Silk Based Matrices as Wound Dressings and Bioartificial Skin Graft

A Thesis

Submitted in Partial Fulfillment of the Requirements for the Degree of

DOCTOR OF PHILOSOPHY

by

DIMPLE CHOUHAN

Department of Biosciences and Bioengineering
Indian Institute of Technology Guwahati
Guwahati-781039, Assam, India

June 2019

Dedicated to my Family and Friends

INDIAN INSTITUTE OF TECHNOLOGY GUWAHATI

DEPARTMENT OF BIOSCIENCES AND BIOENGINEERING

STATEMENT

I do hereby declare that the research findings of this thesis is the result of research work carried out by me in the Department of Biosciences and Bioengineering, Indian Institute of Technology Guwahati, Guwahati, India, under the supervision of Dr. Biman B. Mandal.

As per the general norms of reporting research findings, due acknowledgments have been made, wherever the research findings of other researchers have been cited in this thesis.

Date: 04/06/2019

Dimple Chouhan

INDIAN INSTITUTE OF TECHNOLOGY GUWAHATI

DEPARTMENT OF BIOSCIENCES AND BIOENGINEERING

CERTIFICATE

It is certified that the work described in this thesis entitled "**Silk based matrices as wound dressings and bioartificial skin graft**" by **Ms. Dimple Chouhan** for the award of degree of Doctor of Philosophy is an authentic record of the results obtained from the research work carried out under my supervision in the Department of Biosciences and Bioengineering, Indian Institute of Technology Guwahati, India, and this work has not been submitted elsewhere for the award of any other degree.

Dimple Chouhan
(Candidate)
Roll No: 136106012

CERTIFIED

Biman B. Mandal, Ph.D.
(Thesis Supervisor)

Date: 04.06.2019

ACKNOWLEDGEMENT

The work presented in this thesis would not have been possible without the support from following wonderful people. I feel the opportunity to pen down an acknowledgement, is one of the finest privileges and an equally great responsibility that one can have. It is a privilege to remember all with whose help, this scientific journey has been possible.

First and foremost, I would like to express my sincere gratitude and heartfelt thanks to my supervisor Dr. Biman B. Mandal for giving me an opportunity to be a part of his amazing group. Thank you very much for providing me constant support and encouragement to conduct research over these years. I am grateful for his advice, great ideas and scientific discussions, which are part of this thesis. Being a part of the BBM lab group is an invaluable learning experience for me both scientifically and personally. The wonderful support, valuable suggestions and encouragement are the main factors behind shaping my thesis work.

I would also extend my gratitude to the members of my Doctoral committee, Dr. Manish Kumar and Dr. Rajkumar P. Thummer of the Department of Biosciences and Bioengineering and Dr. Kingsuk Mahata of the Department of Chemistry for their valuable suggestions throughout this journey. I would also like to thank my former Doctoral committee member Dr. Piruthivi Sukumar for his valuable suggestions and constant motivation during the initial annual evaluations.

I would like to thank the present and former Heads of the Department, Dr. Latha Rangan, Dr. Kannan Pakshirajan and Dr. V. Venkata Dasu and the other faculty members for their support and teachings. I would like to acknowledge the Department of BSBE for providing the infrastructural facility for my research work. I would also like to acknowledge Central Instrumentation Facility (CIF), IIT Guwahati for providing high-end instruments to execute some of the experiments.

My Special thanks to the project collaborators Dr. My Hedhammar, KTH Royal Institute of Technology, Sweden and Dr. Samit K. Nandi, West Bengal University of Animal and Fishery Sciences (WBUAFS), Kolkata for their constant help. I would also like to thank

Dr. Pawan K. Samudrala, National Institute of Pharmaceutical Education and Research (NIPER) and Dr. VGM Naidu, NIPER for providing animal house facilities.

I would also like to acknowledge Dr. Nandana Bhardwaj, NIPER for being an admirable person and helping me throughout my Ph.D. study and providing me valuable inputs and suggestions during the research work. It is really my pleasure to be a co-author in two review articles and one book chapter, which helped me in improving my writing skills. The scientific and casual chats we have had over all these years were indeed very beneficial. Thank you very much for the interesting scientific and general discussions, which have inspired me to a great extent.

My special thanks to project collaborators and co-authors from other institutes Piyali Das (WBUAFS), Bijayashree Chakraborty (WBUAFS), Naresh Thatikonda (KTH), Mona Widhe (KTH), Linnea Nileback (KTH) and Ronnie Jansson (KTH). I would also like acknowledge the master students from NIPER whom I mentored - Tshewuzo-u Lohe and Vasu Kedarnath. It was great working with you guys. I will always miss such a good team.

It is my pleasure to thank all members of the BBM lab group who have given me a really nice and happy environment in the lab. I would like to acknowledge the help I got from Sween, Bibhas and Prerak for their constant co-operation when I started my work. The very beginning of my PhD journey would not have been so smooth without your help, thanks a lot! My heartfelt thanks to my best friend Garima during my initial phase of this journey. I would like to thank co-authors and team members from the group, Janani and Shreya for helping me in experimental works. A special thanks to my favourite student Tshewuzo-u Lohe for helping me with two manuscripts and a good company. I would also like to thank all the lab members Praveen, Yogendra, Ankit, Joseph, Sohenii, Ashutosh, Dr. Rajiv, Dr. Chandramauli, Dr. Bhaskar, Bibrita, Chitra, Sangeeta, Suvro, Souradeep and Monisha for their feedback, co-operation, and great discussions. I am also thankful to my former lab members Dr. Manishekhar, Dr. Rocktotpal, Dr. Biswajeet, Dr. Deepika, Dr. Aparajita, Dr. Vimal, Salma, Krishnamurthy, Prerna, Triya, Sakhsi, Princy, Tarishi, Namit, Omkar, Ahana, Ranjana, Deepak, Smriti, Surojeet, Korah, and Sonu for their great company during my Ph.D. journey. Thank you all for constantly providing me a friendly environment in the lab. I am grateful to all of you for your constant support, encouragement and suggestions for this work. We have gathered some great memories while working together as colleagues and

even more recollections as friends. I would always cherish the memories I made with all of you, who have played varied roles of colleagues, life coaches, teachers, and mischief-makers, thus making the journey an eventful experience.

My next thanks go to my alma mater, IIT Guwahati which gave me an opportunity of embarking on this fine endeavour of learning with ample facilities and an equally enchanting natural bounty of the North-east. I have no words to explain the beauty of this campus.

Next, I would thank the funding agencies that provided me the financial support to conduct my research. I am grateful to Ministry of Human Resource Development (MHRD) for the fellowship during my Ph.D. tenure. I would also like to acknowledge the support from Department of Biotechnology, Govt. of India.

I wish to acknowledge my friends, Siddharth, Abhimanyu, Radhika, Durga, Sushmitha, Payel, Arun, Sharbani, Reshmi, Vibha, Himanshu, Sunanda, Manasa, Bandhan, Sambhavi, Hitesh, Mohan, Gaurav, Amit, Babul, Karukriti, Nijil, Sachin, Samarth, Pawan, Nisha, Iffat, Somya, Gowtham, Amrutha, Rahul, Yoganand and Ulrika for having enriched me as a person. I would like to thank all the individuals, who supported me throughout and contributed significantly to the outcome of this dissertation; their time and effort are greatly appreciated. A very big thanks to all these people and other people who have made my stay in Guwahati as a memorable and enjoyable journey.

Finally, I would like to remember my parents and family for their never-ending love, support and patience towards me. It is their numerous personal sacrifices that have enabled me to reach this juncture in life. Simple thanks are not enough to convey my deep respect and gratitude towards my family.

Thanks to the Lord, the Almighty for showering his grace at each and every step!

Dimple Chouhan

CONTENTS

ABBREVIATIONS

3D	Three-dimensional
4RC	4RepCT recombinant spider silk
A	Alanine
AaSF	*Antheraea assama* silk fibroin
ADMSCs	Adipose derived mesenchymal stem cells
AFM	Atomic force microscopy
AGF	Angiopoietin-related growth factor
AMPs	Antimicrobial peptides
AMP-4RC	Antimicrobial peptide conjugated with 4RepCT
ANOVA	Analysis of variance
A. mylitta	*Antheraea mylitta*
A. assama	*Antheraea assama*
ASTM	American society for testing and materials
ATR	Attenuated total reflection
AU	Arbitrary unit
bFGF or FGF2	Basic fibroblast growth factor
BMSCs	Bone marrow mesenchymal stem cells
BmSF	*Bombyx mori* silk fibroin
B. mori	*Bombyx mori*
BSA	Bovine serum albumin
cDNA	Complementary deoxyribonucleic acid
CFU	Colony forming unit
CIP	Ciprofloxacin
CM	Compressive modulus
Col	Collagen
Col-I	Collagen type I
Col-III	Collagen type III
CK 10	Cytokeratin 10

CK 14	Cytokeratin 14
CD31	Cluster of differentiation 31
CD68	Cluster of differentiation 68
CD163	Cluster of differentiation 163
cm	Centimetre
°C	Degree celsius
D	Aspartic acid
DAB	3,3′- diaminobenzidine
DAPI	4′,6-diamidino-2-phenylindole
Da	Dalton
DD	Duoderm dressing
DFU	Diabetic foot ulcer
DMEM	Dulbecco's modified eagle medium
DMSO	Dimethyl sulfoxide
DNA	Deoxyribonucleic acid
ECM	Extra cellular matrix
EDC	1-ethyl-3-(3-dimethylaminopropyl) carbodiimide hydrochloride
EGF	Epidermal growth factor
ELISA	Enzyme-linked immunosorbent assay
ESCs	Epidermal stem cells
FBS	Foetal bovine serum
FDA	Food and drug administration
FESEM	Field emission scanning electron microscopy
FGF-4RC	Basic fibroblast growth factor conjugated with 4RepCT
FITC	Fluorescein isothiocyanate
FN	Fibronectin
FN-4RC	Fibronectin domain conjugated with 4RepCT
FTIR	Fourier transform infrared spectroscopy
G	Glycine
G″	Loss modulus
G′	Storage modulus

GAGs	Glycosaminoglycans
GAPDH	Glyceraldehyde-3-phosphate-dehydrogenase
GM-CSF	Granulocyte-macrophage colony stimulating factor
GOI	Gene of interest
gm	Gram
h	Hours
H & E	Haematoxylin and eosin
HDF	Human dermal fibroblasts
HDMEC	Human dermal microvascular endothelial cells
HGF	Hepatocyte growth factor
HUVEC	Human umbilical vascular endothelial cells
H_2O_2	Hydrogen peroxide
IgG	Immunoglobulin G
IGF	Insulin like growth factor
IHC	Immunohistochemistry
Inv	Involucrin
IP	Intraperitoneal
iPSCs	Induced pluripotent stem cells
ISO	International organization for standardization
K10	Keratin 10
K5	Keratin 5
kDa	Kilodaltons
KGF	Keratinocyte growth factor
L	Litre
Lac	Lactoferricin
Lac-4RepCT	Lactoferricin domain conjugated with 4RepCT
LDH	Lactate dehydrogenase
LiBr	Lithium bromide
M	Molar
Mag	Magainin
Mag-4RepCT	Magainin domain conjugated with 4RepCT

MaSpI	Major ampullate spidroin I
MaSpII	Major ampullate spidroin II
MIC	Minimum inhibitory concentration
Min	Minute
mL	Millilitre
MMPs	Matrix metalloproteases
MRSA	Methicillin-resistant *Staphylococcus aureus*
mRNA	Messenger RNA
MSCs	Mesenchymal stem cells
MT	Masson's trichrome
MTCC	Microbial type culture collection
mg	Milligram
µg	Microgram
µL	Microlitre
µm	Micrometre
µM	Micromolar
MTT	3-(4,5-dimethylthiazol-2-yl)-2,5-diphenyltetrazolium bromide
MWCO	Molecular weight cut-off
Na_2CO_3	Sodium carbonate
NaOH	Sodium hydroxide
NBF	Neutral buffer formalin
NCCS	National centre for cell science
NF-κB	Nuclear factor kappa enhancer binding protein
NGF	Nerve growth factor
nm	Nanometre
NMSF	Non-mulberry silk fibroin
O.D.	Optical density
PA	*Pseudomonas aeruginosa*
PanCK	Pancytokeratin
PBS	Phosphate buffer saline
PC	Panniculus carnosus

PCL	poly(ε-caprolactone)
PDGF	Platelet derived growth factor
PEG	poly(ethylene glycol)
PEI	poly(ethylenimine)
PEO	poly(ethylene oxide)
%	Percentage
PGA	poly(glycolic acid)
PHBV	poly(3-hydroxybutyrate-co-3-hydroxyvalerate)
PLA	poly(lactic acid)
PLGA	poly(lactic co-glycolic acid)
PlGF	Placenta growth factor
PRP	Platelet rich plasma
P. ricini	*Philosamia ricini*
PrSF	*Philosamia ricini* silk fibroin
PVA	poly(vinyl alcohol)
PVAAA	PVA + AaSF nanofibrous mat
PVABM	PVA + BmSF nanofibrous mat
PVAPR	PVA + PrSF nanofibrous mat
PVP	poly(vinyl pyrrolidone)
PVDF	poly(vinylidene fluoride)
R	Arginine
RDT	Recombinant DNA technology
RGD	Arg-Gly-Asp or Arginine-Glycine-Aspartic acid
RNA	Ribonucleic acid
RH	Relative humidity
Rpm	Revolutions per minute
RT	Room temperature
RT-PCR	Real-time polymerase chain reaction
s	Seconds
SDS	Sodium dodecyl sulphate
SE	*Staphylococcus epidermidis*

SELP	Silk elastin like protein
SF	Silk fibroin
SS	Silk sericin
STSG	Split-thickness skin grafting
SVF	Stromal vascular fraction
TCP	Tissue culture plate
t_{gel}	Gelation time
TGF- β1	Transforming growth factor- β1
TNF-α	Tumour necrosis factor-α
UCS	Ultimate compressive strength
UNT	Untreated
UTM	Universal testing machine
UTS	Ultimate tensile strength
UV	Ultraviolet
VEGF	Vascular endothelial growth factor
vWF	van Willbrand factor
WAXD	Wide angle X-ray diffraction
WHO	World health organization
w/v	Weight/volume
WVTR	Water vapour transmission rate
XRD	X-ray diffraction
YM	Young's modulus

LIST OF TABLES

LIST OF FIGURES

Chapter 1

Introduction and Literature Review

भारतीय प्रौद्योगिकी संस्थान गुवाहाटी
Indian Institute of Technology Guwahati

Introduction and Literature Review

1.1. Introduction

The skin, also known as protective barrier, is the largest organ of our body [1, 2]. It plays multiple roles in protecting the body against external environment, pathogens and mechanical disturbances [2-4]. The skin is composed of three layers: epidermis, dermis and hypodermis as shown in the schematic diagram (**Figure 1.1.**). The three-layered skin structure plays a vital role in protecting the body against any mechanical damage [5]. The outermost thin layer is epidermis, which is highly cellular and mainly composed of keratinocytes and melanocytes. The basal cell layers of mammalian epidermis maintain homeostasis. It also consists of skin appendages such as hair follicles, sweat and sebaceous glands. The middle layer is dermis, which acts as a connective tissue and constitutes the bulk of the skin. It is mainly composed of fibroblasts, extracellular matrix (ECM) components such as collagen, glycosaminoglycans (GAGs) with some elastin and blood capillaries [1, 5]. Fibroblasts represent the major cell type in the dermis, which secrete ECM components and remodelling enzymes (such as proteases and collagenases) that accounts for most of the skin's biomechanics and resilience. The well vascularized hypodermis represents the final layer underneath the dermis, which is mainly composed of adipose tissue contributing towards thermoregulatory and mechanical properties of the skin, and acts as a cushion between the skin and other skeletal structures [1, 4, 5].

Damage to the skin due to cutaneous wounds results in fatal consequences, leading to significant imbalance in physiological activities of internal organs [6, 7]. Dermal wounds represent a major healthcare problem owing to an increasing number of trauma and pathophysiological conditions. Substantial imbalance in physiological activities due to prolonged open wounds may cause significant disability or even death. In addition, increased widespread presence of non-communicable diseases such as diabetes, vascular diseases and obesity also contribute to the rising number of diabetic ulcers, venous ulcers, pressure ulcers and chronic wounds [7, 8]. Cutaneous wounds are broadly categorized as superficial, partial-thickness and full-thickness wounds depending on the depth of tissue injury [5, 8]. The full-thickness wounds, often caused by trauma or wound chronicity, impose a great threat, because such wounds lose the ability of self-repair and may lead to substantial organ failure in the absence of surgical

interventions [8]. Burn injuries and chronic wounds affect more than 11 million and 6.5 million people respectively every year, leaving millions of patients with disability, distress and discomfort [7, 9, 10]. Diabetic foot ulcer (DFU) is a major complication for diabetic patients and more than 85 % of the patients suffering from chronic ulcers end up in limb amputation surgeries [10-12]. Burn injuries have contributed to almost 180,000 deaths (as of 2018) according to the world health organization (WHO) [9]. The annual expenses on wound care may go beyond $ 22.4 billion by 2024, which was $ 14 billion in 2015 [9]. Despite a variety of available treatments, wound healing is still a great challenge due to poor clinical outcomes.

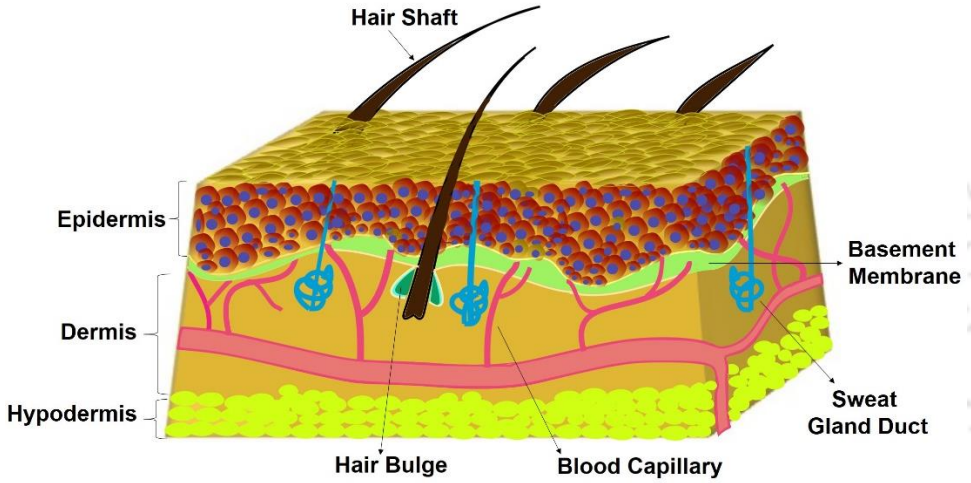

Figure 1.1. *Diagram of a three-dimensional (3D) structure of the skin representing three layers, namely, epidermis, dermis and hypodermis. The anatomy of skin constitutes of various important structures like blood capillaries, sweat gland ducts and hair shafts that play major roles in protecting the body against external environment.*

Superficial or epidermal injuries include typical sunburns or scalds, characterized by minor pain and erythema [13]. The regeneration of epidermal wounds is rapid and without any scarring, as there is no excessive ECM deposition. In addition, there is no requirement of surgical treatments because only the skin epidermis is affected. In contrast, superficial partial-thickness wounds, which include thermal trauma or burns, are characterized by epidermal blistering and severe pain. These wounds also affect superficial parts of the dermis in addition to the epidermis. Herein, healing is carried out by re-epithelialization of the wound boundaries through cell migration from the marginal dermal regions [13]. The epithelial regeneration is also performed by the residual hair follicles and sweat glands, which contain a reservoir of stem cells having self-renewal capability [14]. Furthermore, deep partial-thickness and full-thickness injuries (for

instance third degree burns) involve greater damage to the dermis with loss of skin appendages and complete destruction of regenerative elements of the epithelium. These wounds are healed by epithelialization from the wound edges through contraction, which leads to severe cosmetic deformities due to excessive scarring and functional defects [13, 15]. However, larger full-thickness skin defects (> 4 cm in diameter) lack the ability of self-epithelialization and fail to heal, thereby requiring surgical interventions [1, 16]. Other types of full thickness wounds occur due to pathophysiological conditions such as diabetes. The patients suffering from diabetes often develop chronic cutaneous wounds due to neuropathy and abnormal cellular activity [12]. Unlike acute wounds, which are healed by the self-repair mechanism of skin tissue, chronic wounds fail to heal by themselves [8]. Diabetic wounds are difficult to manage owing to an extreme level of wound chronicity, hyperglycaemia and bacterial colonization, which progress with time unless treated in an efficient way [8, 12]. The complex and dynamic process of natural wound healing process flops in chronic wounds due to cell senescence and persistent inflammation. Therefore, wound repair and regeneration is an intense area of research, requiring clinical interventions to treat millions of patients suffering from various types of cutaneous wounds.

Towards this goal, extensive research is being carried out by taking advantage of the emerging concept of tissue engineering and functional biomaterials [8]. Skin tissue engineering is a complex process involving appropriate choice of biomaterial, cell selection and designing of suitable platform in order to mimic the structural and functional properties of skin [8, 17]. The current 'gold standard' treatment is considered as split-thickness skin grafting (STSG), which is composed of autologous epidermis with some part of the dermis [18]. However, autologous STSG approach suffers from problems like unavailability of donor skin site, high cost, inconsistent engraftment and secondary donor site wounds [1, 3]. Therefore, several other alternative treatments have been adopted that utilize various technological methods to fabricate artificial matrices or constructs. These matrices act as a template to cover the wounds or serve as a bioartificial skin graft to fill the wound cavity. In this context, various biomaterials have been explored that have inherent regenerative properties to accelerate the wound healing process [19, 20]. In the last 25 years, with the worldwide advancement in material development and tremendous demand for skin-replacement products, many natural and synthetic biopolymers have been examined for wound repair and regeneration [19, 20].

The major properties required for wound dressing materials are biocompatibility, non-toxicity, biodegradability and ideal mechanical properties to recapitulate the properties of native skin tissue [7]. In addition, biomaterials based wound dressings and artificial skin grafts provide protection against wound infection and prevent loss of fluid/moisture from the wound surface. Numerous natural biomaterials explored in this field are cellulose, collagen, chitosan, fibrin, gelatin, silk fibroin, silk sericin and hyaluronic acid [8, 19, 20]. Synthetic polymers like poly(vinyl alcohol) (PVA), poly(glycolic acid) (PGA), poly(lactic acid) (PLA), poly(ε-caprolactone) (PCL), nylon and silicone have also significantly contributed in the development of wound dressings [21].

Wound healing process is a very well-orchestrated and regulated process, consisting of series of events such as haemostasis, inflammation, proliferation and ECM remodelling [6]. The wound healing cascade begins with haemostasis and inflammation. The proliferation phase comprises of numerous events like granulation tissue development (formation of provisional ECM), angiogenesis (formation of blood vessels) and re-epithelialization (formation of epidermal skin layer), resulting in wound contraction. The final phase constitutes the remodelling event, in which the previously formed matrix is slowly morphed towards forming either a functional skin or a semi/non-functional scar tissue [6]. With the help of a wound dressing or artificial skin graft acting as a platform over wounds, the healing rate is accelerated towards tissue regeneration pathway [8]. Herein, we have explored affordable silk biomaterials to develop bioactive wound dressings and artificial skin grafts to bridge the gap between number of patients and available wound care regimens.

Application of silk in healing the cutaneous wounds commenced decades ago in the form of silk sutures [22]. Silk fibres, directly isolated from the cocoons were used as sutures in the ancient times. Silk is a protein biopolymer that is produced by a variety of insects such as silkworms, flies, spiders, mites and scorpions [22]. All the varieties of silk fibres differ from species to species due to significant changes in their amino acid sequences. Being a versatile biopolymer, silk has been hugely explored in the applications of tissue engineering and regenerative medicine [23]. Silk has been considered as a biomaterial since decades and has been widely explored in the fields of drug delivery, organs re-construction and wound healing applications [22, 23]. Silk extracted from domesticated mulberry silkworm, *Bombyx mori*, has been the most extensively studied variety of silk since few decades [23]. However, limited study is

available on the potential of non-mulberry silk varieties such as *Antheraea assama* and *Philosamia ricini* that are available in the North East regions of India [24]. Non-mulberry silk possesses inherent Arginine, Glycine and Aspartate (RGD) motifs in the protein sequence, facilitating binding to the integrin receptors of cells [24]. This may provide functional advantage of mediating cell-material interactions for wound repair and regeneration. Therefore, in the present thesis work, we aim to explore the potential of silk from various other varieties and harness their regenerative properties towards developing wound dressings and artificial constructs for skin regeneration.

Apart from providing a physical support, the platform of artificial constructs or wound dressing should also offer cell conducive properties to aid rapid recruitment of host cells and stimulate the wound milieu towards skin regeneration [8, 25]. Such materials confer a physical connection between cells and material, and also mediate biochemical signals controlling cell growth, proliferation and migration [8, 26]. Silk biomaterial holds extraordinary properties for drug delivery applications and has been utilized as a cargo to deliver drugs, biomolecules and growth factors at a slow and sustained rate [27]. Taking advantage of this property of silk, we have applied several strategies to functionalize the silk matrices with growth factors, antibacterial molecules, bioactive compounds and bioactive materials in order to trigger the wound healing process. Our aim is to develop acellular wound dressings and tissue-engineered constructs, which mimic the attributes of wound provisional matrix by functionalizing the silk biomaterials.

Herein, the thesis presents possible strategies to develop various types of silk-based constructs such as nanofibrous matrices, microporous scaffolds and hydrogels for wound-specific treatments. Furthermore, we have explored two approaches to fabricate functionalized wound dressings: 1) functionalization of silk matrices that are embedded with bioactive compounds, which act as a cargo to slowly deliver the additives at wound site and 2) binding of bioactive molecules or its functional mimics that remain adhered to the silk matrices. In the first approach, we have used growth factors, antibiotic drug and antimicrobial peptides as the additives, which are released from the silk matrices at a slow and sustained rate. In the second approach, we have used functionalized spider silk fusion proteins that are physically adsorbed to the silkworm silk matrices due to inherent interaction between the two silk types. Both the approaches help in accelerating the wound healing process. Based on this rationale, the functionalized nanofibrous

wound dressings have been examined for their healing efficacy in diabetic rabbit model. Furthermore, functionalized porous silk scaffolds have been explored for its healing efficacy in treating full-thickness burn wounds *via* one-step grafting procedure. In the final objective, we have developed a unique strategy to fabricate *in situ* forming silk hydrogel for the treatment of third degree burn wounds in comparison to the well explored collagen biomaterial. The detailed studies are organized in various chapters to be followed after an extensive review of literature pertinent to the current research area. In the literature review, we critically appraise the research efforts concerned with the technologies using various biomaterials, growth factors, cells and fabrication strategies. We also touch upon the most recent advances in wound healing applications using silk as a biomaterial, describing various properties of silk that make it a potential candidate for fabricating wound dressing and artificial grafts. Finally, we lay down our research work in this area, showcasing our efforts to develop bioactive silk matrices for skin regeneration towards improved wound healing technology through the following chapters.

1.2. Review of Literature

1.2.1. Wound healing and skin repair: an overview

Wound healing process is a very well-regulated process consisting of series of events such as haemostasis, inflammation, proliferation and extracellular matrix remodelling as illustrated in the image (**Figure 1.2.**) [6, 28]. The four healing phases involve interactions between various types of cells, bioactive factors and a supporting platform, which is usually the natural ECM secreted by cells. The wound healing cascade begins with haemostasis and inflammation. This stage involves recruitment of blood platelets and immune cells to control loss of blood and clearing of pathogens. The initially recruited immune cells play a major role in secreting chemokines and growth factors, which attract other cells and thereby lead the healing process to its next phase of proliferation [28]. The proliferation phase comprises of numerous events like formation of provisional matrix, blood vessels and re-epithelialization, resulting in wound contraction. This particular phase is regulated through crosstalk between various cells, mainly macrophages, fibroblasts, endothelial cells and keratinocytes [28]. The final phase constitutes remodelling event, in which the previously formed matrix is slowly modified into a more resilient tissue through activity of numerous matrix metalloproteases (MMPs) and new ECM components [28].

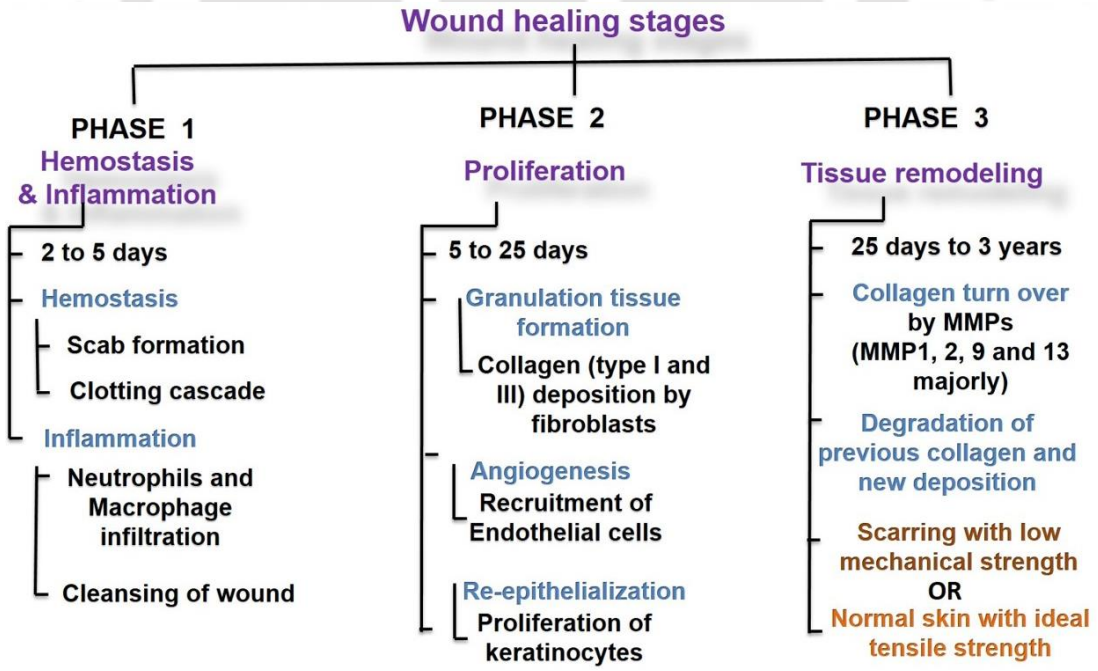

Figure 1.2. *Schematic illustration showing three main phases of the wound healing process and major events associated with each stage.*

This normal healing process gets severely dysregulated in case of pathophysiological conditions. Majority of severe wounds are associated with accidents or disease conditions like diabetes. Large trauma wounds due to burns or accidents result in loss of majority of skin tissue and thus fail to heal [15]. In case of non-healing wounds, for example DFU, the healing process gets obstructed due to persistent inflammation at the very initial phase and gradually turns to be chronic, leading to failure in healing [12]. Depending on the type of chronic wounds (like pressure sores, venous ulcers or diabetic wounds), the process may get hindered during any of the four stages. In case of large burn wounds, natural healing is affected due to significant loss of skin tissue or failure to develop a provisional ECM matrix as a result of tissue necrosis [1, 7]. In case of normal wounds, which possess self-repair potential, the healing cascade runs normally as described above without any failure. Herein, a fibrin clot is formed at the wound-site that acts as a natural provisional matrix for cellular recruitment [26].

The fibrin clot is composed of fibrin matrix, which sequesters growth factors and supports cell adhesion, migration and proliferation through its cell binding motifs [26, 28]. The fibrin clot also helps in slow and sustained release of sequestered growth factors and cytokines during the complete course of healing [8, 26]. Thus, the natural wound milieu consists of fibrin clot platform having cell adhesive sites, instructive biochemical cues, growth factors and various types of cells. Therefore, in order to treat non-healing and large wounds, the biomimetic approach is considered outstanding, wherein the microenvironment of normal wound is imitated with the help of bioactive matrices. However, mimicking the natural wound milieu is very challenging and requires interdisciplinary approaches in terms of biomaterials, bioactive molecules and structural framework of the constructs. The most successful strategy to treat the non-healing wounds is to provide an artificial matrix in the form of wound dressing or skin graft, which serves as a provisional matrix or supporting platform, and thereby aid in the healing process [17].

Significant improvement in the development of bioactive templates and pro-regenerative matrices has been going on because such matrices trigger the key events of natural healing cascade and help in the regeneration of functional skin tissue [29]. Furthermore, depending on the type of functionalization of matrix, a definite stage or event of healing process can be stimulated by certain biomolecules like specific growth factors, cytokines, chemokines and cell adhesive peptides. The regenerative cues

provided by such biomolecules are fine orchestra of signalling molecules, which along with the structural framework of scaffolds, help in accelerating the healing process [30]. Another approach for skin regeneration therapeutics lies in the structural engineering of scaffolds or hydrogels. Numerous construct designs like woven/non-woven mat, nanofibrous matrices, microporous scaffolds, bilayer or trilayer constructs, hydrogel lattices, injectable gels, microspheres and 3D bioprinted grafts have been employed for wound healing applications [31, 32]. Herein, we have briefly reviewed scaffold fabrication approaches, various biomaterials and functionalization strategies to fabricate tissue-engineered skin and bioactive wound dressings.

1.2.2. Basic requirements of constructs for wound healing applications

A range of biomaterials and advanced fabrication strategies have led to the development of plethora of scaffolds for wound healing applications. The basic properties required for making such matrices are – biocompatibility, non-immunogenicity, non-toxicity, biodegradability, good mechanical stability, moisture retention property, adequate water vapour transmission rate (WVTR) and adequate porosity with well-connected pores to support exchange of nutrients and gases [32-34]. The scaffolds should promote ingrowth of fibrovascular tissue and angiogenesis, integrate well into the wound bed, prevent infection, avoid maceration, prevent skin contracture and scarring [32-34]. Moreover, the artificial skin construct in the form of a final scalable product should also be cost-effective and off-the-shelf available with longer shelf-life [1]. Some of the major properties of matrices for wound healing applications are discussed in details in the following sections:

1.2.2.1. Scaffold architecture and strategies for construct design

Tissue engineering aims at repair and regeneration of damaged tissues by constructing artificial grafts, which closely mimic the anatomy and physiology of the native organ [35, 36]. Hence, it is essential to achieve the similar structure, chemical make-up, mechanical properties, adequate porosity and interconnecting pores while fabricating the scaffolds. Considering the biomimetic approach, different scaffold fabrication strategies have been applied to match the layered and fibrous architecture of skin since decades [32, 33]. Integra, the most studied biosynthetic artificial skin was developed for the first time in early 1980s by Burke and Yannas, who adopted the biomimetic approach by fabricating a bilayered acellular construct [37]. Integra constitutes of porous scaffold

made up of bovine collagen and GAGs serving as a dermal substitute, which has been covered with semipermeable polysiloxane (silicone) layer mimicking the barrier properties of epidermal layer [37]. Since then, advancement in the biomanufacturing techniques has led to the development of a variety of scaffolds like foams, hydrogels, microporous sponge, nanofibrous matrices and microfibrous scaffolds using a variety of natural and synthetic biomaterials [8, 34].

A scaffold is a 3D supporting framework that serves as a platform for cellular localization, adhesion, migration, proliferation and differentiation, which ultimately guides the development of new functional tissue [32, 38]. The conventional fabrication methodologies for 3D scaffold involve freeze drying, phase separation, self-assembly, particle leaching, decellularization and chemical crosslinking [31]. The advanced fabrication methodologies involve photopolymerization processes, electrospinning, microfluidic assembly, 3D bioprinting and extrusion-based techniques such as 3D fibre deposition [39-41]. The scaffold architecture should not only mimic the porous and fibrous architecture of dermal component but should also support the development of epithelial layer with its primary characteristics like – (1) stratification of keratinocytes, (2) polarization of cells, (3) contact with the basement membrane and (4) effective barrier properties [42].

The natural structural hierarchy of skin has also been precisely reproduced by applying micro-, nano- and macro-fabrication technologies. In this context, electrospinning has attracted substantial interest in the technological and healthcare sectors in recent years [43]. This technique enables easy fabrication of nanofibrous mats in large scale. Electrospun nanofibrous matrices using various natural and synthetic materials have become advantageous over microfibrous or microporous scaffolds as the size of nanofibres can be tuned to mimic the size of natural fibres present in the ECM of skin [40, 43]. Moreover, the unique features like larger surface area to volume ratio, more interconnected pores, reproducibility and easy fabrication methodology have encouraged the use of electrospun matrices in the field of skin regeneration and therapeutics [40, 43]. The nano-range architecture provided by the electrospun mat bestows improved cellular adhesion and migration, and are considered as excellent cell recruiters because the nanoscale dimensions of nanofibres help in cell binding and thus aid in their migration towards wound site [40, 43]. Moreover, incorporation of bioactive molecules becomes easier in the nanofibrous wound dressings

owing to the facile technology of electrospinning [44]. The bioactive molecules like growth factors provide an adequate niche required to communicate with the surrounding tissue and relay signals back to the cells growing in the scaffold [7]. Such smart matrices have gained much attention in this field in recent times. Building a 3D construct is not enough for tissue regeneration; developing a cell instructive microenvironment is the current aim of tissue engineers [8]. In this regard, such types of scaffolds are currently being fabricated, which are capable of maintaining a crosstalk between cells and ECM focusing on the ‘‘dynamic reciprocity’’ occurring between them.

Furthermore, particular design of a scaffold also depicts its application for a specific type of wound. For example, electrospun nanofibrous matrices have largely been utilized in the form of a wound dressing and rarely as dermal replacement due to limitations in cell migration within the construct [45, 46]. Dermal replacements are mostly used in the form of hydrogel lattice or microporous scaffolds, which could be permanently applied at the wound site either *via* one-step or two-step grafting surgeries [3, 17, 47]. The microporous network or hydrogel environment helps in migration of cells within the construct and thereby aid tissue ingrowth; hence, such constructs could be permanently implanted [1, 17, 48]. However, it should meet the essential characteristics like its integration to the wound bed, vascularization or graft take capacity, biodegradability, immune-compatibility and most importantly its capability to repair the wound defect while supporting the remodelling events that would occur throughout a patient’s life.

Artificial templates for skin regeneration commenced with the development of thin cell sheets. The optimized cell culture conditions have facilitated lab-grown cell sheets of autologous origin to treat partial thickness skin wounds [49, 50]. However, the cell sheets can be applied only on the epidermal and split-thickness wounds and not on full-thickness wounds. This led to the development of porous scaffolds and hydrogels, which can be applied as an artificial template over full-thickness cutaneous wounds [8]. The microporous scaffolds have been considered suitable for fabricating tissue engineered skin grafts, especially in case of dermal replacements [1]. The pore size may vary from 20 to 500 μm depending on the biomaterials used and fabrication methods like freeze-drying, particle leaching or others [51]. The most significant feature of microporous matrices is interconnectivity among pores, which provide a 3D microenvironment for cellular migration and ingrowth [47, 52, 53]. Matrices with pores

in micro range furnish spatial distribution of cells throughout the construct and thus coordinate numerous cell fate processes, including a myriad of signals for angiogenesis and graft take [53].

Furthermore, the architecture of natural ECM with components like collagen or fibrin appear as a hydrated gel-like matrix with intricate fibrillar architecture [54]. From the structural perspective, hydrogels closely mimic the native ECM structure [48, 54, 55]. The skin extracellular microenvironment, which surrounds cells, is a highly hydrated network due to presence of GAGs chains. Hydrogels are hydrophilic lattices of polymeric network or protein fibrils interwoven within a hydrated network due to chemical or physical crosslinking [55, 56]. Hydrogel made up of various biomaterials also hold excellent potential in skin regeneration and wound healing applications. In the progress of strategies for wound repair and regeneration, *in situ* forming hydrogels and injectable systems have largely been explored in the last few years [56, 57].

For example, thermosensitive gels and pH responsive gels behave as a solution, but forms a hydrogel at near-physiologic conditions like 37 °C and physiological pH [58]. This may facilitate *in situ* crosslinking within the biopolymer and also with native wound edge tissue. Another advantage of this strategy is that it is easy to apply and does not require additional glue or sutures because gels take the exact shape of wound defect. Such injectable systems have also been used for cell delivery applications [58]. This demonstrates future possibility of delivering autologous stem cells or autologous tissue specific cells in the gel, which crosslinks at the wound site and forms a cellular matrix immediately. All these examples demonstrate that the scaffold architecture should be considered as one of the important factors for wound healing applications. Overall, the platform of a wound dressing or skin graft assists in healing the wounds at a faster rate in addition to the inherent healing process as illustrated in the schematic image (**Figure 1.3.**).

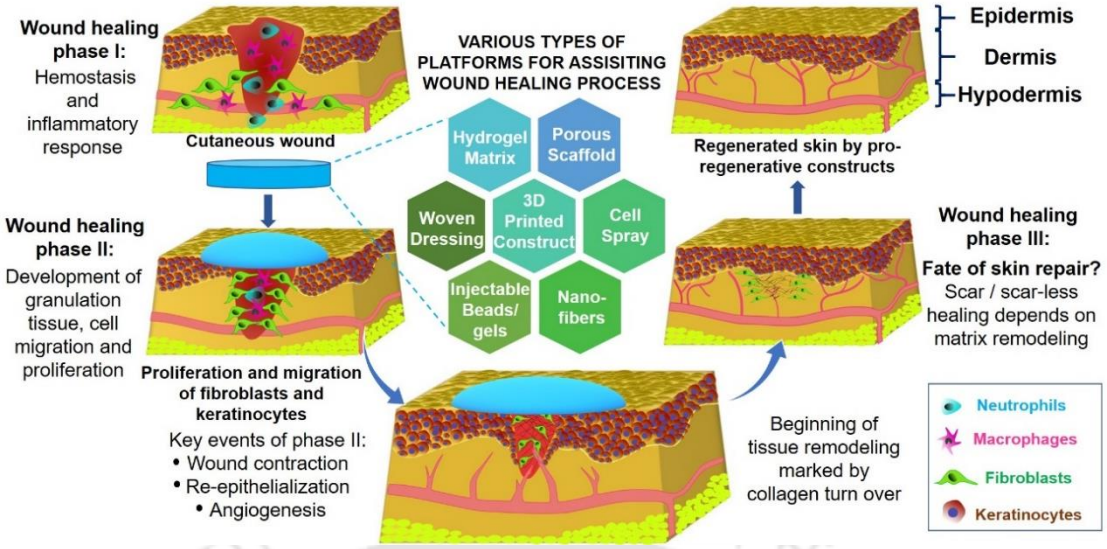

Figure 1.3. *Schematic image depicting the concept of wound healing process assisted by a dressing material or skin graft.*

1.2.2.2. Biocompatibility

Biocompatibility is the ability to support cellular localization, proliferation and normal cellular activities like molecular signalling, differentiation and ECM secretion without eliciting local or systemic immunogenic response or adverse effects to the host [59, 60]. To assess the biocompatibility of artificial grafts, undesirable effects like inflammation, cytotoxicity, genotoxicity, carcinogenicity, immunogenicity, mutagenicity, thrombogenicity and fibrosis overgrowth should be thoroughly verified and examined under both *in vitro* and *in vivo* conditions [59, 60]. Bioengineered skin grafts must show favourable biocompatibility and non-immunogenicity for quicker graft take by the host, which is investigated by examining the integration of graft with the wound bed tissue [54, 60]. The signature characteristics of graft take are determined by angiogenesis, ingrowth of fibrovascular tissue and vascular anastomosis [54]. New biomaterials are often tested *in vivo* by implanting them subcutaneously in animal models prior to their examination for wound healing applications [61]. Biocompatibility of materials is confirmed if they provoke minimal or mild early inflammation; negligible fibrosis, support tissue ingrowth and vascularization [60]. Examination of presence of macrophages, giant immune cells and their quantification further reveal immune response of the host body against materials [62]. Such studies are often carried out for several months to examine their effect for prolonged time period. In addition, the preparatory steps play major roles in deciding the biocompatibility of scaffolds. Green synthesis of constructs is highly appreciable owing to the minimal or negligible toxic

effect on the environment. For instance, methods using aqueous based solvents should be preferred over harsh organic chemicals. Similarly, sterilization methods may contribute to the immunogenicity of grafts and hence should be thoroughly optimized.

1.2.2.3. Biodegradability

Biodegradability is the ability of materials to degrade into harmless and non-toxic substances with time under both *in vitro* and *in vivo* conditions [62]. The degraded products are often resorbed by the host system and if the degradation rate matches with the resorption rate, it is termed as bioresorbable property [63]. Biodegradability is also related with biocompatibility because the products of degradation process should not evoke immune response in the host; the degraded products should be non-toxic, non-immunogenic, easy to metabolize and easy to eliminate from the host system [62, 63]. A variety of degradable natural and synthetic materials have been used for wound healing applications, which can be degraded enzymatically or hydrolysed by themselves without producing harmful degradation products. The biodegradable scaffolds should not degrade at a much faster or slower rate, as it may result in reduced mechanical properties or reduced tissue regeneration ability. Hence, materials with tunable degradation rate provide functional advantage to the scaffold as they can match the degradation rate and thereby create space for new tissue by the deposition of cell-mediated ECM components [64]. Such matrices are also called as smart matrices because they enable the turnover of an artificial graft into a biological matrix with time, thereby serving the true purpose of tissue engineering by restoring the structure and function of damaged tissue.

1.2.2.4. Mechanical properties

The mechanical strength of tissue is closely related to its functional performance and signifies a crucial role in the development of skin. The dermal layer of skin is composed of a complex architecture of enzymatically cross-linked ECM (collagen and elastin fibres) that provides biomechanical properties and elasticity [65]. The mechanically inferior skin substitutes may lead to skin contraction, fibrosis, and scarring with failed skin repair [5]. Therefore, a coherent approach should be considered for both the designing and testing of the mechanical properties of skin substitutes. In addition, the mechanical properties of scaffolds also regulate many cellular behaviours such as cell-matrix interactions, cellular phenotype, differentiation, and vascularization [66]. Soft hydrogels made up of biomaterials such as collagen and fibrin often suffer from matrix

contraction due to low mechanical strength [67, 68]. Contraction mechanism of collagen gels is a well-known phenomenon, and therefore strategies to prevent the contraction have been applied by increasing the mechanical strength *via* chemical or physical crosslinking in various reports [69-71]. In an earlier study, researchers have demonstrated improved mechanical properties in collagen scaffolds through crosslinking with 1-ethyl-3-(3-dimethylaminopropyl) carbodiimide hydrochloride (EDC) [72]. The cross-linked, mechanically stable matrices showed a reduced rate of contraction during the culture period and wound healing process. Such techniques are useful in modulating the bulk properties of certain biomaterials.

In this context, other biomaterials can be explored with relatively high mechanical strength. For example, unlike collagen, silk possesses higher mechanical strength and does not contract; thus, the graft contracture loophole often caused by collagen-based constructs can be circumvented by using mechanically strong biomaterials [73]. Another commonly used method to improve the bulk properties of matrices is to use composite materials by blending mechanically strong synthetic or natural biopolymers [74]. Therefore, various techniques such as blending, chemical crosslinking, functionalization with bioactive molecules and co-polymerization have been employed for the improvement of mechanics of developed matrices [74, 75]. For instance, silk-collagen composite hydrogels were fabricated for developing artificial skin tissue, which were soft gels as well as contained sufficient mechanical strength to prevent matrix contraction [76]. Hence, mechanical properties also hold equal importance while fabricating a suitable construct and needs to be optimized as per the requirement.

1.2.3. Biomaterials for wound healing applications

A wide variety of polymeric matrices are routinely utilized in skin tissue engineering, wound healing and other therapeutic applications, which hold important properties of biocompatibility, biosorption ability and biodegradability [20, 21, 25]. A list of some representative natural and synthetic polymers being utilized in this field is presented in **Table 1.1.** Among different polymers, synthetic polymers are generally much easier to tailor in terms of mechanical, degradation and other properties [21, 56]. However, lack of cell-recognition signals and production of acidic degradation products limit its utilization in therapeutic reconstruction of tissues. In tissue engineering approach, natural polymeric matrices are generally well adapted and tolerated within the host body

compared to other surgical procedures due to presence of intrinsic biological cues/cell binding motifs, biocompatibility and biodegradation properties [20, 22, 26]. Herein, we have discussed different polymers (natural and polymeric) being utilized for wound healing applications.

Table 1.1. *List of some representative polymeric biomaterials utilized for wound healing applications.*

Type of polymer	Biomaterial	Form	Findings	References
Natural	Collagen	Reinforced scaffolds, gels, electrospun dressings	Augmentation of early cutaneous wound healing, improved rate of wound healing	[77-79]
	Gelatin	Membrane, wound dressings, bilayered graft	Acceleration of re-epithelization of wounds and improved neo-vascularization	[80-82]
	Chitosan	Bio-inspired bi-layered hydrogels, Nano-membrane	Improved biostability, nanofibrillar wound dressings, promotion of stem cell delivery and wound healing	[83-85]
	Hyaluronic acid	Hydrogel based system, nanofibrous mats	Cytokine release and growth factors delivery; improved wound healing	[86, 87]
	Fibrin glue	Suspension, gel, membrane	Improved wound closure and faster re-epithelialization	[88, 89]
	Silk fibroin	Dermal substitutes, electrospun and bi-layered dressings	Improved re-epithelialization, wound closure, biological functions	[47, 90-92]

Synthetic	PCL	Electrospun dressings	Improved healing of chronic wounds	[93]
	Polyurethane	Nanofibrous mats, membranes	Improved wound healing and re-epithelialization in diabetic wounds	[94, 95]
	Polyglycolic acid/poly lactic acid	Nanofibrous mesh, knitted membrane	Improvement of full-thickness diabetic foot ulcers	[96, 97]
	Poly(lactic-co-glycolic acid	Electrospun mesh, Sutures	Treatment of full-thickness diabetic foot ulcers	[98, 99]
	PVA	Electrospun wound dressings, membranes	Enhancement of wound repair in a full-thickness dermal defect model	[74, 100]

1.2.3.1. Collagen

Collagen is a naturally derived structural protein present in the skin and is also abundantly present in the body in various forms [5, 67, 101]. Being a major component of native skin, collagen is the most preferable natural biomaterial for skin tissue engineering [5, 17, 33]. Development of artificial skin began with the fabrication of Integra, which contains collagen type I [37]. Since then, collagen has been exploited in different forms such as hydrogel, sponge, film, sheet, lattice, nanofibrous mat or gels for the development of advanced bioengineered constructs [102-104]. A large number of collagen-based dressings or matrices have been widely utilized as a temporary covering for ulcers and burns. In initial studies, either anchored or floating collagen gels were introduced as a dermal-substitutes for investigating the effect of cellular force on collagen contraction and wound contraction [105]. Afterwards, several other collagen-based skin substitutes starting from acellular dermis, cellular epidermis/dermis, to bilayered skin equivalents have been developed for wound healing and tissue engineering of skin [1]. Many of the collagen based matrices have been commercially used such as

Promogram®, Johnson & Johnson, and Puraply®, Royce Medical under various clinical conditions and showed favourable results [105, 106].

Pre-vascularized bioengineered 3D graft using collagen type I has recently been developed, where capillary-like networks were observed in the skin substitute on co-culturing endothelial and fibroblast cells in the collagen gel [54]. A fully functional 3D integumentary system has recently been developed using collagen gel drop where iPSCs embryoid bodies were grown, showing regeneration of sebaceous glands and hair regeneration with proper hair eruption and hair cycles in the mice model [107]. Several research groups have utilized collagen lattice, which was fabricated by condensation of collagen solution populated with fibroblasts to mimic the *in vivo* dermal layer [78, 79]. However, collagen lattices showed significant matrix contraction, which in turn led to the chemical modification of the material to reduce contraction rate [108]. Regardless of the inherent biocompatibility property of collagen, the collagen-based lattices were found to be mechanically weak as they suffered from rapid degradation and matrix contraction. Therefore, in order to increase the biostability, mechanical properties and also to prevent wound contraction during wound healing process, collagen matrices have been modified by cross linking treatment or by combining other natural or synthetic polymers [105, 108, 109].

1.2.3.2. Gelatin

Gelatin is the hydrolysed form of collagen, which is relatively cost-effective and less antigenic compared to collagen due to its denatured form [110]. Gelatin has been used in various formats and blends for skin tissue engineering applications owing to its biodegradability, biocompatibility and easy processing properties [110-112]. The easy gelation property of gelatin has been exploited to develop a bilayered skin graft, where tissue engineered ECM served as dermal layer and growth factor loaded gelatin hydrogels served as epidermal layer [81]. Gelatin microparticles were utilized as implantable cell carriers for skin regeneration. Porous gelatin particles in the form of microparticle complex loaded with cultured cells and growth factors were developed to repair dermal defects and skin regeneration [81]. Electrospun gelatin nanofibres in the form of dual drug delivery system exhibited accelerated wound healing, earlier neo-vascularization, collagen deposition and re-epithelialization of deep burn wounds [80]. Gelatin based artificial constructs also exhibited improved wound healing and enhanced

granulation tissue formation in the formats of scaffolds and films [110, 111]. In another study, gelatin membrane encapsulated with usnic acid-loaded liposomes demonstrated ameliorated healing of full thickness burn wounds in a porcine model [82]. Furthermore, a combination of gelatin scaffolds with moist wound-healing nursing intervention has demonstrated improved wound healing in phase III bedsore, thereby depicting the beneficial properties of gelatin [113].

1.2.3.3. Chitosan

Chitosan is an amino polysaccharide derived by deacetylation of chitin obtained from insects' exoskeletons [114, 115]. Chitosan is also a preferred biomaterial for skin tissue engineering owing to its potential to be moulded into a variety of formats with varied biological properties by simply changing the degree of acetylation [114, 115]. The easy processing and fabrication methods have led to the development of chitosan-based sponges, hydrogels, films, and nanofibres [83, 114, 116]. Chitosan based matrices have been widely explored for the development of wound dressings, as it is a good haemostatic agent, and it also has bacteriostatic and fungistatic activities; thereby leading to enhanced wound healing rate [117]. Being positively charged and biocompatible, it also facilitates easy incorporation of bioactive molecules and triggers proliferation rate of various cells [118]. A bilayered structure composed of chitosan film on top of collagen sponge was developed as skin substitute with antibacterial activity [119]. In another study, chitosan based hydrogel filled with Dulbecco's modified eagle medium (DMEM)/F12 (medium-Az-CH-LA) showed early angiogenesis and improved healing of full-thickness burn wounds [120]. Blended nanofibrous mats of chitosan/poly(3-hydroxybutyrate-co-3-hydroxyvalerate) (PHBV) also exhibited faster wound healing in another study [121]. However, chitosan suffers from a drawback of rapid degradation in acidic environment, which is often observed during wound healing process [122]. In order to overcome this, various crosslinking treatments were introduced for enhancement of structural stability of chitosan [123]. In addition, development of blended matrices of chitosan with one or more polymers were escalated recently to balance its benefit and shortcomings [114, 119, 121].

1.2.3.4. Hyaluronic acid

Hyaluronic acid is a natural ECM component of skin and thus has been widely utilized for the development of artificial skin grafts [124]. Some of the commercially available grafts are Hyalomatrix, Hyaff (Fidia Advanced Biopolymers), Laserskin® (cultured epidermal graft) and Hyalograft 3D (dermal graft) [1, 124, 125]. It promotes enhanced proliferation of keratinocytes and fibroblasts, and it is effective as both dermal and epidermal substitutes [126]. Improved granulation tissue formation and vascularization was also observed in the wounds treated with hyaluronic acid-coated artificial skin constructs as compared to non-coated artificial constructs [126]. Transdermal delivery of essential proteins and growth factors has been successfully achieved using hyaluronic acid for therapeutic applications to treat skin diseases [127]. It can be applied topically and has also been used in dermal filler injectable system for the treatment of skin disorders [128]. Hyaluronic acid matrices incorporated with various drugs and bioactive molecules have been developed for sustained drug delivery applications. In a recent study, hydrogels containing DNA-polyethylenimine (PEI) polyplexes were developed using hyaluronic acid for sustained delivery [87]. In another study, hyaluronic acid cross-linked with heparin was formulated into a tunable hydrogel system for long-term release of amniotic fluid-derived stem cells-secreted cytokines and growth factors [86]. However, therapeutic potential of hyaluronic acid is limited due to the low availability of material.

1.2.3.5. Fibrin

Fibrin glues and fibronectin are the natural proteins present in the blood clot of acute wounds and serve as cell attracting sites due to the presence of RGD tripeptide sequence [26]. The natural blood clot acts as a provisional matrix made up of fibronectin fibres and recruit cells towards the wound for healing purpose [26]. Hence, artificial constructs containing fibrin material have been developed in various forms such as suspension, gel, sheet or membrane for faster wound closure and faster re-epithelialization [8, 129]. The RGD sequences present in fibrin attract blood platelets and has also been utilized as glue for promoting haemostasis [129]. Large sheets of keratinocytes grown on fibrin sealants have been used as autologous grafts for epidermal skin substitutes [1, 129].

Fibrin based commercially available skin constructs like BioSeed-S, AcuDress, Allox and Cyzact are currently under investigation for skin tissue engineering applications on a larger scale [1]. Combination of fibrin glue and fibronectin has demonstrated enhanced migration of fibroblast and keratinocytes, leading to accelerated wound healing [129]. The endogenous fibrin clots have been proven to sequester VEGF and thereby promote angiogenesis by slowly releasing the growth factors during the initial phase of wound healing [8, 26]. This property of sequestering growth factors by binding them and protecting them from proteases has been exploited to develop fibrin based artificial matrices as a sustainable growth factor delivery vehicle for enhancing the wound healing rate [8, 26, 116]. Autologous cell delivery system using fibrin glue and cell-fibrin complex have been developed to deliver autologous keratinocytes, fibroblasts and mesenchymal stem cells directly at the wound site [116]. In another study, matrices of fibrin glue cultured with allogeneic bone marrow mesenchymal stem cells (BMSCs) were developed, which showed promoted skin repair and regeneration in wounded rat model [102]. Despite its good biological efficacy, the material is highly expensive and requires high volume of blood for its isolation, leading to heavy expenses on the treatments.

1.2.3.6. Silk fibroin

Silk, a natural biopolymer is a well-known suture material and has been used for incisional wound healing since centuries. It is increasingly recognized as a potential material for biomedical and tissue engineering applications since last few decades [22, 23]. Silk holds essential biomaterial properties like haemostasis, biocompatibility, tunable degradability and tunable tensile properties [22, 23, 91]. Silk cocoon contains two kinds of proteins – silk fibroin (SF), which is the fibrous protein component of cocoon and silk sericin (SS), which is the glue-like protein, responsible for sticking the silk fibres with each other [22]. SF and SS have been individually explored for the development of artificial tissue constructs in various formats like scaffolds, nanofibrous mats, films, hydrogels and fibres [22, 23, 130, 131]. Silk based bioengineered constructs have shown better wound healing properties in various formats in comparison with commercially available products under *in vivo* conditions [23]. For example, silk lamellar scaffolds and electrospun mats demonstrated better wound healing than Tegaderm; silk films healed the wounds quicker than Duro Active; SF applied as gel dressing showed improved wound healing as compared to Cutinova hydro dressing [23, 91, 132, 133]. In

a recent study, silk scaffolds containing silk fibres have been fabricated, which mimicked the fibrous dermal layer of natural skin [134]. Nanofibrous SF scaffolds cultured with mesenchymal stem cells (MSCs) and epidermal stem cells (ESCs) also showed earlier re-epithelization, regeneration of the skin appendages and ECM secretion in a recent study [135]. A detailed review of literature on silk based wound dressing and healing applications has been described in the later sections.

1.2.3.7. Synthetic polymers

In search of new biomaterials and functional skin substitutes, a wide variety of synthetic polymers have been developed and explored for wound healing and skin tissue engineering applications. Material properties like mechanical strength, degradability, geometrics and architecture can be easily modulated in case of synthetic matrices [21, 25, 136]. Other benefits of using synthetic polymers for scaffold fabrication are better handling, reproducibility, uniformity, no batch to batch variation, no chance of disease transmission, easy processing and inexpensiveness [21, 25, 136, 137]. Silicone is the most extensively used synthetic material for skin tissue engineering [137, 138]. Other polymers like PVA, PLA, PCL, poly(ethylene glycol) (PEG), polyglycolide (PGA), poly(lactic co-glycolic acid) (PLGA) and polyurethane have been widely explored alone or in blends with natural biomaterials [25, 137, 139].

Polyurethane based matrices like Tegaderm^{TM} (3M Health Care) and OpSite (Smith & Nephew) are commercially available wound dressings [1, 21]. In another study, dressing made up of polyurethane foam containing epidermal growth factor (EGF) demonstrated accelerated wound healing and early re-epithelialization, along with the formation of skin appendages in diabetic animal model [140]. TransCyte® and Biobrane^{TM} are commercially available grafts, which contain nylon mesh and have been used as a temporary covering for treating deeper wounds [1, 141]. Dermagraft® (Advanced Tissue Sciences) has gained much attention for treating full thickness DFU owing to its faster wound healing properties [96, 97]. It is made up of knitted PGA/PLA mesh pre-seeded with human neonatal fibroblasts [96, 97]. The allogenic fibroblasts cultured in the Dermagraft promote faster healing by secreting various ECM components in the wounds [96, 97]. Although researchers have demonstrated appreciable epithelialization of keratinocytes using synthetic polymer based matrices, but currently there is no successful epidermal graft or skin substitutes available using synthetic

polymers due to lack of biological cues and tissue compatibility [142]. Therefore, synthetic polymers are generally utilized in combination with natural polymers for development of skin substitutes such as temporary wound dressings, epidermal grafts, or partial-thickness skin substitutes.

1.2.4. Cells and growth factors utilized for skin regeneration therapeutics

A tremendous change in the field of skin tissue engineering and wound healing emerged with the development of cellular and bioactive constructs (also known as smart scaffolds), which overcome the drawbacks of acellular grafts conventionally used before. Cells and growth factors, being the essential components of skin have major roles in wound repair [7, 8]. Presence of senescent cells and proteases in the wound microenvironment of chronic wounds delay the healing process and can be easily treated by re-establishing the cellular and growth factor pool using the cultured skin grafts [7, 8, 12]. For instance, cultured skin substitute using collagen-GAG scaffolds showed comparable results with split thickness autografts for treating full thickness burns demonstrating significance of cellular artificial constructs [143]. Scaffolds delivering growth factors and cells have been found to be highly effective in stimulating the wound healing pathway as compared to acellular constructs [91, 144]. Hence, advanced strategies have been developed by combining cells and growth factors to biomaterials for activating interactions between them to quickly restore the damaged tissue. The following sub-sections describe the significance of various cells and growth factors that have been utilized for wound healing applications.

1.2.4.1. Cells

Application of pre-cultured cellular grafts has become a common therapeutic strategy to quickly repair, restore and regenerate the skin [145, 146]. Among 20 different cell types present in the skin, only fibroblast and keratinocytes have been cultured in the commercially available artificial skin grafts at present [34, 143, 147]. However, culture of other cells like endothelial cells, melanocytes, hair follicular stem cells, adipose derived stem cell and BMSCs have also been recently started in advanced pre-clinical practices for skin regeneration applications [54, 148-150]. Currently, the commercial skin grafts developed using various strategies are available with pre-cultured autologous or allogeneic keratinocytes and fibroblasts. Keratinocytes were the first among all cell

types, which were cultured *in vitro* to form epidermal sheets and have been commercially available as graftable epidermis since decades [1, 143].

The epidermal-sheet forming ability of keratinocytes evolved numerous strategies to develop large sheets of epidermis from a very small biopsy punch (1 - 3 cm^2) and thus minimized the donor-site morbidity by quickly re-epithelializing the wounds [151, 152]. This unique feature of keratinocytes to form a stratified epithelium layer *in vitro* has been exploited by many commercially available epidermal grafts like cultured epidermal autografts, Epicel, Epidex, Laserskin, Bioseed-S, Cryoskin, Myskin [1, 152]. Delivery of proliferating autologous keratinocytes to the wound bed by spraying the cells has also been in practice (cell spray) to improve the healing of chronic cutaneous ulcers and partial thickness wounds [153]. Thus, epidermal constructs using various natural and synthetic polymers have been developed, which effectively deliver pre-confluent keratinocytes or cultured epithelial cell sheets to quickly heal the epithelial and partial thickness wounds [143, 145]. Next, fibroblasts are considered as the wound healers due to their role in secreting ECM fibres to form granulation tissue and their high proliferation capacity [154, 155]. Fibroblasts are the most important mesenchymal cell type, which are also responsible for secreting a variety of growth factors and matrix modulation [156]. Dermal and bilayered constructs pre-seeded with fibroblasts are commercially available such as Dermagraft, TransCyte, OrCel, Apligraf and Theraskin [1, 143]. Commercially available cell seeded grafts are listed below (**Table 1.2.**).

Table 1.2. *List of some representative commercially available skin grafts using keratinocytes and fibroblasts [1, 34, 157].*

Cell type	Commercial forms	Properties	Applications
Autologous keratinocytes	EpiDex	Confluent cell sheet on a silicone membrane using keratinocytes	Cutaneous ulcers like DFU, venous and pressure sores
	Epicel	Cultured epidermal sheets of keratinocytes delivered using petroleum gauze	Cutaneous chronic ulcers
	Laserskin or vivoderm	Scaffold of hyaluronic acid membrane with confluent cell sheet of keratinocytes	Chronic wounds
	MySkin	Epidermal keratinocytes cultured on silicone layer	Chronic wounds; split-thickness burns and donor graft sites
	Cell spray	Sub-confluent suspension of keratinocytes delivery by spraying	Partial thickness burns
Autologous fibroblast	Bioseed-S	Allogenic fibrin sealant scaffold cultured with keratinocytes isolated from oral mucosa	burns, venous ulcers and replacement of oral mucosa
	Hyalograft 3D	Hyaluronic acid membrane scaffold cultured with autologous fibroblast	Feet ulcers and deep burns
Autologous fibroblast and keratinocytes	TissueTech (Hyalograft 3D + Laserskin)	Cultured fibroblast and keratinocytes on hyaluronic acid membrane	Chronic wounds
	PolyActive	PEO/PBT synthetic scaffold cultured with autologous fibroblast and keratinocytes	Split thickness wounds

Allogenic keratinocytes	Cryoskin	Monolayer of keratinocytes cultured on silicon matrix kept in frozen condition	Burns, donor graft sites and venous ulcers
Allogenic fibroblasts	Dermagraft	Polyglactin mesh cultured with allogenic neonatal fibroblast	DFU, burns and dystrophic epidermolysis bullosa full thickness wounds
	ICX-SKN	Collagen matrix with neonatal foreskin fibroblast	Partial thickness wounds
	TransCyte	Silicon film, nylon mesh, porcine dermal collagen cultured with allogenic neonatal fibroblast	Partial/full thickness burns, donor graft sites or over meshed autografts
Allogenic keratinocytes and fibroblast	OrCel	Lyophilized bovine collagen type I sponge cultured with neonatal foreskin fibroblast and keratinocytes	DFU, burns, venous ulcers and recessive dystrophic epidermolysis bullosa and skin graft donor sites
	Apligraf	Bovine collagen sponge cultured with allogenic neonatal fibroblast and keratinocytes	DFU and venous leg ulcers

Furthermore, stem cells found in the bulge region of hair follicles (hair follicle stem cells) was a ground-breaking discovery in the recent times [158]. These stem cells have the potential of forming skin equivalents and *de novo* generation of hair follicles, which made hair regeneration possible in the artificial skin [158, 159]. Bioengineered skin using other types of stem cells like BMSCs, adipose derived mesenchymal stem cells (ADMSCs) and induced pluripotent stem cells (iPSCs) have also shown the potential of making skin equivalent [160-162]. Patients having severe burns, chronic and infected wounds treated with collagen sponge impregnated with autologous MSCs showed accelerated healing along with dermal repair and less scarring [163]. Hence,

cellular constructs cultured with stem cells have the potential of differentiating to almost all the cell types and form a biomimetic skin; however, the clinical application of stem cells is still not encouraged due to loopholes in the certain properties of stem cells, which might lead to cancer growth [164]. Research has been going on to populate the scaffolds with various cell types and mature the tissue in co-culture conditions. For example, co-culture of fibroblasts and endothelial cells has been well-established to fabricate a pre-vascularized artificial skin [54]. This may circumvent the major drawback behind the delayed graft take due to absence of blood vessels in the skin grafts. Prevascularized skin grafts have higher "graft take" rate as the capillaries present in the wound bed anastomose easily with the pre-existing capillaries. Easy exchange of nutrients and oxygen is another factor describing need of prevascularized grafts [54]. However, these strategies have still not come out of the research laboratories and needs clinical trials before reaching to the patients.

1.2.4.2. Growth factors

Growth factors are biologically active proteins secreted by many kinds of cells and perform functions *via* signalling pathways after binding with specific receptors [7]. Numerous growth factors are involved in wound healing pathways and play major roles in the proliferation and migration of various cells [7, 165]. Upon skin wounding, various types of cells secrete growth factors, which create a growth factor pool in the wound microenvironment to trigger cells for initiating the wound healing process. Therefore, biomimetic approach for skin tissue engineering and wound dressings has led to the development of artificial constructs delivering essential growth factors in their active state [165]. Various natural and synthetic polymers have been used to conjugate growth factors, capable of releasing them at a sustainable rate for the development of effective matrices [166].

Different approaches of providing similar active and stable growth factor pool in the bioengineered construct have been taken, which mainly include immobilization or adsorption of growth factors within the scaffolds [166]. Among all growth factors, EGF plays major roles in wound healing pathways by stimulating cell migration and cell proliferation; it also induces fibroblasts to express ECM components and has remodelling effect on collagen type I fibres [140, 167]. For instance, increment in the ECM tensile strength (200 %) was found in murine cutaneous wounds treated with liposome-

encapsulated EGF [167]. Heberprot-P, a product containing EGF, originally registered in the Republic of Cuba and later on by 15 more countries has been serving more than 100,000 patients with chronic wounds [168]. Betacellulin, a member of EGF family has also been found to regulate epidermal homeostasis, wound angiogenesis, hair follicle morphogenesis and hair cycle induction [169]. Basic fibroblast growth factor (bFGF) is also actively involved in wound healing and demonstrated comparable results like EGF [170]. FGF have major roles in wound healing and showed neovascularization, epithelial morphogenesis, granulation tissue formation and increased dermo-epidermal proliferation in wounds [109, 170]. Fiblast Spray (Kaken Pharmaceutical Co. Ltd., Tokyo, Japan), which contains genetically recombinant bFGF showed accelerated wound healing rate in second degree burn wounds and approved for clinical use in Japan [7].

Apart from EGF and bFGF, there are several reports on application of other types of growth factors as well. For example, vascular endothelial growth factor (VEGF) carry out neovascularization by stimulating migration and proliferation of endothelial cells and is secreted by platelets, fibroblasts, keratinocytes and macrophages during the wound healing process [7, 171, 172]. Platelet derived growth factor (PDGF) is the only growth factor, which got approval by Food and drug administration (FDA) in its recombinant form to be used for treating diabetic ulcers [8]. Regranex, a gel dressing containing recombinant PDGF has been used to treat diabetic foot ulcers by topical application [173]. Transforming growth factor- β1 (TGF- β1) acts in an autocrine manner with fibroblasts and is responsible for the production of ECM components along with wound contraction promotion by differentiating the fibroblasts to myofibroblast [174]. Keratinocyte growth factor (KGF) plays a major role in repairing the growing epidermis and promotes re-epithelialization [175]. Hepatocyte growth factor (HGF) is mainly secreted by fibroblasts during wound healing and has mitogenic effect on keratinocytes and VEGF secretion [176]. Insulin like growth factor (IGF) also has mitogenic effect on keratinocytes, induces angiogenesis and is highly secreted by fibroblasts in the wound bed to accelerate wound healing [177]. Placenta growth factor (PlGF), also known to be related to VEGF, has role in neovascularization during wound healing [178]. Angiopoietin-related growth factor (AGF), which belongs to angiopoietin-like protein family binds to α_v integrins through RGD peptide, and stimulate keratinocytes proliferation and angiogenesis [179]. Nerve growth factor (NGF) and granulocyte-

macrophage colony stimulating factor (GM-CSF) are secreted by keratinocytes in skin and stimulate proliferation of keratinocytes in an autocrine manner to aid in rapid re-epithelialization [180, 181]. There are many advantages of growth factors as listed below (**Table 1.3.**) and thus, wound healing can be accelerated by providing adequate growth factors through bioengineered matrices.

Table 1.3. *List of growth factors involved in the wound healing process.*

Growth factor	Functions	Formulations	Applications	References
EGF	Keratinocytes migration and proliferation, fibroblast proliferation (granulation tissue formation during wound healing), endothelial cell migration and cytokine production	Liposomes, microspheres, nanospheres, nanoparticles, sponge, film, hydrogel, nanofibres	Chronic wounds, partial thickness wounds	[7, 166, 167, 182, 183]
FGF	Recruitment of fibroblasts, keratinocytes and endothelial cells; granulation tissue formation and matrix remodelling	Nanofibres, fibrin hydrogel, chitosan hydrogel/film, collagen matrix, gelatin sponge	DFU, pressure ulcers	[109, 118, 166, 170]
PDGF	Chemoattractant for immune cells and fibroblasts; stimulation macrophages	Hydrogel	DFU, pressure ulcers	[9, 184, 185]
VEGF	Endothelial cell migration and proliferation; vascularisation and lymph angiogenesis	Alginate microspheres	DFU	[172]
IGF	Fibroblast proliferation; keratinocytes migration and proliferation	Liposomes	DFU	[177, 186]
TGF-β1	Fibroblast migration and proliferation; granulation tissue formation and increased collagen synthesis.	Collagen sponge	DFU	[187]

1.2.5. Smart technologies and cellular based emerging approaches for skin therapeutics

1.2.5.1. Portable electrospinning technology

Electrospinning has attracted substantial interest in the technological and healthcare sectors in recent years. This technique has enabled easy fabrication of nanofibrous mats in large scale [43]. The latest technology further developed improvised electrospinning instrument by miniaturizing its size and led to the development of handheld electrospinning device [188]. A portable instrument with broad range polymer specificity is easy to use and reduce wound edema or pain. In a study, a portable handheld electrohydrodynamic multi-needle spray gun was developed for practical day-to-day applications using the frame of Dremel glue gun [189]. The glue gun was modified into a multi-needle electrospray gun. Different variations of similar handheld electrospinning apparatus were also developed, which were battery operated by further minimizing the size [46, 190]. The new device weighed only 120 g and could electrospun various polymers such as poly(vinyl pyrrolidone) (PVP), PCL, polystyrene, PLA and poly(vinylidene fluoride) (PVDF). *In situ* deposition of a nanofibrous dressing directly on the cutaneous wounds demonstrate advanced healthcare system. The approach can also be utilized to fabricate patient-specific dressings by incorporating particular drugs or molecules in the electrospinning solution [46, 190]. Such an equipment if used in first aid or in emergency cases can generate wound patches at the injury site to stop wound bleeding and provide instant dressing. Portable electrospinning equipment could be a temporary solution in case of emergencies; however, in case of large size wound defects, the acellular nanofibrous patch face drawback in long-term treatment. Similar to portable electrospinning, the handheld cell spray and bioprinting techniques developed recently could be an effective solution to deliver living autologous cells over the wounds.

1.2.5.2. Spray based approach

Of critical importance for large-sized cutaneous wounds, cell spray system has also emerged in recent years. Cell spray system has been developed long back using Badger 100G airbrush and demonstrated successful delivery of bovine dermal fibroblast with more than 50 % cell viability [191]. Viability of cells post-spray is an important concern since direct spraying may induce cellular damage. The problem was resolved by the

aerosol delivery method with encouraging outcomes. In a recent study, researchers have optimized calculations for non-cultured autologous skin cell-spray grafting [192]. The calculation was performed by considering variables like yield of donor site skin tissue, cell density, distribution area, spray volume and the percentage of surface coverage. The mathematical approach demonstrated possible ratios of 1:80 to 1:100 (donor site area: treatment area); thereby revealing significant improvement over the conventional mesh grafting technique [192]. In a comparative study against fibrin membrane transfer system, aerosol cell spray was found to be effective with pre-confluent keratinocytes [193]. Cell suspension experienced various types of stress conditions like hydrostatic, shear or elongation stress when sprayed directly onto a wound [193].

Although aerosol-based cell spray technique has shown huge potential in re-epithelialization of superficial wounds, the technique is further improved using biopolymers for severe cutaneous injuries. Recent work on the delivery of human keratinocytes using microcarriers and compressed collagen demonstrates the excellent utilization of spray technique [194]. Support of biomaterial based microcarriers could further improve cell viability, a major concern in direct cell spraying due to lack of cell-adhesion in the suspension conditions. Gelatin microcarriers provided cell adhesion sites and thereby increased the overall distribution of cells in the keratinocyte cell therapy while maintaining the clinically-relevant time-frame [194]. Such examples of customized cell spray equipment paves way for next generation smart system for efficient delivery of autologous skin cells for wound healing applications.

1.2.5.3. Portable 3D skin printer

Technical advancement in recent years has led to the development of handheld skin printer to be applied for *in situ* formation of skin tissues at the wound site. The remarkable work by Hakimi *et al* represented development of a portable 3D bioprinter (weight < 0.8 kg) that enabled bioprinting of skin tissue sheets using a microfluidic cartridge [41]. The study illustrated *in situ* formation of skin sheets in the porcine and murine wound models as a direct treatment using skin specific cells in the bioink. Such portable 3D printers can be revolutionary in the current healthcare market as patients do not have to wait for the laboratory grown cellular skin grafts. This technology can also be used for emergency cases like burn trauma cases and can be carried in ambulances for immediate treatment in real time.

1.2.5.4. Immunomodulation and vascularization based approach

Principal goals in wound management include vascularization in the regenerated tissue to achieve rapid wound healing and skin regeneration. Many pioneering approaches have utilized cellular and molecular biology for the development of pre-vascularized skin grafts over the past decade [54, 195]. During the course of development of advanced cellular therapies, a greater comprehension of basic biology has been considered by the researchers in recent years. Targeting immune system for enhanced angiogenesis has recently been explored leading to significant advances in wound healing therapy [196, 197]. This approach stands apart from the orthodox approach of using only endothelial cells in making vascularized grafts. Clearly, immune system has a major role in the healing process because inflammation is the very initial phase of wound healing [197]. The early immune response delivers signals to the subsequent phases through cytokines and chemokines. The crosstalk between immune cells and endothelial cells plays a major role in the rate of healing process, showing their interdependence during the tissue repair. Macrophages deliver a continuing supply of cytokines essential for cell growth and angiogenesis; and newly formed blood vessels carry oxygen and nutrients necessary for cell metabolism [198]. The chemokines secreted by macrophages have also been shown to induce migration of endothelial under *in vitro* conditions [199]. This interplay between immune system and vascularization has recently been exploited in various strategies to increase the wound healing rate and develop pre-vascularized skin grafts. These strides have ultimately led to advancements in skin regeneration. Therefore, tailoring the immune response or modulating the behaviour of immune cells may impart major breakthroughs in wound repair and skin tissue engineering.

Formation of blood vessels in the wounded tissue during healing process is a common phenomenon and is known as angiogenesis [200]. In this process, new vessels sprout from existing vessels to establish the supply of oxygen and nutrients to the newly formed tissue at the injured site. Vascularization is a complex process requiring interaction between various cells, the ECM and numerous growth factors [200]. However, in certain pathophysiological conditions like diabetic wounds or large burn wounds, this natural angiogenesis process is severely obstructed. Artificially developed implants on such wounds often fail to develop vascularized network and clinical outcomes remain poor. To cope with this problem, fabrication of pre-vascularized skin

grafts has been a recent area of research where the bioengineered tissue is already well developed with a vascular network. Several strategies have been explored with the aim of developing pre-vascularized constructs using cellular therapy, growth factor delivery, and use of bioactive materials.

Co-culture system has been the most explored and highly efficient strategy for developing pre-vascularized grafts so far. Endothelial cells, which make wall of the blood capillaries, have cellular crosstalk with fibroblast cells. Co-culture of both the cells has been very successful in bioengineering the vascularized dermo-epidermal skin grafts [54]. Human dermal microvascular endothelial cells (HDMECs) when co-cultured with human dermal fibroblasts (HDF) in 3D hydrogels developed vasculature networks within 3 weeks [54]. It was also shown that HDMECs when cultured alone in the hydrogels failed to develop capillary like structures proving the significance of co-culture system. Marino *et al* went one step ahead by developing skin grafts with lymph vessels along with blood vessel network. The tissue engineered skin grafts containing blood and lymph vessels when transplanted on wounds of nude rats demonstrated connections with existing vessels and formed functional skin layers. The bioengineered grafts also drained the wound fluid away through pre-formed vessels thereby helping in accelerated wound healing [54].

In another study, researchers used growth factor therapy by encapsulating a cocktail of growth factors along with endothelial colony forming cells to develop vascularized grafts [201]. The growth factor cocktail consisted of recombinant human VEGF165, bFGF, angiopoietin-1, tumour necrosis factor alpha (TNF-α) in the constructs demonstrated accelerated diabetic wound healing [201]. Another recent emerging approach in the fabrication of vascularized grafts is culturing stromal vascular fraction (SVF), which is a cocktail of cells that can be obtained from adipose tissue through enzymatic digestion or mechanical dissociation [202, 203]. The popularity of SVF in wound healing is gaining momentum as it seems to contain all components that not only take care of the underpinned properties of accelerated scar-less wound healing, but can also be valuable in terms of providing vascularization. This can in turn enormously contribute towards better graft acceptance for full thickness skin grafts and wound patch. Fabrication of SVF based pre-vascularized grafts and their integration with host skin demonstrate the benefits of SVF application in healing critical wounds [204]. Overall, it

is seldom in nature that most desired components for therapy are found in a well-balanced cluster. SVF seems to be such a component, which if harnessed properly can be an ingenious approach towards regeneration therapy.

1.2.6. An update on clinical trials

The clinical implementation of technology is necessary to validate proof of concept and pre-clinical studies performed in animal models. Clinical study not only reveals the treatment outcomes, but also unfolds the basic information like cost of treatment, patient safety and risks involved during the particular treatment. Efficacy of wound dressings and skin grafts have been constantly under evaluation through the regulated clinical trials on patients in multiple clinical set-ups over a period of 5-10 years [3]. The aim of clinical study is to transfer the technology from bench to bedside for harnessing the emerging wound management strategies and realistic advancements over the conventional methods. Clinicians and scientists are nowadays applying mathematical calculations, statistical methods and resource expenditure assessment to demonstrate the results in a more realistic and accurate manner. Herein, we try to summarize the outcomes of some recent trial reports on the bioengineered skin grafts.

Clinical practices have evolved in the past few years by taking trial deigns, patient population, accurate wound measurements and specialized tools into consideration. Integra, the well-explored acellular bioengineered skin graft has been constantly under frequent clinical trials since last 3 decades. In a recent clinical trial on severely wounded military soldiers, Integra was found to be highly successful in the management of complex and devastating wounds with a success rate of 78 to 86 % [205]. Integra is also commonly used as a positive control in clinical trials of novel constructs like CellonexTM (a viscose cellulose sponge), which revealed comparable healing efficacy of the cellulose based construct in a recent study [206]. In a comparative study with Integra, Hyalomatrix demonstrated better cell regulation, ECM production and stimulation activity; whereas, Integra showed dermal regeneration with more elastic, physical and mechanical properties [207].

Another well-studied commercially available dermal substitute is Dermagraft, which is made up of polyglactin mesh seeded with HDF [208]. It serves as a cryopreserved cellular dermal substitute for chronic wounds and has been found to be

very effective in treating DFU and venous leg ulcers [3, 208]. Successful clinical trials on various well-established artificially developed living cellular grafts like Apligraf, CEA and Orcel reveal their safety and efficacy [3, 49]. Grafts made up of decellularized tissues include Epifix (dehydrated human amnion/chorion membrane), Grafix (placental allograft) and Neox [209, 210]. Their clinical trial on extreme diabetic foot ulcers not only revealed their safety, but also their cost effectivity and efficient treatment. Recent report on the clinical trial of a fibrin patch containing concentrated leukocytes and blood platelets revealed excellent outcomes in treating DFU and also its feasibility in clinical practice [211]. Application of cadaveric dermal allografts on trauma wounds has been a common practice since centuries. Although allogenic in nature, skin allografts are still considered as a good option for treating a variety of wounds ranging from chronic wounds to burn and trauma injuries. In a recent comparative study, Theraskin (cryopreserved human skin allograft) proved to be cost effective (42.2 % decrease in cost) in comparison to the bioengineered skin Apligraf with no significant differences in the healing outcomes [212].

Although many novel types of constructs and dressing materials have been developed in the past 2-3 decades, only a handful of products have undergone clinical trials. Prospective and retrospective analysis of clinical trials of the commercially available acellular and cellular skin grafts provide a clear picture of their utility. Such studies have side by side improved our understanding of the pathophysiology of hard to heal wounds like chronic wounds and burn injuries. The clinical trials done so far thus represent encouraging results in the field of wound healing and could motivate the experts to conduct such studies on emerging techniques and novel bioengineered grafts.

1.2.7. Exploring silk as a potential biomaterial for wound healing applications

Silk is a protein biopolymer that is produced by a variety of insects such as silkworms, flies, spiders, mites and scorpions [22]. Silk produced from silkworms and spiders has been widely studied and explored for various biomedical applications [22, 23]. Silk is a broad term and often referred as protein fibres spun by insects; however, it varies from species to species and function to function [24]. Silkworms develop silk cocoons by spinning silk fibres, which provide them shelter during their period of metamorphism [24]. Spiders produce silk fibres to develop webs, capture preys and for their movements [213]. All the varieties of silk fibres differ from species to species due to significant

changes in their amino acid sequence [24, 213]. For instance, different silkworm varieties, broadly categorized as mulberry and non-mulberry silkworms produce silk fibres with different composition having variation in their amino acid sequences [214].

Silks also vary in their structure and physical properties owing to the variation in composition [24, 214]. Being a versatile biopolymer, silk has been hugely explored in the applications of tissue engineering and regenerative medicine [22, 24, 213]. SF extracted from domesticated silkworm, *B. mori*, has been the most extensively studied variety of silk since few decades [22, 23]. It has been completely characterized in terms of physical properties, chemical composition and biological properties [215]. Herein, we focus on the fibrous types of silk biomaterials such as silkworm SF protein and spider silk fibres to understand their structural and biological properties, which make them one of the sought-after materials in the field of biomedical engineering. Various types of sources of silk biomaterials and structures generated out of the material are represented as below (**Figure 1.4.**). The following sub-sections provide a detailed literature on the various types of silk biomaterials, their properties and applications in wound repair and regeneration.

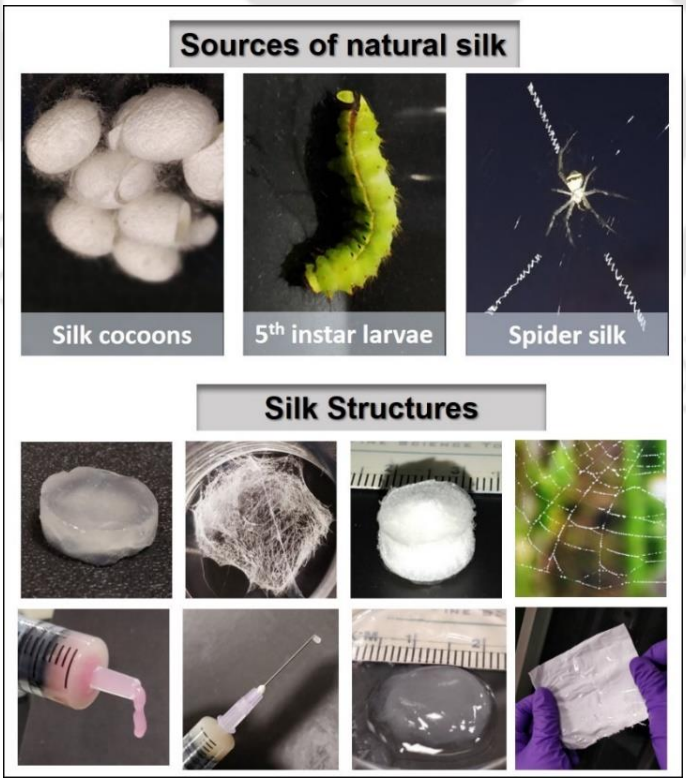

Figure 1.4. *Schematic image showing various natural sources of silk protein and structures made up of various silk biomaterials.*

1.2.7.1. Silk types, chemistry, structure and properties

There are many varieties of silkworms and based on their feeding habits, they are broadly classified into two: mulberry and non-mulberry silkworms [24]. The host plants that give shelter and food to the silkworms are considered as key players behind their classification [24]. Silkworms that feed on the mulberry leaves are mulberry silkworms, for example *Bombyx mori*. Other varieties that do not feed on mulberry leaves are categorized under non-mulberry silkworms. There are numerous non-mulberry silkworm varieties world-wide; for example, *A. assama* (Indian Muga silk), *A. mylitta* (Indian Tasar silk), *A. pernyi* (Chinese Oak Tussah silk), *A. yamamai* (Japanese silk) and *P. ricini* (Indian Eri silk) [24]. The major differences in the protein sequence are responsible for variations in the physical, chemical and biological properties of different silk proteins. Silk, known for its regenerative properties has been found to aid many events throughout the wound healing process (**Table 1.4.**). Besides the silkworm SF, spider silk is also discussed in the following sections to provide a clear picture on the available fibrous silk proteins and their application in skin tissue engineering.

1.2.7.1.1 Mulberry silk

B. mori silk fibroin (BmSF), also known as mulberry silk, include two polypeptide chains: a heavy chain of 391.367 kDa and a light chain of 25 kDa. BmSF also contains a glycoprotein known as P25 [216]. Assembly of H-chains, L-chains and P25 is in the ratio of 6 : 6 : 1, which is also considered as a signature of BmSF protein [216]. The SF protein remains in α-helix and random coil conformation in the silk glands of silkworms, which transforms to mechanically strong silk fibres or threads during spinning [216]. Stability of silk fibres at the time of construction of silk cocoons is due to transition of the SF protein from random coils to β-sheet conformation [217]. These β-sheet structures are majorly formed due to the presence of repetitive stretches of $(GAGAGS)_n$ in the protein sequence [218]. The fibroin heavy chain of silk is the structural protein complex that consists of long crystallizable hydrophobic domains along with amorphous hydrophilic domains. The packed β-sheet structures of the crystallizable domains in SF play significant roles in manipulating the properties of the protein [218]. The hydrophobic repetitive domains of glycine-alanine repeats contribute to more than 50 % of total fibroin and thus confer crystallinity to the overall protein structure [22, 218]. The

crystalline structures of silk are majorly responsible for their high mechanical strength and structural properties that make this natural material unique [22, 27, 218].

Isolation of SF from cocoons involves sequential procedure of degumming and dissolving the silk fibres in organic solvents or ionic liquids to obtain the liquid state of SF protein [215]. Degumming is performed to remove the sericin component by boiling the silk cocoons in aqueous solution of 0.02 M sodium carbonate (Na_2CO_3). Dissolution of degummed silk fibres has been well established in the chaotropic lithium bromide (LiBr) solution. The SF fibres get easily dissolved in 9.3 M LiBr at 60 °C, which upon subsequent dialysis against water yields aqueous silk solution [215]. The obtained aqueous silk solution can be easily modulated in various types of designs by tuning the β-sheet formation induced by numerous well-established physical and chemical methods. For instance, changes in solution conditions like fibroin concentration, pH, temperature, solution aging, ionic strength or blending with other polymers lead to permanent crosslinking within the protein chains and cause an overall increase in β-sheet content in the SF, which lead to fabrication of stable structures [219-221]. Physical methods of β-sheet induction include mechanical shear (vortexing), sonication and electric field, which result in enhanced physical permanent crosslinking [222-224]. Being a bulk material, it has been well-explored in constructing scaffolds of various size and shapes, thereby making it a versatile biomaterial for tissue engineering applications.

1.2.7.1.2. Non-mulberry silk

Non-mulberry silk fibroin (NMSF) consists of a heavy chain and lacks both the L-chain and P25 glycoprotein unlike BmSF [24, 214]. This marks the prime difference in the composition of BmSF and NMSF proteins. Further, differences in the protein sequence of fibroin heavy chains signify their important characteristics. Unlike BmSF, which consists of GAGAGS repeats, NMSF consists of repeats of polyalanine (AA)n and polyglycine (GG)n blocks [24]. For example, *A. assama* silk fibroin (AaSF) protein consists of two main motifs, namely, polyalanine motifs (Alanine content 44.5 %) and polyglycine motifs (Glycine content 30.1 %) [214]. The polyalanine blocks contribute to the main crystalline core of AaSF; whereas, in BmSF, glycine rich blocks are responsible for crystallinity of protein. Another major difference in between BmSF and AaSF is the amount of arginine content (R-motif). Consisting of 17 R-motifs, AaSF is rich in Arg

content among all reported H-fibroins [214]. A/G/R-motifs present in AaSF together represent hydrophobic and hydrophilic regions of the protein that has been responsible for a wide variety of applications.

Presence of RGD tripeptide in AaSF, a well explored cell binding motif has provided additional advantage to the silk in tissue engineering applications [214]. Similarly, other non-mulberry silk varieties also differ from BmSF and possess extraordinary properties owing to the variations in the protein sequence. Silkworms of *Antheraea* genus (such as *A. assama, A. mylitta, A. pernyi*) share similarities in silk fibroin protein like presence of dominating polyalanine blocks, RGD tripeptide and high arginine content [24]. *P. ricini* NMSF also contains polyalanine blocks as the repeating unit and is speculated to contain RGD motif in the peptide sequence [24]. *A. assama* NMSF is highly explored in the field of biomedical engineering owing to its known protein sequence. Like BmSF, induction of β-sheets in the NMSF based constructs is also performed by treating them with ethanol or vapours of water and ethanol [225, 226]. Variation in the protein sequence of NMSF is another major reason for discrepancies in the protein dissolution methods in comparison to BmSF. The dissolution method of BmSF from silk cocoons has been well established using 9.3 M LiBr as the degummed *B. mori* silk fibres readily dissolve in the aqueous solution of LiBr [215]. However, the same method is not feasible for silk fibres of non-mulberry silkworm cocoons. It is speculated that due to the presence of hydrophobic core of A-motifs and excessive hydrogen bonding among the alternated hydrophilic sequences, the NMSF fibres do not dissolve in chaotropic reagent like LiBr. The ionic solvent systems like LiBr disrupt the intermolecular hydrogen bonding of fibroin chains, thereby dispersing the fibroin polypeptides for proper dissolution. This readily works for *B. mori* silk fibres; however, this solvent fails to completely dissolve non-mulberry silk fibres and result in significantly lower yield. Therefore, researchers have sorted to an alternative method as invented by Mandal and Kundu, 2008 [227].

SF isolated from silk glands of mature silkworms is easy to solubilize in surfactant like sodium dodecyl sulphate (SDS). Silkworms extrude the raw form of SF from their silk glands while spinning cocoons. The protein changes its conformation from α-helix to β-sheets during the spinning process. Therefore, the silk fibres present in silk cocoons contain high amount of stable β-sheets, which make the fibres difficult to dissolve. By dissolving the raw form of SF isolated directly from the glands, is an easy

and versatile method [227]. This method works for a wide variety of NMSF like *A. mylitta*, *A. assama* and *P. ricini* [226]. Non-mulberry silks have outperformed mulberry silk fibres (BmSF) in terms of mechanical properties [226]. The crystallinity of A-motifs present in NMSF is much higher and requires higher energy to break than that of (GAGA)n repeats of BmSF [214, 228]. For example, the β-nanocrystal formed by short polyalanines repeats present in the spider silk fibres of *Nephila clavipes* confer high mechanical strength along with high elasticity to the fibres [228]. Similarly, *A. assama* silk possessing polyalanine repeats holds outstanding tensile strength because of stronger polyalanine crystals [214]. *A. assama* silk showed 40 % elongation at break, which was found to be comparable with *N. clavipes* spider silk fibres (40 %); however, *B. mori* silk showed only 15 % elongation at break, thereby revealing lower mechanical strength in comparison to non-mulberry silk [214]. The polyalanine blocks offer a unique property of stretching ability to non-mulberry silk that lacks in the mulberry silk. Conclusively, the unique polypeptides of NMSF and their (intra/inter)molecular structural organizations are cumulatively responsible for various extraordinary properties.

1.2.7.1.3. Spider silk

Varieties of spider silk proteins are produced by a single insect depending on its particular movements and functions like dragline, orb web or cocoon construction [229]. The chemistry and structure of different silk proteins slightly vary depending on its function. The unique physical properties of spider silk have led to an increased interest in harbouring the protein for various biomedical applications [229]. Dragline silk is the most studied and highly explored spider silk variety owing to the unique tensile and light-weight properties [229]. Spiders store the soluble form of dragline silk in the sac of their major ampullate glands and spontaneously form silk fibres through the duct during their spontaneous movements [230]. The spider silk is composed of assembly of spidroins, which contains crystalline repetitive regions along with non-repetitive N-terminal and C-terminal domains [230]. Spider silk protein is rich in glycine and alanine blocks in its repetitive region similar to silkworm silk fibroin protein; however, the overall protein sequence is quite different from silkworm silk fibroin [230].

Another feature of spider silk is its high elasticity due to the presence of short repeats of semi-amorphous regions like GPGXX (β-spirals or β-turns) and GGX (helix) in the non-crystalline regions [229]. The β-sheet crystalline regions serve as connecting

links to the amorphous chains and form a network structure, thereby maintaining the tensile and elastic properties of spider silk. Dragline silk of *N. clavipes* is the most studied spider silk variety and it consists of two spidroins, namely, major ampullate spidroin I (MaSpI) and major ampullate spidroin II (MaSpII) [229]. The dragline silks share structural similarities with other dragline silks, consisting of non-repetitive N/C terminals and a repetitive central domain of glycine rich or polyalanine blocks that makes its core region [231]. However, they differ in the number of hydrophobic domains and presence of proline residues in their protein sequence, which lead to variations in their physical properties. Similar to *N. clavipes*, another variety of dragline silk is produced by spider *Araneus diadematus* [231]. This spider produces ADF-3 and ADF-4, which are analogous MaSpI and MaSpII proteins in the context of structural and functional properties [231].

Harvesting large numbers of spiders is difficult in comparison to silkworms. In addition, the yield obtained from spiders ranges from 12 – 137 m, which is far lesser than that of a single silkworm (600 – 900 m) [229, 232]. Therefore, researchers have resorted to exploit the recombinant DNA technology for production of recombinant spider silk [233]. Technological advancements in genetic engineering have enabled the integration of spider silk encoding genes and successful expression of spider silks through a range of host systems. Numerous varieties of recombinant spider silks have been generated over the years that mimic the native structural and functional properties of dragline silk produced from spiders like *N. clavipes, A. diadematus* and *Euprosthenops australis* [213, 233]. For example, MaSpI and MaSpII of *N. clavipes*, ADF-3 and ADF-4 dragline silks of *A. diadematus* and 4RepCT (4RC) partial dragline silk of *E. australis* [213, 229, 231]. Till date, recombinant spider silk production from micro-organisms like *E. coli* bacteria is the most exploited host organism owing to the simple bacterial system, easy purification process and relatively high yield [213]. However, recombinant spider silks have been produced from a wide variety of host systems like potato, tobacco, mammary glands of mice and goats [213].

Mammalian cell systems have also been efficient in the expression of recombinant spidroins [234]. The method of producing recombinant spider silk holds another advantage of synthesizing silk containing additional bioactive domain in the protein sequence and thereby obtaining desired functionalized spider silk biomaterials [213, 233]. Successful production of recombinant spider silk conjugated with human

bioactive peptides like cell binding RGD peptide, growth factor peptides and antimicrobial domains are perfect examples of this technology [235-237]. This smart strategy of making functionalized spider silk demonstrated possible modulation of silk protein at post-production level. Therefore, recombinant spider silk holds great potential in tissue engineering applications.

Table 1.4. *List of silk materials used for cutaneous wound healing applications.*

Material format	Wound model	Response	References
Silk film	Full-thickness in nude mice	Improved healing response than Duoactive dressing and comparable results with AlloaskD.	[132]
Silk film	Full-thickness in rabbit and porcine	Faster healing and better skin regeneration in comparison to commercially available Suprathel and Sidaiyi dressings.	[238]
Porous silk scaffold	Full-thickness wound in rat	Better healing outcomes and dermal regeneration in comparison to PVA scaffold.	[239]
Aligned Nanofibrous hydrogel matrix	Full-thickness wound in rat	Vascularization, tissue ingrowth, improved cell migration with rapid wound closure in comparison to non-aligned nanofibrous scaffolds.	[240]
Silkworm cocoon sol-gel film	Full-thickness in rabbit	Faster wound healing than Mepitel wound dressing. Reconstruction of intact epidermal layer.	[241]
Silk elastin like protein (SELP) hydrogel	Full-thickness chronic and acute wounds in mice and guinea pigs	Better healing outcomes in comparison with conventional product carboxymethyl cellulose gel. SELP hydrogel demonstrated higher epithelialization rates in comparison with Granugel.	[242]
Silk based nanofibrous mat	Burn wound in rat	Reduced expression level of pro-inflammatory cytokine in comparison to the medical gauze.	[243]

Silk based xerogel	Pressure sore in mice	Silk xerogel promoted sore-healing without scarring.	[244]
Powdered *A. pernyi* silk	Second degree burn rat	The powder showed good biocompatibility and promoted re-epithelization on burn wound.	[245]
Silk film, nanofibre and lamellar porous film	Full-thickness wound in mice	Silk matrices showed faster wound healing rate with minimal scarring in comparison to commercially available Tegaderm™ controls.	[91]
Native spider silk fibres	Full-thickness in rabbit	Improved healing outcomes in comparison to standard control groups (Vaseline and phenytoin)	[246]
Native spider silk fibres	Full-thickness in sheep	Neovascularization in the bundles of spider silk matrix, migration of cells on spider silk fibres.	[247]

1.2.7.2. Biological properties of silk biomaterials and their application in skin regeneration

Silk has been considered as a biomaterial since decades and has been widely explored in the fields of drug release, engineering of artificial organs or tissues and wound healing [90, 248, 249]. Being a biocompatible and non-immunogenic material, BmSF silk-based scaffolds have been approved by the FDA for biomedical applications [23]. Easy processability of the SF to mould into various shapes is an additional advantage of this material that makes it a suitable candidate for fabricating wide varieties of structural constructs. The bulk SF biopolymer is easy to transform into numerous types of constructs like thin films, hydrogels, porous scaffolds, nanofibrous mats, nanoparticles and injectable systems [47, 90, 91, 217, 248, 250, 251]. If we look deeply into the wound healing process supported by a silk-based matrix, we find that the platform of silk is involved in every major step of healing process. Commencing with the first phase of wound repair, silk holds excellent property to bind with blood platelets and fibrinogen protein, thereby aiding the healing process from the very first event of haemostasis [252, 253]. The entrapped fibrinogen and platelet cells in the silk matrix act as a reservoir of

secreted growth factors and cytokines, which keep on releasing at a slow and sustained rate, thereby help in migration of cells from wound edges towards the cavity [253].

Next, it has been proven that BmSF stimulate cell migration through upregulation and phosphorylation of c-Jun that lead to activation of various signalling pathways [254]. Therefore, silk matrix plays the most important role of cell migration during the wound healing process. Other additional factors that enhances the cell migration process are presence of bioactive sites in the amino acid sequence of various types of fibroin proteins. For example, NMSF silk varieties like AaSF possesses well-established RGD cell binding tripeptide [24]. In another recent study, it has been proven that BmSF activates nuclear factor kappa enhancer binding protein (NF-κB) signalling pathway to promote the wound healing process [255]. Thus, influence of silk on the cell migration process leads to accelerated wound healing process. This ultimately influence a lot of main events associated with cell migration process, like neovascularization (by migration of endothelial cells), granulation tissue development (by migration and proliferation of fibroblasts) and re-epithelialization (by migration of keratinocytes) and other unknown events by migration of numerous other cells [90]. Therefore, silk is an excellent choice of biomaterial for wound healing applications. In order to harness the regenerative properties of silk, various strategies have been applied to fabricate wound dressings using silk as a biomaterial (discussed in details in later chapters).

Silk has been used as sutures, tissue scaffolds, and drug delivery agents since decades [22, 90, 249]. Both physical and biological properties of silk material are easily manipulated simply by structural re-adjustments. Apart from the biocompatible properties of silk as a biomaterial, it holds extraordinary properties for drug delivery applications [249]. The bulk material of SF has been utilized as a cargo, which delivers drugs, biomolecules and growth factors at a slow and sustained rate [249, 256]. This property of silk has been extensively exploited for wound healing applications as the silk-based matrix can be easily functionalized with antibiotics or growth factors to be delivered at the wound site [91]. In addition to the drug delivery applications, silk also helps in stabilization of biomolecules and preserve the bioactivity of drugs/molecules for longer time [256]. For example, antibiotics like penicillin and tetracycline incorporated in silk films demonstrated higher stability in comparison to their storage in solution and powder form [257]. In another study, silk microneedle arrays containing tetracycline

demonstrated sustained release and preserved bioactivity of the antibiotic against *Staphylococcus aureus*, the most commonly found bacteria in the infected wounds [258].

Drug entrapment and stabilization within silk biomaterial depend on various factors like hydrophobic/hydrophilic interactions, electrostatic interactions or hydrogen bonding [256]. The aqueous solution of silk is generated by dissolving silk fibres in LiBr solution. This process breaks the highly stable hydrogen bonds in the β-sheet structures of fibroin fibres and silk in its solution form is obtained [215]. While fabricating constructs using aqueous solution of silk, the hydrogen bonds are re-formed and the stable β-sheet structures render stability to the structure of silk construct [259]. For functionalization, drug or biomolecules are directly added in the silk solution and thereafter the solution is processed into particular type of construct [27]. For example, during the fabrication of a thin film, drug loaded silk solution upon air-drying lead to reformation of the hydrogen bonds and entrapment of drugs or biomolecules [257].

In a study, drug release mechanism from silk films was examined by loading the films with different molecular weight fluorescein isothiocyanate (FITC)-dextrans ranging from 4 to 40 kDa [260]. The study revealed that the diffusion mechanism was the major factor for sustained release rate as determined by the Peppas equation [260]. Therefore, silk matrices can be considered as a potential drug delivery material for slow and sustained release of drugs and bioactive molecules. Overall, the results of the current literature on silk based matrices demonstrate that the silk is a promising material and can be used as a wound dressing platform for healing applications. Exploring other varieties of this material and fabricating various types of matrices might reveal their unique properties towards tissue regeneration therapeutics. Summarizing the review of literature, we hypothesize the wound healing process assisted by a dressing platform as represented in the schematic image (**Figure 1.5.**). Further, keeping in mind the above-mentioned research using silk as a biomaterial, we target to explore other varieties of silk in wound healing applications and develop novel strategies to contribute in this particular field.

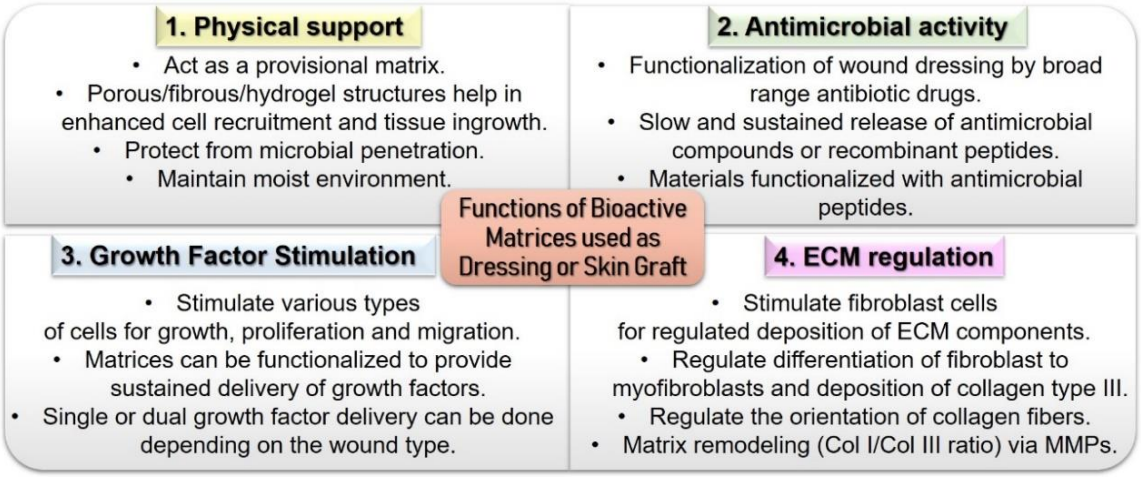

Figure 1.5. *Illustrative representation demonstrating functions of bioactive constructs and how such matrices may trigger the key events of wound healing process for skin regeneration applications.*

MOTIVATION AND OBJECTIVES

OF THE PRESENT INVESTIGATION

MOTIVATION AND OBJECTIVES OF THE PRESENT INVESTIGATION

Skin wounds represent a major healthcare problem owing to an increasing number of trauma and pathophysiological cases like burns and diabetic wounds. Such conditions hamper the normal self-healing process of skin and their treatment has been a foremost clinical challenge since decades. Based on the literature of currently used highly expensive treatments, there is a significant demand of affordable technology to bridge the gap between the need and the availability. Silk, being a natural biomaterial possessing inherent regenerative properties holds immense potential towards the development of cost-effective and efficient treatments. In the course of developing strategies for wound repair and regeneration, our main aim is to develop pro-regenerative matrices using inexpensive silk biomaterials. Our research focusses on harnessing the regenerative properties of numerous types of available silk biomaterials to aid wound healing through various strategies. The origin of the present research work and the salient motivating factors are as follows:

1. Current therapeutic approaches for treating cutaneous wounds include natural biomaterials like collagen, fibrin and allogenic cadaveric grafts. However, these materials are human origin, leading to low-availability and high cost. Materials obtained from xenogeneic sources like bovine or porcine suffer from disease transmission, short shelf-life, immune response and graft rejections. The gold standard approach of applying autologous split-thickness skin grafts depends on the availability of healthy skin left in the patient and faces a major drawback of secondary donor-site wounds. Based on these loopholes, there is an urgent need of affordable alternative therapeutic approaches, which are available off-the-shelf and holds efficient wound healing properties.
2. Fabrication of bioactive wound dressings that possess inherent biological cues to stimulate the cells residing at wounded tissue happens to be a promising strategy for treating chronic wounds. Bioactivity rendered by topical application of growth factors might be fruitful; however, the proteolytic wound milieu of chronic wounds is prone to degenerate the active peptides and demands high

amount of such molecules for topical application. Therefore, efficient delivery of stable growth factors through biomaterials, which act as a cargo is beneficial in reducing the dose amount and sustained release of biomolecules. Considering the natural wound milieu, the instructive biochemical cues can be recapitulated in the developed matrices by incorporating materials containing cell adhesive peptides and bioactive molecules such as growth factors and antibacterial compounds.

3. Silk biomaterial, well-known for its application in the form of sutures to treat incisional wounds, holds immense potential in skin regeneration therapeutics. Furthermore, there are numerous varieties of silk biomaterials, which needs to be explored. This motivated us to explore various other varieties of silk ranging from silkworm SF to recombinant spider silk proteins. Among the silkworm SF varieties, unlike mulberry *B. mori* silk, non-mulberry silk possesses inherent cell binding motifs, which attracted us to further explore this particular silk variety in wound healing applications.
4. Silk is a fibrous structural protein and thereby is easy to formulate into various types of constructs such as woven/non-woven mat, porous scaffold, hydrogel, thin films and nanofibrous mats. Along with structural properties, silk possesses extraordinary properties like biocompatibility, non-immunogenicity, biodegradability and high mechanical strength. The abundant bioresources of silk materials and inexpensiveness provide further advantage in using this material over other biomaterials in the field of regenerative medicine.
5. Fabrication of wound dressing not only requires biological properties but also demands ideal physical properties like porous architecture to allow cell migration, moisture retention properties to keep the wound bed moist, integral stability and suitable mechanical properties to prevent disruption of wounded tissue. Giving equal importance to the physical parameters along with biological properties, silk biomaterial is selected for fabrication of matrices for wound healing applications.
6. Surgical interventions for skin grafting prefer one-step grafting procedures for efficient clinical outcomes. In this context, acellular porous scaffolds and *in situ* forming hydrogel matrices are gaining much attention for treating full-thickness wounds, especially burn injuries. Artificial graft in the form of a porous scaffolds and *in situ* forming hydrogel can be easily applied at the wound site *via* one-step grafting surgery. Furthermore, fabrication of hydrogel using cross-linker free

approach is desirable to avoid side effects of chemical based crosslinking agents. Using materials that hold self-assembly properties like silk, provide additional advantage in facile hydrogel fabrication strategies. Silk matrices in the form of wound dressing and artificial grafts are effective and inexpensive, which hold great potential for wound repair and regeneration.

In the light of enormous scope of exploring various silk biomaterials and unravelling the regenerative properties of different silk proteins, we have utilized various strategies to develop silk-based matrices. With the aim to fabricate bioactive wound dressing and bioartificial skin grafts for wound healing applications. We analysed our different hypothetical strategies through the following objectives:

Objectives:

1. Development of silk based nanofibrous dressings for wound healing applications.
2. Functionalization of silk based nanofibrous dressings for treating diabetic wounds.
3. Development of functionalized bioactive materials using silk-silk interactions between silkworm silk fibroin and recombinant spider silk variants.
4. Investigation of recombinant spider silk coated silk based constructs in treating chronic diabetic wounds and full-thickness burns.
5. Development of *in situ* forming silk hydrogel for treating full thickness burn wounds.

Chapter 2

Development of silk based nanofibrous dressings for wound healing applications

This chapter discusses the fabrication methodology of nanofibrous mats using three types of SF varieties through electrospinning technique. The work focuses on the physico-chemical characterization of the mats and demonstrates the efficacy of non-mulberry silk dressings for scarless wound healing.

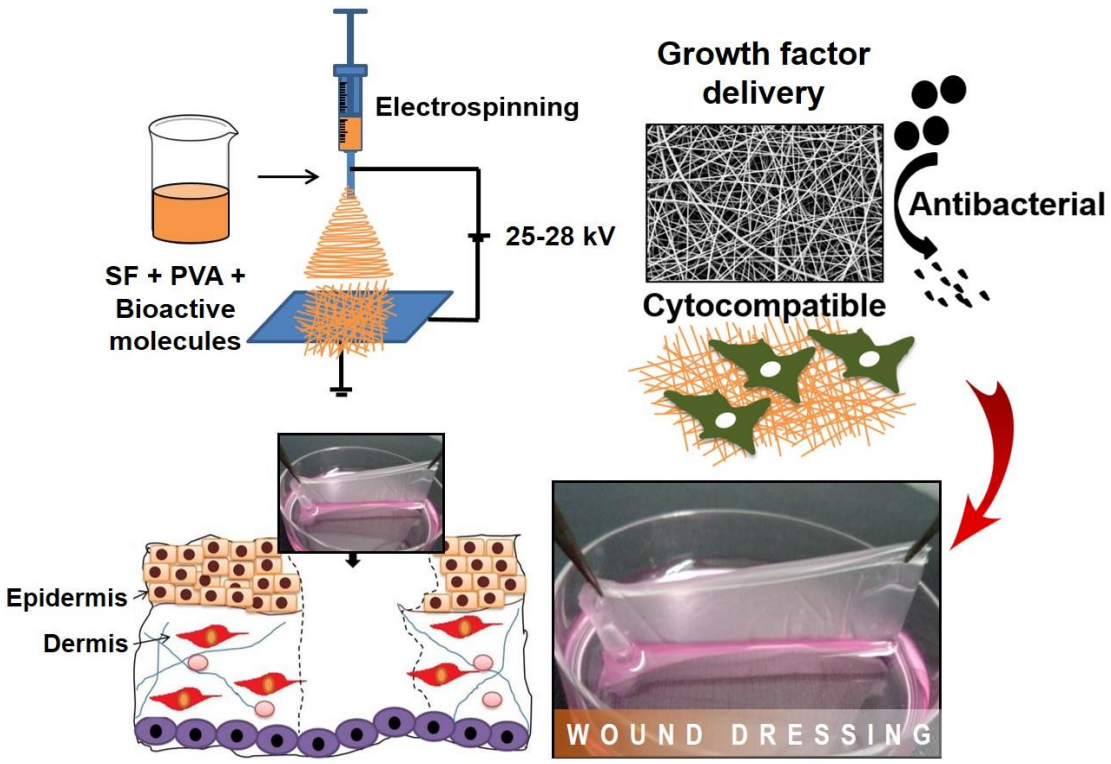

The work embodied in this chapter is published:
Chouhan D, Chakraborty B, Nandi SK, Mandal BB. Role of non-mulberry silk fibroin in deposition and regulation of extracellular matrix towards accelerated wound healing. *Acta Biomaterialia* 2017; 48: 157-74.

भारतीय प्रौद्योगिकी संस्थान गुवाहाटी
Indian Institute of Technology Guwahati

ABSTRACT

Bombyx mori silk fibroin (BmSF) as a biopolymer, has been extensively explored in wound healing applications. However, limited study is available on the potential of silk fibroin (SF) from non-mulberry (*Antheraea assama* and *Philosamia ricini*) silk variety. Herein, we have developed non-mulberry SF (NMSF) based electrospun mats as potential wound dressing, which can also be functionalized with bioactive molecules like epidermal growth factor (EGF) and ciprofloxacin antibiotic drug. The NMSF based mats exhibited essential properties of wound dressing like biocompatibility, high water retention capacity (440 %), water vapour transmission rate (~2330 $gm^{-2}day^{-1}$), high elasticity (~2.6 MPa), sustained drug release and antibacterial activity. Functionalized NMSF mats enhanced the proliferation of human dermal fibroblasts and HaCaT cells *in vitro* as compared to non-functionalized mats ($p \leq 0.01$) showing effective delivery of EGF. Extensive *in vivo* wound healing assessment demonstrated accelerated wound healing, enhanced re-epithelialization, highly vascularized granulation tissue and higher wound maturity as compared to BmSF based mats. NMSF mats treated wounds showed regulated deposition of mature elastin, collagen and reticulin fibres in the extracellular matrix of skin. Finally, presence of skin appendages and isotropic collagen fibres in the regenerated skin demonstrated scar-less healing and aesthetic wound repair.

2.1. Introduction

Skin protects the internal organs from various foreign elements, pathogens and mechanical stress [7]. Breaching of skin may lead to physiological imbalance of the body, often resulting in fatal consequences. More than 6.5 million people are suffering from chronic cutaneous wounds such as diabetic foot ulcers, venous ulcers, pressure sores and traumatic injuries [7]. Wound healing is a complex process comprising four sequential phases – haemostasis, inflammation, cell proliferation and tissue remodelling [261]. Obstruction in any phase of the healing pathway may lead to complications like wound chronicity or fibrosis [12]. There is a necessity of bioactive wound dressing, which not only accelerates the healing process but also regulates the extracellular matrix (ECM) deposition to avoid further scarring complicacies. Hence, efficient wound dressing, which aims to improvise all the four phases of wound healing is the ultimate need for aesthetic wound repair.

Electrospinning technique holds immense potential in the wound healing applications, as it not only facilitates the easy incorporation of bioactive molecules but also closely mimics the nanofibrous structure of natural ECM, thereby providing a 3D environment for better cell recruitment [43, 262]. Over the past decades, extensive research endeavours have been directed towards the development of nanofibrous mats using various synthetic and natural polymers. The most explored biopolymers in wound dressing applications are collagen, chitosan, silk fibroin, hyaluronic acid, cellulose, alginate, dextran, elastin, poly(vinyl alcohol) (PVA), poly(ethylene glycol) (PEG), poly(lactic co-glycolic acid) (PLGA), polylactic acid (PLA), poly(caprolactone) (PCL) and silicone [25, 263]. Current strategies to develop dressing materials focus only on the accelerating healing events to quickly seal the wound. However, scar-less skin regeneration is not addressed by most of the products [264]. Achieving regulated ECM deposition by tuning the fibroblast response using functional wound healing substrate needs to be explored more [265]. The current study focuses on fabricating bioactive wound dressings and their role in the regulated deposition of ECM towards wound repair.

Among the various biomaterials reported till date, silk fibroin (SF) from mulberry silkworm *B. mori* has been proven to be an accepted material for biomedical applications due to its biocompatibility, biodegradability, low immunogenicity, material versatility, cost-effectiveness, easy processing and tensile properties [22]. In the present study, we

explored the potential of silk from non-mulberry varieties, namely, *A. assama* silk fibroin (AaSF) and *P. ricini* silk fibroin (PrSF). Non-mulberry silk fibroin (NMSF) possesses inherent Arginine, Glycine and Aspartate (RGD) motifs in the protein sequence, facilitating binding to the integrin receptors of cells [214]. This provides functional advantage of mediating cell-material interactions for wound repair.

To fabricate NMSF based electrospun mats, PVA (a non-protein polymer) was used as the blending material, because the proteolytic rich environment of chronic wounds demands a stable wound dressing [266]. Blend of PVA and BmSF has been previously used in the format of membranes, manifesting the efficacy of the blend for wound dressing applications [100]. In the present study, blends of PVA with three different types of SF were electrospun using aqueous solvent, which were also functionalized with epidermal growth factor (EGF) and ciprofloxacin (CIP) to re-establish the growth factor pool in wound microenvironment and prevent infection respectively [166, 267]. The present study focuses on the assessment of essential physical properties and functional advantage of the novel material for wound healing applications. Four different functionalized mats were prepared: one pristine mat of only PVA and three hybrid mats from the blends of PVA with three varieties of SF for comparative study. We have also looked into the substrate's ability to accelerate the *in vivo* wound healing process and potential to regulate the deposition of collagen, elastin and reticulin fibres that majorly constitute the ECM of skin.

2.2. Materials and methods

2.2.1. Preparation of silk fibroin solutions

BmSF was isolated from the silk cocoons as described in the standard protocol [215]. Briefly, *B. mori* cocoons were degummed twice for 15 min in boiling water using 0.02 M sodium carbonate (Merck, India). The dried silk fibres were dissolved in 9.3 M lithium bromide solution (Sigma Aldrich, USA) at 60 °C for 4 h and subsequently dialyzed against distilled water using a MWCO 12 kDa cellulose dialysis membrane (Sigma Aldrich, USA) for 3 days at room temperature (RT) to obtain aqueous BmSF solution. NMSF silk solutions, namely, AaSF and PrSF were extracted from the silk glands of 5^{th} instar matured larvae of *A. assama* and *P. ricini* silkworms respectively according to previously described protocol [227]. Briefly, the fibroin protein was extruded out from

the glands using forceps and was subsequently dissolved in 1 % (w/v) aqueous sodium dodecyl sulphate (SDS) (Himedia, India) solution. The protein solution was further dialyzed against distilled water using a 12 kDa cellulose dialysis membrane for 4 h at 4 °C to obtain pure AaSF and PrSF aqueous solutions. Isolation procedure of SF from the three silk varieties was completely aqueous and further fabrication steps also involved all-aqueous procedures bringing green synthesis of the nanofibrous mats.

2.2.2. Fabrication of functionalized nanofibrous mats using electrospinning

PVA (1,700–1,800 degree of polymerization and 98-99 mol % hydrolysis) was procured from LobaChemie Pvt. Ltd., India. PVA stock solution (13 % w/v) was prepared by dissolving PVA granules in lukewarm de-ionized water at 40-50 °C for 6 h with constant stirring. PVA aqueous solution was then blended separately with the three different aqueous solutions of SF (3 % w/v) (BmSF, AaSF and PrSF) in the ratio of 4:1 (PVA: SF; w/w) to make hybrid mats. Pristine nanofibrous mat of PVA was fabricated using 8 % PVA (w/v) solution. Viscosities of pristine PVA solutions and blend solutions were measured using a viscometer (Fungi Lab, Visco Basic Plus) with the spindle calibrated at 0 cP for water, rotating with a speed of 100 rpm. The four types of nanofibrous mats were electrospun using electrospinning machine (E-spin nanotech, India). Briefly, the solution was filled in a syringe and spilled with a flow rate of 0.800 ± 0.100 mL/h *via* a 21-gauge blunt needle. Rotating drum collector (at a rotating speed of 500 rpm) was placed at a distance of 15 cm from the needle, while the voltage was kept at 25 ± 3 kV. Four different mats were prepared under the similar electrospinning parameters: one pristine mat of only PVA solution (PVA) and three hybrid mats from the blends of PVA and SF: PVA + *B.mori* (PVABM), PVA + *A. assama* (PVAAA) and PVA + *P. ricini* (PVAPR).

To fabricate functionalized nanofibrous mats, human recombinant EGF (expressed in *E. coli*) (Sigma Aldrich, USA) was mixed in the spinning solution prior to electrospinning. The final concentration of EGF in all the solutions was 1 µg/mL. β-sheet in the hybrid silk mats were induced by slightly modifying the solvent vapour method [268]. For this, mats were kept in a vacuum desiccator saturated with 70 % ethanol vapours for 6 h. The average thickness (300 µm) was kept constant for all the mats by spinning 12 mL solution. For the evaluation of preliminary antibacterial assessment, the nanofibrous mats were coated with ciprofloxacin hydrochloride monohydrate (Himedia,

India, MW 385.82 Da). Drug incorporation was done by coating onto the processed mats instead of co-spinning to achieve higher burst release. The mats (6 mm diameter) were coated with 50 µL of CIP solution (30 mg/mL), by which a total amount of 1.5 mg CIP was adsorbed on each sample. Coating of CIP was performed in 5 cycles by adding 10 µL of drug solution and drying after every one hour.

2.2.3. Physico-chemical characterization of nanofibrous mats

Morphology and size of nanofibres were investigated using field emission scanning electron microscopy (FESEM; Zeiss, sigma). Image J software (Wayne Rasband, National Institute of Health, USA) was used to determine the diameter of nanofibres by measuring 100 randomly selected nanofibres from the magnified images. The surface topography and roughness of the nanofibres were assessed using atomic force microscopy (AFM; Agilent, Model 5500 series, non-contact mode) with silicon cantilever having a spring constant of 42 N/m at a resonance frequency of 320 kHz. AFM images were further analysed by WSxM software. The functional groups and chemical bonds of SF and PVA in the nanofibrous mats were analysed by Fourier transform infrared spectroscopy (FTIR; Perkin Elmer spectrum two spectrometer). All spectra were obtained in the range of 400–4000 cm^{-1} with a resolution of 8 cm^{-1} by taking 32 scans per spectra under ambient conditions. Tensile properties of nanofibrous mats were determined by following American society for testing and materials (ASTM) D-638 standard using Universal Testing Machine (UTM, Zwick Z010, Germany) equipped with a 500 Newton load cell operated at a crosshead speed of 20 mm/min. Rectangular specimens (10 × 100 mm) were taken for tensile testing. Ultimate tensile strength (UTS), Young's modulus (YM) and elongation at break (%) were estimated from the stress versus strain plots obtained for each sample. The results were reported as average ± standard deviation (n=5).

In vitro degradation analysis of electrospun mats was carried out by evaluating the digestion of mats using protease XIV (Sigma Aldrich, USA) with an activity of 2 U mL^{-1} at 37 °C for 14 days. For comparative study, we examined the degradation profile of nanofibrous mats by taking phosphate buffer saline (PBS, pH 7.4) solution without protease as control. Briefly, the samples were cut into 10×10 cm^2 size and put into protease solution as well as in control solution (only PBS). The samples were replenished with fresh protease solution after every 3 days so as to retain the activity of protease. The

dry weight of mats was measured using an electronic balance (Sartorious, AG Germany). Degradation profile was plotted by calculating the change in mass using the standard formula –

Percent mass remaining = (mass at time t / initial mass) x 100 …….. (2.1.)

Morphology of nanofibrous mats after *in vitro* proteolytic treatment was examined by FESEM. Integral stability of the nanofibrous mats was examined by calculating the amount of protein released from the mats using Bradford assay for 28 days under *in vitro* conditions. The hybrid mats (10 × 10 cm^2) were incubated in 10 mL of PBS containing 0.05 % sodium azide (pH 7.4) at 37 °C. Solutions from incubated samples were then collected at specific time points (0, 1, 3, 7, 14, 21 and 28 days), mixed with Bradford reagent and absorbance of the mixture was recorded at 595 nm. To examine the amount of released protein, each type of sample was compared with the standard plots of respective SF solutions. The results were reported as average ± standard deviation (n=4).

2.2.4. Drug release profile and antibacterial action

The drug released from CIP coated nanofibrous mats was quantified by submerging them in 1 mL PBS (pH 7.4) at 37 °C. 100 µL of releasate was taken out and replaced with 100 µL of fresh PBS at pre-specified time-points (*viz*., 1, 3, 12, 24, 48 and 72 h). Released percentage of CIP was determined by measuring absorbance of the releasate at 270 nm using a microplate reader (Tecan Infinite Pro M200) and comparing the concentration with the standard curve of CIP. Cumulative drug release behaviour was calculated for 3 days using the following formula –

Dug release (%) = $(M_t/M) \times 100$ ……..……..… (2.2.)

Where M_t was the amount of drug released at time t and M was the theoretical value of drug present in the nanofibrous mat.

Antibacterial action of CIP coated nanofibrous mats was checked against four types of skin infecting bacteria obtained from Microbial Type Culture Collection and Gene Bank (MTCC, IMTECH, India). *Staphylococcus aureus* MTCC 3160, *Staphylococcus epidermidis* MTCC 435, *Escherichia coli* MTCC 40 and *Pseudomonas aeruginosa* MTCC 1688 were cultured for susceptibility test [269]. Uniform spreading of 100 µL microbial culture with cell density 6.4 x 10^8 cells/mL was carried out on

solidified nutrient agar (Himedia, India). CIP coated nanofibrous mats (6 mm) were subsequently placed on the cultured bacterial plates and incubated at 37 °C. Zone of inhibition was observed on the bacterial plates after 24 h.

2.2.5. *In vitro* swelling studies, dehydration rate and water vapour transmission rate

Swelling capacity or water gain (%) of all the nanofibrous mats was analysed by comparing the weights of dry and swollen samples at different time points. Nanofibrous mats (10 × 10 cm^2) were incubated in 10 mL of PBS (pH 7.4) at 37 °C and weight of wet sample was measured at pre-defined time-points till saturation level was attained. Swelling ratio was calculated using the formula –

Water gain (%) = {(mass of swollen mat – mass of dry mat)⁄ mass of dry mat} × 100 ……. (2.3.)

After the saturation was attained, swollen mats were kept in an incubator at 37 °C. At pre-determined time points, weight of wet mats was examined till they were completely dry to measure the rate of water loss. Percentage water loss was calculated using the same formula as used for swelling ratio. Dehydration rate was calculated by determining the slope of the curve plotted for water loss (%) vs. time. Water vapour transmission rate (WVTR) measurements were performed using PERMATRAN-WR Model 1/50 (Mocon, USA) by following the ASTM standard E398-03. Circular electrospun mats were placed in between two aluminium foil cards with small holes and a total exposure area of 18 cm^2. A driving force of 80 % relative humidity (RH) was applied by setting 100 % RH in the wet chamber and 20 % in the dry chamber. The experiment was carried out at a temperature of 37.8 °C for more than 150 cycles to obtain the WVTR value. Four samples were carried out for each group for all the experiments.

2.2.6. Release profile of epidermal growth factor

The amount of active EGF released in PBS solution was determined using enzyme-linked immunosorbent assay (ELISA) kit specific for human EGF (Sigma Aldrich, USA, sensitivity < 1 pg/mL). Briefly, nanofibrous mats weighing 50 mg each were soaked in 5 mL PBS and placed in an incubator at 37 °C and 95 % RH. 100 µL of PBS containing EGF releasate was taken out at different time points (1, 12, 24 and 72 h) and replaced with 100 µL of fresh PBS so as to maintain the volume. ELISA assay was conducted following the manufacturer's protocol. Cumulative percentage release was plotted for

each sample (n=4) against time. Cumulative EGF release (%) was calculated using the formula –

$$\% \text{ EGF release} = (M_t/M) \times 100 \quad \text{..... (2.4.)}$$

Where M_t was the amount of EGF released at time t and M was the theoretical value of EGF present in the nanofibrous mat. Four samples were taken for each group.

2.2.7. *In vitro* cell culture on nanofibrous mats

Primary human dermal fibroblasts (HDF) (Himedia, India) at passage number 4 and human keratinocyte cell line (HaCaT cells procured from NCCS, India) were cultured separately on the four types of mats in static culture conditions. Briefly, both the cells were maintained in an incubator at 37 °C, 95 % RH and 5 % CO_2 using high glucose Dulbecco's Modified Eagle's Medium (DMEM; Gibco, USA) containing 10 % Fetal bovine serum (FBS; Gibco), 3.7 g/L $NaHCO_3$ (Himedia, India) and 1 % antibiotics. The four types of mats were UV-sterilized for 20 min and conditioned overnight in media prior to cell seeding. Circular mats (diameter 2 cm) were used for proliferation assay carried out in a 12-well cell culture plate. Cells were seeded at a density of 1×10^4 cells per sample. Fresh medium was replenished every alternate day. Tissue culture plate (TCP) was taken as control and culture conditions were kept similar for further experiments.

2.2.8. Cell proliferation on functionalized nanofibrous mats

Cell proliferation of HDF cells and HaCaT cells was analysed by quantifying the reduction of alamar blue dye (Invitrogen, USA) at specified time-points. Briefly, the spent media was taken out from the culture, alamar dye (diluted 1:10 in complete DMEM medium) was added to the culture and kept in an incubator at 37 °C and 5 % CO_2 for 3 h. Absorbance at 570 nm and 600 nm were taken using a microplate reader to quantify the dye-reduction performed by live cells. Alamar blue assay was performed on both the sets of nanofibrous mats *i.e.*, mats functionalized with EGF and non-functionalized mats to check the activity of EGF on cells. Four samples were carried out for each group for both the experiments.

2.2.9. Viability and morphology of cells on nanofibrous mats

Viability of both HDF and HaCaT cells cultured on the functionalized nanofibrous mats was investigated by live/dead assay after 7 days of culture. Cultured mats were carefully washed twice with sterile PBS before the addition of live/dead solution. Green fluorescence ($\lambda_{ex/em}$ ~495 nm/~515 nm) was produced by the live cells treated with Calcein AM (2 mM) dye (Sigma Aldrich, USA) due to active esterase activity; whereas dead cells were visible in red fluorescence ($\lambda_{ex/em}$ ~495 nm/~635 nm) due to binding of ethidium homodimer-1 (4 mM) dye (Sigma Aldrich, USA) with nucleic acids in the damaged cells. Imaging was done using fluorescent microscope (EVOS FL cell imaging system).

Morphology of cells was visualized using Rhodamine Phalloidin (Invitrogen, USA) and Hoechst 33342 (Invitrogen, USA) fluorescent dyes, which stain actin filaments of cytoplasm and nucleus respectively. After 7 days of culture, media was taken out and the cultured mats were gently washed with sterile PBS. Cells cultured on nanofibrous mats were fixed with 10 % neutral buffer formalin (NBF) overnight, subsequently permeabilized with 0.1 % Triton X-100 (Sigma Aldrich, USA) and blocked with 1 % bovine serum albumin (BSA, Sigma Aldrich, USA) prior to staining. Imaging was done under red and blue filters of fluorescence microscope and overlaid images were produced.

2.2.10. *In vitro* cytocompatibility of nanofibrous mats

MTT assay was carried out to examine the cytocompatibility of HDF and HaCaT cells on PVA, PVABM, PVAAA and PVAPR. Separate cultures were prepared for different time points (1, 7 and 14 days). Briefly, the cultured mats were incubated with 1:10 ratio of 3-(4,5-Dimethylthiazol-2-yl)-2,5-Diphenyltetrazolium Bromide (MTT) reagent (Sigma, USA) and serum-free DMEM medium for 4 h at 37 °C and 5 % CO_2. Post removal of the media containing MTT, dimethyl sulfoxide (DMSO; Sigma, USA) was added to dissolve the purple formazan crystals. Absorbance was measured at 570 nm using multiplate reader and cell proliferation index was calculated by comparing the optical density (O.D.) obtained at desired time points relative to the O.D. obtained on day 1. This experiment was carried out only on the non-functionalized mats in order to examine the biocompatibility of different silk matrices.

2.2.11. *In vivo* tissue response against the nanofibrous mats in mice

Following acclimatization, twenty-four Swiss albino mice, each weighing 30-35 g of either sex, were taken in two groups for two time points (2 and 6 weeks). Prior to operation, all the mice were anaesthetized by inhalant isoflurane along with 1-3 % oxygen using a precision vapourizer. The operative regions were wiped with 70 % ethanol and 5 mm incisions were made in the subcutaneous pocket of lateral side of thoraco-lumber region of mice. Sterile nanofibrous mats (1×1 cm^2) were implanted and incisions were closed using non-absorbable nylon suture stitches. All the mice were kept in separate cages and monitored daily. The animals were sacrificed after 2 weeks and 6 weeks post cervical dislocation and implanted samples with small portion of surrounding tissues were carefully peeled off for histological examination. The implants were fixed with 10 % NBF, dehydrated through a series of graded ethanol, embedded in paraffin and sliced with a microtome (Leica, RM2235, Germany) to obtain sections of 5 µm thickness. All the sections were stained with haematoxylin and eosin (H & E) and were observed under bright field microscope to assess the cellular response of the host to the implants. The images were then semi-quantified according to the 4-grade criteria given in International Organization for Standardization (ISO)-10993-6 as listed (**Table 2.1.**). This experiment was also carried out only on the non-functionalized mats in order to examine the tissue response against different silk-based matrices *in vivo*.

Table 2.1. *The scoring system used for examining the biological response against subcutaneously implanted materials as per ISO-10993-6.*

Response	Score 0	Score 1	Score 2	Score 3	Score 4
Immune cell infiltration	0	Rare, 1-5 per field	5-10 per field	Heavy infiltrate	Packed
Fibrosis	0	Narrow band	Moderately thick band	Thick band	Extensive band
Neovascularisation	0	Minimal capillary like structures	Fully grown few blood capillaries with supporting fibroblastic structures	Broad band of capillaries with supporting fibroblastic structures	Extensive band of many capillaries with supporting fibroblastic structures

Tissue or cellular ingrowth	0	Minimal fibroblast invasion	Moderate fibroblast invasion	Fibroblast invasion with moderate graft remodelling	Extensive fibroblast invasion with extensive graft remodelling

2.2.12. *In vivo* wound healing assessment of nanofibrous mats in rabbit model

All the animal experiments were performed in accordance with "Principles of laboratory animal care" from the Institutional Animal Ethical Committee, West Bengal University of Animal and Fishery Sciences, West Bengal, India (Permit No. Pharma/IAEC/136 dated 30.6.2014). Twenty-four adult New Zealand white rabbits each weighing 1.2 – 1.5 kg of either sex were randomized into two groups in three time points (7, 14 and 21 days), consisting of 4 animals per group in each time point. Surgeries were performed under aseptic conditions after giving intramuscular anaesthesia using xylazine hydrochloride (6 mg/kg) (Xylaxin®, Indian Immunologicals, India) and ketamine hydrochloride (33 mg/kg) (Ketalar®, Parke-Davis, India). Dorsal surface of mid thoraco-lumbar region was shaved, wiped with 70 % ethanol and three full-thickness skin wounds (6 mm diameter) were created using 6 mm biopsy punch in each animal. The full-thickness wounds covered with functionalized mats in the form of nanofibrous dressing patch were termed as the treated wounds. The wounds covered with surgical gauze bandage were termed as the control. Dressing patches were replaced with fresh ones after every three days till 14 days post-wounding and animals were regularly monitored. No haemorrhage or abnormality was found during the operation or post-operation. The progress of wound healing was evaluated by periodic monitoring of the rabbits. Digital photographs were taken on day 4, 7, 14 and 21 to evaluate wound closure rate. Rate of wound healing was calculated by measuring the size of wounds through analysis of the photographs using image J software. Following formula was used –

$$\text{Wound area (\%)} = A_t/A \times 100 \quad \text{(2.5.)}$$

Where A_t was the area of wound at time (t) and A was the initial wound area. Accordingly, wound closure rate was determined by considering the area of wound closed with respect to time. Four animals were taken for each group and average value was plotted.

2.2.13. Histopathological examination

Tissues from the wound bed were excised on post-wounding days 7, 14 and 21 for histological examination. Briefly, tissue samples were preserved in 10 % NBF, dehydrated with series of graded ethanol and embedded in paraffin to get sections of 5 µm thickness. Slides containing sections were then stained with H & E for general morphological observations. Masson's trichrome staining method was applied to stain collagen fibres, Gridley's modification of the silver impregnation method was applied to stain reticulin fibres and Weigert's Resorcin–Fuschin method was applied to stain elastin fibres according to manufacturer's protocol [270-272]. Images were taken by observing at least 10 fields per section under bright field microscope.

2.2.14. Skin maturity quantification

H & E stained histologic sections were assessed on day 21 post-treatment according to previously published methods [184, 273]. Specific 4-grade criteria for dermal differentiation, epithelial maturation and skin appendage regeneration were used to quantify the skin maturity level. Thickness of epidermis after 21 days post injury was analysed by Image J software from the histological sections. Scoring of granulation tissue on day 7 was done to assess the degree of proliferation by modifying the previously published protocol to 4-grade criteria based on histological results [184, 273]. Scoring was based as underneath: Score 1 = no granulation tissue formation; score 2 = thin, immature granulation with few fibroblasts and dominated by inflammatory cells; score 3 = moderately thick granulation tissue with few neovascularization regions, fibroblasts infiltration and minimal collagen deposition. Score 4 = thick, vascularized granulation tissue with extensive collagen deposition dominated by fibroblast cells.

2.2.15. Quantitative evaluation of elastin and hydroxyproline in wounds

The tissue samples from wound bed were excised on post-wounding days 7, 14 and 21 and stored at - 80 °C. All the samples were analysed altogether after 21 days in order to quantify the content of elastin and hydroxyproline in the tissues. Elastin and hydroxyproline secretions were quantified using rabbit elastin ELISA kit (Mybiosource, USA) and hydroxyproline assay kit (Sigma Aldrich, USA) respectively according to manufacturer's protocol. Tissue samples from 4 animals were taken for each group.

2.2.16. Scar tissue assessment

Formation of scar tissue from different treatments was evaluated by visually and histologically examining the regenerated skin. Investigation of scar formation was carried out by considering three key-points: 1. Shape of the wounds post-injury by visual observation – deformed or elongated shape suggests scarring [91]; 2. Histological observation of development of skin appendages in the regenerated skin – scar tissues are devoid of skin appendages [273]; 3. Histological observation of deposition and orientation pattern of collagen bundles – Secretion of collagen is abnormally high and collagen bundles are tightly packed with minimal inter-collagen gaps in parallel fashion in the scar tissue [274].

2.2.17. Statistical analysis

All experiments were carried out for n = 4 samples unless otherwise specified. Data were expressed as mean ± standard deviation and analysed using statistical software OriginPro 8 (Originlab Corporation, USA) at both significant ($*p \leq 0.05$) and highly significant ($**p \leq 0.01$) levels. One-way analysis of variance (ANOVA) was performed to compare between groups and within groups to measure the significance level followed by Tukey's test. Histological examination was performed by capturing at least 10 fields per section and images were analysed using Image J software.

2.3. Results

2.3.1. Fabrication and physico-chemical characterization of nanofibrous mats

Nanofibrous mats of PVA and SF blends were successfully fabricated by the electrospinning technique. Viscosities of the three varieties of SF protein solutions ranged between 10 and 20 cP, posing difficulty in electrospinning. Hence, SF solutions were blended with highly viscous PVA solution in a ratio of 4:1 PVA: SF; (w/w) to bring about optimum viscosity required for electrospinning (**Table 2.2.**).

Table 2.2. *Table showing viscosity of aqueous solutions of PVA, various SF proteins and respective blends.*

Solution type	Viscosity (cP)
PVA (13 %)	1764.5 ± 56
PVA (8 %)	244.5 ± 37
B. mori (3 %)	10.5 ± 2.4
A. assama (3 %)	19.1 ± 3.9
P. ricini (3 %)	16.5 ± 4.2
PVA + *B. mori*	218.5 ± 32
PVA + *A. assama*	256.5 ± 41
PVA + *P. ricini*	234.2 ± 29

Nanofibres of hybrid mats (PVABM, PVAAA and PVAPR) and pure PVA mats were continuous, smooth, bead-less and randomly oriented as shown by the FESEM images (**Figure 2.1.A**). The mats showed highly porous network along with interconnected voids. The morphology and size of nanofibres were not much affected by their treatment with ethanol vapours, as can be seen by the FESEM images before and after the treatment. Among all, nanofibres of PVABM and PVA had tighter distribution of fibre sizes (**Figure 2.1.B**) and their average diameters were 157.69 ± 21.53 nm and 193.91 ± 15.84 nm respectively. The distinguishing feature of PVAAA and PVAPR was non-uniformity in fibre diameter, showing wider distribution of fibre sizes ranging from 50 to 300 nm with average diameter of 179.59 ± 49.41 nm and 172.52 ± 52.07 nm respectively. PVAAA and PVAPR had two distinct populations in fibre distribution, 100 nm/170 nm; 140 nm/190 nm respectively (**Figure 2.1.B**).

The FTIR spectrum for PVA mat showed a broad spectral band from 3600-3200 cm^{-1} corresponding to the O-H stretching, the peak at 2890 cm^{-1} assigned to C-H stretching vibrations from alkyl groups, sharp intense peak at 1627 cm^{-1} assigned to the C=O stretching vibrations resulting from the residual vinyl acetate group and sharp peak at 1085 cm^{-1} corresponding to the C-O stretching vibration (**Figure 2.1.C**) [275]. Hybrid mats containing both PVA and SF showed differences in few peaks along with the overlapping peaks of PVA. Broadening of band at 3600-3000 cm^{-1} in the spectra revealed more stretching of –OH bonds. Emergence of weak peak shouldering the 2890 cm^{-1} corresponded to the –OH stretching of –COOH side chain groups of SF, indicating possible interaction of carboxylic groups with hydroxyl groups to form ester linkages [276]. The peak broadening noticed at 1085 cm^{-1}, may be attributed to this (C-O-C) ester bond formed, confirming blending and subsequent crosslinking of the PVA-silk matrices. The hybrid mats also showed the characteristic fingerprint regions of SF, as observed from 1627 cm^{-1} to 1286 cm^{-1}; the band at 1627 cm^{-1} was associated with the C=O stretching vibrations relating to the β-sheet conformational backbone (amide I), the band at 1450 cm^{-1} was indicative of N-H bending vibrations (amide II), while the weak band at 1286 cm^{-1} was associated with amide-III, resulting from C-N and N-H coordinate displacements. Slight change in the amide I peak of PVABM mat suggested characteristic differences as compared to PVAAA and PVAPR, which might be due to different stretching of amide I bond because of the changes in amino acid composition and hence differences in the β-sheet conformation (**Figure 2.1.C**). Other peaks were more or less similar in all the three types of hybrid mats. Further, AFM images revealed highly rough nano-topography of the nanofibrous mats with high rms roughness – PVA (288 ± 47 nm), PVABM (272.9 ± 52 nm), PVAAA (296.19 ± 61 nm) and PVAPR (289.1 ± 54 nm) **(Figure 2.2.A)**.

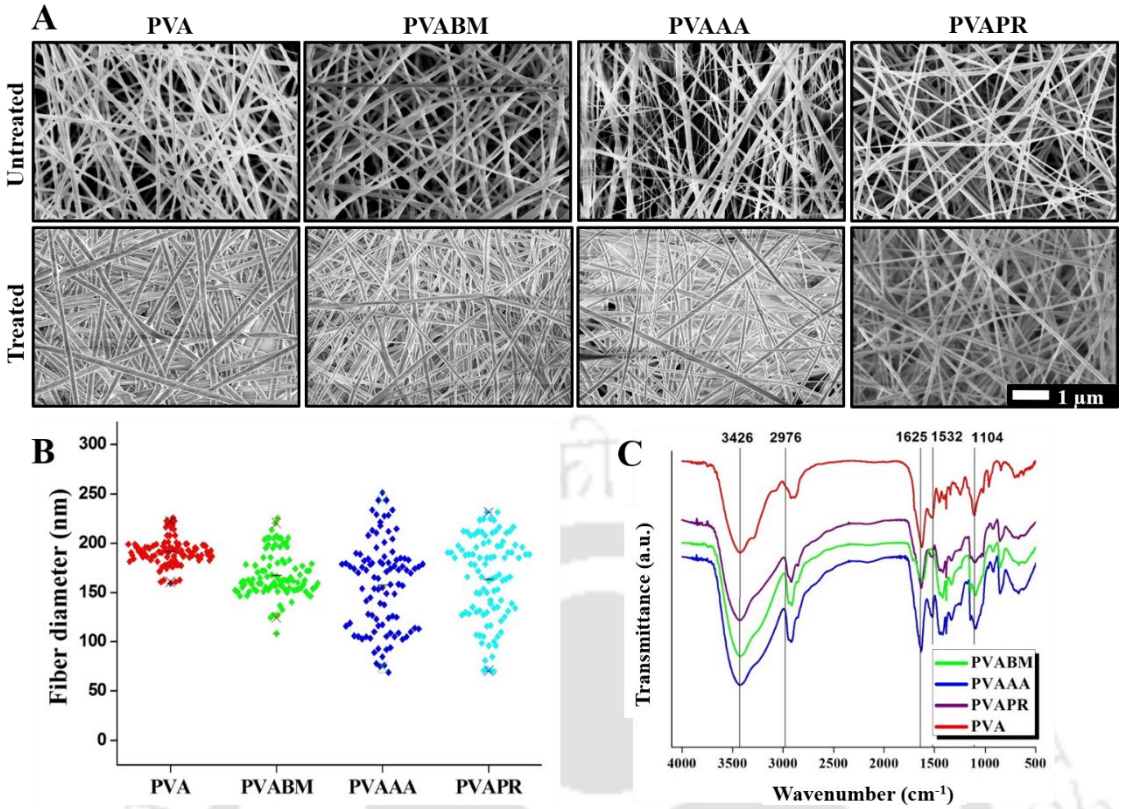

Figure 2.1. *(A) FESEM images representing morphology of nanofibres before and after treatment with 70 % ethanol vapours. (B) Quantification of fibre diameter showing size distribution of nanofibres among various nanofibrous mats. (C) FTIR spectra of nanofibrous mats showing characteristic peaks of PVA and SF. a-I = amide I (1627 cm^{-1}), a-II = amide-II (1450 cm^{-1}) and a-III = amide III (1286 cm^{-1}) signify amide peaks associated with SF.*

2.3.2. Mechanical properties

Tensile testing of the PVA-SF hybrid mats revealed their resilient and elastic nature suggesting their potential to be used as wound dressing (**Figure 2.2.B**). PVA polymer, being well-known for its elastic nature showed the highest tensile strength among all mats. UTS of PVA, PVABM, PVAAA and PVAPR was 24 ± 1.83 MPa, 13 ± 2.35 MPa, 15.35 ± 0.8 MPa and 13.32 ± 1.7 MPa respectively (**Figure 2.2.C**). Modulation in the mechanical properties of PVA was clearly observed by blending SF protein. YM of PVA was 3.58 ± 0.17 MPa, which was significantly higher than that of the hybrid mats, $p \leq 0.01$ **(Figure 2.2.D).** There was no significant difference in the UTS and YM among all hybrid mats, however PVAAA and PVAPR exhibited broad plastic region in the stress vs. strain curve, depicting higher elongation at break (**Figure 2.2.E**). Elongation at break of PVAAA (316.12 ± 33.24 %) and PVAPR (293.62 ± 18.33 %) was significantly higher than that of PVA (248.37 ± 19 %) and PVABM (210.12 ± 24.83 %), $p \leq 0.01$. Our results

were in lines parallel to previous observations attesting higher elongation at break of PrSF and AaSF fibres compared to BmSF fibres [214, 277].

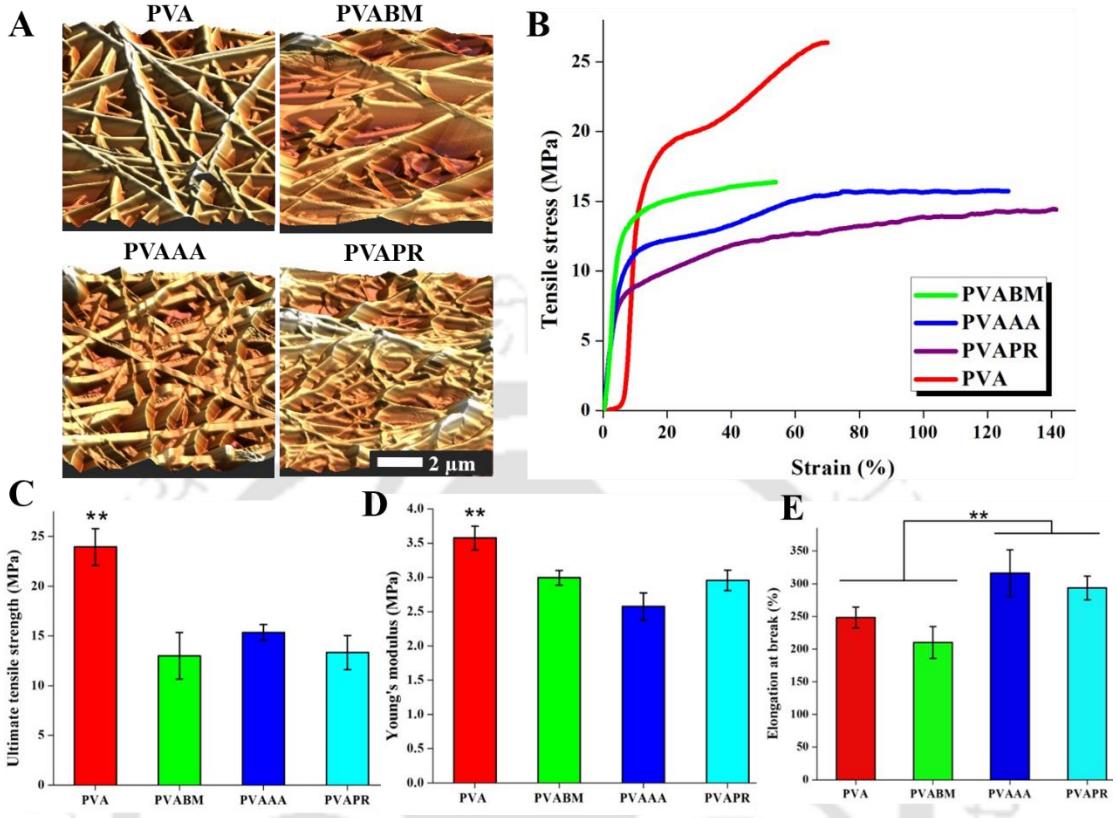

Figure 2.2. *(A) AFM images showing nanotopology of nanofibrous mats. (B, C, D and E) Tensile testing of nanofibrous mats showing curve of stress vs. strain, ultimate tensile strength, Young's modulus and elongation at break respectively, (*p ≤ 0.05, **p ≤ 0.01).*

2.3.3. *In vitro* degradation and integral stability

Gradual degradation of hybrid mats with respect to time was obvious by the proteolytic treatment (**Figure 2.3.**). Hybrid mats containing SF protein showed highly significant mass loss (30-35 %) after 14 days as compared to PVA mat, which did not degrade in the artificial proteolytic environment created by protease XIV, $p \leq 0.01$. There was significant difference in the degradation profile of mats treated with and without protease XIV after 14 days, $p \leq 0.01$. However, no significant difference was observed in the degradation profile among hybrid mats containing different SF proteins. Broken morphology of nanofibres and bigger porous structure of the degraded mats were clearly demonstrated by the FESEM images after 14 days of protease treatment. Mats were highly stable in PBS solution as demonstrated by the negligible mass change over a period of 14 days in control solution (PBS). In addition, SF protein did not leach out

from the hybrid mats due to stable β–sheet structure induced by 70 % ethanol vapours. Stability of the mats against hydrolytic degradation was confirmed by the Bradford assay, which did not show significant protein release from the mats.

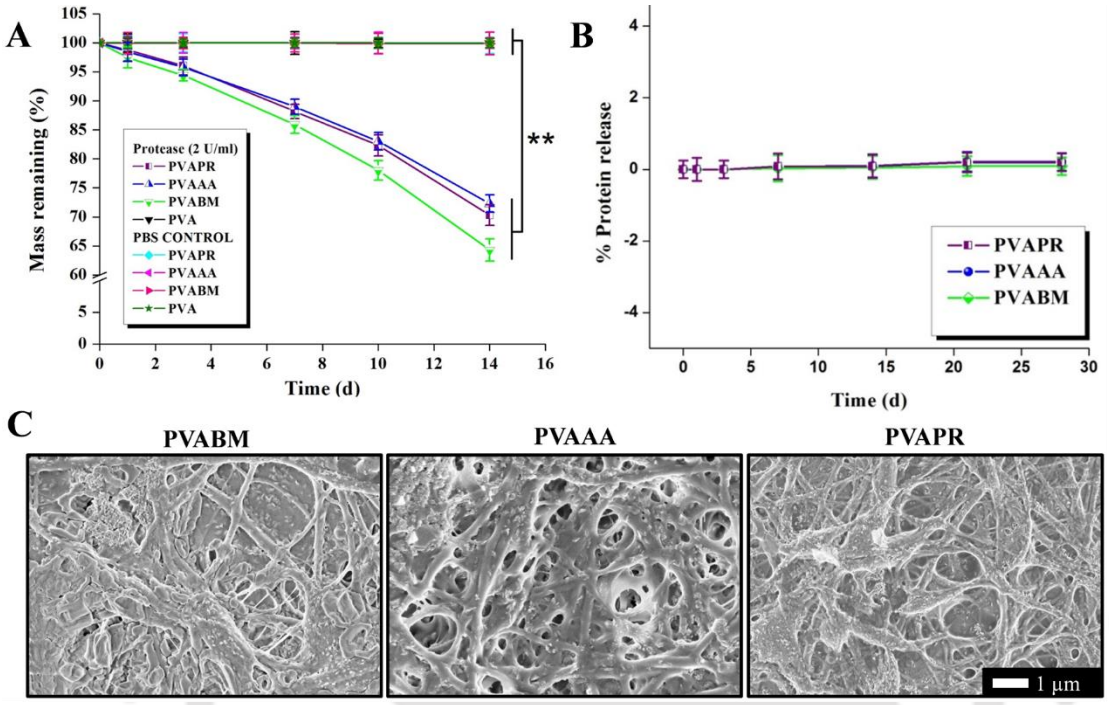

Figure 2.3. *(A) In vitro degradation behaviour of nanofibrous mats in both proteolytic and non-proteolytic solutions for a period of 14 days, (*p ≤ 0.05, **p ≤ 0.01). (B) Protein release profile leached out from mats observed over 28 days, which showed that the SF protein did not leach out from the hybrid mats as confirmed by the Bradford assay. (C) FESEM images showing morphology of nanofibres after 14 days under in vitro protease treatment.*

2.3.4. Antibiotic drug release and antibacterial activity

The nanofibrous mats coated with CIP showed burst release of 60 % within the initial 6 h when submerged in PBS (**Figure 2.4.A**). There was no significant difference in the drug release profile among all mats owing to the weak interactions between the drug and the surface of the mats. 50-70 % of the drug was released within 18 to 24 h showing high drug release. The release behaviour of the drug was quite linear between 24 to 72 h. Antibacterial activity against *E. coli, S. aureus, P, aeruginosa* and *S. epidermidis* was evidenced through the zone of inhibition (**Figure 2.4.B**). There was no significant difference in the zone of inhibition derived from all the four types of antibiotic coated mats owing to equivalent drug release profile.

2.3.5. *In vitro* swelling studies, dehydration rate and water vapour transmission rate

All the nanofibrous mats demonstrated high swelling capacity required for wound healing applications (**Figure 2.4.C**). Swelling ratio of PVAAA and PVAPR ranged from 430-470 %, which was significantly lesser as compared to both PVA (540 %) and PVABM (645 %) mats, $p \leq 0.01$. Within 15-30 min, all the mats got swollen up to a range of 300-500 %, proving high water retention capacity. Dehydration rate of PVAAA (0.024 ± 0.0022 g/min) and PVAPR (0.023 ± 0.0018 g/min) was found significantly lesser than that of PVA (0.036 ± 0.0027 g/min) and PVABM (0.031 ± 0.0029 g/min). This study also disclosed slow dehydrating property of NMSF based mats (**Figure 2.4.D**). Moisture retention capacity of the nanofibrous mats was also corroborated by the high WVTR values (**Figure 2.4.E)**. WVTR of various mats were as follows: PVA – 2526 g m^{-2} day^{-1}, PVABM – 2468 g m^{-2} day^{-1}, PVAAA – 2329 g m^{-2} day^{-1} and PVAPR – 2333 g m^{-2} day^{-1}. WVTR of different mats were found to be in the desired range for wound dressing applications [278].

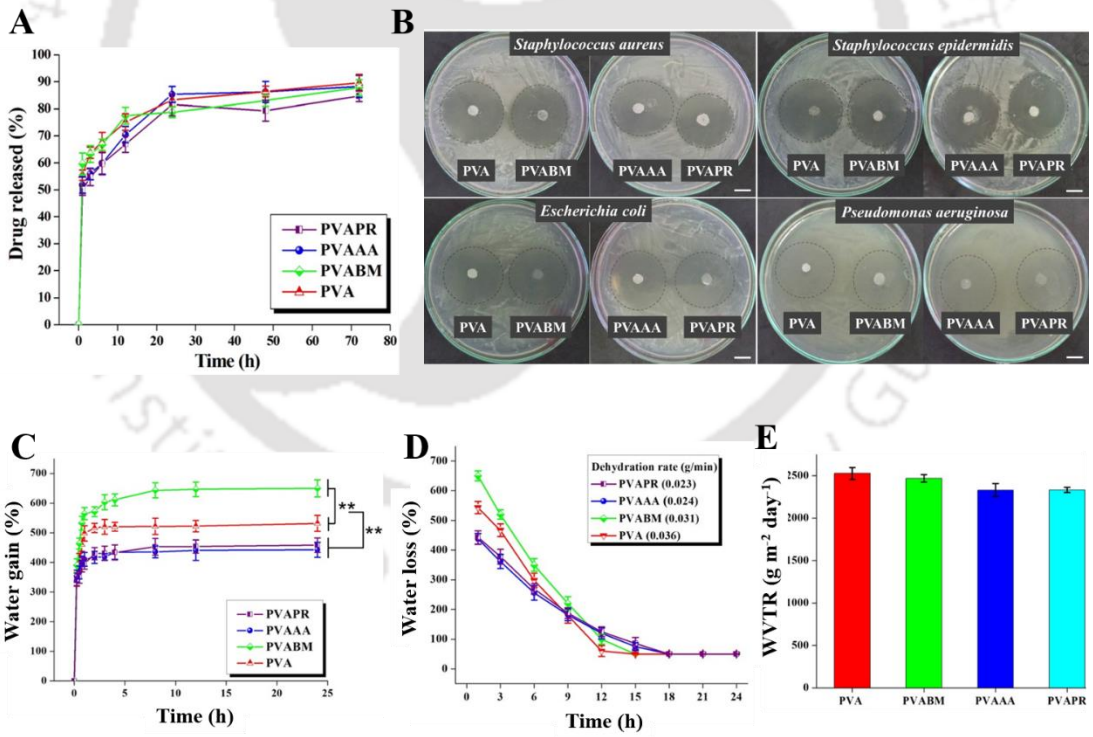

Figure 2.4. *(A) Drug release profile from mats for 3 days. (B) Anti-bacterial activity of mats loaded with CIP drug against four skin infecting bacteria as determined by the disc diffusion method. (C) Swelling behaviour of mats determined by the amount of water uptake with respect to time, (*p ≤ 0.05, **p ≤ 0.01). (D) Dehydration rate of mats showing profile of water loss with respect to time. (E) Water vapour transmission rate of mats showing appropriate WVTR for wound dressing applications.*

2.3.6. *In vitro* release profile of EGF and proliferation of cells on functionalized mats

Nanofibrous mats showed sustained release of EGF as observed for 3 days (**Figure 2.5.A**). Initial burst release of EGF was observed after an hour in all the four types of mats. Initial burst release from PVA and PVABM was 12.04 ± 1.45 % and 15.83 ± 1.04 % respectively. PVAAA and PVAPR mats demonstrated significantly higher initial burst release (20.24 ± 1.50 % and 19.99 ± 1.75 % respectively) than that of other mats, $p \leq 0.01$. EGF was released continuously till 24 h, after which plateau region was observed at 72 h. EGF release was significantly higher from PVAAA and PVAPR than from PVA and PVABM at all the time points, $p \leq 0.01$. PVAAA and PVAPR released 34.71 ± 1.67 % and 31.85 ± 2.02 % EGF respectively after 72 h. This was significantly higher than the amount of EGF released from PVA (17.90 + 1.65 %) and PVABM (26.62 ± 1.65%), $p \leq 0.01$.

The higher cell proliferation on EGF impregnated mats vouched for the functionality of EGF released from the respective mats (**Figure 2.5.B,C**). Alamar blue assay was used to assess the proliferation of HDF and HaCaT cells. Appearance of a plateau phase on day 21 obscured the interpretation of the difference in the cell proliferation between functionalized and non-functionalized mats (**Figure A2.1.**). Hence, proliferation data on day 7 was chosen to figure out this difference. Significantly higher cell proliferation of HaCaT was found on the EGF incorporated hybrid mats (PVABM, PVAAA and PVAPR) as compared to the corresponding non-functionalized mats on day 7, $p \leq 0.01$. HDF cells also showed significantly higher cell proliferation on the EGF incorporated PVAAA and PVAPR compared their non-functionalized counterpart, $p \leq 0.01$. Higher proliferation of HDF and HaCaT cells on the functionalized mats ascertained sustained release of EGF from the PVAAA and PVAPR mats. However, no significant difference was observed for the proliferation of HDF cells on the EGF incorporated PVABM and PVA mats relative to their non-functionalized mat. Functionalized PVABM showed significantly higher cell proliferation as compared to functionalized PVA mat, $p \leq 0.01$. The experiment also revealed significantly higher cell proliferation on PVAAA and PVAPR as compared to PVA and PVABM at all time-points after day 7, $p \leq 0.01$. High proliferation of skin cells on the novel NMSF based blends not only established the latter's cytocompatibility, but also vouched for their aptness for wound healing applications.

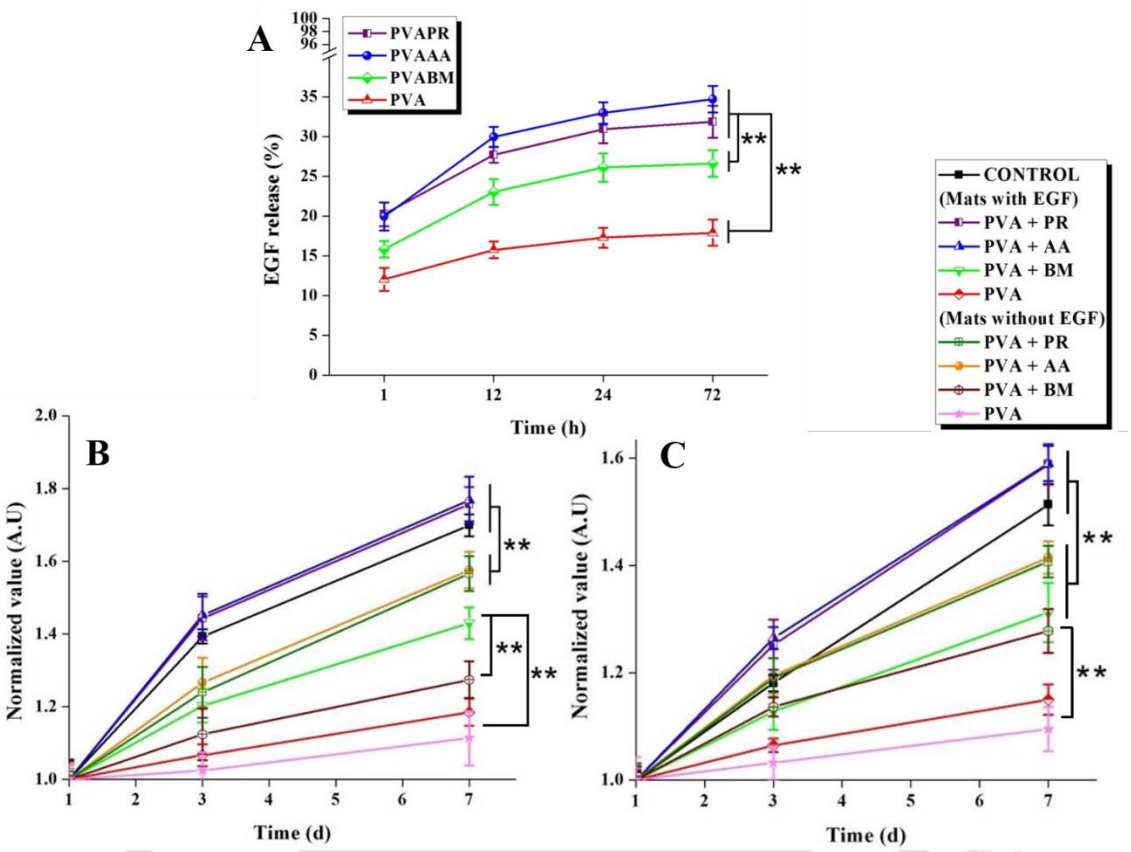

Figure 2.5. *(A) Release profile of EGF by submerging the mats in PBS at 37 °C as determined by ELISA. (B, C) Proliferation profile of HaCaT and HDF cells on blank nanofibrous mats as well as on EGF-functionalized mats respectively over a period of 7 days, (*p ≤ 0.05, **p ≤ 0.01).*

2.3.7. Morphology and viability of cells on nanofibrous mats

Spread-out morphologies were depicted by both HDF and HaCaT cells on PVAAA and PVAPR mats. This was in resemblance to the fully extended morphology as seen on TCP, providing clue of higher cell adhesion (**Figure 2.6.A**). Cells cultured on PVABM formed clumps of elongated HDF, suggesting lower cell adherence as compared to NMSF based mats, which did not show clump formation of cells. Protrusions of elongated HDF cells were clearly visible on PVAAA and PVAPR. Cell density after day 7 could also be visualized through the microscopic images. PVAAA and PVAPR showed higher cell density than PVABM and PVA. Round and clumped cells on PVA mat suggested poor adhesion and consequently a low cell population. Live/dead assay depicted viability of cells on the mats (**Figure 2.6.B**). PVAAA and PVAPR were shown to be fully loaded with live cells; while comparatively low cell density was observed on PVABM and PVA.

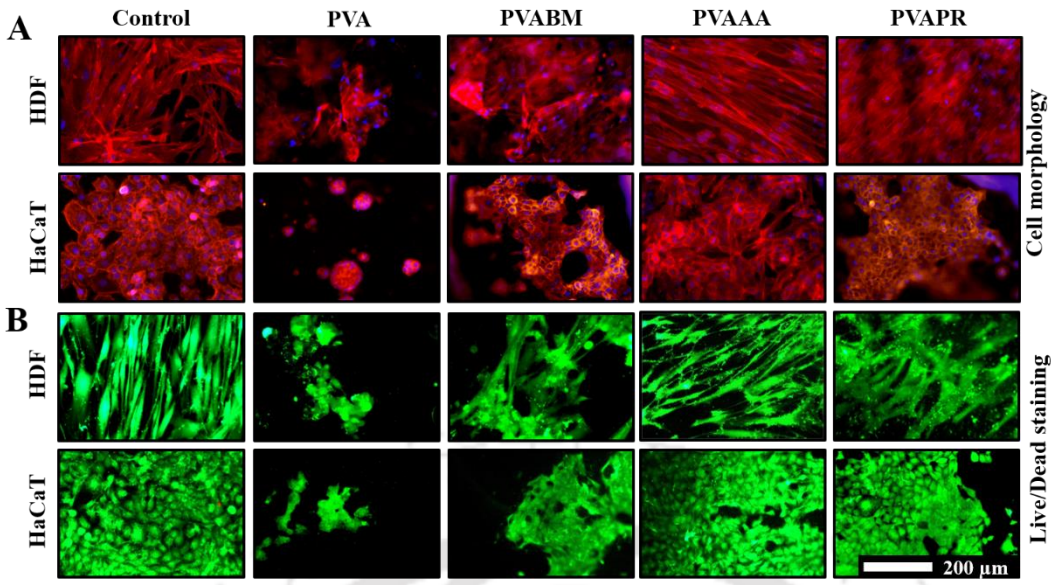

Figure 2.6. *(A) Morphology of HDF and HaCaT cells cultured on various mats, where nuclei were stained with Hoechst dye and actin filaments of cytoplasm were stained with Rhodamine Phalloidin. (B) Live-dead assay of HDF and HaCaT cells: live cells (green) were stained with Calcein AM dye and dead cells (red) were stained with Ethidium Homodimer.*

2.3.8. *In vitro* cytocompatibility of the nanofibrous mats

MTT assay was carried out to analyse cell proliferation index of HDF and HaCaT cells cultured on the non-functionalized nanofibrous mats. Cell proliferation index was the highest in PVAAA and PVAPR mats and lowest in PVA mat among all samples (**Figure 2.7.A,B**). Significantly higher proliferation of both HDF and HaCaT cells were observed in PVAAA and PVAPR as compared to PVABM, $p \leq 0.01$. There was no significant difference between the proliferation index of control (TCP), PVAAA and PVAPR, which further corroborated enhanced cytocompatibility of the NMSF based mats.

2.3.9. *In vivo* tissue response of subcutaneously implanted nanofibrous mats in mice

Histological examination of the subcutaneously implanted mats in mice for the period of 6 weeks revealed biocompatibility of respective materials (**Figure 2.7.C**). The four types of mats were analysed on the basis of H & E stained microscopic images, semi-quantified according to the ISO-10993-6. As observed by the H & E stained sections, cluster of cells at the interface of PVA mat and host tissue was observed after 2 weeks, which is a characteristic feature of immune cells, suggesting early immune response elicited by the host [64]. Slightly milder immune response was shown for PVABM implant, as similar type of cell invasion was observed at the host-implant interface after 2 weeks (**Table**

2.3.). Macrophages and multinucleated giant cells have this distinct property of attacking foreign material by forming cell cluster at the host-implant interface, which is easily detectable by H & E staining [64, 279]. Such type of immune reaction was not observed for PVAAA and PVAPR after 2 weeks time period, suggesting very mild or undetectable immune response within 2 weeks periods. Further, the implants of PVAAA and PVAPR showed early tissue ingrowth (2 weeks), which were signs of early graft acceptance. Presence of early tissue ingrowth in the implants was majorly due to more fibroblast invasion, initiating the graft remodelling of PVAAA and PVAPR within 2 weeks [64, 279]. Tissue ingrowth was observed after 6 weeks in the implants PVA and PVABM, which showed delayed graft acceptance by the host system. Few blood vessels with supportive fibroblastic structures were observed only for PVAAA and PVAPR. The microscopic images at 6 weeks showed remarkable difference in terms of implant morphology, which was attributed to the graft remodelling done by fibroblast invasion and cellular ingrowth. Early graft take of PVAAA and PVAPR was thus validated by neovascularisation, cellular ingrowth and early graft remodelling, which demonstrated biocompatibility of the material.

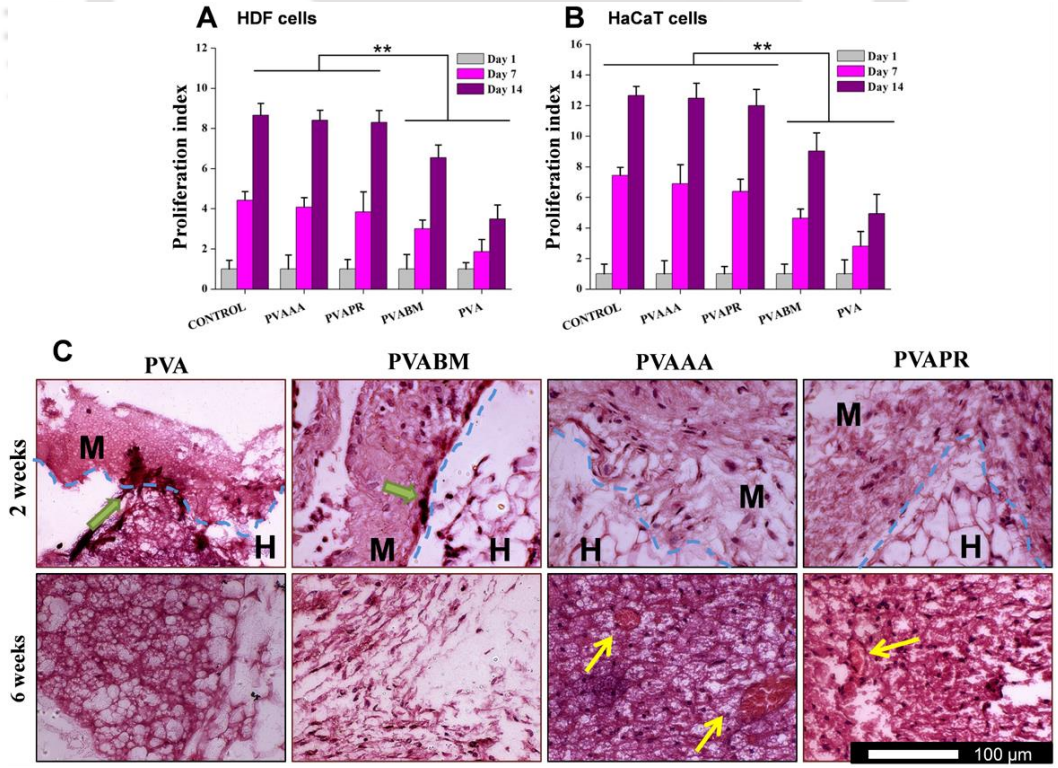

Figure 2.7. *(A, B) Proliferation index of HDF and HaCaT cells on various nanofibrous mats after 1, 7 and 14 days of cell seeding, as determined by MTT assay. Mats containing NMSF have significant difference with mulberry SF blend and PVA, (*p ≤ 0.05, **p ≤*

0.01). (C) Histological analysis of subcutaneously implanted mats by H & E staining after 2 and 6 weeks. Green arrows represent cells trying to invade into the graft at the host-implant interface, where M – Mats (implant) and H – Host tissue. High tissue ingrowth and graft remodelling was observed for PVAAA and PVAPR mats after 2 weeks, which attested their improved biocompatibility and graft take ability as compared to PVA and PVABM. Yellow arrows represent blood vessels, indicating angiogenesis in PVAAA and PVAPR within 6 weeks.

Table 2.3. *Table showing biological response against subcutaneously implanted nanofibrous mats assessed by semi-quantification of histological microscopic images (ISO-10993-6).*

Response	PVA	PVABM	PVAAA	PVAPR
Immune cell infiltration	2	1	0	0
Fibrosis	0	0	0	0
Neovascularization	0	0	2	2
Tissue/cellular ingrowth	2	2	3	3

2.3.10. *In vivo* wound healing activity of nanofibrous mats

Nanofibrous mats (in the form of dressing patch) were applied on full thickness wounds of rabbit model to demonstrate the wound healing activity of various silk-based mats. Gross morphology of wounds treated with various mats are depicted in the images (**Figure 2.8.**). Quantitative measurement of wound area showed different healing profile among various treatments. There was a significant difference in the size of wounds among wounds treated with various nanofibrous mats and control group (surgical gauze). Wound size of control group was similar on day 0 and day 4, suggesting 0 % wound contraction; whereas, the wounds treated with nanofibrous mats began contracting on day 4. Treatment with the dressing patch of PVAAA and PVAPR resulted in 80-88 % wound contraction on day 7. The corresponding values for PVABM, PVA and control were 67.51 ± 3.77 %, 54 ± 4.01 % and 31.81 ± 3.05 % respectively. Higher wound contraction was found for PVAAA and PVAPR than other groups at all the time points with significant difference, $p \leq 0.01$.

Histological examination of the entire wound healing process was performed over a period of 21 days to reveal the healing activity of various dressing patch (**Figure 2.9.**). Nanofibrous mats supported the establishment of haemostasis in the wounds as indicated by the absence of blood cells on day 7 in contrast to the control wounds. Presence of necrotic tissue and less wound contraction till day 7 demonstrated prolonged inflammatory phase of wounds in the control group. Granulation tissue was developed in the wounds within 7 days of injury by all the three hybrid mats and was scored as depicted in **Figure 2.8.C**. Presence of necrotic tissue and absence of granulation tissue on day 7 depicted moderate inflammation in PVA treated wounds, as the proliferation phase did not begin within 7 days. Hence, PVA treated wounds scored ~2 for granulation tissue. Granulation tissue formed by PVABM patch scored low as compared to PVAAA and PVAPR treatments due to relatively thinner granulation tissue and lesser number of blood vessels. Very thick granulation tissue with mature collagen fibres and high number of blood vessels was observed in PVAAA and PVAPR treated wounds on day 7, demonstrating early proliferative stage of wounds and hence scored the highest. A thin epithelial layer completely sealing the wounds was clearly visible in the wounds treated with PVAAA and PVAPR on day 14 (**Figure 2.9.**). The sections depicted a well-formed matrix of dermal structures and different strata of epidermal layers along with budding of collagen fibres and angiogenic points.

Thin epithelial tongue progressing towards the central wound portion was visible on day 14 by PVABM treatment, whereas PVA treated and control wounds were devoid of epidermis on day 14 and demonstrated delayed wound healing. Wounds treated with PVAAA and PVAPR exhibited complete skin regeneration with appendages on the rabbit skin and no sign of wound history on day 21. Epithelial layer regenerated in PVAAA and PVAPR treated wounds on day 21 was significantly thicker than other groups, $p \leq 0.01$ (**Figure 2.8.D**). Overall, wound maturity was scored on the basis of dermal and epidermal regeneration by various treatments as shown in the graph (**Figure 2.8.E**). PVABM presented lower re-epithelialization than PVAAA and PVAPR, but scored higher than PVA and control. Tissue remodelling of healed tissue by PVAAA and PVAPR was validated by the presence of well-formed collagen bundles, skin sebaceous glands, hair follicles, nerve endings and blood vessels on day 21 and hence scored the highest for dermal differentiation and skin appendage formation. PVABM closed the wounds completely by 21 days but appearance of mature collagen bundles and skin

appendages was significantly lower than PVAAA and PVAPR treatments, $p \leq 0.01$. Presence of eschar on wounds till day 14 clearly demonstrated slow healing by PVA and control treatments. PVA mat also failed to regenerate skin appendages and mature collagen fibres by 21 days and hence were scored the lowest, $p \leq 0.01$.

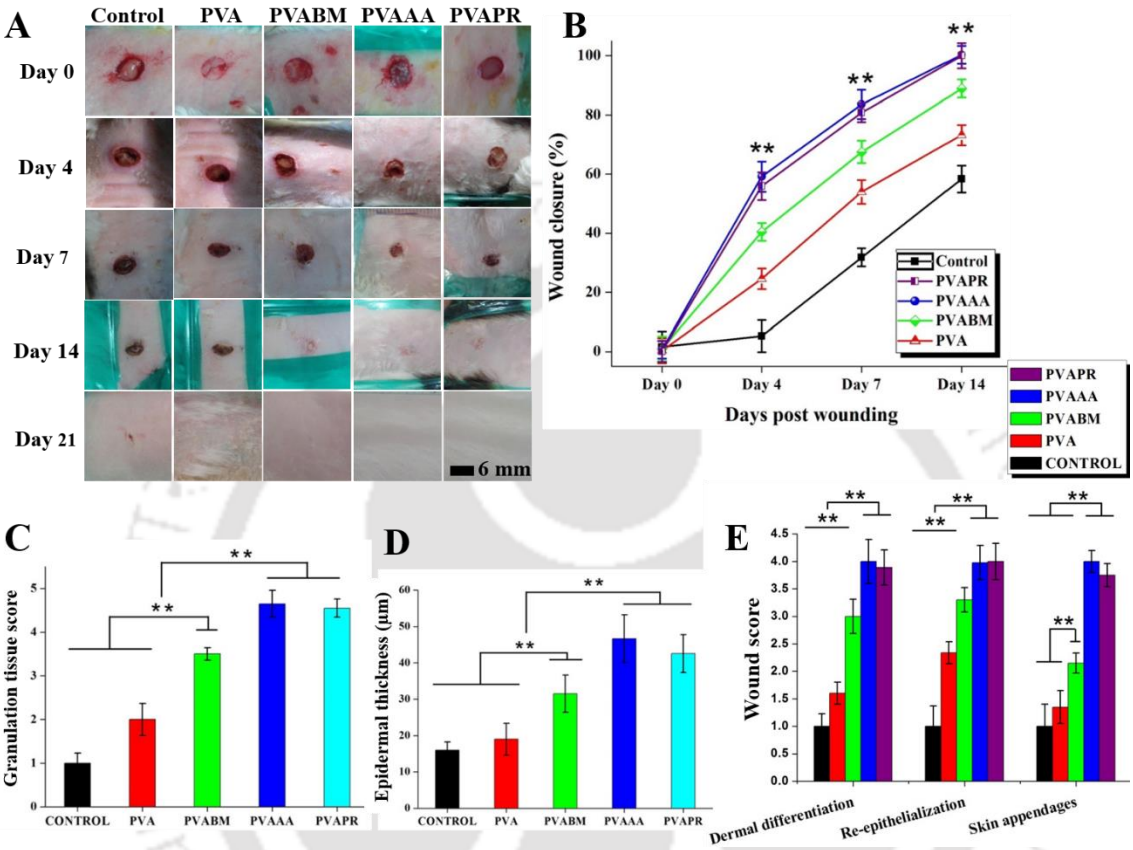

Figure 2.8. *Wound healing profile of the various nanofibrous mats representing (A) Gross images of wounds in rabbit showing extent of wound healing on days 4, 7, 14 and 21. (B) Wound closure percentage determined by calculating the area of wounds on particular time-point using Image J software. (C) Granulation tissue score of wounds on day 7. (D) Epidermal thickness of healed wounds on day 21. Control samples used in the study was surgical gauze bandage. (E) Histology analysis scores of wounds on day 21 in terms of dermal differentiation, re-epithelialization and regeneration of skin appendages, which together represented high wound maturity by PVAAA and PVAPR mats, (*$p \leq 0.05$, **$p \leq 0.01$).*

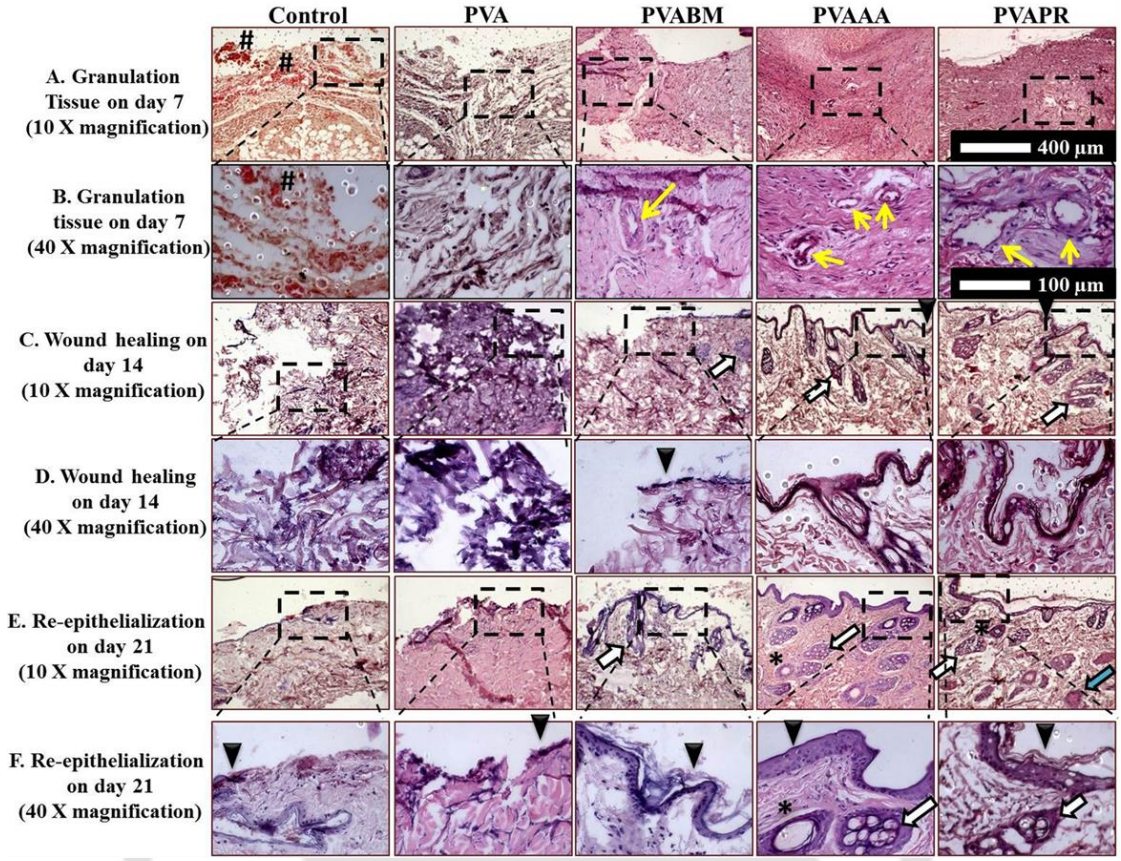

Figure 2.9. *H & E stained sections of wounds on day 7, 14 and 21 by various samples displaying (A, B) Extent of granulation tissue developed by different treatments: absence of the tissue and presence of necrotic tissue on day 7 in control and PVA treated wounds (hash = blood cells). Hybrid mats (PVA-SF) showed development of healthy granulation tissue; among them PVAAA and PVAPR treated wounds developed thicker tissue and more blood vessels as depicted by yellow arrows compared to PVABM. (C, D) Wound healing on day 14 showed complete re-epithelialization by PVAAA and PVAPR, but absence of epithelial layer on PVA and control treated wounds. PVABM showed epithelial tongue growing towards wound, as marked by black arrows. (E and F) Skin regeneration observed in both dermal and epidermal layers on day 21: Dermal regeneration was depicted by mature collagen bundles and skin appendages; epidermal regeneration was depicted by thickness of epithelial layer of skin (black arrowheads = epithelial layer, asterisks = hair shafts surrounded by hair follicles, white arrows = sebaceous glands, blue arrow = nerve ending). Scale bars of 10X and 40X magnified images are 400 µm and 100 µm respectively for all the images.*

2.3.11. Investigation of extracellular matrix deposition

Deposition of elastin and collagen fibres was examined qualitatively and quantitatively to find out the role of various SF based nanofibrous mats in instructing the ECM deposition during the wound healing process. Morphology of elastin fibres secreted in the regenerated skin was demonstrated by staining the elastin fibres with Weigert

Resorcin–Fuschin method after 21 days of treatment (**Figure 2.10.A-E**). The highest elastin secretion was observed in the dermal region of wounds treated with PVAAA and PVAPR, which was obvious due to faster wound healing. Moreover, the elastin fibres were found to be isotropically orientated, as can be clearly seen in the images. Elastin fibres appeared mature, robust and thick distributed all over the dermal tissue healed by NMSF based mats. However, only some young and slender elastin fibres arranged anisotropically were visible in the dermal tissue healed by PVABM mats. PVA treated and control wounds depicted only few slender elastin fibres with high anisotropy and were tightly packed in close association with collagen fibres. Mature elastin fibres were not visible on day 7 and day 14 as the wound healing was in process; however, mesh of thin elastin fibrils was observed in the dermal region of wounds treated with PVAAA and PVAPR on day 14 (**Figure A2.2.**). Quantitative assessment of elastin fibres done using ELISA also supported significant higher elastin deposition in the wound-bed treated with PVAAA and PVAPR, $p \leq 0.01$ (**Figure 2.10.F**).

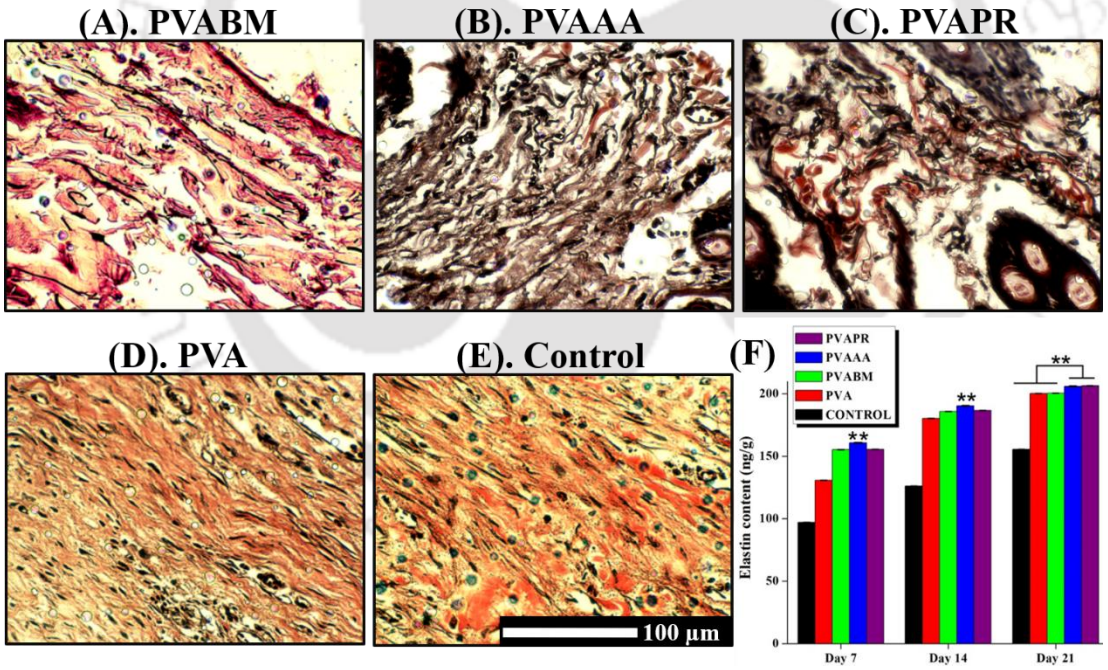

Figure 2.10. *(A-E) Elastin fibres stained by Weigert Resorcin–Fuschin method in the dermal region of regenerated skin by various treatments on day 21 post-wounding. (F) Quantification of elastin on day 7, day 14 and day 21 revealed significantly higher elastin secretion in PVAAA and PVAPR treated wounds than other treatments, (*p ≤ 0.05, **p ≤ 0.01).*

Collagen fibres stained with Masson trichrome in the dermal region of regenerated skin after 21 days were depicted in stained images (**Figure 2.11.A-E**).

Wounds treated with PVABM, PVA and control group showed immature, thin, highly shattered and scanty collagen fibres. However, wounds treated with PVAAA and PVAPR depicted mature and thick collagen bundles throughout the dermal region, which was also responsible for early wound contraction. The collagen bundles were stout, wavy and thick along with moderate inter-collagen gaps exhibiting scar-less healing. Collagen fibres produced in the granulation tissue during the proliferative phase of wound healing (day 7 and day 14) also supported improved healing process in the PVAAA and PVAPR treated wounds on day 14 (**Figure A2.3.**).

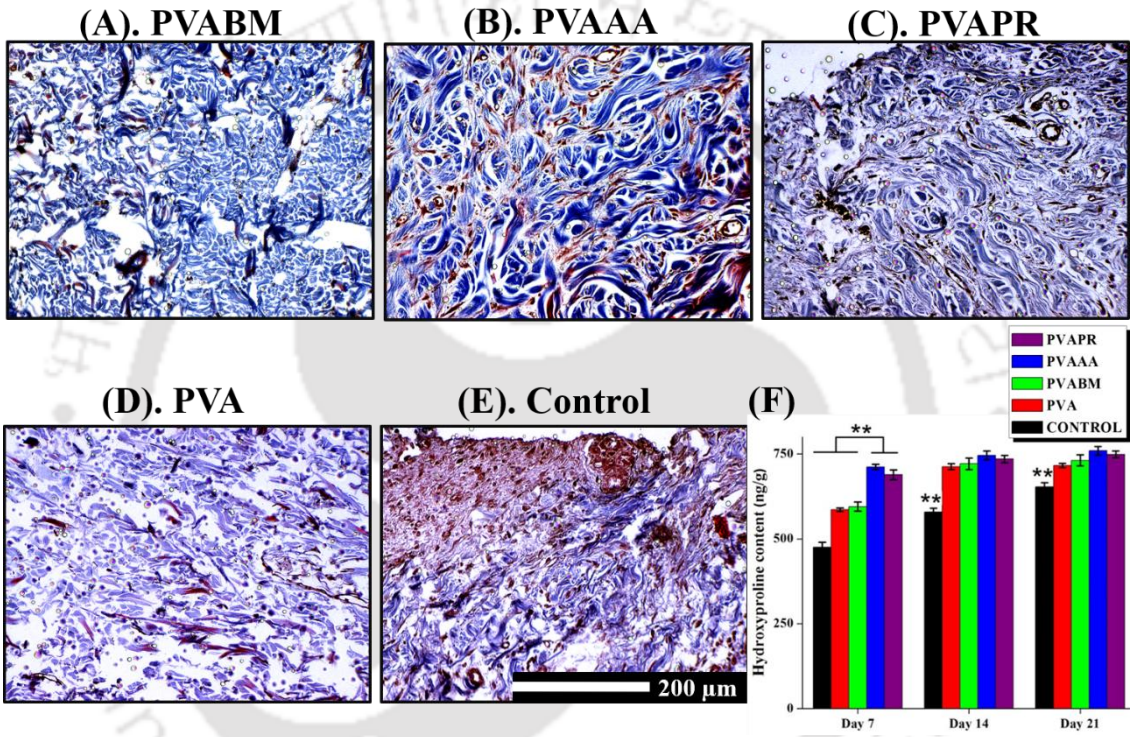

Figure 2.11. *(A-E) Collagen fibres stained by Masson trichrome method in the dermal region of regenerated skin by various treatments on day 21. (F) Quantification of hydroxyproline on day 7, day 14 and day 21 revealed significantly higher collagen deposition in the treated wounds in comparison with control group, (*p ≤ 0.05, **p ≤ 0.01).*

Quantitative assessment of hydroxyproline further revealed significantly higher secretion in the wounds treated with PVAAA and PVAPR on day 7 (**Figure 2.11.F**). However, there was no significant difference in the amount of hydroxyproline produced in the wound beds treated with different types of dressing patches on day 14 and 21 owing to the remodelling phase after day 14. Equivalent secretion of hydroxyproline by PVAAA from day 7 to day 21 attested the influence of AASF to regulate collagen deposition. Sufficient collagen fibres were deposited during the proliferative stage. These

were further re-oriented and modulated during tissue remodelling, which also prevented hyper-deposition of collagen bundles and thereby prevented scarring.

In order to further look into the ECM deposition, qualitative inspection of reticulin fibres was carried out to examine the basement membrane of regenerated skin on day 21 post-wounding (**Figure 2.12.**). Distribution of mature reticulin fibres in the form of whirling threads was found mainly in association with collagenous and fibroblastic stroma underneath epidermis in the wounds treated with PVAAA and PVAPR. Due to non-occurrence of re-epithelialization in all the wounds, typical structure of reticulin fibres were not observed in the tissues on day 7 and day 14 (**Figure A2.4.**). But PVAAA and PVAPR treated wounds exhibited good and mature reticulin fibres in the basement region of regenerated skin, as can be seen on day 21. Whereas, scanty reticulin fibres appeared in the wounds treated with PVABM and PVA even on day 21. Control groups were devoid of reticulin fibres in the basement membrane region after 21 days as the wounds were not completely re-epithelialized.

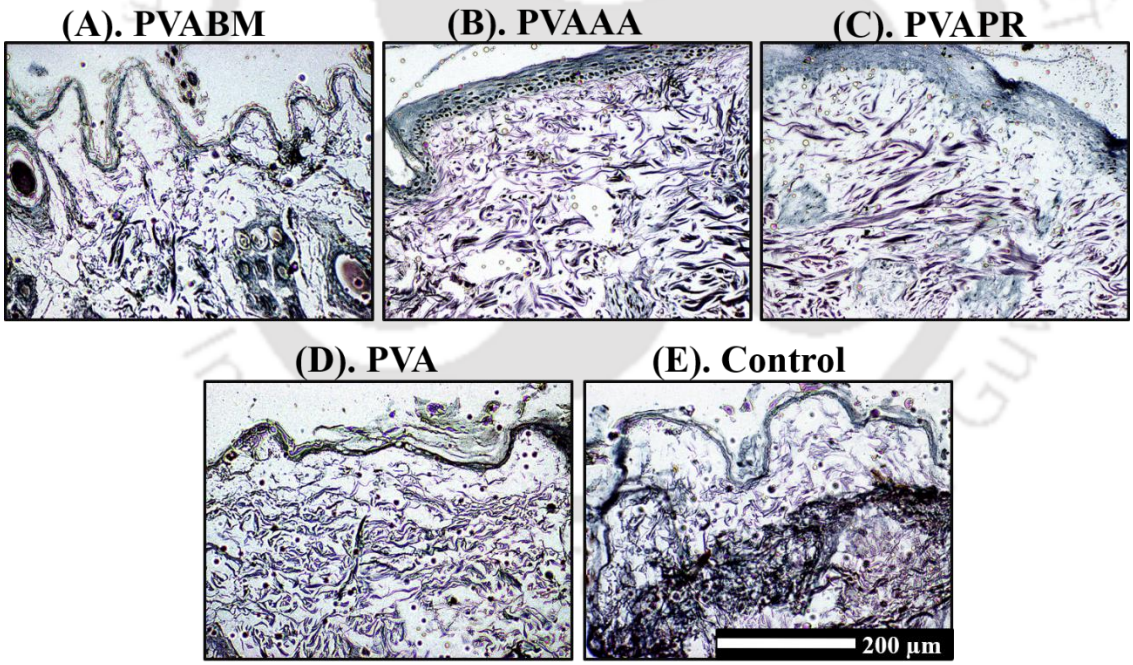

Figure 2.12. *(A-E) Reticulin fibres stained by Gridley silver impregnation method in the basement membrane region of regenerated skin by various treatments as observed on day 21.*

2.3.12. Scar tissue assessment

Histological and gross examination of wounds revealed the morphology of healed tissue after 21 days of treatment. Control and PVA treated wounds were elongated in shape, as

can be seen by the gross images of wounds (**Figure 2.8.A**). Interestingly, wounds treated with hybrid mats retained the round shape representing correct regeneration pattern of the growing dermal and epidermal tissues. PVAAA and PVAPR supported complete regeneration of the skin. Skin appendages like sebaceous glands, hair follicles, nerve endings were absolutely absent, suggesting development of scar tissue for the PVA and control treatments; whereas hybrid mats showed presence of mature skin appendages by day 21 (**Figure 2.9.**). PVAAA and PVAPR exhibited significantly greater number of skin appendages compared to PVABM, $p \leq 0.01$ (**Figure 2.8.E**). Elastin fibres interwoven between collagen bundles showed anisotropy in control wounds and the wounds treated with PVA and PVABM on day 21, representing formation of a scar tissue (**Figure 2.10.**). Presence of isotropic and mature collagen bundles with moderate inter-collagen gaps suggested loosely packed irregular collagen fibres after 21 days, which provided clues of scar-less healing outcomes by PVAAA and PVAPR (**Figure 2.11.**).

2.4. Discussion

Promotion of wound healing, repairing of the detrimental wound microenvironment and alleviation of infection and inflammation are the key parameters to evaluate wound dressing material [266]. Moreover, for complete repair and regeneration of injured tissue, it should also stimulate other aspects of wound healing process. Regulation of ECM deposition is of utmost importance for structural and functional regeneration of skin [6]. Adequate secretion of major ECM components (collagen and elastin) and their orientation decide the fate of healing tissue [265]. Our approach for aesthetic wound repair is to use biomimetic and physicomimetic materials, which promote cell-material interactions and concomitantly regulate the ECM deposition along with accelerated wound healing. In the present study, we mimicked the tissue matrix both biologically and physically by fabricating NMSF based electrospun mats functionalized with EGF and antibiotic. Presence of inherent RGD motifs in biomaterial (also a hallmark feature of our NMSF based dressing patch) offers functional advantage of cell recruitment to accelerate the wound healing process [26, 214]. PVA, an FDA approved polymer (GRAS notice no. GRN 000141) was used as a base material to provide optimum viscosity for electrospinning (**Table 2.2.**) and to render structural support in highly proteolytic wound environment. PVA fetches its application in wound dressing material for its non-toxicity,

non-immunogenicity, non-carcinogenicity, low cost, water-solubility, durability, high swelling capacity and high elasticity [100, 275, 280, 281].

The natural ECM architecture was mimicked by PVAAA and PVAPR due to heterogeneous size distribution of nanofibres (**Figure 2.1.A,B**). Morphological differences among the four different mats were due to different stretching force and uneven evaporation of different solutions. More hydrophilic domains in PVA and PVABM solutions led to the formation of homogeneously distributed nanofibres due to same stretching force throughout the solution [226, 281]. Presence of more hydrophobic domains such as polyalanine stretches (AA)n along with hydrophilic amino acid residues in the non-mulberry silk fibroin solution imposed varied stretching forces responsible for heterogeneous size distribution in PVAAA and PVAPR [226]. Heterogeneity in size of nanofibres ranging from 50 to 300 nm in PVAAA and PVAPR was comparable to the natural collagen fibrils (10 to 300 nm) present in ECM, which created desired environment for more cell recruitment [262, 282]. From the FTIR spectra recorded for various mats (**Figure 2.1.C)**, characteristic bands of both PVA and SF ensured homogeneity of both the materials throughout the hybrid mats. υO-H stretching showing broadened band at 3600-3000 cm^{-1} in the spectra of hybrid mats revealed the intermolecular hydrogen bonding between neighbouring molecules, indicating possible cross-linking between PVA and SF [281]. Other intermolecular interactions like hydrogen bonding between hydroxyl groups of PVA with carboxylic groups of SF and peak broadening at 1085 cm^{-1}, suggesting ester bonds that also signified homogenous blending between both the polymers throughout the mats [276].

The dressing patch should be soft, flexible, comfortable and mechanically strong enough to prevent further mechanical damage to the injured tissue [283]. The mechanical properties of biomaterial also influence cellular response, as the cell-matrix interactions are dependent on the extrinsic shear force and mechanical signalling pathways, which regulate cellular migration, proliferation and differentiation [262, 284]. A study reported YM of stratum corneum layer of human skin to be 2.6 ± 0.6 MPa and combined stiffness of epidermis and stratum corneum to range between 1 and 2 MPa [285]. YM of NMSF based mats being very close to that of reported value of skin holds great potential to provide similar biomechanical signals (**Figure 2.2.D**). The hybrid mats were comprised of nanofibres of various sizes, due to which they were unable to distribute the force uniformly and hence exhibited reduced tensile strength. Whereas, higher UTS and YM

of PVA mat was found owing to the homogenous distribution of force throughout the mat, as all the nanofibres were of same size, allowing uniform force to all the nanofibres and thereby strengthening the overall mat. A study showed reduced tensile strength of PVA-BmSF blended films compared to the PVA films owing to the heterogeneous pore size and pore distribution in the blended films [100]. Current wound dressings made up of collagen, elastin, chitosan, PGA and PLA have good biocompatibility but their poor mechanical properties make them succumb to external forces particularly during wound contraction [282, 283].

High stretching ability and optimal degradability of a dressing material are critical aspects to prevent the disruption of wound-bed during wound contraction and retention of structural integrity to facilitate the barrier functions [92]. Higher elongation at break point of PVAAA and PVAPR was due to greater unfolding of amorphous random coils present in non-mulberry SF protein [214]. Resistivity of PVA towards *in vitro* proteolytic digestion offered stability to the hybrid mats and allowed slow biodegradation of nanofibres (**Figure 2.3.**). A study conducted on biodegradation of PVA proved it a stable polymer and showed its degradation only by the free radical reactions induced in the presence of specific bacteria and fungi present in soil [280, 286]. *In vivo* stability of 2 years has also been reported for PVA hydrogels implanted in rabbits in the form of artificial meniscus [280]. Protease XIV was chosen in the present study, as it has been proven to cleave the SF protein non-specifically at multiple locations [47, 287]. More than 20 % degradation of the hybrid mats after 14 days was due to the proteolytic digestion of silk fibroin protein, which resulted in broken inter- and intra-molecular interactions between PVA-SF. Bigger pores and broken fibres revealed structural modulations of the hybrid mats. The FESEM images were indicative of the plausible altered morphology of the mats under rich proteolytic environment of chronic wounds.

The NMSF based mats acted as moist dressings due to their high water retention capacity for longer time period (**Figure 2.4.C-E**). Hydrated dressings have been shown to promote wound healing by rapid re-epithelialization and normal ECM deposition due to enhanced cellular movements in moist microenvironment [266, 288, 289]. In contrast to dry dressings, moist dressings also contribute to autolytic debridement of wounds by absorbing wound exudates and rehydrating the dried devitalized tissues [266, 288]. According to a study conducted by Queen *et al.* (2007), WVTR of injured skin ranged from 279 to 5138 g m^{-2} day^{-1} depending on the wound type and extent of loss of skin

[278]. Dressings with very high WVTR (~5000 g m^{-2} day^{-1}) might dry the wound bed quickly and make it necrotic; while occlusive dressings with very low WVTR (~300 g m^{-2} day^{-1}) might accumulate exudate fluid due to low moisture permeation and make the wound bed prone to infections. Both the extreme cases delay wound healing process and hence the mid-range WVTR value (2000 to 2500 g m^{-2} day^{-1}) was recommended for an ideal wound dressing material [288-290]. The nanofibrous mats in our study showed WVTR value in the mid-range, further forwarding their candidature as ideal wound dressing material. The nanofibrous mats were semi-occlusive in nature, as they allowed gaseous exchange but did not allow fluid drainage.

Trillions of different kinds of micro-organisms present on skin surface constitute the skin microbiome, which become active pathogens during skin injury and colonize the wounds [288, 291]. Chronicity of wounds is also associated with bacterial infections [288]. Hence, antibacterial property of a dressing patch is very crucial to treat infected wounds. Ciprofloxacin was coated on the nanofibrous mats because of its broad-spectrum activity against a variety of gram positive, gram negative bacteria and Methicillin-resistant *Staphylococcus aureus* (MRSA) [267, 292]. This drug is also considered as the gold standard for treating skin and eye infections [293]. High burst release of the drug from mats was easily achieved to kill pathogens at the initial step of treatment (**Figure 2.4.A**). Similar trend of drug release behaviour from the antibiotic coated nanofibrous mats was due to weak interactions between the drug molecules and processed mats. *In vitro* antibacterial property of the mats against the four major skin infecting bacteria for three days ascertained the active state of the drug and antibacterial properties of the mats (**Figure 2.4.B**). Thus, the silk based nanofibrous mats demonstrated essential physical properties of a wound dressing patch like optimal mechanical properties, slow biodegradability, structural integrity, high swelling capacity, moderate water vapour permeability, antibacterial activity and sustainable drug delivery [263, 264].

High proliferation of skin cells (HDF and HaCaT) on the novel NMSF based blends not only established the latter's cytocompatibility but also vouched for their aptness for wound healing applications (**Figure 2.5.B,C**). Microscopic images also revealed clumped and spherical morphology of cells, suggesting their incapability to spread and proliferate on PVA mat (**Figure 2.6.**). Poor *in vitro* cell proliferation and *in vivo* cell infiltration on PVA mat demonstrated the impact of silk fibroin on cellular

response. Significantly higher proliferation index of HDF and HaCaT cells on NMSF based mats validated their biomimetic and physicomimetic features **Figure 2.7.A,B**) [294]. Minimal inflammatory response and early tissue ingrowth in the implants showed *in vivo* biocompatibility of the NMSF based mats when implanted subcutaneously **(Figure 2.7.C)**. Minimum immune response against the material is a pre-requisite for efficient tissue repair. Signs of angiogenesis on PVAAA and PVAPR implants attested biocompatibility of NMSF based mats and early graft acceptance.

Biological and structural modulations of the implants shown after 6 weeks revealed their capability of being remodelled by the activity of infiltrated fibroblasts. Poor fibroblast recruitment on the PVA implant was supported by the low cell proliferation index (MTT assay). Spread out morphology of cells on PVAAA and PVAPR mats proposed better cellular adhesion, indicating strong cell-material interactions owing to the presence of cell-recognition motifs (RGD) present in NMSF [214]. Greater number of arginine (R) motifs present in non-mulberry silk fibroin might also be responsible for higher cell adhesion and proliferation [214, 265]. *Gupta et al.* (2015) did extensive study on AaSF and categorized the non-polyalanine regions of AASF into arginine rich 'R-motifs' and Glycine rich 'G-motifs' [214]. They found out that the crystalline core of heavy chain of AaSF protein contains 17 R-motifs, which is the highest number reported till date among all saturniid silk varieties [214]. R-motifs are relatively very low in BmSF protein compared to AaSF and PrSF (BmSF=0.6%, AaSF=3.9% and PrSF=3.81%) [214, 295]. Electrostatic attraction between positively charged guanidine group of R amino acid and negatively charged phosphate group of cells facilitates cell-material interactions [265]. Guanidine head group of Arg are also known to mediate hydrogen bonding between the material and lipid-phosphate group of cell membrane [183]. All these factors could have possibly enhanced the interactions between cells and the NMSF based mats and thereby, recruitment of more cells to the wound bed was easily achieved.

Natural ECM is a reservoir of numerous growth factors, which is lost in the highly proteolytic environment of chronic wounds [296]. Functionalized nanofibres with EGF (on the surface and trapped inside) re-established the growth factor pool through sustained release. Sequestration of the EGF within the nanofibrous mats masks the former's degradation in the proteolytic environment of chronic wounds [297]. Among all growth factors, we selected EGF in the present study as a model molecule for

assessing wound healing of full-thickness excisional wounds in rabbits. However, for treating specific types of wounds, relevant growth factors may be loaded to develop wound-specific dressing. For example, platelet derived growth factor (PDGF) and fibroblast growth factor (FGF) known to treat diabetic chronic wounds can be loaded in the dressing patch specific for diabetic cutaneous ulcers [184]. EGF is the common growth factor supplement to treat all types of cutaneous wounds because of its highest potency to stimulate re-epithelialization and keratinocyte migration [298]. EGF also plays a major role in granulation tissue formation, wound contraction, cell migration, cytokine production, collagen secretion, nitric oxide suppression and maintenance of tensile properties, which altogether help in accelerating the wound healing process [7, 173, 183, 297, 298].

Complete release of EGF was not observed. This might be due to its loss during electrospinning and further processing of mats [182]. The sequestration within the mats as mentioned previously might be another hindrance to the complete release of EGF [182]. Dissimilar release profile of EGF from different mats was indicative of differences in interactions of the growth factor with the respective material. PVA and PVABM, being more hydrophilic in nature might exhibit more interactions with hydrophilic EGF [226, 281]. Higher EGF release from PVAAA and PVAPR mats suggested weaker interactions of EGF with both the blends owing to the hydrophobic nature of NMSF [226]. Diffusion of EGF from internal nanofibres *via* nano and micro pores might be responsible for the sustained release behaviour [182]. Due to differences in the fibre distribution and overall morphology of nanofibrous mats, release pattern might further be influenced. However, the observed *in vitro* release profile of EGF may not represent the actual *in vivo* picture. This may be corroborated with the various hydrophobic, electrostatic and non-covalent interactions in the wound microenvironment. Higher cellular proliferation and accelerated wound healing process assisted by the NMSF based mats were due to the synergistic effect of higher EGF release and bio-physicochemical resemblance with ECM. Comparable results were also seen in the work done by Schneider *et. al* (2009), where 3.5 fold higher wound contraction was observed in functionalized silk nanofibrous mats due to 20-25 % release of EGF over a period of 7 days [182].

Faster wound healing rate by NMSF treatment was clearly demonstrated by the gross wound images **(Figure 2.8.)**. Sequential examination of the four phases of wound healing further validated accelerated *in vivo* wound healing due to NMSF based dressing

patch (**Figure 2.9.**). Nanofibrous mats supported the establishment of haemostasis in the wounds, as indicated by the absence of blood cells in contrast to the control wounds. Presence of necrotic tissue and less wound contraction till day 7 demonstrated prolonged inflammatory phase of wounds in the control group. Development of granulation tissue in the wounds treated with PVAAA and PVAPR demonstrated early proliferative stage of wounds within 7 days. Early granulation tissue development also signified autolytic debridement of wound exudates, prevention of tissue necrosis and relatively very short inflammatory phase, which were not observed.

Timely cell recruitment, cell infiltration, and vascularization during the proliferation phase is the prerequisite for wound healing [261]. Secretion of various ECM components in the proliferation phase develops a provisional matrix for recruiting various cells. Healing of most of the chronic wounds is challenged due to failure to form the provisional matrix [266]. Fibronectin is the key matrix component that is present in all the phases of wound healing and plays a major role of cell recruitment [26]. Among all cell adhering motifs, RGD motifs facilitate cell-matrix adhesion *via* integrin binding, stimulate certain intracellular signalling pathways and cell recruitment [299, 300]. Interaction of integrins of fibroblasts, keratinocyte and endothelial cells with the RGD motifs of fibronectin is involved in wound contraction, re-epithelialization and angiogenesis respectively [301]. Sutures developed from *A. assama* fibres also promoted healing of incisional wounds in rabbit model in a study [302].

Superior cytocompatibility for endothelial cells was also observed for artificial blood vessels made of non-mulberry silk fibroin protein in a recent study, which further confirmed enhanced recruitment of endothelial cells by NMSF mats [226]. The NMSF based mats containing inherent RGD motifs and incorporation of EGF might mimic the whole mechanism and recruited all types of cells as evidenced by the development of healthy granulation tissue, early re-epithelialization and more vascularization (**Figure 2.9.**) [8, 301]. Faster wound closure rate by PVAAA and PVAPR might be attributed to the synergistic effect of the following factors – (1) unique morphology and topography of nanofibres mimicking the ECM structure, (2) quick re-establishment of EGF pool by higher release profile, (3) high Arg content in NMSF and (4) enhanced cell-material interactions and cell recruitment due to the presence of cell binding 'RGD' motifs [214, 282, 300].

The final phase of wound healing is the tissue remodelling phase, which involves modulation and re-arrangement of matrix components [303]. Events occurring in this phase decide the fate of regenerated tissue. Isotropic and loose orientation of collagen fibres in the ECM lead to regeneration of normal and functional tissue [304]. On the contrary, excessive and aligned deposition of collagen fibres lead to the formation of less-functional scar tissue [304]. Scar formation is common after wound healing by aligned deposition of collagen fibres due to lack of functional support and delayed wound healing [305]. Scar tissues only provide barrier function to the skin; other skin functions are lost due to failure to regenerate skin appendages like hair, sebaceous glands and nerve endings [261]. Presence of all such skin appendages in the histological images of healed tissue treated by hybrid mats on day 14 and day 21, clearly suggested normal skin regeneration without scars (**Figure 2.9.**).

Hypertrophic scar tissues are devoid of elastin fibres and mostly contain packed collagen fibres [306]. Abundant elastin fibres on day 21 in the dermal matrix attested scar-less healing by hybrid mats (**Figure 2.10.**). Random orientation of elastin fibres (conferring elasticity) help the skin to remain in its normal configuration after being deformed [306]. Wounds treated with hybrid mats retained the round shape, which also attested normal deposition and isotropic orientation of collagen fibres as compared to the elongated shape of wounds treated by PVA mats and control group. Control wounds demonstrated the lowest elastin content among all the groups. Studies on the anti-scar properties of EGF reported remodelling effect of EGF on collagen type I and hence it can be said that presence of EGF during the tissue remodelling process helps in the degradation of collagen type I and thereby prevents scar formation [307]. Some studies have also shown that EGF lowers down the expression of transforming growth factor (TGF-β), which has been found to produce scarring effect in wound healing [305]. Increment in the mechanical strength of skin by EGF has also been reported [75]. Hence, sustained EGF release from the mats might have also contributed to tissue remodelling phase.

Equivalent secretion of hydroxyproline by PVAAA from day 7 to day 21 attested the influence of AASF to regulate collagen deposition (**Figure 2.11.**). PVAAA and PVAPR demonstrated high degree of remodelling in reticulin deposition as well (**Figure 2.12.**). Reticulin fibres are uniform collagen type III fibrils, which get deposited as meshwork in association with other types of collagen fibres between the epidermis and

the basement membrane [308]. Sufficient collagen fibres were deposited during the proliferative stage. Another study forwarded poly-L-arginine based biomaterials as instructive substrates for fibroblast-driven collagen orientation and deposition [265]. High Arg content in PVAAA and PVAPR may be projected as a possible reason for normal ECM deposition and tissue remodelling. Presence or absence of RGD motifs in fibronectin has been shown to directly influence the amount of ECM synthesis [309]. Normal deposition of mature collagen, reticulin and elastin fibres in PVAAA and PVAPR treated wounds on day 21 was the distinctive feature of tissue remodelling phase. The heavy chains of AaSF containing crystalline core of many Arg motifs was capable of directing the orientation and deposition of ECM fibres. Role of AaSF in guiding the ECM deposition was clearly noticeable by the normal appearance of collagen, elastin and reticulin fibres.

Accelerated wound healing process by NMSF based mats was confirmed by faster wound healing, early re-epithelialization, dermal regeneration, vascularization, secretion and regulation of ECM constituents like reticulin, collagen and elastin. Among all the four types of mats, both PVAAA and PVAPR (NMSF based mats) showed better wound healing, as there were no significant differences between them. The results indicated that nanofibrous mats containing NMSF are endowed with greater wound healing potency as compared to the mulberry counterpart. Thus, NMSF based mats hold immense potential to be used as dressing patch for aesthetic wound repair and skin regeneration. Study on additional wound models may be required to further check potential of the dressing patch on various types of chronic wounds. The rabbit model used in the present work does not perfectly imitate the human system; hence, further human trials may be conducted to translate the product from the bench to bed-side.

2.5. Significant findings

The salient findings of this chapter are as follows:

1. Electrospinning technique is a facile approach for fabricating nanofibrous mats, as it provides benefit in large scale production of various silk fibroin matrices. The inherent properties of nanofibres such as large surface area to volume ratio, nanofibrous architecture and semi-occlusive properties offer additional advantage to such matrices for wound dressing applications.
2. The silk nanofibrous dressings hold ideal physico-chemical properties like nanoscale surface properties, high swelling capacity, sufficient water vapour transmission rate, integral stability and necessary mechanical properties. All these properties benefit the wound healing process.
3. Exploration of other silk varieties in wound healing applications unfolded regenerative properties of non-mulberry silk category, especially *A. assama* silk, which contains inherent cell binding domains and arginine rich cores, which together promoted accelerated wound repair process.
4. Drug incorporation and release parameters investigated using EGF and ciprofloxacin antibiotic drug revealed slow and sustained release profile of bioactive molecules. The study opened up new avenues in drug delivery applications using nanofibrous patch.
5. *In vitro* cell culture study on various silk mats demonstrated enhanced cell attachment and proliferation on the NMSF variety owing to the presence of inherent RGD sequence. Thus, the mats can be considered as a potential candidate to be used as an alternative substrate for cell culture matrices.
6. Finally, application of silk mats in the form of wound dressing in acute wounds illustrated their healing efficacy *in vivo*. The results revealed accelerated wound healing and higher wound maturity by NMSF mats as compared to BmSF based mats. Presence of skin appendages and isotropic collagen fibres in the regenerated skin demonstrated scar-less healing and aesthetic wound repair owing to the unique cell interacting peptides present in NMSF.

Our effort on developing silk-based wound dressings by exploring various silk fibroin varieties resulted in understanding the inherent regenerative properties of silk proteins.

The chapter presents a promising strategy to produce nanofibrous silk matrices that can be fortified with antibacterial properties and growth factor functionalization. In particular, it would be interesting to validate the scarless healing outcomes in large animal models like porcine system, which closely mimics the conditions of human system. In concurrence with this preliminary study, the next chapter illustrates the potential of the same materials in chronic wound model, thereby validating the regenerative properties of developed wound dressings for treating diabetic wounds.

भारतीय प्रौद्योगिकी संस्थान गुवाहाटी
Indian Institute of Technology Guwahati

Chapter 3

Functionalization of silk based nanofibrous dressings for treating diabetic wounds

This chapter explores the potential of various bioactive molecules along with further elucidating the efficacy of non-mulberry silk in healing chronic diabetic wounds. The release profile of additive molecules from various silk-based dressings are examined to understand the delivery mechanism from nanofibrous mats. Further, investigation of key events like angiogenesis, re-epithelialization and tissue remodelling of wounds are illustrated in detail.

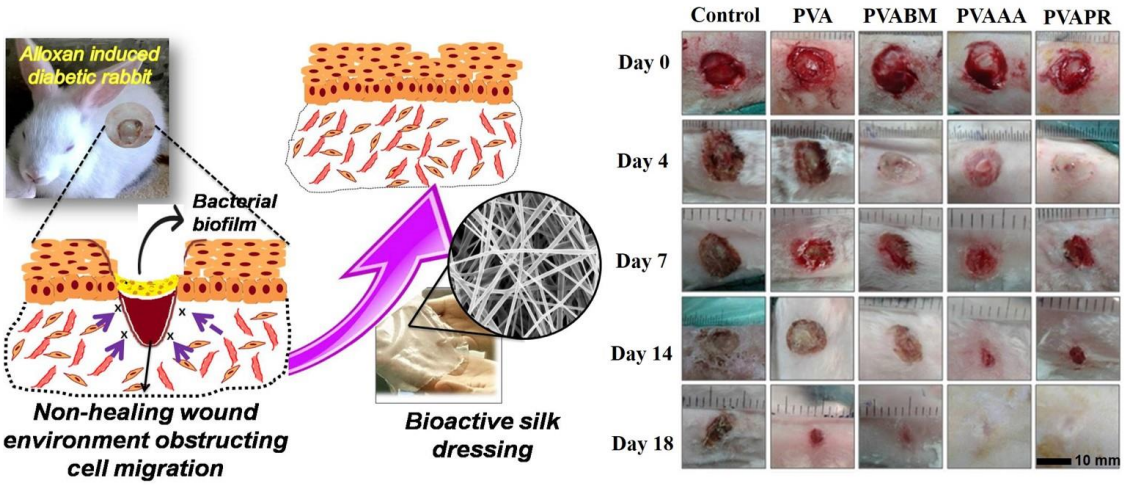

The work embodied in this chapter is published:
Chouhan D, Janani G, Chakraborty B, Nandi SK, Mandal BB. Functionalized PVA-silk blended nanofibrous mats promote diabetic wound healing via regulation of extracellular matrix and tissue remodelling. *Journal of Tissue Engineering and Regenerative Medicine* 2018; 12: e1559-e70.

ABSTRACT

Chronic cutaneous ulcers, a complex pathophysiological diabetic condition, represent a critical clinical challenge, in the current diabetes mellitus pandemic. Consequently, there is a compelling need for bioactive dressings, which can trigger healing processes, and secure quick and complete wound repair. Silk fibroin (SF), a natural protein polymer from mulberry and non-mulberry silkworms, has properties that support accelerated wound healing rate. SF from non-mulberry variety possesses additional cell-binding motifs, which offer added cell material interactions for rapid healing. This study is aimed to investigate wound healing efficacy of various SF varieties in Alloxan induced diabetic rabbit model. Dressings using nanofibrous mats were developed, and functionalized with two types of growth factors and an LL-37 antimicrobial peptide. Non-mulberry SF (NMSF) based dressings healed the wounds more rapidly, in comparison to the mulberry *Bombyx mori* SF (BmSF) counterpart. Post 14 day of operation, wound closure by NMSF dressing was higher than BmSF dressing (85-90 % vs. 73-77 % respectively; $p \leq 0.01$). Granulation tissue development, angiogenesis and re-epithelialization observed earlier in NMSF treated wounds, exhibited accelerated wound healing capacity. Investigation of MMP gene expression, and collagen proteins for 21 days, affirmed higher extent of tissue remodelling in the healed skin. Furthermore, there was an organized ECM deposition (collagen type I, type III, elastin and reticulin) and higher wound breaking strength (~ 60 %), compared to 20 % in control group after 4 weeks. These results validated the potential of NMSF based dressings to influence ECM deposition and tissue remodelling, even under diabetic conditions.

3.1. Introduction

Wound healing is a complex dynamic process involving numerous cell types and bioactive factors. Both these factors, guide four sequential phases of the wound healing process, namely, haemostasis, inflammation, cell proliferation and tissue remodelling [8]. Detrimental alterations in any of the wound healing phases often lead to wound chronicity. Diabetic foot ulcers (DFU) is a perfect example of chronic wounds, aggravated by their hyperglycaemic environment [12]. A large population is suffering from diabetes mellitus worldwide, and the number is expected to rise to 439 million by 2030 [310]. The pathological conditions associated with diabetes mellitus severely impair the normal healing process due to cell senescence, bacterial colonization and persistent inflammation [12]. Upregulated Matrix Metalloproteinases (MMPs) secretion, matrix instability and lack of growth factors, further prevent cellular migration. The hyperglycaemic state of the wound fluid also alters the morphology of keratinocytes, thus hindering re-epithelialization of wounds [8, 12].

Bioactive factors like growth factors, cytokines and antimicrobial peptides (AMPs) are normally secreted from a variety of cells, subsequent to skin wounding in normal physiological conditions [7, 311]. In contrast, chronic wound fluid lacks these biomolecules, either due to their degradation by higher MMP secretion, or through failure to recruit cells towards the wound [12, 296]. Among the numerous growth factor, epidermal growth factor (EGF) and basic fibroblast growth factor (bFGF) play major roles in wound repair, as they stimulate and enhance cell proliferation and migration [7]. AMPs, like LL-37 (the only cathelicidin peptide found in humans), concurrently prevents pathogenic attacks and stimulates wound healing, by promoting cell migration [311]. Several strategies have been developed to treat hyperglycaemic wounds by targeting single or multiple pathways. For example, commercially available Regranex gel containing platelet derived growth factor (PDGF), aims at achieving higher cell proliferation rate to accelerate healing of chronic wounds [8].

Preventing infections in the diabetic wounds using silver-based dressings is another concurrent approach [312]. Sustained growth factor delivery *via* nanofibrous matrices, is an emerging technique to treat diabetic wounds, where researchers have used a variety of biomaterials [173]. Unfortunately, as evidenced from poor clinical outcomes, none of these techniques offer holistic options, that stimulate all the four phases of

healing process for complete wound repair. The dynamic nature of wound healing process can be easily modulated through instructive extracellular microenvironment [303]. The substrate or dressing material, plays a central role in deciding the fate of wound healing, through cell-material interactions that spatially and temporally direct cellular behaviour [265, 303]. Hence, natural cues administered by dressing material, are vital for effective cellular mobilization and recruitment towards the wound bed. Our approach is to develop wound dressing, using natural biomaterial, which simultaneously accelerates wound closure rate, and influences cells to remodel the ECM.

Silk fibroin (SF), from both mulberry and non-mulberry varieties, has been extensively explored in wound healing applications. Its biocompatible, non-immunogenic, biodegradable and mechanically robust qualities, can be easily tailored to the desired biological response [22, 23, 313]. SF from non-mulberry silkworms *Antheraea assama* (AaSF), and *Philosamia ricini* (PrSF), possess Arginine, Glycine and Aspartate (RGD) motifs that act as cell-binding sites; which are absent in mulberry SF (*Bombyx mori*) [24]. In our previous study, we observed faster and scar-less healing of acute wounds by nanofibrous mats made up of NMSF blended with poly(vinyl alcohol) (PVA) as compared to mulberry SF blend [314]. The present study focuses on the role of various silk based nanofibrous mats, incorporating EGF, bFGF and LL-37; to evaluate their competence in healing of diabetic wounds. The four types of functionalized dressings developed are: PVA, PVABM (PVA +*B.mori* SF), PVAAA (PVA + *A. assama* SF) and PVAPR (PVA + *P. ricini* SF). Assessing the potential of NMSF based dressings (PVAAA and PVAPR) for remodelling of tissue during the healing process is central to our focus. The nanofibrous format was chosen to mimic the natural ECM; the former acts as a provisional matrix, and a conduit for sustained growth factor delivery in the healing process. Herein, wound healing efficacy of various nanofibrous dressings was determined by applying them on cutaneous wounds of Alloxan induced diabetic rabbits.

3.2. Materials and methods

3.2.1. Preparation of silk fibroin solutions

B. mori silk cocoons were used to isolate silk solution as described in the standard protocol [215]. Briefly, the pieces of cocoons were degummed twice in boiling water containing 0.02 M sodium carbonate (Merck, India) for 15 min. The dried silk fibres were then dissolved in 9.3 M lithium bromide solution (Sigma Aldrich, USA) at 60 °C for 4 h to obtain *B. mori* silk fibroin (BmSF) solution. This was subsequently dialyzed against Mili-Q water using a 12 kDa cellulose dialysis membrane (Sigma Aldrich, USA) for 3 days. Concentration of aqueous BmSF solution thus obtained was measured by gravimetric method, and was further diluted to 3 % (w/v) by adding water. SF solutions from non-mulberry variety were extracted directly from the silk glands of *A. assama* and *P. ricini* silkworms respectively according to previously described protocol [227]. Briefly, the 5^{th} instar larvae were sacrificed and SF protein was extruded out by squeezing the silk glands using forceps. The SF protein was then dissolved in 1 % (w/v) aqueous sodium dodecyl sulphate (SDS) (Himedia, India) solution. This was further dialyzed against distilled water using 12 kDa dialysis membrane for 4 h at 4 °C to get 3 % (w/v) respective SF solutions.

3.2.2. Fabrication of functionalized nanofibrous mats using electrospinning

Electrospinning instrument (E-spin nanotech, India) was used to fabricate four types of nanofibrous mats as already mentioned in the previous chapter [314]. Functionalization of the nanofibrous mats was achieved by the addition of 0.5 µg/mL human recombinant EGF (Sigma Aldrich, USA), 0.5 µg/mL human recombinant bFGF (Sigma Aldrich, USA) and 50 µg/mL LL-37 full length human antimicrobial peptide (M.W. 4493.37 Da) (NeoScientific, USA) to the SF solution prior to blending it with PVA. Similarly, EGF, bFGF and LL-37 loaded pristine PVA mat was also fabricated by directly mixing the peptides in 8 % (w/v) PVA solution prior to electrospinning. Concentrations of the three peptides were kept similar for all the four types of nanofibrous mats: one pristine mat of only PVA solution (PVA) and three hybrid mats from the blends of PVA and SF – PVA + *B.mori* (PVABM), PVA + *A. Assama* (PVAAA) and PVA + *P. ricini* (PVAPR). β-sheet in the hybrid electrospun mats were induced by keeping them in a vacuum desiccator saturated with 70 % ethanol vapours for 6 h. Functionalized nanofibrous mats thus fabricated have been used in all further experiments and referred to as nanofibrous

mats or mats in the text. Morphology of the nanofibrous mats was observed using field emission scanning electron microscopy (FESEM; Zeiss, sigma).

3.2.3. Scratch assay

Primary human dermal fibroblast (HDF) (Himedia, India) and human keratinocyte cell line (HaCaT cells procured from NCCS, India) were accustomed with serum free media and high glucose (25 nM) conditions for 24 h prior to culturing them in a 24-well tissue culture plate with a density of 1 x 10^5 per well. Scratch was created using a 200 µL pipette tip on the confluent monolayer of cells. Four types of treatments were given separately: EGF (50 ng/mL), bFGF (50 ng/mL), LL-37 (5 µg/mL) and combination of EGF, bFGF and LL-37. Healing of scratched wounds was analysed from gross pictures of the cell migration to the wound after 18 h following the protocol [315]. Cells were fixed with 100 % ethanol and stained with crystal violet dye for better visualization. Gap between the scratch edges was calculated using image analysis software (Image J, Wayne Rasband, National Institute of Health, USA). Percentage recovery of scratch was calculated as the ratio of the difference between the original and the remaining wound areas versus the original wound area.

3.2.4. Release profile of EGF and bFGF

The amount of active growth factor released in phosphate buffer saline (PBS) solution was determined using ELISA kit specific for human EGF (Sigma Aldrich, USA and for bFGF (Abcam, U.K.). Briefly, the mats weighing 50 mg each were soaked in 5 mL PBS. 10 µL of PBS containing growth factor releasate was taken out at different time points (1, 12, 24 and 72 h) and diluted with 100 µL of fresh PBS. Releasates at different time points were stored in -20 °C prior to the experiment and ELISA assay was conducted for all the releasates together following the manufacturer's protocol. Cumulative growth factor release was calculated and plotted for each sample (n=4) against time using the formula:

$$\% \text{ Growth factor release} = (Mt/M) \times 100 \quad \text{..... (3.1.)}$$

Where Mt was the amount of growth factor released at time t and M was the theoretical value of growth factor present in the nanofibrous mat. The results were reported as average ± standard deviation (n=4).

3.2.5. Blood platelet adhesion on nanofibrous mats

Blood platelet adhesion assay was carried out to examine the haemostatic property of nanofibrous dressing materials by measuring the lactate dehydrogenase (LDH) activity of adhered blood platelets onto the mats. Briefly, the platelet rich plasma (PRP) was isolated by adding 8 U/mL heparin (Sigma-Aldrich, USA) to the whole blood and centrifuging at 100 g for 20 min at 20 °C. The supernatant containing PRP was collected carefully and used fresh for further studies. Nanofibrous mats were incubated with 200 µL of PRP for 1 h at RT on an orbital shaker at 60 rpm. The mats incubated with PRP were washed thrice with phosphate buffer saline (PBS, pH 7.4) solution and incubated with 1 % Triton-X 100 for 1 h at 37 °C to lyse the adhered platelets. Cell lysate was then centrifuged at 10,000 rpm at 4 °C and LDH enzyme was quantified from the supernatant using LDH assay kit (Sigma-Aldrich, USA) following manufacturer's instructions. Standard surgical cotton gauze was used as control. The results were reported as average ± standard deviation (n=4).

3.2.6. Release profile of LL-37

The amount of LL-37 released from nanofibrous mats was measured using the colourimetric assay of Bradford reagent following the protocol [316]. Mats were prepared by functionalizing them only with LL-37 peptide in order to prevent error by the release of growth factor peptide. Briefly, LL-37 functionalized mats were dipped in PBS and 100 µL of releasate was taken out at pre-defined time points (1, 12, 24 and 72 h). The releasate was mixed with Bradford reagent (Sigma, USA), incubated for 15 min at 37 °C and absorbance was measured at 595 nm using multiplate reader (Tecan). Serially diluted solutions of LL-37 ranging from 5 to 50 µg/mL were taken as the standard solutions. To calculate exact released amount of LL-37 from SF-PVA hybrid mats, releasates collected from non-functionalized mats were used as blank in order to exclude the interference of released SF protein of hybrid mats. The release profile was plotted for each sample (n=4) against time using the same formula as in equation 3.1.

3.2.7. Antibacterial activity and antibiofilm activity of LL-37 loaded nanofibrous mats – *in vitro* and *in vivo* study

Antibacterial action of LL-37 loaded nanofibrous mats was evaluated against skin infecting bacteria *Staphylococcus epidermidis* MTCC 435 and *Pseudomonas aeruginosa* MTCC 1688 obtained from Microbial Type Culture Collection and Gene Bank (MTCC,

IMTECH, India). 10 µL of bacterial culture containing bacteria with cell density of 1 × 10^5 colony forming unit (CFU)/mL was taken, diluted with 1 mL of fresh nutrient broth (Himedia, India) and cultured for 6 h. The nanofibrous mats (1 cm diameter) were immersed in 1 mL of bacterial suspension culture and incubated at 37 °C. 100 µL of bacterial culture was withdrawn at specific time points (1, 3, 6, 12, 18, 24 h) and analysed spectroscopically at 600 nm using multiplate reader (Tecan Infinite Pro M200). Ampicillin (500 µg/mL) and Gentamicin (500 µg/mL) were used as the positive control for the gram positive and gram negative bacteria respectively. To examine the antibiofilm activity of LL-37, crystal violet staining of biofilms was exhibited following the protocol [317]. Briefly, overnight cultures (1 × 10^5 CFU/mL) of *S. epidermidis and P. aeroginusa* were inoculated separately on the nanofibrous mats (1 cm diameter) in 24-well plates. Plates were incubated for 24 h in static condition.

To quantify the biofilm formation, bacteria cultured on the mats were fixed using 100 % ethanol, washed thrice with PBS and stained with 0.1 % crystal violet for 30 min. Acetic acid (30 %) was then added and incubated for 30 min at RT with shaking. The collected crystal violet solution was measured by taking absorbance at 595 nm using multiplate reader (Tecan Infinite Pro M200) and plotted with respect to the biofilm formed by bacteria cultured on the mats without LL-37 i.e non-functionalized mats. Results were reported as average ± standard deviation (n=4). To examine the effect of LL-37 loaded nanofibrous mats under *in vivo* conditions, wound exudates were collected on day 1, day 3 and day 5 from the wounds treated by different kinds of functionalized nanofibrous mats and surgical gauze as control. 25 µL of wound exudate was diluted with equal amount of PBS and the exudates-PBS mixture were plated onto the nutrient agar plates, which were subsequently incubated at 37 °C for 24 h. Negative control was taken as sterile PBS. The colonies grown on each agar plate were counted and plotted as bar graph. The results were reported as average ± standard deviation (n=4).

3.2.8. Induction of hyperglycaemic condition in rabbits for making *in vivo* diabetic wound model

All the animal experiments were performed in accordance with ‘‘Principles of laboratory animal care” from the Institutional Animal Ethical Committee (IAEC), West Bengal University of Animal and Fishery Sciences (WBUAFS), West Bengal, India (Permit No. Pharma/IAEC/136 dated 30.6.2014). Twenty-four New Zealand white rabbits (1.2 – 1.5

kg) were acclimatized by controlling their 12 h light/dark cycle, temperature and were given standard diet prior to the study. Twelve out of twenty-four rabbits were taken separately for diabetic induction. Briefly, subcutaneous injection of Acepromazine (1 mL/kg) was given to sedate the rabbits; hair at the back of ears were shaved off followed by administration of Alloxan (Sigma-Aldrich, USA) (150 mg/kg) in 30 mL saline at a rate of 1.5 mL/min *via* ear vein following the protocol [310]. After the treatment with Alloxan, rabbits were given water containing glucose (12 g/L) for a period of 48 h and monitored regularly afterwards. Blood glucose was examined using blood glucose meter (Accuchek_test advantage meter, Accu-chek_advantage II strips, Roche Diagnostics, U.K.). Diabetic condition of rabbits was confirmed in the rabbits having constant high blood glucose level (350 ± 16 mg/dL) for a period of at least 4 weeks. Diabetic rabbits were randomized into three groups for time points (day 7, day 14 and day 21). Each time point contained four rabbits. Proper aseptic conditions were taken while creating wounds, hair of mid thoraco-lumbar region of dorsal surface were shaved off and skin was wiped with 70 % ethanol. Intramuscular anaesthesia of xylazine hydrochloride (6 mg/kg) (Xylaxin®, Indian Immunologicals, India) and ketamine hydrochloride (33 mg/kg) (Ketalar®, Parke-Davis, India) was given prior to wounding.

Biopsy punch of diameter 12 mm was used to create full thickness wounds on dorsal surface and a total number of five wounds were created in each rabbit. Each rabbit was wounded with a total number of five wounds and the following treatments were given. Dressing patches were replaced with fresh ones after every three days till 14 days post-wounding and animals were regularly monitored. One wound taken as control was treated by surgical gauze and four wounds were treated using four different types of nanofibrous mats in the form of dressing patch: PVA, PVABM, PVAAA and PVAPR. Similarly, other twelve normal healthy rabbits (without hyperglycaemic condition) were also wounded as described above for comparative study. Blood glucose of rabbits with diabetic condition was found to be 350 ± 16 mg/dL as compared to the healthy rabbits (143 ± 9 mg/dL) throughout the study. All the animals were regularly monitored and no abnormality was found during the surgery or post-operation.

3.2.9. *In vivo* wound healing assessment in rabbit model

The wound closure rate was evaluated by measuring the size of wounds periodically. Photographs of the wounds were taken on day 0, 4, 7, 14, 18 and 21 to measure the

wound closure rate using Sony digital camera. Image J software was used to analyse the photographs for measuring the wound size. Following formula was used –

Wound area (%) = $A_t/A \times 100$ …… (3.2.)

Where A_t was the area of wound at time (t) and A was the initial wound area. Accordingly, wound closure rate was determined by considering the area of wound closed with respect to time. The results were reported as average ± standard deviation (n=3).

3.2.10. Histological examination

Histological examination of healing tissue was carried out on day 7, 14 and 21 post-wounding. Briefly, 10 % neutral buffer formalin (NBF) was used to preserve the tissue samples, which were then washed with water and dehydrated with series of graded ethanol prior to embedding in paraffin wax. Sections of 5 μm thickness taken on the glass slides were stained with haematoxylin and eosin (H & E) for general morphological observations.

3.2.11. Gene expression of MMP 1, MMP 2, MMP 9, Collagen-I and Collagen-III

Real time polymerase chain reaction (RT-PCR) was used to determine expression of collagen type I (Col-I), collagen type III (Col-III), MMP-1, MMP-2, MMP-9 and glyceraldehyde-3-phosphate-dehydrogenase (GAPDH) mRNA transcripts. Tissue samples collected from wounds on day 7, 14 and 21 were preserved in -20 °C using RNA later (Sigma Aldrich, USA), subsequently all the tissues were processed altogether. Briefly, tissues were chopped, treated by TRIzol reagent (Sigma Aldrich, USA) for 30 min and centrifuged at 13,000 rpm for 10 min in 4 °C. The supernatant containing mRNA was collected in fresh tubes followed by chloroform treatment and centrifuged at 13,000 rpm for 15 min at 4 °C. Subsequently, the upper aqueous phase containing mRNA was treated by isopropanol to obtain RNA pellet, which was further dissolved in water. The isolated equal amount of mRNA was taken to synthesize cDNA using reverse transcription kit (Applied Biosystems, USA) and PCR equipment (Takara, Japan). Real-time PCR reactions were performed using SYBR Green PCR Mastermix on a 7500 Fast Real Time System (Applied Biosystems, USA). Expression of each target gene was normalized with the Ct value of GAPDH. Primer sequences used are listed in **table 3.1.** The results were reported as average ± standard deviation (n=3).

Table 3.1. *Primer sequences used for the gene expression study.*

Target gene	Forward primers	Reverse primers
Rabbit GAPDH	5'-TCGGCATTGTGGAGGGGCTC-3’	5'-TCCCGTTCAGCTCGGGGATG-3'
Rabbit Col-I	5'-CCTGGCACCCCAGGTCCTCA-3’	5'-TCGCTCCCAGGGTTGCCATC-3'
Rabbit Col-III	5'-AAGCCCCAGCAGAAAATTG-3’	5'-TGGTGGAACAGCAAAAATCA-3'
Rabbit MMP 1	5'-TCAGTTCGTCCTCACTCCAG-3’	5'-TTGGTCCACCTGTCATCTTC-3'
Rabbit MMP 2	5’-TTGGATCCTCCTACAGCAGCTGCACCAG-3’	5’- AAGAATTCCCGTAGAGCTCTTGAATGC-3’
Rabbit MMP 9	5'-TGCCAGGAGTACCTGTTCCGCTATG-3’	5'-TGCCACTTGAGGTCACCCTCGAA-3'

3.2.12. Morphological examination of collagen, reticulin and elastin fibres

Tissues from the healed wound portion were taken out on day 21 and 28 post-wounding and preserved using 10 % NBF. Tissues were washed with water and dehydrated with series of graded ethanol prior to embedding in paraffin wax. Sections of 5 μm thickness were taken on the glass slides and used for different types of staining. Extracellular matrix components collagen, elastin, and reticulin were stained using Masson’s trichrome (MT) staining method, Weigert’s Resorcin–Fuschin method and Gridley’s modification of the silver impregnation method respectively, according to the manufacturer’s protocols [270-272].

3.2.13. Immunofluorescence of CD31 and pancytokeratin markers in the regenerated skin

Formalin fixed paraffin embedded sections (5 µm thickness) of skin tissue excised from the wound bed on day 7 and day 21 were analysed by immunofluorescence staining for CD31, and Pancytokeratin (PanCK) markers. Briefly, sections were rehydrated, permeabilized with 0.1 % Triton X-100 in PBS for 10 min, and blocked in PBS containing 1 % BSA for 1 h. The sections were then incubated with monoclonal primary antibody anti-CD31 and anti-pancytokeratin (Abcam, U.K.), diluted in blocking buffer (1:300) for 1 h at RT. After washing with PBS, the sections were incubated with FITC labelled secondary antibody, and counterstained with Hoechst 33342 to mark the nuclei. Furthermore, the sections were washed 4 to 5 times and mounted. Fluorescence images were taken using respective green and blue filters of the microscope (EVOS FL, Life technologies, USA).

3.2.14. Immunohistochemistry of Col-I and Col-III

Formalin fixed paraffin embedded sections (5 µm thickness) of skin tissue, excised from the wound bed were analysed by Immunohistochemistry (IHC), to evaluate the extent of collagen type I and collagen type III deposition in the regenerated skin, using IHC kit (Vectastain Elite Universal ABC kit, Vectors lab, U.K.). Briefly, sections were rehydrated and incubated with 0.1 % (v/v) blocking serum for 30 min at RT prior to applying monoclonal primary antibody (Abcam, U.K.) against Col-I and Col-III (1:300 dilution). After washing with PBS, the sections were incubated with biotinylated universal secondary antibody (Vectastain Elite Universal ABC kit, Vectors lab, USA). The ABC reagent containing avidin-horseradish peroxidase, was then applied to the sections before exposure to Peroxidase substrate 3,3′- diaminobenzidine (DAB) and H_2O_2 to develop a brown reaction product. Furthermore, sections were counterstained with haematoxylin, dehydrated, cleared, mounted, and images were taken using bright field microscope (EVOS FL, Life technologies, USA).

3.2.15. Quantitative evaluation of hydroxyproline and elastin in wounds

The excised tissue samples from wound beds were collected at different time points (day 7, 14 and 21), stored at - 80 °C and analysed altogether to quantify the content of ECM components. Hydroxyproline secretions were quantified using hydroxyproline assay kit (Sigma Aldrich, USA) according to the manufacturer's protocol. Elastin was quantified

using rabbit elastin ELISA kit (Mybiosource, USA) as per manufacturer's protocol. The results were reported as average ± standard deviation (n=3).

3.2.16. Tensile strength of regenerated skin

Full thickness skin with healed tissue in the central area was excised after 4 weeks post wounding; tensile strength of the wounds was determined using a Universal Testing Machine (UTM) (Instron 5944, USA), fitted with 100 N load cell and Bluehill version 3.66 software. Young's Modulus (YM) was calculated only between the starting point and initial wound break point. The results were reported as average ± standard deviation (n=3). Ultimate tensile strength (UTS) at the initial wound breaking point was taken as the wound breaking strength, which was calculated as per the formula –

Wound strength (%) = (UTS of normal unwounded skin/ UTS of wounded skin) × 100 ……(3.3.)

3.2.17. Statistical analysis

All the experiments were carried out for n = 4 samples unless otherwise specified; results of the *in vivo* experiments were considered for n=3 animals at each time point. Data were expressed as mean ± standard deviation. Data analysis was done using statistical software OriginPro 8 (Origin lab Corporation, USA) at both significant (* $p \leq 0.05$) and highly significant (** $p \leq 0.01$) levels. The significance level was measured by comparing the data between groups and within groups by performing one-way analysis of variance (ANOVA) followed by Tukey's test. Microscopic images were analysed using Image J software and images were observed at least 10 fields per section for histological examination.

3.3. Results

3.3.1. Morphology of functionalized nanofibrous mats

Functionalized nanofibrous mats of only PVA and hybrid mats of various PVA-SF blends (PVABM, PVAAA and PVAPR) were successfully fabricated by electrospinning technique. The nanofibrous dressing developed herein contained EGF, bFGF and LL-37. Nanofibres of all the four types of functionalized mats were continuous, smooth and randomly oriented as shown by the FESEM images (**Figure 3.1.A**). The mats showed

highly porous network along with interconnected voids. The variation in morphology and size of nanofibres was dictated by the variety of SF protein as also observed in the study conducted in chapter 1.

3.3.2. Scratch assay

Migration of HDF and HaCaT cells was assessed by *in vitro* scratch assay to examine the effect of EGF, bFGF, LL-37 and combination of all these three bioactive molecules on wound healing (**Figure 3.1.B**). Gross images of scratches showed complete wound healing after 18 h in high glucose media, when treated with the combination dosage (EGF + bFGF + LL-37). The faster wound healing is attributed to their synergistic activity on cell migration as compared to individual treatments. Percentage recovery of scratches created in monolayers of HDF and HaCaT was almost 100 % under the combination treatment (**Figure 3.2.**), which was found to be significantly higher than individual treatments of EGF, bFGF and LL-37, $p \leq 0.01$.

3.3.3. Release profile of EGF, bFGF and LL-37

Sustained release of EGF and bFGF from the nanofibrous mats was observed for 3 days following an initial burst at 1 h (**Figure 3.3.A,B**). EGF and bFGF was released continuously till 24 h, after which plateau region was observed till 72 h. Growth factor release pattern was different for EGF and bFGF, with all the hybrid mats showing higher release of bFGF as compared to EGF. Initial burst release of EGF from the four types of mats is as follows: PVA = 12 ± 1.05 %, PVABM = 14 ± 1.24 %, PVAAA = 20.19 ± 1.16 % and PVAPR = 19.5 ± 1.9 %. Initial burst release of bFGF from PVAAA and PVAPR was found to be 23.95 ± 1.67 % and 25.09 ± 1.87 %, significantly higher than the EGF burst release from same mats. PVAAA and PVAPR mats demonstrated significantly higher growth factor release in comparison to other mats after 72 h, $p \leq 0.01$. Similarly, Sustained release of LL-37 from the nanofibrous mats was observed for 3 days, following an initial burst at 1 h (**Figure 3.3.C**). Release of LL-37 from nanofibrous mats was also found to be higher than the minimum inhibitory concentration (MIC) at all the time-points, which further validated the sustained antibacterial activity of functionalized mats for a period of 3 days.

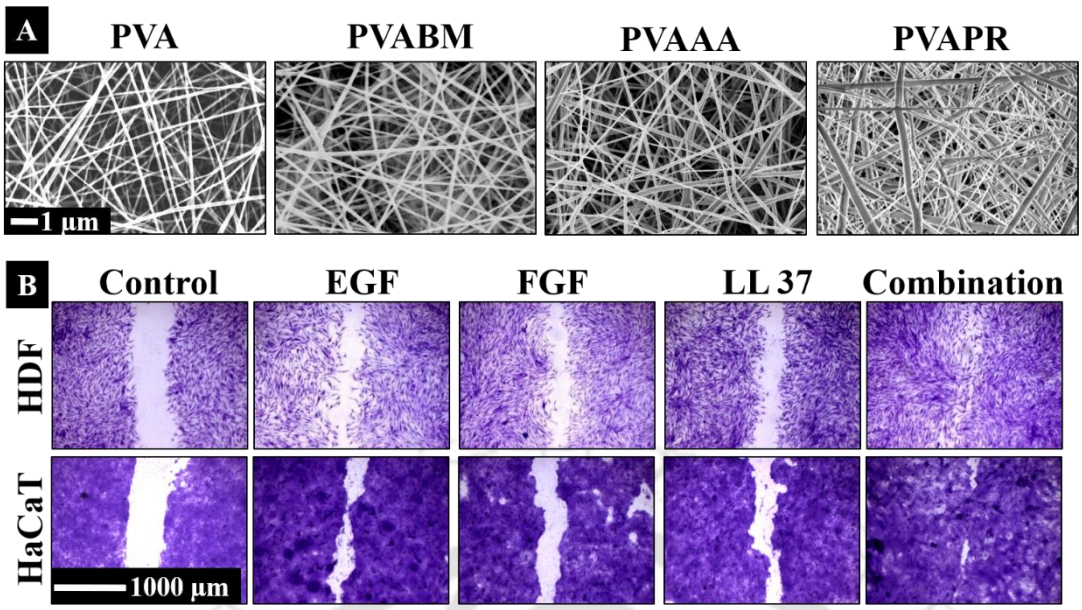

Figure 3.1. *(A) FESEM images of various functionalized nanofibrous mats representing morphology of nanofibres. (B) In vitro scratch assay on cell monolayers depicting effect of various bioactive molecules on the cell migration.*

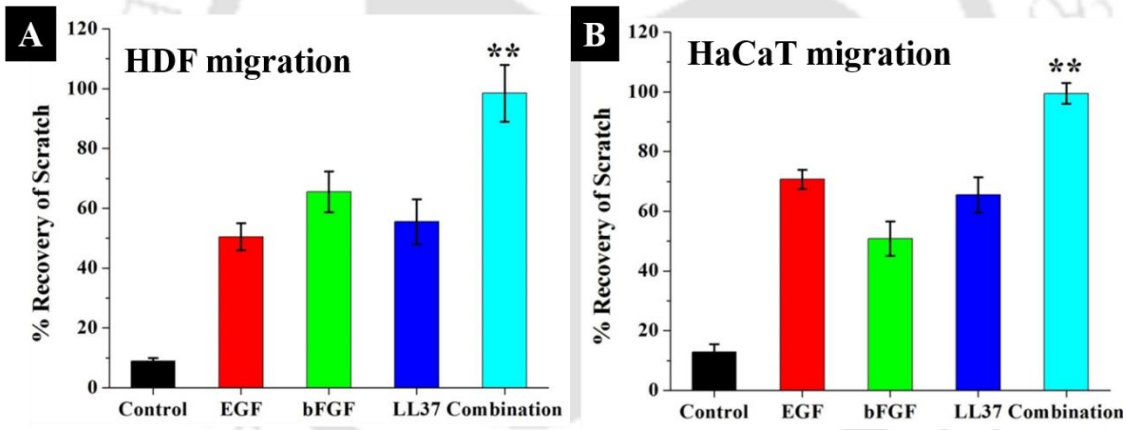

Figure 3.2. *Quantification of cell migration as recovery of scratch by (A) HDF cells and (B) HaCaT cells in the presence of various bioactive molecules.*

3.3.4. LDH activity

Silk based nanofibrous mats showed haemostatic activity, when examined by quantifying the LDH activity of adhered platelets (**Figure 3.3.D**). Commonly used surgical cotton gauze taken as control, exhibited significantly lower LDH activity as compared to the silk based mats ($p \leq 0.01$); the control thus demonstrated ineffective haemostasis. PVAAA and PVAPR mats showed higher LDH activity 4.32 ± 0.72 and 4.04 ± 0.54 milliunits/mL respectively, which was significantly higher than all the other samples, suggesting higher number of platelets adhered to the NMSF based mats ($p \leq 0.01$).

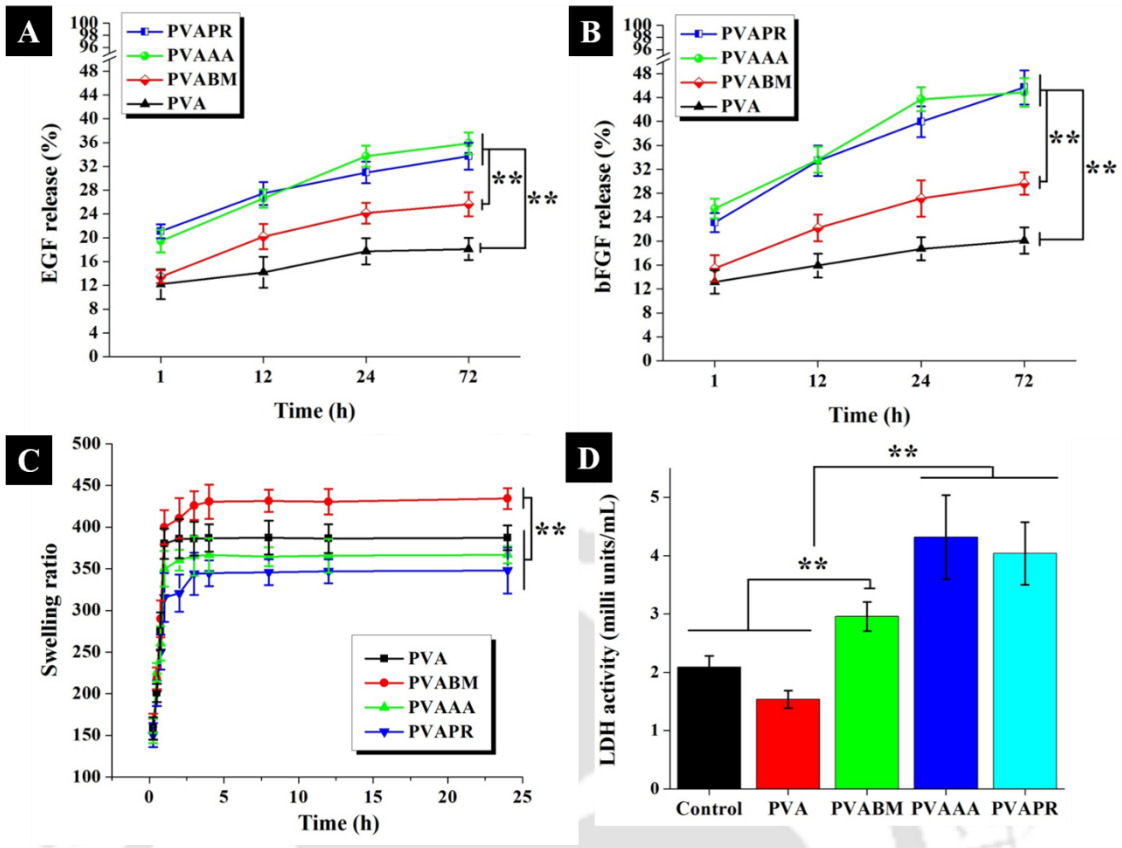

Figure 3.3. *(A, B and C) Release profile of EGF, bFGF and LL-37 from the nanofibrous mats showing sustained growth factor release for 3 days respectively. (D) LDH activity of adhered platelets on various nanofibrous mats, representing superior haemostatic activity of silk-based mats compared to conventionally used surgical gauze (control), (*p ≤ 0.05, **p ≤ 0.01).*

3.3.5. Antibacterial activity and antibiofilm activity of mats

Antibacterial activity of LL-37 loaded nanofibrous mats observed against skin infecting *P. aeruginosa* and *S. epidermidis* bacteria revealed their efficient bacteria killing properties for 24 h (**Figure 3.4.A**). High bacterial growth was observed on the non-functionalized mats, as compared to LL-37 functionalized mats, suggesting efficient antibacterial property of LL-37 under *in vitro* conditions. These functionalized mats clearly inhibited biofilm development, from both the types of bacteria; whereas, bacterial biofilm developed on the non-functionalized mats was seen within 24 h (**Figure 3.4.B**). Lesser number of bacterial colonies in the treated wounds compared to control wounds was also evident from the wound-exudate study carried under *in vivo* conditions using diabetic rabbits (**Figure 3.4.C**). Control wounds exhibited significantly higher number of bacterial colonies on day 3 and day 5 showing 500 to 650 bacterial colonies. In contrast, functionalized nanofibrous mats treated wounds showed significantly lower

number of colonies, $p \leq 0.01$; 100 to 150 on day 3 and less than 100 on day 5. The lower number of colonies observed in the wound-exudate study revealed efficient reduction in the bacterial growth even in diabetic condition, which supported the potential of LL-37 in significantly lowering the polymicrobial infections.

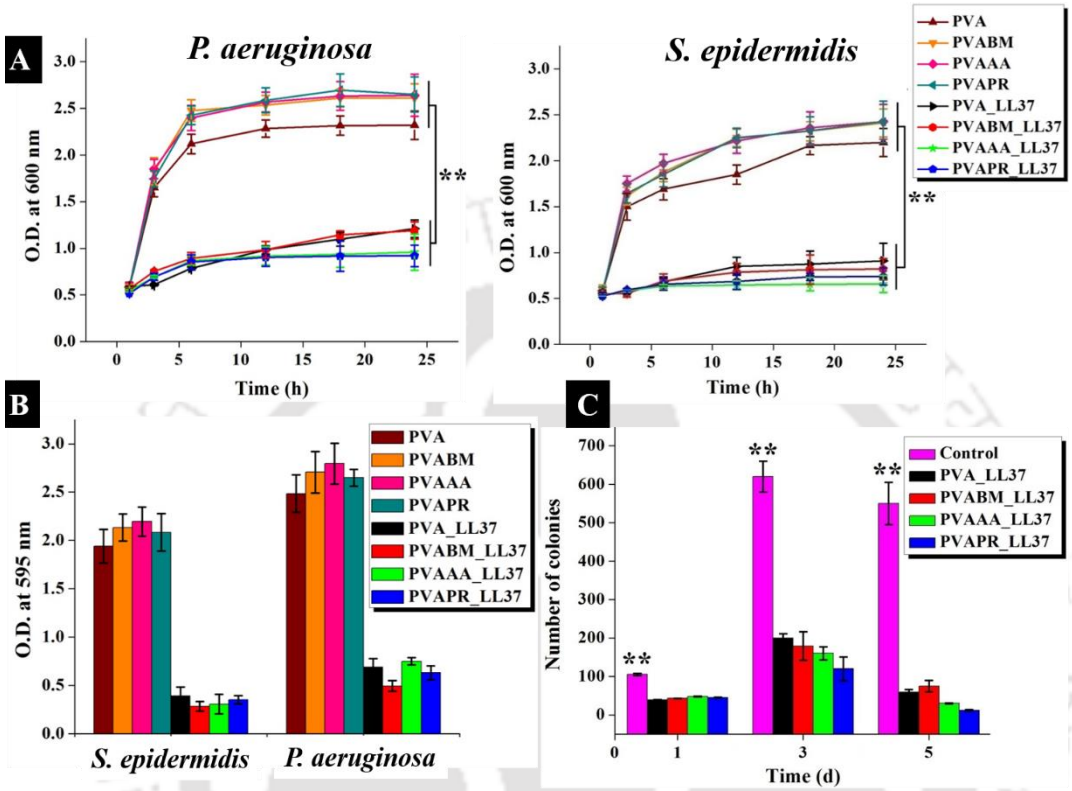

Figure 3.4. *(A) In vitro anti-bacterial activity of functionalized nanofibrous mats against skin infecting bacteria. (B) In vitro anti-biofilm activity of mats showing inhibition of biofilm formation by LL-37 antimicrobial peptide; whereas non-functionalized mats formed biofilm within 24 h. (C) Anti-bacterial activity of mats under in vivo conditions as determined by the wound exudate study representing number of colonies in the wounds of diabetic rabbits, (*$p \leq 0.05$, **$p \leq 0.01$).*

3.3.6. *In vivo* wound healing assessment in rabbit model

Wound healing rate was first compared between diabetic and non-diabetic rabbits to examine the effect of functionalized mats on both acute and chronic wounds. Wounds created in diabetic rabbits healed at a slower rate as compared to normal rabbits; the difference was distinctly visible when compared with the images of control wounds (**Figure 3.5.A**). Alloxan induced diabetic rabbits showed high blood glucose levels (350 ± 16 mg/dL) as compared to healthy rabbits (143 ± 9 mg/dL) throughout the study (**Figure A3.1.**). Control wounds showed two-fold wound closure recovery on day 7 in non-diabetic (30.65 ± 2.57 %) compared to diabetic rabbits (18.81 ± 3.05 %), depicting

wound chronicity in the diabetic model (**Figure 3.5.B,C**). Among the treated wounds, PVAAA and PVAPR promoted wound healing at a faster rate in both non-diabetic and diabetic models, resulting in wound closure within 14 to 18 days. Wound closure by PVAAA and PVAPR was significantly higher than other treatments on day 7 and day 14 in both the diabetic and non-diabetic rabbits, $p \leq 0.01$. Wound closure on day 14 by PVAAA and PVAPR was 85 to 90 % in diabetic model and 95 to 98 % in non-diabetic model, which was significantly higher than the rest of the treatments, $p \leq 0.01$. PVABM treated wounds healed faster than PVA treated wounds and control wounds; PVABM achieved 75.28 ± 2.08 % and 84.50 ± 4.34 % wound closure on day 14 in diabetic and non-diabetic rabbits, respectively. Similar results have been reported in another study, where BmSF nanofibrous mats functionalized with EGF healed the wounds of healthy animals within 14 days.

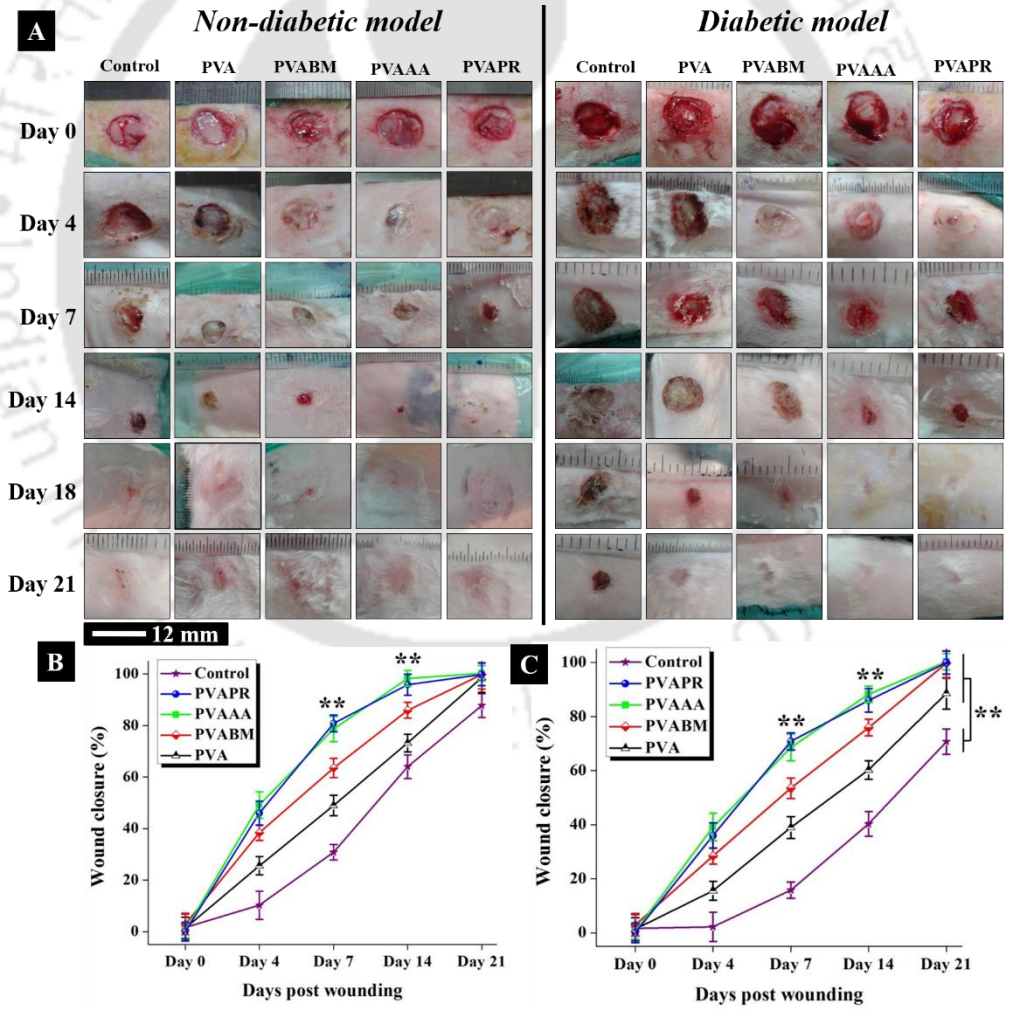

Figure 3.5. *(A) Wound healing assay under in vivo conditions showing gross wound images under various treatments in both healthy and diabetic rabbit model, depicting rapid wound closure by PVAAA and PVAPR samples. (B, C) Wound healing efficacy of*

various nanofibrous mats represented by wound closure percentage in healthy rabbits and diabetic rabbits respectively as determined by calculating the area of wounds using ImageJ software, ($p \leq 0.05$, **$p \leq 0.01$).*

3.3.7. Histological examination of wounds

Histological study of wound tissues on day 7, 14 and 21 revealed sequential wound healing process by different treatments in the diabetic rabbits (**Figure 3.6.A**). On day 7, a blood clot mass was observed in the control wounds, indicating delayed haemostasis. PVA treated wounds showed absence of granulation tissue with redness, suggesting inflammation and tissue necrosis. Conversely, proliferating granulation tissue was developed in the wounds treated by silk-based dressings. A higher extent of granulation tissue development, and an increased occurrence of thick collagen bundles, were distinctly observed in case of PVAAA and PVAPR treated wounds. It is noteworthy that even under hyperglycaemic conditions, the wounds treated with NMSF based mats displayed relatively thick and mature granulation tissue all over the wound area; providing a head start to the healing process.

Greater numbers of blood vessels were observed in the granulation tissue developed by PVAAA and PVAPR dressing patches as compared to PVABM. Immunostaining the sections against CD31 marker demonstrated highly vascularized tissue on day 7 (**Figure 3.6.B**). This suggested early recruitment of endothelial cells, and angiogenesis by the NMSF based mats owing to the presence of cell binding peptides and high bFGF release. On day 14, sections of control wounds exhibited presence of eschar, demonstrating very slow progression in wound healing process. The growing epithelial tongue appeared in the wounds treated by PVAAA and PVAPR on day 14, but not in the other treatments. The healed wounds also displayed a well-formed matrix of dermal structures. Different strata of epidermal layers along with budding of hair follicles and sebaceous glands were also visible on day 21, whereas they were not observed in other treatments. Wound healing events in the non-diabetic rabbits were seen to proceed at a relatively faster rate compared to diabetic rabbits, with wounds in the former healing completely in 14 days (**Figure A3.2.**). Re-epithelialized tissues demonstrated higher pancytokeratin expression in the wounds treated by silk based dressings (**Figure 3.6.C**). Control and PVA treated wounds could not express pancytokeratin as shown by the absence of green fluorescence in epidermis. In contrast, dressing made up of SF-PVA blend re-epithelialized the wounds expressing pancytokeratin marker all over the new

epidermal layer. PVAAA treated wounds also showed cornified layer above epidermis, suggesting fully grown mature epidermal layer. Herein, the ability to recruit keratinocytes, and retain normal morphology of epithelial cells, was unequivocal even in high glucose regimes.

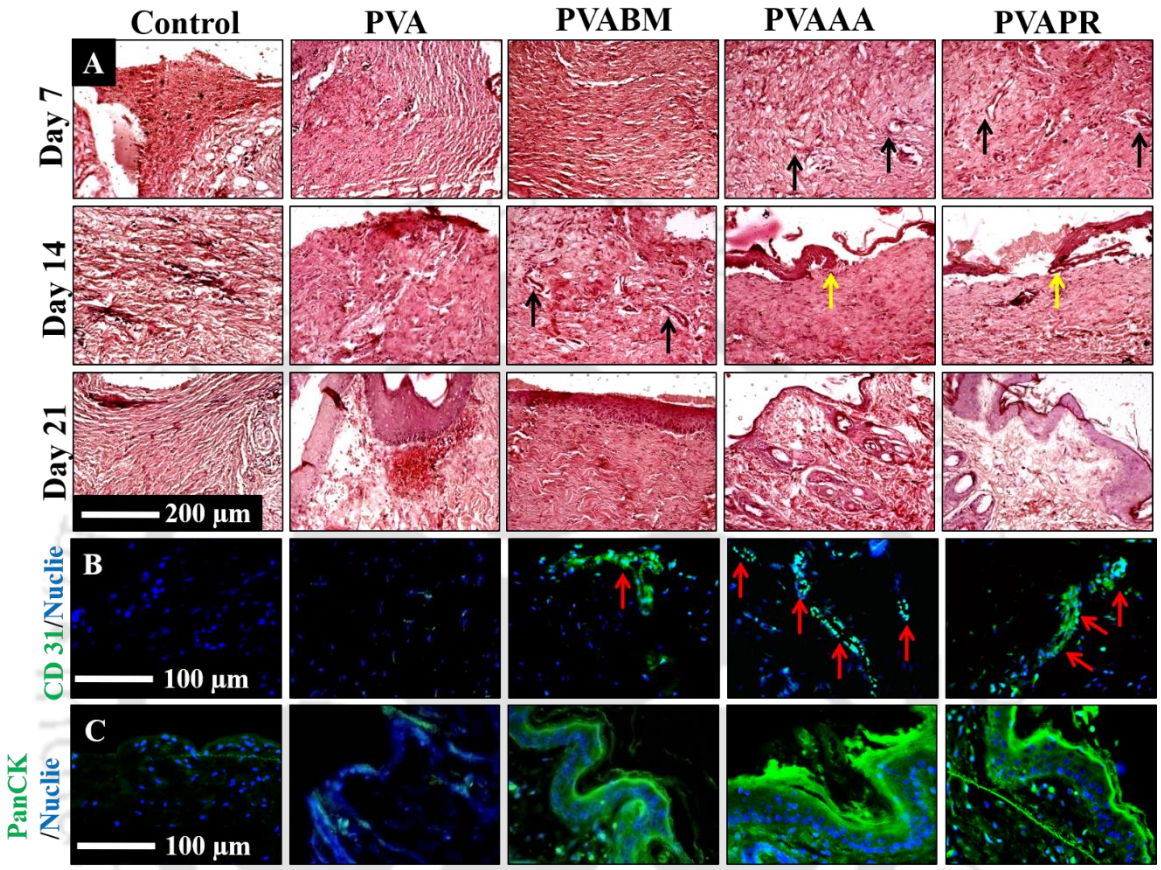

Figure 3.6. *(A) Histological study (H & E stain) of wounds on day 7, 14 and 21 post wound creation in diabetic rabbit model shows: early development of healthy granulation tissue on day 7 in PVABM, PVAAA and PVAPR treated wounds (black arrows = blood vessels); re-epithelialization in PVAAA and PVAPR treated wounds on day 14, exhibiting growing epithelial tongue (yellow arrows) and complete epidermal and dermal regeneration on day 21, depicting mature dermal matrix. (B) Extent of angiogenesis on day 7 (red arrows = endothelial cells immunostained by anti-CD31 antibody). (C) Immunostaining against pancytokeratin marker revealing normal morphology of epithelial cells on day 21 under hyperglycaemic conditions.*

3.3.8. Gene expression of MMP 1, MMP 2, MMP 9, Col-I and Col-III

Analysis of various MMPs and collagen gene expression was quantified by RT-PCR, which demonstrated their varied expression associated with ECM turn over with time (**Figure 3.7.)**. Balanced secretion of various MMPs and ECM components is critical to the wound healing process. Control wounds showed increasing trend in the gene

expression of MMP 1 as compared to the other wounds, with the highest value on day 21, $p \leq 0.01$. While wounds treated with silk based mats showed an initial increment in the MMP 1 expression till 14 days, but regressed expression on day 21. Expression of MMP 2 was seen similar in all the wounds at all time points except control wounds on day 14. MMP 9 expression was relatively lower than MMP 1 but higher than MMP 2 in all the nanofibrous mats treated wounds till day 14; MMP 9 expression was regressed many folds on day 21, showing non-chronic condition of wounds at the later stages of healing. Wounds treated by the nanofibrous mats showed an upregulated expression of MMP 9 on day 7 suggesting an early inflammatory response, followed by resumption of normal physiological conditions at later stages. Control wounds showed significantly higher gene expression of MMP 9 on day 14 and day 21, clearly demonstrating wound chronicity in the untreated wounds, $p \leq 0.01$.

On co-relating the gene expressions of MMP 1, 2, 9, Col-I and Col-III, the study revealed greater extent of ECM remodelling by the silk dressings (**Figure 3.7.)**. Collagen type I expression continued to increase from day 7 to day 21 in all the wounds showing continuous secretion of Col-I and progression of wound healing. PVAPR showed significantly higher secretion of Col-I on day 7 compared to other wounds, $p \leq 0.01$. Higher Col-I gene expression was observed in the silk mats on day 14, demonstrating wound healing progression with time compared to PVA treated mats and control, $p \leq 0.01$. In contrast, expression of Col-III was observed to be completely different on day 21, showing significantly higher expression in control and PVA treated wounds in comparison with other wounds, $p \leq 0.01$. On correlating the expression of Col-I and Col-III, control wounds showed significantly higher gene expression of both types of collagens on day 21, suggesting collagen secretion in process; whereas nanofibrous mats treated wounds showed lowered gene expression of Col-III on day 21 compared to Col I.

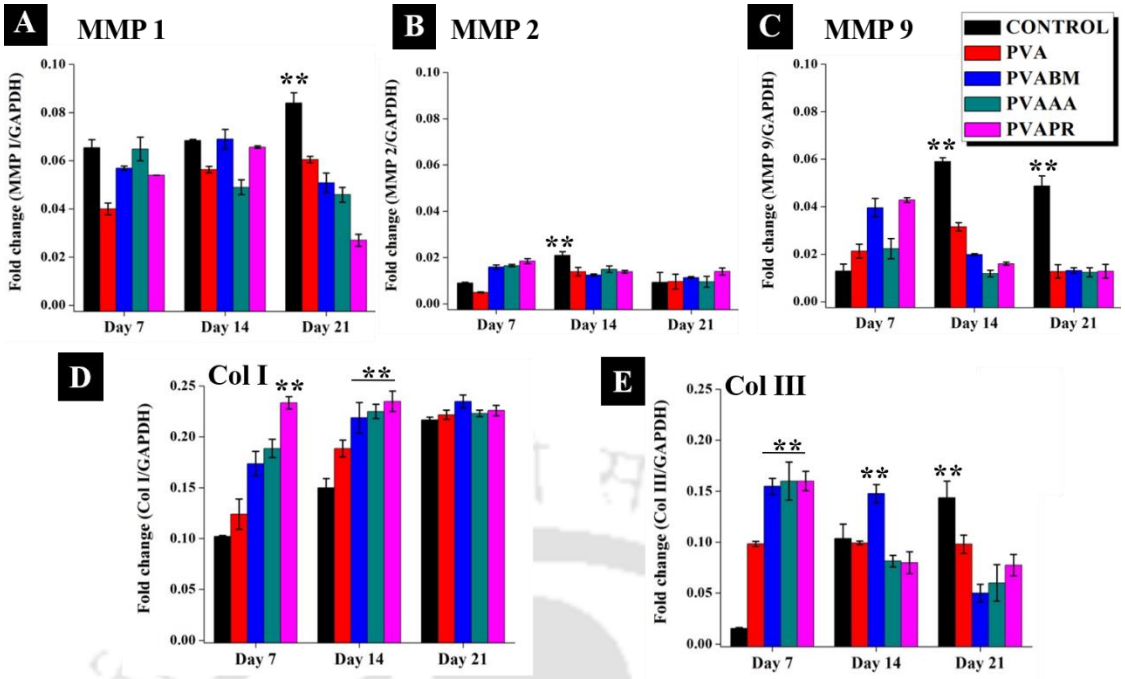

Figure 3.7. *(A-E) Gene expression of various MMPs and collagen components in the wounds, showing ECM remodelling during the wound repair process in diabetic rabbit model (*p ≤ 0.05, **p ≤ 0.01).*

3.3.9. Immunohistochemistry and assessment of ECM deposition

IHC of dermal sections was carried out in order to further evaluate the distribution of Col-I and Col-III (**Figure 3.8.A,B**). Wounds treated by silk dressings showed lighter density of Col-III as compared to Col-I, suggesting lower deposition of Col-III. In addition, collagen fibres stained with MT revealed overall collagen secretion in the dermal matrix formed after 21 days (**Figure 3.8.C**). Mature, thick collagen bundles with wavy appearance were visible throughout the dermal region of regenerated skin in the wounds treated with PVAAA and PVAPR. Distribution of mature collagen bundles was not observed homogeneously in the wounds treated with PVABM, as can be seen in the image where the intensity of MT stain was lesser in the central zone as compared to the peripheral region. Contracted collagen fibres were clearly visible in the dermal region of wounds treated with PVA mat, suggesting wound healing majorly due to contraction mechanism. In contrast, control wounds showed immature collagen secretion, depicting presence of granulation tissue on day 21, demonstrating delayed wound healing process.

Whirling threads of reticulin fibres distributed all over the regenerated skin was clearly visible in the wounds treated with PVAAA and PVAPR on day 21 (**Figure 3.8.D**). Reticulin fibres were arranged as slender threads, suggesting mature development of reticulin fibres in the regenerated skin. They were arranged in diffused patterns as

delicate mesh of fine fibrils throughout the wounds. PVABM demonstrated only few reticulin fibres with lower intensity on day 21. On the contrary, mature reticulin fibres were not visible in the wounds treated with PVA and control group. Thick and mature elastin fibres were found in the dermal regions of wounds treated with PVAAA and PVAPR (**Figure 3.8.E**). They were mostly found underneath the epidermal layer, depicting their role in integrating the dermal and epidermal layers. PVABM treated wounds showed immature thin elastin fibres, suggesting delayed secretion or lesser intense elastin fibres in the wounds. Visible elastin fibres were not found in the PVA treated and control wounds. Similar observations on day 28 further validated the mature deposition of ECM fibres in the regenerated tissue (**Figure A3.3.**). Controls groups showed minimum ECM secretion (hydroxyproline and elastin) at all the time points as compared to the wounds treated with nanofibrous mats (**Figure 3.9.**).

Among all treatments, ECM secretion was found to be significantly higher in the wounds treated with PVAAA and PVAPR as compared to other groups on day 14 and day 21, $p \leq 0.01$. Time dependant increment in the concentration of hydroxyproline and elastin suggested progression of wound healing and varied ECM deposition by all the treatments. Significantly higher elastin secretion was found in PVAAA and PVAPR treated wounds on day 14 and day 21 compared to PVA, PVABM and control, $p \leq 0.01$. Similarly, higher secretion of hydroxyproline was also found in the wounds treated with PVAAA and PVAPR. There was no significant difference in the amount of hydroxyproline produced in the wound beds on day 14 and 21, suggesting saturation in the collagen deposition by 21 days, which indicated remodelling stage of wounds. Progressively increased secretion of hydroxyproline from day 7 to day 21 in the control, PVA and PVABM treated wounds indicated proliferative stage of wounds.

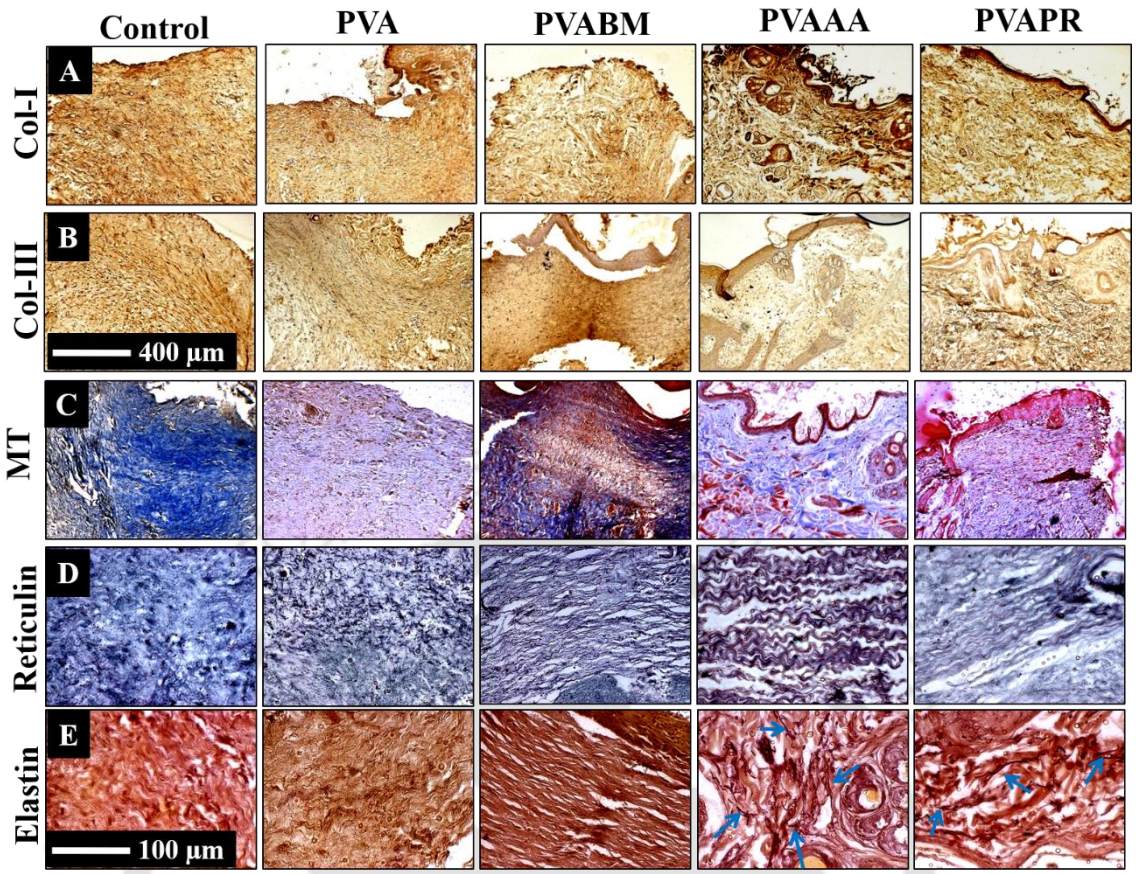

Figure 3.8. *(A, B) IHC images showing distribution of collagen type I and collagen type III in the healed tissue on day 21 respectively. (C-E) Stained ECM components – collagen (MT), reticulin and elastin fibres deposited in the healed skin tissue on day 21; deposition of mature elastin fibres (blue arrows) could be visible only in the healed tissue treated with PVAAA and PVAPR.*

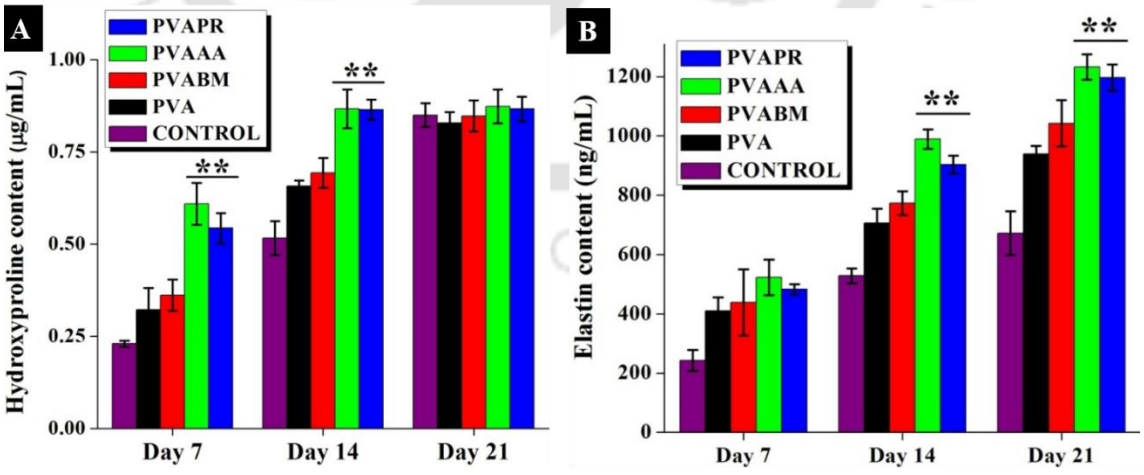

Figure 3.9. *(A, B) Quantification of ECM components: hydroxyproline and elastin on day 7, day 14 and day 21 post wounding (*p ≤ 0.05, **p ≤ 0.01).*

3.3.10. Wound breaking strength

Mechanical testing of the regenerated skin revealed strength of the new tissue formed in the wounds after 4 weeks (**Figure 3.10.**). Control and PVA treated wounds broke at a very early stage, giving 1.8 to 2 MPa YM and 20 – 30 % wound strength. The wounds recreated by stretching of skin during the mechanical testing, were bigger in size, as evidenced in the gross images. On the contrary, silk-based hybrid mats treatments, significantly increased the wound strength. PVABM treated wounds showed 2.86 ± 0.25 MPa YM and 39.12 ± 4.34 % wound strength. PVAAA and PVAPR showed significantly higher YM and wound strength (5 to 6 MPa YM and 55 to 63 % wound strength), suggesting faster and improved wound healing within 4 weeks, $p \leq 0.01$. Gross images of stretched wounds also revealed that wound breakage occurred at the edge of healed wound in case of PVAAA. This supported higher wound strength of tissue and wound was not re-created on applying the force.

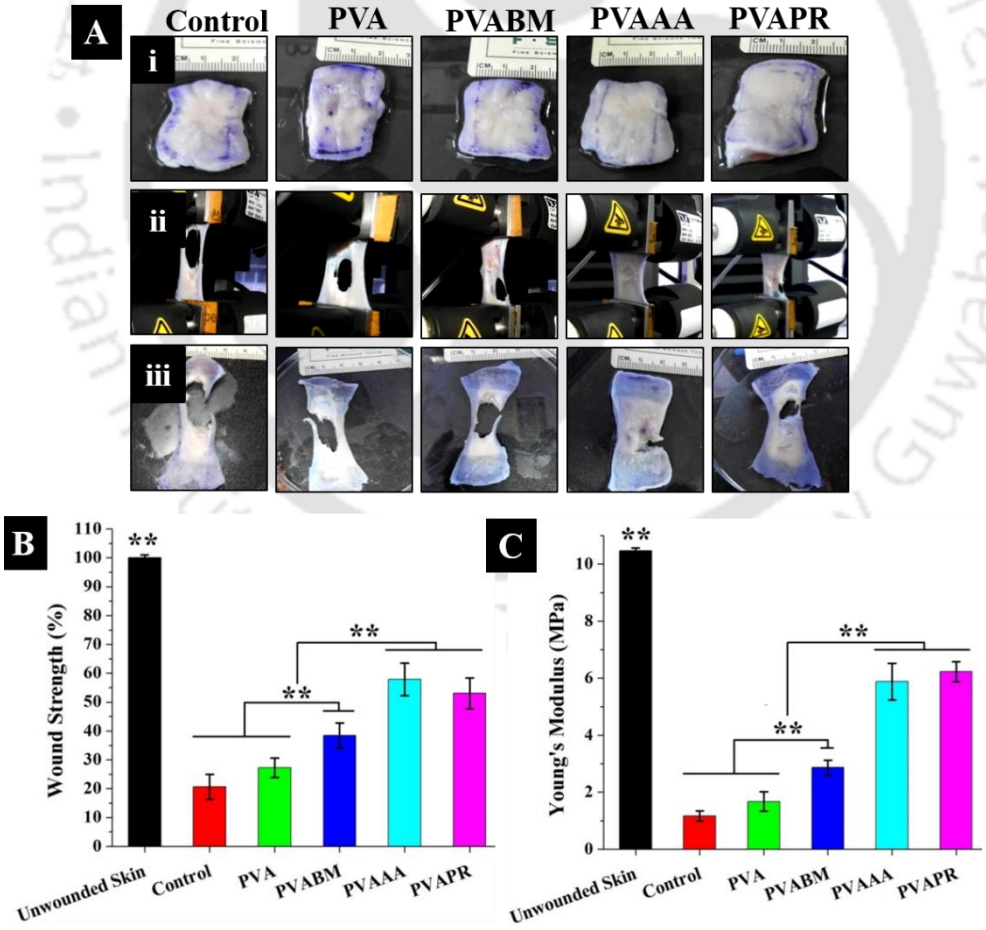

Figure 3.10. *(A) Determination of mechanical tensile strength of healed skin tissue by measuring the wound break strength on day 28 (i) skin samples before measuring the mechanical strength, (ii) samples at wound break point showing re-occurrence of*

wounds and (iii) morphology of samples after stretching. (B) Wound break strength of healed tissues measured by taking UTS of intact unwounded skin as 100 %. (C) Young's Modulus of healed tissues by various treatments compared to normal unwounded skin ($p \leq 0.05$, **$p \leq 0.01$).*

3.4. Discussion

Development of an efficient bioactive dressing material for wound healing applications aims at stimulating the healing mechanism by various strategies. Wound dressings should not only seal open wounds temporarily, but also provide a supportive substrate or matrix that stimulate cells from nearby tissue towards wound repair. Successful wound healing involves alleviation of infection, non-persistent inflammation, earlier cell recruitment and organized ECM deposition for quick wound repair [6]. In our previous work as described in chapter one, role of NMSF on accelerated healing of acute wounds and organized ECM deposition in the repaired tissues was observed owing to the cell interacting material properties [314]. The current study reveals benefits of NMSF based wound dressing in treating chronic wounds in diabetic conditions. Hyperglycaemic condition of wound bed impairs cell morphology, obstruct cell migration and de-stabilize the matrix components [12]. Our approach is to trigger impaired healing mechanism of diabetic chronic ulcers by providing suitable growth factor microenvironment along with influencing the ECM deposition during the healing process, leading to complete wound repair.

Structural advantage of nanofibrous format and incorporation of growth factors and AMPs were the constant factors for comparative study among various silk based nanofibrous wound dressings. Nanofibrous architecture of dressing substrate mimics the natural ECM web, offering nanotopographical cues for enhanced cellular migration and recruitment in the wound bed (**Figure 3.1.**). Our previous study also dealt with essential physico-chemical properties of NMSF based mats for wound dressing applications like rough surface nanotopology, ideal water vapour transmission rate (~2330 g/m^2/day), high elasticity (~2.6 MPa) and sustained drug release behaviour [314]. The present study focuses on the healing effect of various nanofibrous mats under hyperglycaemic conditions in diabetes. EGF, bFGF and LL-37 together showed 100 % recovery of scratches by both types of cells, demonstrating synergistic role of the cocktail on accelerating the cell migration (**Figure 3.2.**). Sustained release of such bioactive

molecules through our developed wound dressing played crucial roles in rapid wound re-epithelialization and cell proliferation.

Nanofibrous format of dressing patch provided advantage of sustained growth factor delivery as compared to the topical application, in which growth factor may get inactive due to rich proteolytic environment of chronic wounds. Dissimilarity in the growth factor release patterns among various mats has been attributed to difference in the SF protein sequences (**Figure 3.3.A,B**). Electrostatic interaction clearly played a major role in growth factor release behaviour. The isoelectric point and overall crystallinity of both mulberry and non-mulberry SF are similar as verified by the protein sequence and FTIR spectroscopy in previous studies [314, 318]. However, the isoelectric point of EGF (pI 4.78) and bFGF (pI 9.58) is considerably different. This justifies the dissimilar release profile from the nanofibrous mats. Higher release of bFGF as compared with EGF might be because of transient binding and diffusion due to opposite charge interactions. Similar findings were observed in case of nerve growth factor with pI 9.3, alike bFGF in another study [318]. However, other factors such as Van der Waals forces of interaction and hydrogen bonding may also influence the growth factor release [256]. The difference in swelling capacity, which corresponded to the hydrophilicity and hydrophobicity of mulberry and non-mulberry SF, in turn also affected growth factor release. Hydrophilic nature of EGF and bFGF might induce increased interaction with relatively more hydrophilic PVABM mat as evidenced by significantly lower growth factor release. NMSF-based dressings released higher amount of growth factors, which reinforced its potential as a wound dressing material.

The sequential healing process starting with haemostasis, going through proliferative phase and ending with tissue remodelling revealed outstanding attributes of PVAAA and PVAPR in wound healing applications. Open wounds often lead to elevated bleeding, causing blood loss from the body. Therefore, development of haemostatic wound dressings that induce rapid blood clotting is very important. More platelet adhesion on NMSF based mats compared to other mats and surgical gauze demonstrated their superior haemostatic property (**Figure 3.3.D**). High LDH activity on PVAAA and PVAPR mats was due to the presence of cell binding 'RGD' sequences, attracting more platelets. The results were in parallel with another study, where greater amount of platelet interaction was observed with another non-mulberry SF variety *A. mylitta*, as compared to BMSF due to the presence of intrinsic RGD sequences in Am protein [252].

Bacterial colonization and biofilm development are commonly observed in diabetic wounds owing to high glucose condition of wound bed, which obstruct the healing process and aid in wound chronicity [319]. Bioburden on chronic wounds due to the presence of polymicrobes has been evidenced from many studies, particularly in diabetes condition [320]. Hence, it is of utmost importance to provide antibacterial property in the dressing patch used to treat DFU. The nanofibrous mats loaded with LL-37 exhibited effective antibacterial and antibiofilm activities against *P. aeruginosa* and *S. epidermidis*, which commonly infect DFU (**Figure 3.4.**). *In vivo* wound-exudate study revealed efficient bacterial prevention in the wounds by functionalized nanofibrous mats even under the hyperglycaemic conditions, supporting potential of LL-37 in eradicating polymicrobial infections.

The silk based nanofibrous dressing demonstrated accelerated wound healing, also shown by early development of granulation tissue, angiogenesis and re-epithelialization (**Figure 3.5. and 3.6**). Greater extent of angiogenesis shown by higher number of blood vessels demonstrated highly vascularized wound bed, suggesting early recruitment of endothelial cells by the NMSF based mats. Wound bed with high glucose condition is known to alter the normal physiological functions of keratinocytes hampering re-epithelialization during diabetic conditions [321]. Higher expression of multiple cytokeratin proteins shown in the re-epithelialized skin treated with silk dressing proved normal morphology of epithelial cells. On the contrary, control wounds and PVA treated wounds could not re-epithelialize efficiently within 21 days. Further, balanced ECM deposition is crucial for wound repair especially in the chronic wounds due to high MMP concentration, which is responsible for ECM disintegration. Detrimental wound physiology often leads to impaired ECM secretion, making it hard to heal. Therefore, balanced secretion of various MMPs and ECM components becomes critical.

On co-relating the gene expressions of MMP 1, 2, 9, Col-I and Col-III, the study suggested greater extent of ECM remodelling during the wound repair process (**Figure 3.7.**). Higher MMP 1 expression along with higher Col-1 expression in the wounds treated with silk dressings, suggested the simultaneous secretion and degradation of Col-I fibres. MMP 1 is also reported to support re-epithelialization by helping the keratinocytes to migrate over collagen type I provisional matrix, by degrading and modulating the collagen fibres [322]. Higher MMP 1 expression on day 7 and day 14 supported faster re-epithelialization in the wounds treated with NMSF mats. Sustained

increase in the expression of Col-I in all wounds, was a clear indicator of progression in the wound healing process. The constant expression of MMP 2 in treated wounds, pointed to its constitutive expression in wounds treated with nanofibrous mats. Higher MMP 9 expression in control wounds signified prolonged inflammatory condition along with higher degradation of basement membrane inhibiting re-epithelialization [323]. Higher Col-III expression in the wounds treated by silk based dressings on day 7, signified early beginning of wound repair; since fibroblasts are known to secrete high amount of Col-III, in the early proliferative phase. Lowered expression of Col-III at the later phases (day 14 and 21) may be explained as collagen turn over, or beginning of tissue remodelling phase.

Variations in the morphology and amount of ECM fibres deposited in the healed tissues further revealed the role of different SF based biopolymers on ECM deposition and tissue remodelling (**Figure 3.8.**). The guidance provided by biomaterials during tissue regeneration process influence ECM deposition to a greater extent owing to cell-material interactions [265]. As discussed above regarding the upregulation and downregulation of certain MMPs and collagen gene expression during wound healing process; continuous ECM deposition, degradation, modulation of matrix and MMP-ECM crosstalk were shown. Higher expression of both MMP 1 and Col-1 was supported by the unaltered secretion of hydroxyproline in the wounds treated by NMSF dressings (from day 14 to day 21). It also implied modulation of provisional granulation tissue, towards a more resistant and mature dermal matrix. Presence of mature and thick collagen bundles distributed homogeneously in the wounds treated by PVAAA and PVAPR demonstrated better collagen deposition. Morphology of mature elastin and reticulin fibres distributed underneath the epidermal layer of regenerated skin signified role of NMSF in their early regeneration. Higher levels of elastin and hydroxyproline quantified on day 7 and 14 further supported faster ECM deposition by PVAAA and PVAPR mats (**Figure 3.9.**).

The ECM remodelling events further confirmed that the extent and quality of ECM deposition is directly proportional to their physiological role, which was measured by their maximum tensile strength (**Figure 3.10.**). Within 4 weeks, control wounds could reach only 20 % tensile strength of intact skin, as also observed in another study [324]. In comparison to control and PVA treated wounds, wounds treated with silk dressing showed higher wound strength, suggesting role of SF in organized secretion of ECM

components. Gross images of stretched skin also signified some hidden wound strength properties of different dressings. The wounds recreated on stretching the skin were bigger and central to the wound area as seen in case of control, PVA and PVABM. On the other hand, PVAAA treated wound was smaller in area and skin was torn off from the edge of wound, instead of main central wound zone, thus supporting higher wound strength. Similar result was found in case of PVAPR. The force required to break the wound directly measures the effective deposited ECM fibres and crosslinked collagen fibres present in the healed tissue. Further long-term study on the wound strength could reveal more aspects of NMSF based mats on their wound healing and ECM deposition properties. Among silk based nanofibrous mats, NMSF based mats represented potential wound healing material to be used as a dressing patch for treating chronic diabetic cutaneous ulcers. Thus, the present study addressed current unmet requirements of wound dressings for complete wound repair and regeneration.

3.5. Significant findings

The salient findings of this chapter are as follows:

1. The bioactive dressings thus developed provided vital support in enhancing cell migration towards the wound bed, even under high glucose environment of chronic wounds.
2. The combination therapy of EGF, bFGF and LL-37 triggered the healing process of diabetic wounds through functionalized silk-based nanofibrous mats.
3. Sustained release of bioactive molecules helped in re-establishing the growth factor pool of chronic wounds, thereby helping in stimulating the cells towards tissue regeneration.
4. Occurrence of biofilm and bacterial colonization in the diabetic wounds were effectively avoided by the human antimicrobial peptide incorporated in the wound dressings.
5. NMSF based dressings demonstrated functional advantage of providing cell-material interactions, which encouraged early angiogenesis, re-epithelialization and regulated ECM remodelling, including organized deposition of collagen type I, collagen type III, elastin and reticulin fibres. Greater wound strength of regenerated skin further supported the influence NMSF based dressings on ECM deposition.
6. Investigation of all the four phases of wound healing events occurring during the repair process highlighted NMSF based mats as bonafide dressing material, with great potential for treating compromised chronic wounds like DFU.

Based on the findings of the present study, it is evident that silk-based dressings provide vital support in wound repair and regeneration. Further study in other wound models like venous ulcers or pressure sores will be an interesting proposition to examine healing efficacy of the developed dressings for treating various other types of chronic wounds.

Chapter 4

Development of functionalized bioactive materials using silk-silk interactions between silkworm silk fibroin and recombinant spider silk variants

This chapter describes the methodology to functionalize silkworm silk matrices using recombinantly produced spider silk fusion proteins for the fabrication of bioactive constructs in the form of wound dressings and skin grafts. Herein, variety of SF matrices, namely, coatings, nanofibrous mats and porous scaffolds are explored in the form of a bulk material, which are further functionalized, representing successful development of a potential multifunctional wound dressing material and cellular skin graft.

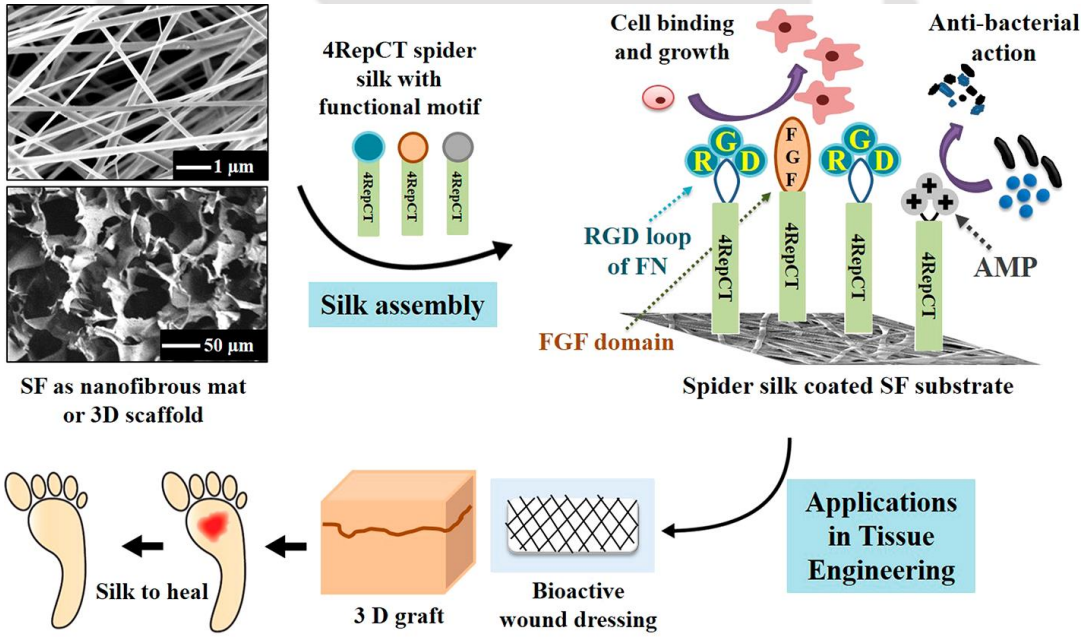

The work embodied in this chapter is published:
Chouhan D, Thatikonda N, Nileback L, Widhe M, Hedhammar M, Mandal BB. Recombinant spider silk functionalized silkworm silk matrices as potential bioactive wound dressings and skin grafts. *ACS Applied Materials & Interfaces* 2018; 10: 23560-72.

ABSTRACT

Silk is considered to be a potential biomaterial for a wide number of biomedical applications. Silk fibroin (SF) can be retrieved in sufficient quantities from the cocoons produced by silkworms. While it is easy to formulate into scaffolds with favourable mechanical properties, the natural SF does not contain bioactive functions. Spider silk proteins on the other hand, can be produced in fusion with bioactive protein domains, but the recombinant procedures are expensive and large-scale production is challenging. Herein, we combined the two types of silk to fabricate affordable, functional tissue engineered constructs for wound healing applications. To achieve this, nanofibrous mats and microporous scaffolds made of natural silkworm SF were used as a bulk material, which were top-coated with the recombinant spider silk protein (4RepCT) in fusion with a cell-binding motif, antimicrobial peptides and a growth factor. For this, the inherent silk properties were utilized to form interactions between the two silk types by self-assembly. The intended function, *i.e.* improved cell adhesion, antimicrobial activity and growth factor stimulation, could be demonstrated for the obtained functionalized silk mats. As a skin prototype, SF scaffolds coated with functionalized silk were co-cultured with multiple cell types to demonstrate formation of a bi-layered tissue construct with a keratinized epidermal layer under *in vitro* conditions. Thus, the encouraging results supported fabrication of an affordable bioactive SF-spider silk based biomaterial matrices as potential wound dressings and skin substitutes.

4.1. Introduction

Skin regeneration is an important challenge due to complexity of different kinds of wounds as well as costly treatments. Wounds like diabetic foot ulcers, venous ulcers or pressure sores are chronic wounds, where the healing process stalls due to the pathophysiological conditions [12, 325]. Around 6.5 million people are suffering from chronic wounds, with an estimated cost of $ 25 billions [10]. Increasing number of such cases impose a great demand of effective solutions for healing at low cost. Other traumatic wounds like full thickness burn wounds and lacerations impose a great threat due to the significant skin loss and damaged tissue integrity [8]. Use of autografts, artificial grafts, polymeric dressings, tissue engineered acellular grafts and other therapeutic approaches have resulted in improved wound healing outcomes [1, 8]. However, the limitations of available grafts and wound dressings necessitate advancement in the current technology. Another challenge in therapeutic approaches for treatment of chronic wounds is to combat cellular senescence, bacterial bioburden and prolonged inflammation [8, 12, 30]. Therefore, there is a great demand of bioactive wound dressings or grafts, which not only stimulate cells for proliferation but also provide antibacterial action; and thereby improve the wound healing process.

In this context, fabrication of functionalized scaffolds through various strategies have emerged in the field of tissue engineering [303]. Due to lack of bioactivity in the commercially available materials, researchers have resorted to the recombinant DNA technology to functionalize protein-based materials [326]. As such, functionalized recombinant spider silk proteins expressed in bacteria holds great potential for the development of advanced biomaterials [213]. The recombinant partial dragline spider silk protein 4RepCT (herein denoted as 4RC) is a self-assembling protein derived from *Euprosthenops australis* [327, 328]. 4RC is a part taken from the natural spidroin, and comprises four sequential repeats of poly-alanine/glycine-rich moieties and a non-repetitive C-terminal domain [327, 328]. Further, 4RC possesses the property to self-assemble into materials, which are suitable as cell culture matrices [326, 328].

The 4RC protein can be functionalized by means of recombinant DNA technology, wherein the gene encoding a functional peptide sequence or a fold-dependent protein domain can be fused to the silk gene [237, 300, 329]. For instance, the recombinant technology has enabled fusion of functional motifs like antimicrobial

peptides (AMP-4RC) and a cell adhesion motif from fibronectin (FN-4RC) to the partial spider silk protein [237, 300]. The 4RC protein has shown promising results for tissue engineering applications due to mechanical strength, non-immunogenicity and biocompatibility of the matrices made thereof, and improved bioactivity when conjugated with functional motifs [213, 235, 237, 300, 326]. However, due to rather expensive production procedures and limited yields obtained from recombinant expression systems, spider silk is less suitable as a bulk material for fabricating grafts or tissue engineered organs in large scale. In order to efficiently develop bioactive grafts, we resorted to use silk-assembly to combine a bulk of natural silkworm silk fibroin (SF) with a top-coating of functionalized spider silk fusion proteins.

Silk has been explored in various biomedical applications like tissue engineering and drug delivery during the last few decades [22, 23, 47, 249]. As an example, silk based bilayer skin constructs have recently been developed by using SF nanofibrous matrix on top of decellularized human amniotic membranes, and shown to guide scarless healing of burn wounds [330]. Improvement of SF based constructs have previously been performed by mixing or chemical coupling with bioactive compounds like growth factors, antibiotics or other molecules [91, 331]. Here, we aim to immobilize functional motifs on SF substrates in a facile and cost-effective manner by coating them with bioactive spider silk fusion proteins instead. In our recent study, we already explored the interactions between the recombinant spider silk protein 4RC with silkworm SF and established a procedure for easy functionalization of the SF substrates with various 4RC fusion proteins [332]. We could then conclude that 4RC and its functionalized variants can self-assemble into stable coatings onto the SF substrates. Therefore, through the present study, we aimed to fabricate multifunctional bioactive silk matrices using silk assembly, which can be used as potential wound dressing and artificial skin graft. The combined materials of silkworm SF and spider silk fusion proteins were thus selected to gain cell-binding, antimicrobial and growth factor activity through the top-coating with 4RC fusion proteins.

This chapter demonstrates fabrication of silk constructs with bioactivity that is of interest for advanced skin healing. For this, recombinant 4RC proteins fused with a cell-binding motif from fibronectin (FN), a growth factor (FGF) or cationic peptides with antimicrobial properties (AMPs), were used. We used two types of silkworm SF to further look into the development of stable functional grafts. *Bombyx mori*, the mulberry

silk variety, which is available world-wide and has been extensively explored as a biomaterial for tissue engineering applications [23]. *Antheraea assama*, a non-mulberry silk variety, which possesses excellent biocompatibility and has great potential in tissue engineering, although less explored [214]. SF from both silkworm varieties holds properties like biocompatibility, low immunogenicity, biodegradability and tunable mechanical strength, which is essential for developing 3D tissue engineered products [23, 24, 248]. The ease of processability and flexibility also allows fabrication of various formats like films, sponges, nanofibrous mats, hydrogels, microparticles or nanoparticles [23, 24, 248, 333]. Herein, we use the formats of thin coating, nanofibrous mats and 3D porous scaffolds coated with spider silk protein as shown in the macroscopic and macroscopic images (**Figure A4.1. and A4.2.**). The results of the study reveal an easy, efficient and affordable way to develop functionalized constructs for tissue engineering applications.

4.2. Materials and methods

4.2.1. Preparation of silk fibroin solutions

SF solutions were obtained from *B. mori* silk cocoons and *A. assama* silk glands following the standard protocols [215, 227]. Briefly, B. *mori* cocoons were cut into small pieces and subsequently washed using 0.02 M sodium carbonate solution in boiling water to remove sericin. The degummed silk fibres were dissolved in 9.3 M lithium bromide (LiBr) solution and incubated at 60 °C for 4 h. The solution was subsequently dialyzed against water at room temperature (RT) using a cellulose dialysis membrane (12 kDa, Sigma Aldrich) to obtain an aqueous BmSF solution.

A. assama SF was isolated directly from the silk glands of fifth instar larvae of *A. assama*. The obtained silk protein was washed with distilled water thrice prior to its dissolution in 1 % (w/v) aqueous SDS solution. The debris from the dissolved SF solution was removed by centrifugation at 5000 rpm for 10 min at 4 °C. The supernatant SF solution was collected and dialyzed against water using the 12 kDa cellulose dialysis membrane for 4 h at 4 °C. The concentration of aqueous AaSF and BmSF solutions obtained after dialysis was measured using gravimetric method. Both SF solutions were further diluted to the desired concentration by adding water.

4.2.2. Fabrication of SF coatings, nanofibrous mats and scaffolds

Silk coatings were fabricated using re-constituted SF solutions. The aqueous silk fibroin solutions (AaSF and BmSF) were initially freeze-dried using lyophilizer Alpha 1-4 LD plus (Martin Christ Gefriertrocknungsanlagen) and re-constituted back to the aqueous state at the concentration of 1 mg/mL. The reconstituted SF solution was subsequently diluted ten folds in 20 mM Tris (hydroxymethyl) aminomethane (Tris) buffer, pH 8.0. The concentration of final SF solutions used for developing SF coatings was 0.1 mg/mL in Tris buffer. The SF solutions were poured onto the wells of hydrophobic plates (TC Plate 96 Well, Suspension, F, Sarstedt) and incubated for 1 h at 37 °C. The remaining solution was collected and coated wells of the plate were used for cell culture studies.

Nanofibrous mats were prepared by blending the respective SF solutions with poly(vinyl alcohol) (PVA) using electrospinning method [314]. Two types of nanofibrous mats were prepared: one blended mat from BmSF + PVA solution (called as BmSF mat herein) and another from AaSF + PVA solution (called as AaSF mat herein) described as PVABM and PVAAA respectively in chapter 1. Blend of SF and PVA (1:4 w/w) solution was filled in the syringe and respective nanofibrous mats were fabricated using electrospinning unit Super ES1 (E-spin nanotech). The instrument parameters for the fabrication of mats were set as follows: voltage = 25 ± 3 kV, flow rate = 0.800 ± 0.100 mL/h, tip to collector distance (d) = 15 cm, and rotating speed of drum collector = 500 rpm. The fabricated as spun mats were treated with 70 % ethanol for 2 h for β-sheet induction. Subsequently, the mats were washed four to five times with sterile water in order to remove residual ethanol. Further sterilization was carried out on the wet mats using UV radiation for 20-30 min on each side of the mat prior to cell culture studies.

Silk based microporous scaffolds were fabricated using well-established freeze-drying technique [334, 335]. Briefly, 300 µL of 2.5 % (w/v) BmSF and AaSF solutions, respectively, were poured into each well of a 24-well plate. The plates were frozen at -20 °C overnight and then subjected to freeze dry for 24 h. The freeze-dried scaffolds obtained as such were treated with 100 % ethanol for 1 h followed by 70 % ethanol for 6 h to induce β-sheets. The treated scaffolds were extensively washed with water four to five times and were subsequently autoclaved in wet condition for sterilization prior to use.

4.2.3. Recombinant spider silk proteins and their coating on SF substrates

Recombinant spider silk proteins were provided from Spiber Technologies AB (Spiber®, Sweden) and stored frozen in 20 mM Tris buffer, pH 8.0. Four types of recombinant spider silk proteins have been used in the present study: FN-4RepCT (cell-binding motif with the sequence CTGRGDSPAC from fibronectin fused to 4RepCT), Mag-4RepCT (antimicrobial motif with the sequence GIGKFLHSAGKFGKAFVGEIMKS fused to 4RepCT), Lac-4RepCT (antimicrobial motif with the sequence FKCRRWQWRMKKLG fused to 4RepCT) and FGF-4RepCT (fibroblast growth factor (FGF2) with the sequence AAGSITTLPALPEDGGSGAFPPGHFKDPKRLYCKNGGFFLRIHPDGRVDGVREK SDPHIKLQLQAEERGVVSIKGVCANRYLAMKEDGRLLASKCVTDECFFFERLE SNNYNTYRSRKYTSWYVALKRTGQYKLGSKTGPGQKAILFLPMSAKS fused to 4RepCT). Proteins were thawed, centrifuged briefly to remove aggregates, and diluted in 20 mM Tris, pH 8.0 to obtain 0.1 mg/mL solutions.

The spider silk proteins (0.1 mg/mL solutions) were then coated onto the SF coatings, mats and scaffolds following the below mentioned procedure. Briefly, for the coatings format, pristine AaSF and BmSF coatings were first developed onto the wells of hydrophobic plates as mentioned earlier. SF coatings were washed gently with Tris buffer twice and spider silk solution was added to the wells. After the incubation of 1 h at 37 °C, the excess spider silk solution was removed and the wells were again washed three times with Tris buffer before cell seeding. Similarly, coating of spider silk on the SF mats was also performed. The sterile nanofibrous mats were cut in circular shape to fit in the well of 24-well plate (Sarstedt, suspension cells). The mats were then made wet by incubating in sterile PBS for 30 min. Subsequently, PBS was removed and 100 µL of spider silk solution was added on top of the mats. After incubating them at 37 °C for 1 h, the excess spider silk solution was removed and washed three times with Tris buffer before cell seeding. For coating the porous SF scaffolds with spider silk, dip coating method was applied. Briefly, sterile scaffolds (6 mm in diameter) were washed with 20 Tris buffer twice, submerged into the spider silk solution and incubated for 1 h at 37 °C. The scaffolds were retrieved back from the spider silk solution, placed into transwells in a 24-well plate and washed with Tris buffer twice prior to culturing cells. All the cell

culture experiments on SF substrates were performed without prior conditioning with media.

4.2.4. Cell culture on coatings and cellular assays

Human dermal fibroblasts of neonatal origin (HDFn, passage 6, ECAAC, Salisbury, UK) and the human keratinocyte cell line HaCaT (Cell line service, Germany) were used for cellular studies on various silk coatings. Five different types of silk coatings were developed in the wells of 96-well HP plate. Three coatings of silk varieties were FN-4RC, AaSF, BmSF. Two dual coatings developed were AaSF/FN-4RC and BmSF/FN-4RC denoting to coating of FN-4RC on top of AaSF and BmSF coatings. Cells were harvested with TrypLE Express (Life Technologies) when reaching a confluency of 80 – 90 % for subculture or experiments. DMEM nutrient mixture F12 ham (Sigma) supplemented with 5 % foetal bovine serum (Sigma), penicillin (100 U/mL), and streptomycin (100 µg/mL) was used for expanding and maintaining the culture of HDFn and HaCaT cells. Cells were cultured with a density of 3500/cm^2 in each well of a 96 well plate and cell adhesion test was performed. Briefly, after 1 h of incubation in cell incubator, the media was removed gently and the culture was washed with pre-warmed PBS to remove non-adhered cells. The adhered cells were fixed using 96 % ethanol for 10 min and stained with 0.1 % crystal violet in H_2O for 30 min. The wells washed with water and cell adhesion was observed by taking micrographs at 2X and 10X magnification in an inverted bright field microscope.

Next, quantification of cell proliferation and viability test was performed by culturing cells on the coatings for a period of 7 days. Proliferation of cells cultured with a density of 3500/cm^2 on various silk coatings was analysed by quantifying the reduction of Alamar blue (Invitrogen) at specified time-points *viz.*, 0, 2, 4 and 7 days. Briefly, the spent media was removed from the culture, Alamar blue (diluted 1:10 in fresh medium) was added and incubated at 37 °C for 2 h. The reduced dye solution was collected back from the culture and fluorescence intensity of the solution was measured with a fluorescence plate reader (CLARIOstar, BMG Labtech) using excitation at 544 nm and emission at 595 nm. The experiment was terminated and cell viability was analysed on day 7 using live/dead assay (Life technologies). Culture media was removed, washed gently with PBS and live dead solution Calcein AM (4 µM) and ethidium homodimer (2 µM) in complete medium was added. After the incubation for 20-30 min, the live dead

solution was removed and samples were washed twice with PBS. Live cells appeared green in colour owing to the active esterase activity upon treatment with Calcein AM dye. The dead cells were visible in red fluorescence due to binding of ethidiumhomodimer-1 dye to the DNA of dead and damaged cells. Imaging was done using an inverted fluorescence microscope (Nikon Eclipse Ti) and whole well images were taken at 2X magnification using NIS elements BR (Nikon).

4.2.5. Antibacterial and antibiofilm examination of coated SF mats

Lac-4RepCT and Mag-4RepCT spider silk variants were coated on the nanofibrous mats as described above. Antibacterial action of spider silk coated nanofibrous mats was evaluated against two skin infecting bacteria *Staphylococcus epidermidis* (SE) MTCC 435 and *Pseudomonas aeruginosa* (PA) MTCC 1688 obtained from Microbial Type Culture Collection and Gene Bank (MTCC, IMTECH, India) in comparison with uncoated mats. 10 µL of bacterial culture containing bacteria with cell density of 1×10^6 CFU/mL was withdrawn from the individual inoculums, which was further diluted with 990 µL of fresh nutrient broth (Himedia, India) before culturing onto the mats. The nanofibrous mats immersed in 1 mL of bacterial suspension culture was incubated at 37 °C for 24 h in static condition. 100 µL of bacterial culture was withdrawn at specific time points (1, 3, 6, 12, 18, 24 h) and analysed spectroscopically at 600 nm using multiplate reader (TECAN infinite M 200 pro). Ampicillin (500 µg/mL) and Gentamicin (500 µg/mL) were used as the positive control for the gram-positive and gram-negative bacteria respectively. Samples were taken in triplicates.

The experiment setup used for above experiment was carried further to examine the anti-biofilm activity of mats using crystal violet staining. The bacterial culture in the plates previously incubated for 24 h was removed; mats were washed gently with sterile PBS and 99 % ethanol was added to fix the adhered bacteria or biofilm. The mats were stained with 0.1 % crystal violet (Himedia, India) for 30 min and rinsed twice. Acetic acid (30 %) was then added and incubated for 30 min at RT with gentle shaking. The collected crystal violet solution was measured by taking absorbance at 595 nm using multiplate reader (TECAN infinite M 200 pro) and plotted with respect to the biofilm formed by bacteria cultured on uncoated mats.

4.2.6. Cell culture on FN-4RC coated SF nanofibrous mats and cellular assays

AaSF and BmSF mats coated with FN-4RC denoted as AaSF/FN-4RC and BmSF/FN-4RC respectively were first examined using HDFn and HaCaT culture. Uncoated AaSF and BmSF mats were used as controls for the study. Cell seeding was performed as described earlier with the density of 10000/cm^2 and culture was maintained for a period of 14 days. Medium was changed every alternate day. Cell proliferation was quantified by the reduction of Alamar blue at specified time-points, *viz*., 1, 3, 7, 10 and 14 days as described previously. Similar set of experiment was performed and maintained for 7 days to assess the cell viability by live/dead assay. Further, for morphological observations, another set of similar experiment was maintained for 3 and 14 days. Briefly, the cultured cells on various mats were washed with PBS and fixed with 4 % paraformaldehyde. Blocking with 1 % BSA and permeabilization with 0.1 % Triton X 100 was done prior to staining. Specific dyes for actin filaments and nuclei used for cell morphological observations were: Phalloidin-Alexa Flour 488 diluted 1:500 and DAPI 1:1000 respectively. Samples were viewed under a Nikon Eclipse T*i* inverted fluorescence microscope and pictures were taken at 10 X magnification using NIS elements BR (Nikon). All the experiments described in this section were performed using complete media (with FBS) in cell incubator at 37 °C with 5 % CO_2 and 95 % humidity.

4.2.7. Cell culture on FGF-4RC coated SF nanofibrous mats and cellular assays

To study the effect of FGF-4RC coating on SF mats, human umbilical vascular endothelial cells (HUVEC) were used. Six different types of SF mats were developed: uncoated AaSF, uncoated BmSF; FGF-4RC coated SF mats denoted as AaSF/FGF-4RC and BmSF/FGF-4RC respectively; and combined coating of FN-4RC and FGF-4RC proteins denoted as AaSF/FN + FGF-4RC and BmSF/FN + FGF-4RC. HUVECs were expanded in gelatin coated T-75 flask using specialized media for endothelial cells (endothelial cell growth medium (C-22010, Promocell containing 2 % fetal bovine serum, PromoCell GmbH, Germany) prior to cell seeding. After spider silk coating on SF mats, cells were seeded at the density of 10000 /cm^2 and maintained in medium lacking supplemented growth factors and reduced serum (0.5 %) for 48 h in cell incubator. Difference in the cellular activity among various mats after 48 h of culture was evaluated using Alamar blue reduction assay. For morphological observation of HUVEC after 48 h of culture in similar reduced serum (0.5 %) conditions, the cells were

fixed and stained with Phalloidin-Alexa Flour 488 and DAPI as described in previous section.

4.2.8. Cell culture in SF scaffolds and development of skin substitute

Co-culture of two or three cell types was carried out in the porous silk scaffolds for developing *in vitro* skin construct. HDFn and HaCaT cells were maintained as described before. Human dermal microvascular endothelial cells (HDMEC, PromoCell GmbH, Germany) were expanded in gelatin coated T-75 flask using specialized media for endothelial cells (endothelial cell media, containing 5 % FBS, PromoCell GmbH, Germany). HDF and HDMEC were co-cultured in the scaffolds with the density of 20000/cm^2 and 2000/cm^2 respectively. The transwells were maintained in submerged conditions and media was changed every alternate day. On the 7th day of culture, HaCaT were seeded at the density of 100000/cm^2 on top of the co-cultured scaffolds. The transwells were air-lifted on day 2 after seeding HaCaT cells, i.e. 9th day of culture and then maintained in such a way to provide air-liquid interface to the uppermost layer of the scaffold. The culture was sustained for 21 days from the beginning; in which air-liquid interface conditions were maintained for 12 days. The bottom layer was in submerged condition to provide nutrition to the cells. The media used in the co-culture study contained DMEM nutrient mixture F12 and endothelial cell media mixed in equal volume. For control studies, scaffolds were co-cultured with HDF and HDMEC at the same density without subsequent seeding of HaCaT cells.

4.2.9. Histological and immunofluorescence examination of the co-cultured scaffolds

The cultured scaffolds were fixed using 4 % paraformaldehyde, stored in 20 % sucrose solution and 25 µm thick sections were made using cryomicrotome (Leica). Both transverse cross section and lateral sections were taken. The sections were stained with haematoxylin and eosin (H & E; Sigma-Aldrich) for general morphological observations following manufacturer's protocol prior to antibody staining. Specific marker study was performed by immunofluorescence using specific antibodies for epidermal layer. The sections were incubated with 0.1 % Triton X 100 and 1 % BSA for permeabilization and blocking respectively. Primary antibodies were used at the following concentrations: mouse IgG1, unconjugated (BioSite, 10 µg/mL), mouse anti human Involucrin (SY5,

Sigma, 10 µg/mL), rabbit anti human Keratin 5 (BioSite, 1 µg/mL), and rabbit anti human Keratin 10 (Bio Legend, 5 µg/mL). After 30 min incubation with primary antibody, the sections were washed with PBS and then secondary antibody (Alexa-Flour 488 goat anti mouse IgG (Invitrogen, 4 µg/mL) was applied for 30 min. Counterstaining was done using DAPI and incubated for 10 min. The slides were mounted and images were taken using Nikon Eclipse T*i* inverted fluorescence microscope.

4.2.10. Statistical analysis

All the experiments were carried out for n = 3 samples (replicates) unless otherwise specified. Data were expressed as mean ± standard deviation. Data analysis was done using statistical software OriginPro 8 (Origin lab Corporation, USA) at both significant (* $p \leq 0.05$) and highly significant (** $p \leq 0.01$) level. The significance level was calculated by comparing the data between groups and within groups by performing one-way analysis of variance (ANOVA) followed by Tukey's test.

4.3. Results

4.3.1. Effect of combined silk coatings on skin cells

We first examined the effect of silk proteins on cell adherence by culturing skin cells on various combined silk coatings through quick adhesion assay. A spider silk protein with a cell binding motif from fibronectin FN-4RC was coated on top of SF coatings; whereas pristine SF coatings (AaSF and BmSF) were used as control. The density of HDFn and HaCaT cultured for 1 h was observed using crystal violet stain (**Figure 4.1.**). Coating with FN-4RC resulted in a significant improvement in attachment of HaCaTs for both types of SF (**Figure 4.1.A**). In contrast, a clear difference was not visible in case of HDFn cells among AaSF and AaSF-FN (**Figure 4.1.B**), which might be due to the presence of inherent RGD motifs in AaSF that binds to integrins of HDFn quickly. Lack of RGD sequence in BmSF led to low binding of HDFn cells in comparison to BmSF-FN, suggesting significance of spider silk coating.

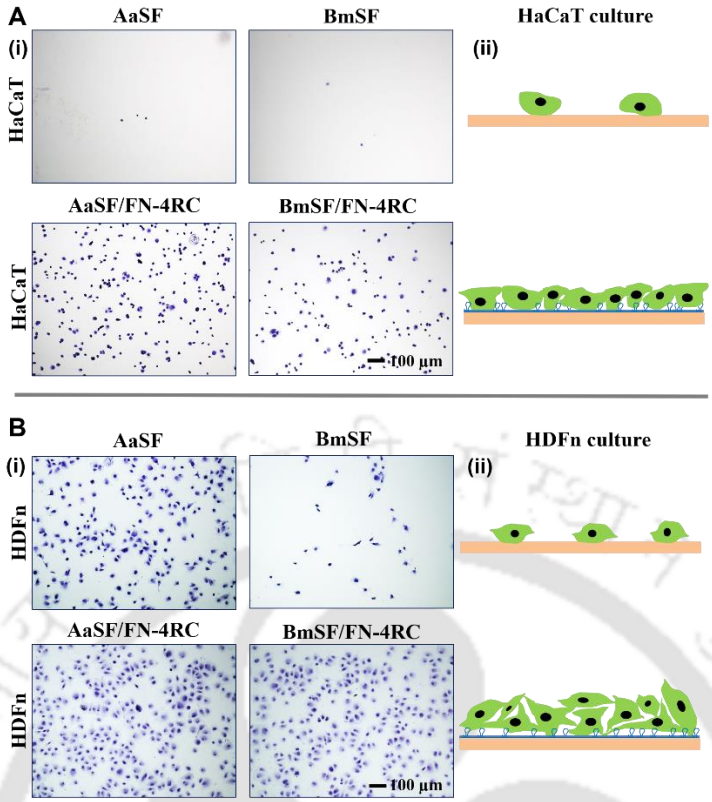

Figure 4.1. *Quick adhesion study on various silk coatings using (A) HaCaT cells and (B) HDFn cells stained with crystal violet. (i) Macrographs at 10X magnification demonstrate density of cells after 1 h adhesion to various silk coatings. Scale bar represents 100 µm. (ii) Schematic representation of cell (green) attachment to pristine SF coatings (beige) and FN-4RC (blue) coated SF coatings. The RGD loop present in FN-4RC promotes cell binding.*

To further investigate the ability of combined silk coatings to support cell growth, we monitored the cultures with Alamar blue viability assay for 7 days (**Figure 4.2.**). Hydrophobic plates intended for suspension cell culture were used throughout the study to avoid the interference of cell attachment to the plastic. Therefore, barely any cell proliferation was observed in the uncoated wells. In contrast, the wells coated with AaSF or BmSF alone, as well as SF coated with FN-4RC, all showed cell viability and proliferation. For HaCaT cultures, both types of SF coatings covered with FN-4RC outperformed the pristine AaSF and BmSF coatings, suggesting a high impact of FN-4RC on cell proliferation. This further validated the results obtained from quick adhesion study. For HDFn, cultures on pristine BmSF showed significantly lower proliferation than other groups on day 7, $p \leq 0.01$. Except that, there was no significant difference in the cell proliferation among all the groups. A live dead assay performed after 7 days of culture further validated higher cell density on FN-4RC coatings at the end time-point.

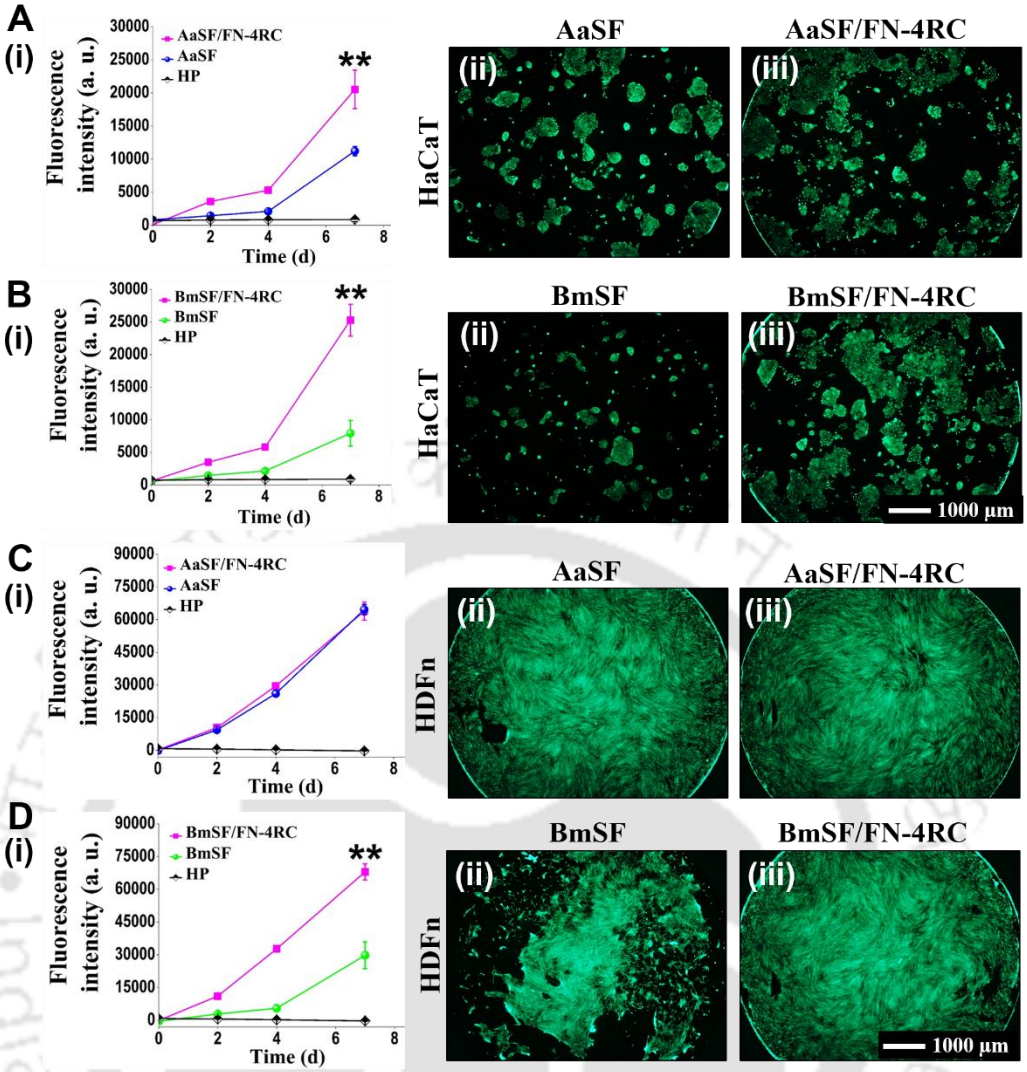

Figure 4.2. *Effect of FN-4RC coated SF on the proliferation and viability of (A, B) HaCaT and (C, D) HDFn cells, seeded at 3500/cm^2 density. (i) Alamar blue viability assay graphs of cells cultured on silk coatings for 7 days, ** represents $p \leq 0.01$. HP represents the uncoated wells. Micrographs of live (green)/dead (red) stained cells after culture for 7 days on (ii) pristine SF coatings and (iii) FN-4RC coated SF coatings. Scale bar represents 1000 µm.*

4.3.2. Functionalization of SF mats with antimicrobial peptides conjugated to spider silk

To prevent bacterial colonization in case of chronic wounds, we further targeted to functionalize the developed SF mats with antimicrobial activity. For this purpose, we coated the mats with spider silk fusion proteins containing the cationic AMPs Magainin I (Mag-4RC) and Lactoferricin (Lac-4RC), respectively. We selected two of the major skin infecting bacteria, *P. aeruginosa* and *S. epidermidis*, to investigate antibacterial action of SF mats coated with Mag-4RC and Lac-4RC (**Figure 4.3.**). The anti-biofilm

action of the coated mats was examined by estimating bacterial adhesion on mats using crystal violet staining after 24 h of bacterial culture on the mats (**Figure 4.3.B**). A significantly higher $O.D._{595nm}$ observed by crystal violet staining demonstrated almost 5-fold increase in bacterial population on uncoated mats as compared to the coated mats ($p \leq 0.01$).

We further measured bacterial growth to see the effect of AMP-silk on both types of bacteria growing on coated and uncoated SF mats (**Figure 4.3.C,D**). Both types of bacteria continued to grow on the uncoated mats during 12 h. In contrast, the coated mats (both Mag-4RC and Lac-4RC) were found to be highly efficient in decreasing bacterial growth ($p \leq 0.01$). However, significantly higher $O.D._{600nm}$ was observed for the coated mats in comparison to the positive control i.e. an antibiotic drug in solution. This suggested that the AMP-4RC coated SF mats slowed down the bacterial growth but did not kill the bacterial population completely. In summary, the coating with recombinantly produced spider silk in fusion with Mag or Lac allowed a facile method to functionalize SF mats with antibacterial motifs.

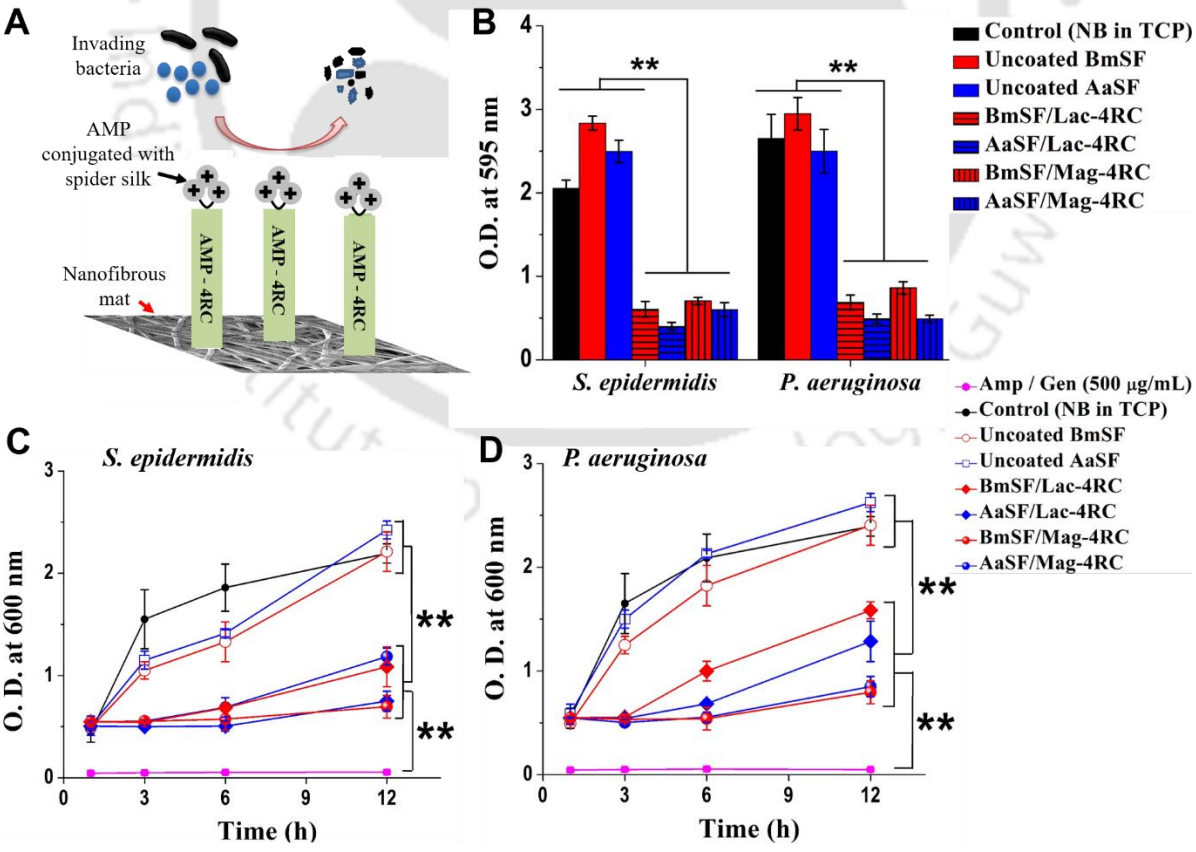

Figure 4.3. *Antibacterial assay on nanofibrous SF mats coated with 4RC conjugated with Mag or Lac cationic peptides. (A) Schematic representation shows the function of*

Mag-4RC or Lac-4RC that had been assembled onto SF nanofibrous mats. (B) Anti-biofilm assay using crystal violet staining shows significantly less biofilm formation on the spider silk coated SF mats compared to uncoated mats, $p \leq 0.01$. (C, D) Growth curve of bacteria inoculated at 1 x 10^6 CFU depicts significantly lower bacterial growth on the spider silk coated SF mats compared to uncoated mats; $p \leq 0.01$. Spider silk conjugated with AMPs slowed down the bacterial growth. The positive controls, antibiotic drugs Gentamicin and Ampicillin (500 µg/mL), showed significantly lower bacterial growth than the AMP-silk coated SF mats, $p \leq 0.01$.

4.3.3. Functionalization of SF mats with FN-silk

Here, we first used the recombinant spider silk 4RC conjugated with the cell binding motif from fibronectin FN-4RC to investigate cellular behaviour of fibroblasts and keratinocytes on the coated mats. Alamar blue viability assay revealed differences in the proliferation of fibroblasts and keratinocytes when cultured on the SF mats coated with FN-4RC compared to uncoated SF mats (**Figure 4.4.A,B**). Significantly higher proliferation of HaCaT was observed on AaSF/FN-4RC and BmSF/FN-4RC compared to the respective uncoated mats, suggesting a considerable impact of FN-4RC ($p \leq 0.01$). For HDFn cultures, highest proliferation was observed on AaSF/FN-4RC mats from day 1 to day 7 ($p \leq 0.01$). In addition, BmSF/FN-4RC showed higher proliferation in comparison to both uncoated AaSF and BmSF mats up to day 10, suggesting affirmative bioactivity of FN-4RC coated SF mats ($p \leq 0.01$). Higher fluorescence values were obtained from coated mats, depicting significantly higher cell adhesion already 24 h after cell seeding ($p \leq 0.01$). To further look into it, we examined the morphology of HDFn and HaCaT after day 3 of culture (**Figure 4.4.C,D**).

Similar type of extended cell morphology was observed for HDFn on uncoated AaSF mats, probably due to the RGD sequence present in the AaSF protein. This implies a higher degree of cell adhesion of HDFn, as observed by the protrusions of cells all around the mats. In contrast, cells with narrow and constricted cell morphology were found on uncoated BmSF mats, while extended cells were found on BmSF mats coated with FN-4RC. Morphological differences of HaCaTs on SF mats on day 3 attested the variation of cellular behaviour between coated and uncoated SF mats. The results were also validated by the cell viability test performed on day 7, where coated mats showed a higher density of live cells in comparison to uncoated mats (**Figure 4.5.**). After 14 days

of culture a similar cell density was observed on all the mats, suggesting good biocompatible properties of all individual silk proteins (**Figure 4.6.**).

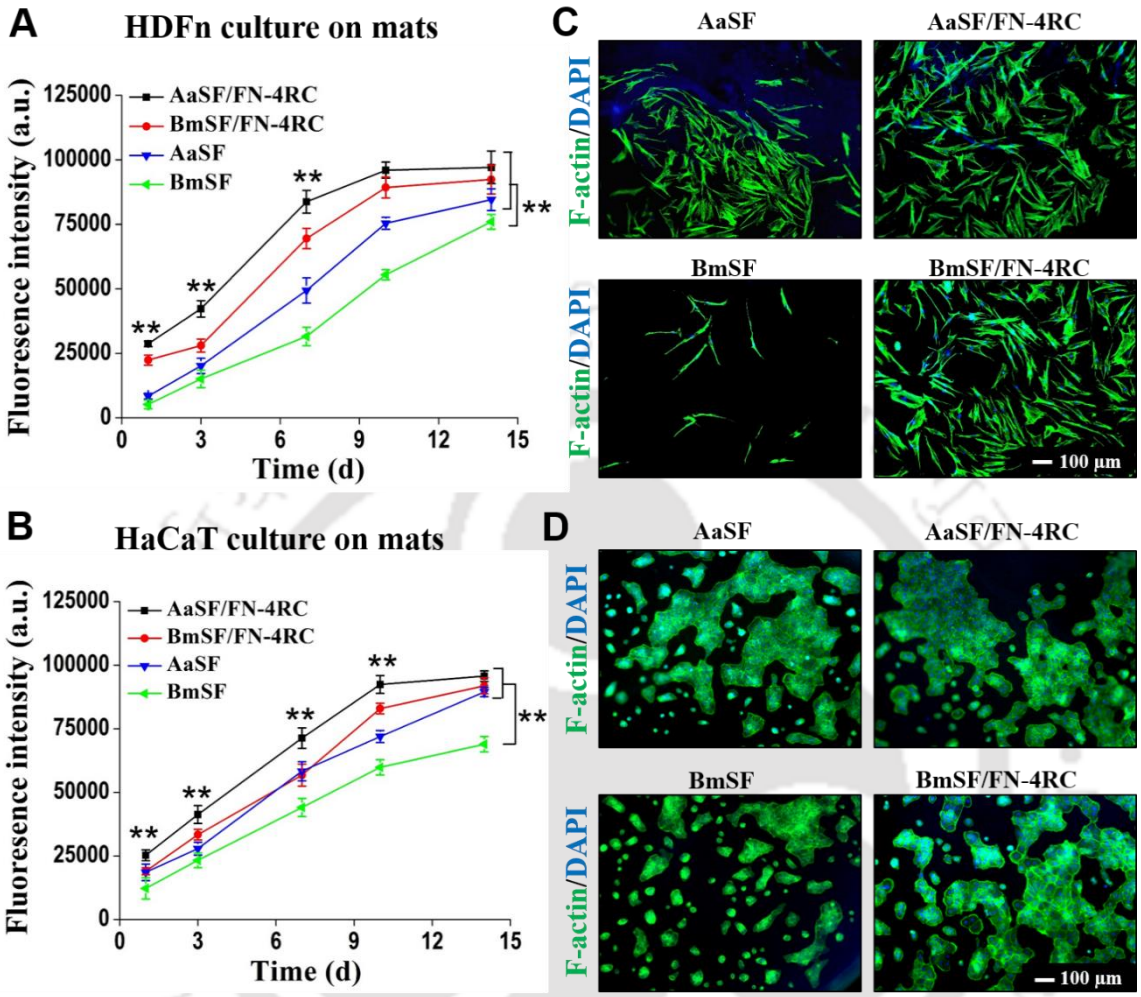

Figure 4.4. *Two weeks-cell culture study on SF nanofibrous mats coated with FN-4RC. Alamar blue viability assay graphs depict difference in the proliferation of (A) HDFn and (B) HaCaT seeded at 10000/cm^2 density on FN-4RC coated and uncoated SF mats. AaSF/FN-4RC mats demonstrated highest proliferation of both cell types compared to other mats on day 1, 3 and 7, $p \leq 0.01$. Morphological examination of (C) HDFn and (D) HaCaT on various mats after 3 days of culture. Cytoskeleton (f-actin) was stained with AlexaFluor Phalloidin (in green) and nucleus was stained with DAPI (in blue). Scale bar represents 100 µm.*

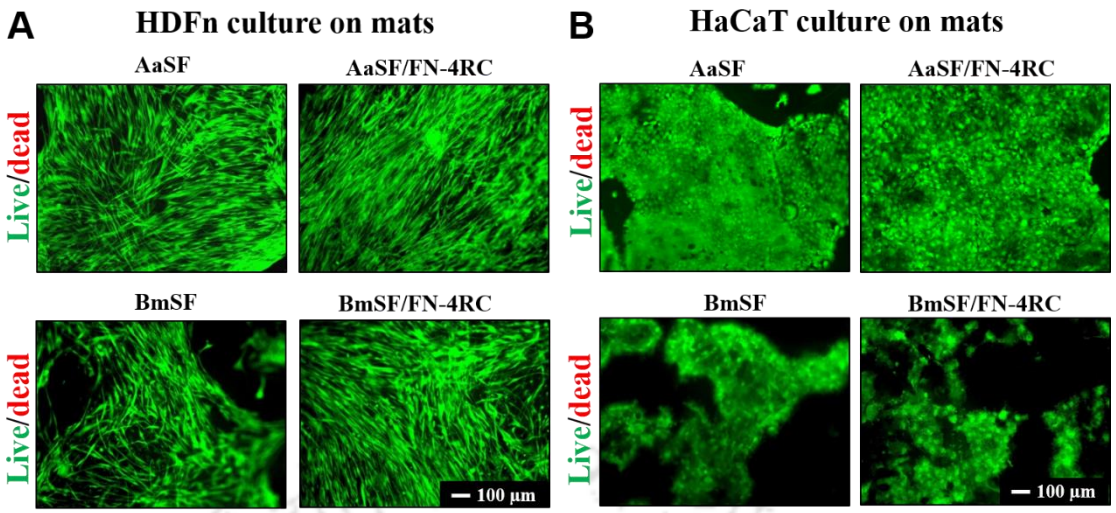

Figure 4.5. *Live/dead assay of (A) HDFn and (B) HaCaT seeded at 10000/cm^2 density after 7 days of culture on FN-4RC coated and uncoated SF mats. Scale bar represents 100 µm.*

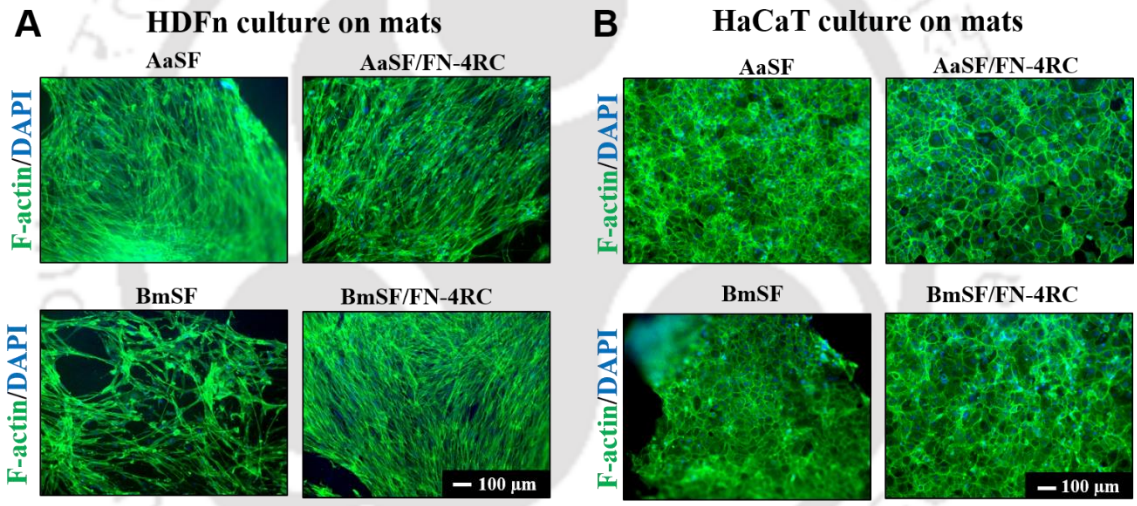

Figure 4.6. *Morphology of (A) HDFn and (B) HaCaT cells cultured on SF mats for 14 days. Cytoskeleton was stained with AlexaFluor Phalloidin showing f-actin (in green) and nuclei were stained with DAPI (in blue). Scale bar represents 100 µm.*

4.3.4. Functionalization of SF mats with FGF conjugated spider silk

Next, we coated SF mats with 4RC genetically fused to a fibroblast growth factor FGF-4RC, to examine the response of endothelial cells. HUVECs were cultured on SF mats with and without coating with FGF-4RC, in media without supplemented growth factors and in reduced serum (0.5 %). By quantifying the metabolic activity of adhered cells and observing morphological differences after 48 h, we investigated the effect of FGF-4RC coatings on the SF mats. Alamar blue viability assay performed after 48 h showed a higher cellular activity on the SF mats coated with FGF-4RC compared to uncoated mats

($p \leq 0.01$) (**Figure 4.7.A**). A significantly higher proliferation of HUVEC on AaSF/FGF-4RC compared to BmSF/FGF-4RC was also revealed ($p \leq 0.01$). Next, to investigate the effect of a combination of both FN-4RC and FGF-4RC, we coated SF mats with a mixture of both types of spider silk fusion proteins, and examined their synergistic effect on HUVEC culture. Combined coatings with FN-4RC and FGF-4RC demonstrated 4-fold higher adhesion of HUVEC in comparison to AaSF coated with only FGF-4RC. Morphological observations of HUVEC cultured on the SF mats with combined coatings indicated enhanced cell activity due to FN-4RC and FGF-4RC (**Figure 4.7.B,C**). In comparison to uncoated mats, the coated mats showed a high cell density of HUVECs with extended cytoskeleton and spread out morphology.

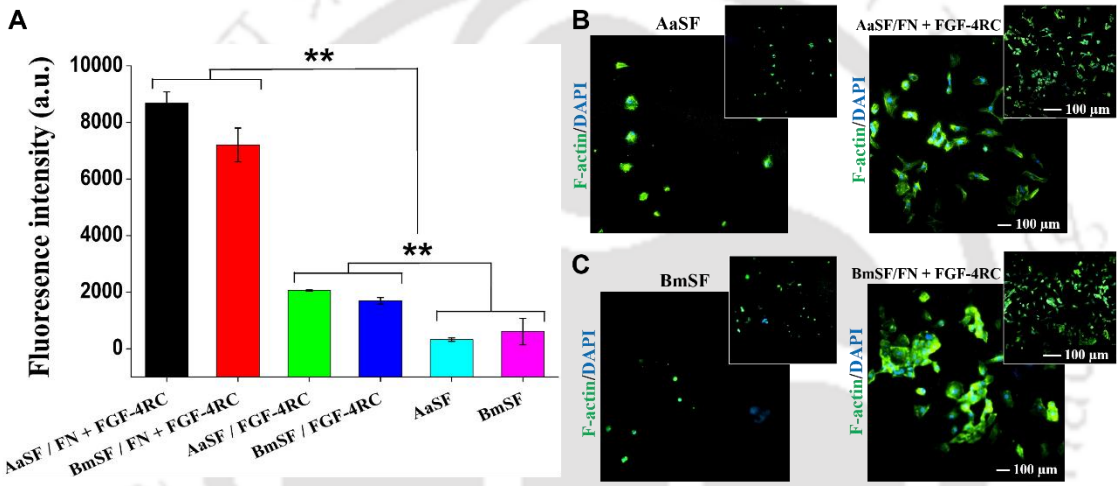

Figure 4.7. *Effect of FGF-4RC in combination of FN-4RC on HUVEC cells. (A) Alamar blue viability assay graph depicts quantitative measurement of the cell population adhered on coated and uncoated SF mats after 48 h culture of HUVECs in medium without supplemented growth factors and low serum (0.5 %). Combined coating of FN-4RC and FGF-4RC showed almost 4-fold higher cell activity in comparison to only FGF-4RC coating. (B, C) Morphology of HUVEC cultured on coated and uncoated mats after 48 h culture, captured at 20X and 10X (inset) magnification. Cytoskeleton (f-actin) was stained with AlexaFluor Phalloidin (in green) and nuclei were stained with DAPI (in blue). Scale bar represents 100 µm.*

4.3.5. Functionalization of SF scaffolds and co-culture of cells into a 3D skin graft

In order to simulate the bilayer structure of skin, we utilized porous architecture of 3D silk scaffold by co-culturing necessary dermal and epidermal cells *in vitro*. Dermal bed was first prepared by co-culturing skin derived HDFn and HDMEC in the FN-4RC

coated SF scaffolds. After 7 days of co-culture, we further seeded HaCaT on top of the cultured scaffolds, and provided an air-liquid interface for keratinization and development of epidermal layer, as represented in the schematic image (**Figure 4.8.A**). Cellular proliferation in the co-cultured scaffolds was confirmed using Alamar blue viability assay (**Figure 4.8.B**).

The combination of HDFn and HDMEC proliferated well in the co-culture system, as observed by the control scaffolds where HaCaT cells were not seeded. An abrupt rise in the growth profile was observed by day 10, was due to the highly proliferating HaCaT cells, which were seeded at 5 times higher density compared to HDFn after 7 days of culture. The higher intensity observed on day 10 also demonstrated that the air-liquid interface provided on the 9th day of culture did not lead to any substantial cell death or other abnormality. The coated SF scaffolds contained cell populations densely distributed throughout the scaffolds, in comparison to the low cellular density found in the uncoated scaffolds (**Figure 4.9.**). Proliferation of all the three cell types was higher in AaSF/FN-4RC and BmSF/FN-4RC as compared to pristine AaSF and BmSF scaffolds, probably due to the cell binding motif from fibronectin present in FN-4RC.

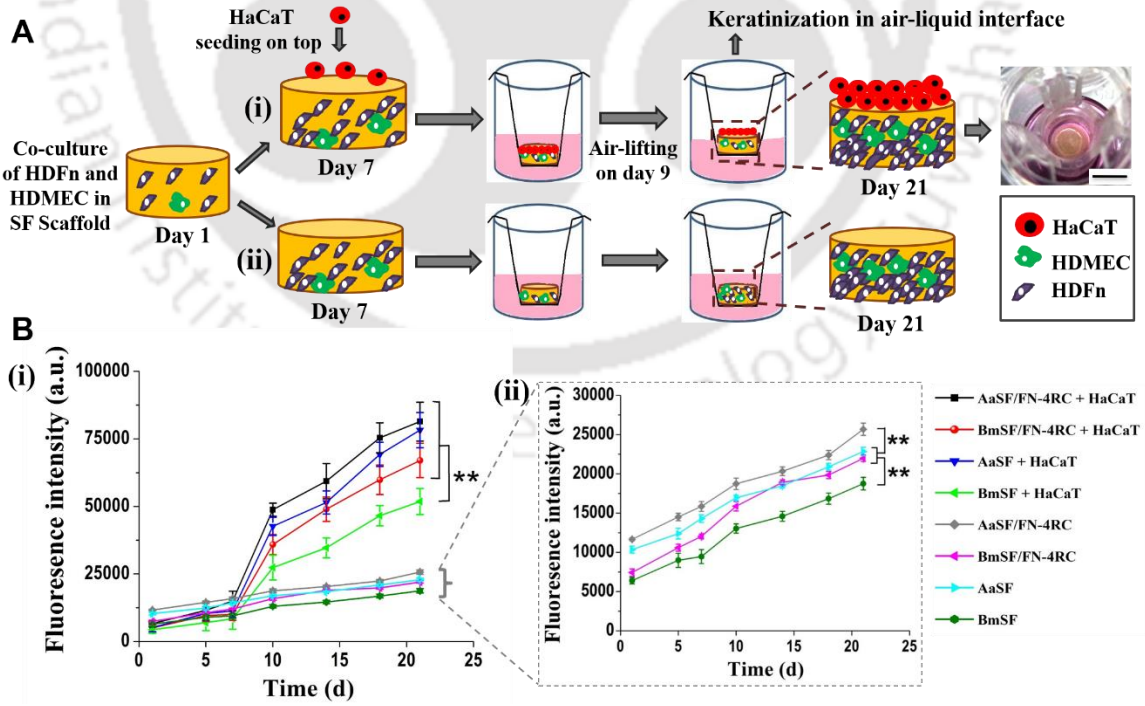

Figure 4.8. *(A) Schematic representation of the development of a skin graft by co-culturing various cell types on SF scaffolds coated with FN-4RC. (A.i) The co-cultured scaffolds (HDFn: HDMEC 10: 1) were maintained in immersed conditions, seeded with HaCaT (5 times density with respect to HDFn) on top at day 7; air-liquid interface*

conditions were provided from day 9 to day 21. (A.ii) Co-cultured scaffolds without subsequent HaCaT seeding and maintained in submerged conditions for 21 days were used as control. (B) Alamar blue viability assay performed on the (B.i) Bilayered scaffolds and (B.ii) Control scaffolds depicted cell proliferation for a period of 21 days.

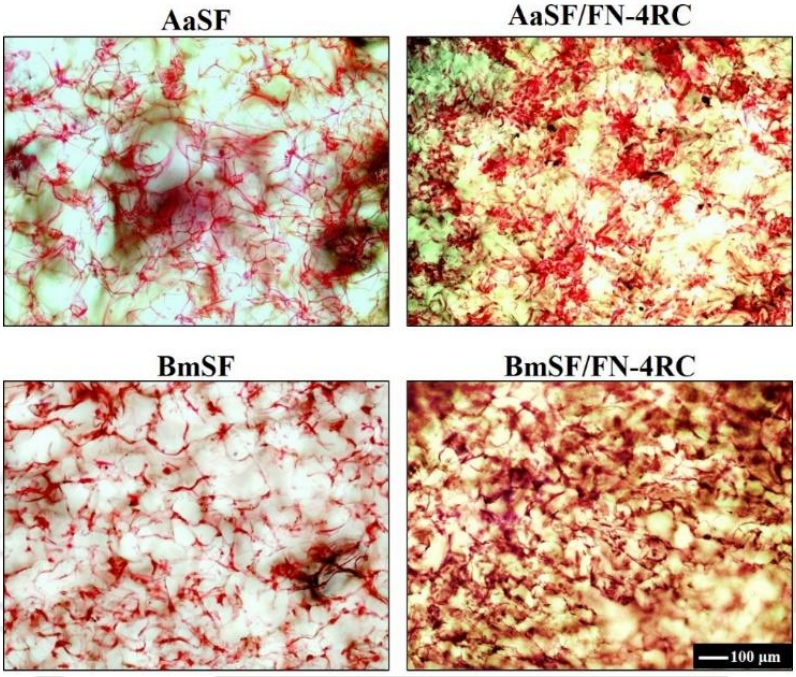

Figure 4.9. *H & E stained lateral sections of coated and uncoated SF scaffolds after 14 days of culture, showing distribution of cells all over the scaffolds in the co-cultured conditions. FN-4RC coated SF scaffolds demonstrated higher cell density in comparison to pristine SF scaffolds. Scale bar represents 100 µm.*

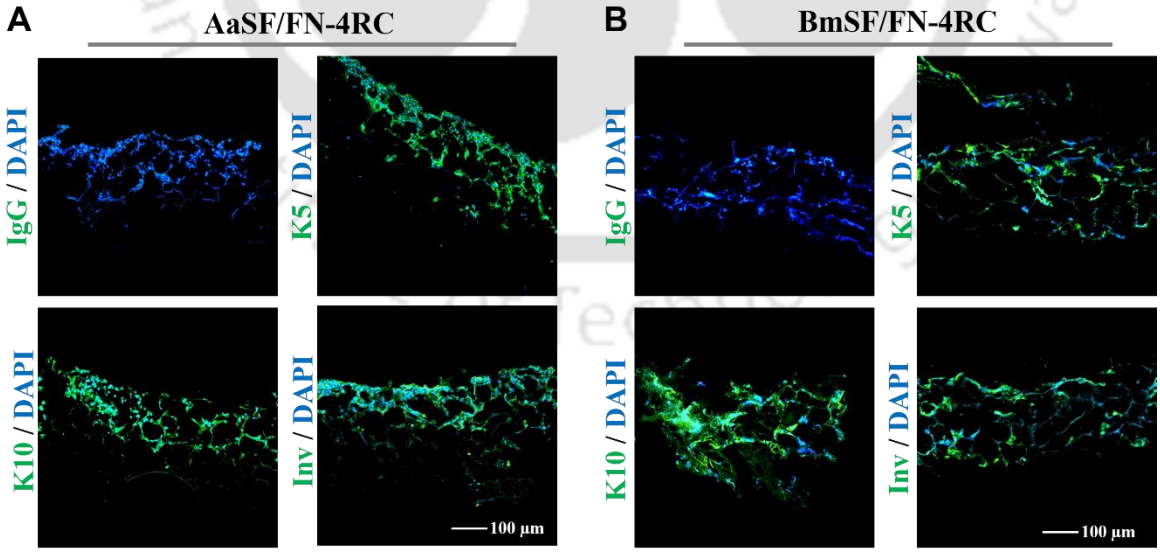

Figure 4.10. *Immunostainings on cross-sections of co-cultured scaffolds depicts prominent cytokeratin markers: keratin 5, keratin 10 and Involucrin (in green) in the coated scaffolds. (A) FN-4RC coated AaSF scaffolds showed more prominent and even keratinization in comparison to (B) BmSF counterpart. IgG represents isotype control.*

Counterstaining of nuclei was performed with DAPI (in blue). Scale bar represents 100 µm.

To investigate keratinization in the co-cultured silk scaffolds, three cytokeratin markers: Keratin 5 (K5), Keratin 10 (K10) and Involucrin (Inv) were studied (**Figure 4.10.**). A confluent cell multilayer was clearly visible on top of the AaSF/FN-4RC scaffolds. The upper layer appeared continuous with few gaps among the cells. Just beneath this layer, cells appeared with interspaces between the pores of the silk scaffold and showed dermal like structures with intact pores for further cellular growth and migration. In contrast, BmSF/FN-4RC scaffolds showed discontinuous epithelial inclusions or relatively thin epithelial layer. AaSF/FN-4RC scaffolds thus seemed to provide better structural support compared with BmSF/FN-4RC scaffolds, leading to higher cell attachment, growth and maturation of keratinocytes on the uppermost layer. Concurrent mature layers expressing K5, K10 and Inv, thus resembling neo-epidermis, was apparent in AaSF/FN-4RC scaffolds. Involucrin was clearly visible on the uppermost layer of AaSF/FN-4RC scaffolds.

4.4. Discussion

Our aim is to fabricate 'bioactive matrices' that mediate cell-material interactions and contains cues for rapid cellular recruitment and stimulation. Such biologically active systems hold great potential in developing 'interactive materials', through which tissue regeneration can be promoted at a much faster rate. Improvement of tissue engineered grafts have previously been performed by linking various bioactive compounds to the grafts *via* click chemistry, enzyme mediated coupling or chemical reactions in several studies [336, 337]. Our strategy is to functionalize SF bulk material using spider silk assembly, without any chemical reaction to avoid the toxicity associated with reagents and by-products. By coating the silkworm SF matrices with desired functionalized spider silk fusion protein, we could successfully develop multifunctional wound dressing and bioactive scaffold.

The quick adhesion assay revealed clear effects of different silk coatings on early cell attachment (**Figure 4.1.**). Higher cell density observed on SF coated with FN-4RC compared to pristine SF coatings revealed that FN-4RC promotes adherence of fibroblasts and keratinocytes. For HDFn, there was a clear effect of FN-4RC on BmSF

but no marked difference between pristine AaSF and AaSF/FN-4RC. Here, the adherence of HDFn onto pristine AaSF was almost as good as on AaSF/FN-4RC, possibly due to the presence of an inherent RGD motif in the AaSF sequence but lacking in BmSF, as has been discussed previously. However, culture of HaCaT cells revealed significant difference in the attachment and proliferation between AaSF and AaSF/FN-4RC, indicating improved cellular activities due FN-4RC coating over AaSF. The RGD cell binding motif in FN-4RC is presented in a turn loop, which mimics the natural conformation present in the full-length fibronectin protein [300]. The results from these adhesion studies supports previous findings that cells prefer RGD motifs present in a loop format as in fibronectin rather than the linear RGD present in AaSF [300]. This was further corroborated by the long-term culture for 7 days, which demonstrated that the SF coated with FN-4RC showed enhanced cell viability and proliferation (**Figure 4.2.**). The difference in the cell density among various coatings was probably due to that FN-4RC provides a natural integrin-ECM interaction to the cells. The RGD motif found in the tenth type III domain of native fibronectin is the best characterized cell-adhesion ligand, and binds to almost 50 % of the receptors in the integrin family [300, 338]. Overall, the functional bioactive motifs from fibronectin was thus efficiently provided to SF bulk material *via* spider silk fusion proteins.

Chronic wound care is one of the most challenging tasks in the global healthcare system. Impaired healing process and bacterial colonization in chronic wounds make them hard to heal [339]. One way to treat such wounds is to eradicate bacterial infection and prevent biofilm formation [339]. Keeping this in mind, we aimed to functionalize the developed SF mats with antimicrobial activity. For this purpose, we coated the mats with spider silk fusion proteins containing the cationic AMPs Magainin I (Mag-4RC) and Lactoferricin (Lac-4RC), respectively. Both types of AMP-silk coatings on SF mats were shown to be capable of inhibiting biofilm development and bacterial growth (**Figure 4.3.**). Bacteria residing in the wound biofilms often develop resistance to the immune system and antibiotic drugs, which in turn aggravate the wound chronicity [263, 339]. Currently, the common strategy to combat infection involves loading of antibiotic drugs or silver nanoparticles in dressing material [91, 263, 312, 336]. Due to the emerging increase in resistance towards conventional treatments, novel antibacterial interventions are needed [340]. AMPs are gaining interest as an alternative to antibiotics, since they are part of the innate immune system of most multicellular organisms, with

less propensity of inducing resistance among microbes [340]. AMPs are short cationic peptides that commonly interact with the outer membrane of microbes causing disruption and leakage, although various mechanisms have been reported for different AMPs [340, 341]. The natural AMPs found in human system, like LL-37 and defensins, are activated during infection and promote the wound healing process [311, 316, 342]. Other AMPs, like Magainin (Mag) and Lactoferricin (Lac), are well known for their antibacterial activity [343, 344]. Lac is homologous to the natural cleavage product of the mammalian glycoprotein Lactoferrin, which is a part of the innate immune response [344, 345]. Lactoferrin has been shown to modulate cellular behaviours to favour the wound healing process [344]. Thus, application of AMPs in treating infected wounds is a new approach to cope with drug resistance.

Another challenge in treating chronic wounds is to combat cellular senescence and promote cell migration [12]. Chronic wound physiology is different from that of acute wound due to multiple factors e.g. lack of growth factors, abnormal cellular response and obstruction in cell migration [12]. An ideal wound dressing should possess physical properties like integral stability, swelling capacity for exudate absorption and moisture retention to create desirable environment favourable for healing process [314]. In addition, if the dressing is made of biomaterials containing cell binding peptides or growth factor peptides it helps in developing an "interactive matrix" by guiding cell behaviour through specific cell-material interactions [7, 8, 303]. Considering all these properties, we used SF based nanofibrous mats with well-studied physical and biological properties as demonstrated in previous chapters. The SF mats were then functionalized by a coating of spider silk fusion proteins aimed to improve the cell-interactive properties. Both types of SF mats coated with FN-4RC showed higher cell proliferation rate with extended morphology of cells (**Figure 4.4.**). Cellular proliferation at initial time points (day 1 to day 3) is highly critical from the wound healing perspective, as it also depict cellular adherence and growth of cells from the very beginning. The apparent demarcation on uncoated BmSF mats in terms of cell morphology is probably due to the lack of cell binding sites, also in line with the lower proliferation of cells. Nevertheless, extended morphology of spread out cells on the FN-4RC coated mats demonstrates the bioactivity of FN-silk rendered to the coated SF mats. Similar behaviour was observed for HaCaT cells as well.

FGF is an important factor for angiogenesis and granulation tissue development during the wound healing process [6, 7]. FGF mediated signalling on endothelial cells results in rapid angiogenesis and is also responsible for up-regulation of $\alpha_v\beta_3$ integrin [346, 347]. Therefore, next we coated SF mats with FGF-4RC to examine the response of HUVEC cells. The Alamar blue viability assay performed after 48 h showed higher cellular activity on the SF mats coated with FGF-4RC compared to uncoated mats, suggesting positive effect of the spider silk coatings (**Figure 4.7.**). The RGD motif derived from fibronectin is known to interact with the integrin receptors present on endothelial cells and promote cell adherence [300]. The results presented here indicate that a combination of FGF-4RC and FN-4RC may lead to rapid and augmented angiogenesis. By examining the behaviour of three of the cell types present during wound healing, we can confirm that functionally active mats have been achieved. In addition, we show that functionalization of silk with antimicrobial motifs helps in preventing biofilm formation and bacterial colonization. Thus, the basis for construction of a multi-biofunctional 'silk to heal' dressing with potential for treating chronic wounds has been developed.

The observed higher cellular activity on AaSF mats coated with spider silk compared to BmSF counterpart could be attributed to two factors: 1). Additional RGD sequences present inherently in the AaSF protein and 2). Higher physical adsorption of spider silk fusion proteins on AaSF mats, which provide more functional motifs to the AaSF based substrate [214, 332]. Spider silk fusion proteins tend to self-assemble more quickly and strongly to AaSF in comparison to BmSF, likely due to amino acid sequence similarity between AaSF and 4RC. Both these proteins contain long polyalanine blocks, which attribute to higher silk interaction between AaSF and 4RC, as observed in our previous study [214, 332]. In contrast, lower interaction of 4RC fused proteins with BmSF leads to overall lower cell binding sites on BmSF coated mats and hence, attribute to lower cellular adhesion compared to AaSF coated mats. Thus, bioactivity of the spider silk fusion proteins was successfully delivered to the bulk SF material even when using a low concentration (0.01 %) of the functionalized 4RC silk variants.

Scaffold architecture plays a major role in developing artificial grafts not only for mimicking the native structure, but for also providing structural and mechanical cues to the cells [334, 348]. For the development of a skin substitute, a porous sponge is more

suitable in comparison to electrospun mats due to limitations in the pore size provided by the nanofibrous mats. Skin is a complex structure comprising almost 20 different cell types and migration of cells within the construct is an important criterion to consider while developing a skin substitute [34, 143]. Herein, we successfully demonstrated development of a keratinized bilayer skin construct by co-culturing three cell types in SF scaffolds coated with functionalized spider silk. The Alamar blue viability assay validated cellular proliferation in the co-cultured scaffolds (**Figure 4.8.**). Analysis of H & E stained lateral sections of the co-cultured scaffolds further validated presence of high density of cells in the scaffolds (**Figure 4.9.**). The coated SF scaffolds contained cell populations densely distributed throughout the scaffolds, in comparison to the low cellular density found in the uncoated scaffolds, indicating positive effect of coating on the scaffolds. Further validation of keratinization in the epidermal layer was corroborated by various cytokeratin markers (**Figure 4.10.**). The K10 is a late differentiation marker represented by the suprabasal keratinocytes in the neoepithelium; whereas, K5 is an early differentiation marker represented by the basal keratinocytes [91, 349]. Involucrin is a marker of terminally differentiated keratinocytes and cornified epidermis [350]. The prominent keratinization in AaSF/FN-4RC scaffolds relative to the BmSF counterpart was probably due to more available RGD motifs and higher adsorption of spider silk in the AaSF scaffolds. In just 21 days of culture, of which 12 days in air-liquid interface environment, SF scaffolds coated with spider silk showed promising results for the development of bilayer skin substitute.

Functionalization of SF scaffolds with spider silk fusion proteins not only provided bioactivity to the construct but also promoted functional development of a skin graft. In previous reports, mesh based on native dragline spider has been used for culturing of keratinocytes and shown to support keratinization of epidermal layer [351]. However, fabrication of such constructs needs a high amount of native spider silk fibres, which is a major limitation. By coating the bulk SF substrate with a low concentration (0.01 %) of recombinant spider silk, we circumvented the shortage of spider silk and could efficiently use the properties of the functionalized spider silk protein. This facile methodology may reduce the cost of artificial grafts many folds owing to the inexpensiveness of SF bulk material. Our approach of coating silkworm SF scaffolds with functionalized 4RC silk *via* physical adsorption further overcomes the drawbacks of chemical based crosslinking techniques. The simplistic technique of coating

functionalized spider silks on the SF substrates might thus be used for construction of bioactive scaffolds for tissue engineering applications. Functionalization of SF substrates can also be done as per the requirement using single or many 4RC fusion proteins like AMP, FN, FGF or a combination of all. Taken together, the various bioactivities of SF constructs coated with functionalized 4RC will provide the composite material a great advantage in healing complex cutaneous defects like diabetic foot ulcers or burn wounds. The encouraging results on both nanofibrous mat and porous scaffold format led to the development of 'silk to heal' bioactive wound dressings and cellular tissue engineered skin grafts. These tissue-engineered models, especially human skin-equivalents, may also be used as an alternative to animal testing for laboratories or industries to study the effect of cosmetic chemicals on skin as a preclinical step at a much affordable cost. Further investigation of these bioactive constructs may be performed under *in vivo* conditions to unfold their healing properties and study cell-material interactions in future.

4.5. Significant findings

The salient findings of this chapter are as follows:

1. Using silkworm SF as a bulk biomaterial, different formats could be easily designed such as, coatings, nanofibrous mats and microporous scaffolds. The inherent silk assembly of recombinant spider silk fusion proteins enabled chemical-free functionalization, thereby leading to a cost-effective production process.
2. The bioactive moieties like the cell-binding motif from FN, the growth factor FGF2 and the AMPs - Lac and Mag were easily applied to SF substrates *via* spontaneous silk assembly. This facilitated intended functions of improved cell adhesion, growth factor stimulation and antibacterial activity to the dressing material.
3. The coated silk mats provided necessary cues for cellular adhesion and proliferation, a pre-requisite for a wound dressing material. Culture of fibroblast, keratinocytes and endothelial cells revealed higher adhesion and proliferation of all cell types on the coated SF mats. Thus, multi-functional mats with antibacterial and cell recruiting properties were projected as a potential candidate for treating complex chronic wounds.
4. Dermo-epidermal grafts developed using co-culture of skin cells on the spider silk coated SF scaffolds demonstrated bilayer tissue formation with a keratinized epidermal layer under *in vitro* conditions.
5. The encouraging results revealed an easy, efficient and affordable way to develop functionalized constructs for skin regeneration applications.

Considering the large availability and versatility of SF bulk material and the various bioactivities that can be provided by coating with spider silk fusion proteins, this chapter reveals a simplistic approach to the fabrication of bioactive dressings and scaffolds as tissue engineering products. The encouraging outcomes of the study further motivated us to validate the healing efficacy under *in vivo* conditions, which have been discussed in details in the next chapter.

Chapter 5

Investigation of recombinant spider silk coated silk based constructs in treating chronic diabetic wounds and full-thickness burns

This chapter illustrates the potential of bioactive silk constructs developed by combining silkworm silk and functionalized spider silk fusion proteins in healing complex cutaneous wounds like diabetic foot ulcers and 3rd degree burn injuries. Two types of constructs, namely, nanofibrous mats and microporous scaffolds are examined for their wound healing efficacy using specific animal models. The study validates the potential of bioactive silk matrices in faster repair of cutaneous wounds as hypothesized in previous chapter.

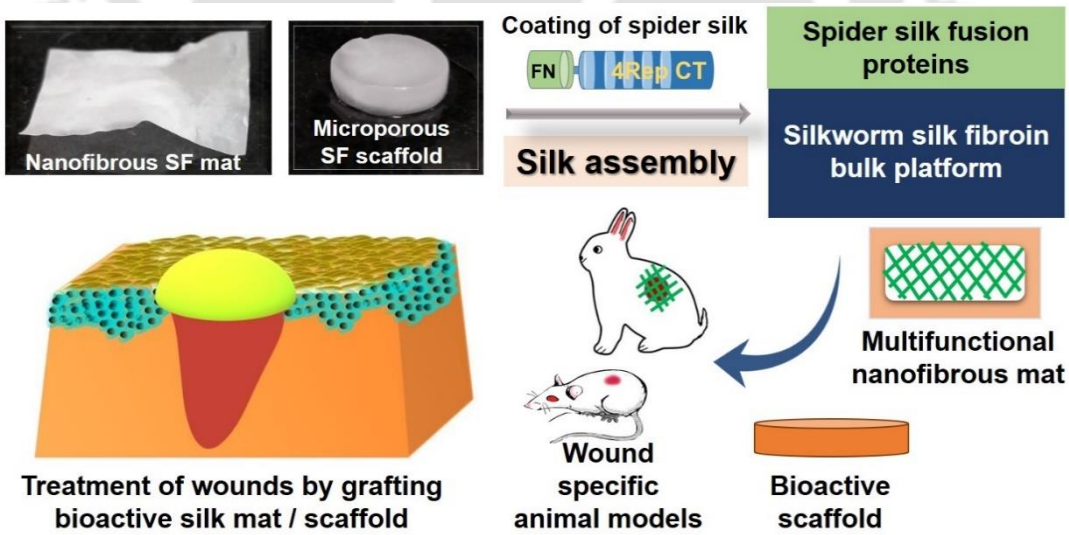

The work embodied in this chapter is under consideration for publication.

ABSTRACT

Complex cutaneous wounds like diabetic foot ulcers and 3rd degree burn injuries represent a critical clinical challenge in the current scenario. The substantial increase in the number of patients suffering from such conditions demands a large-scale and low-cost strategy in addition to effective treatments. Herein, we investigated the efficacy of developed bioactive constructs made up of silk biomaterials in treating diabetic and burn wounds through specific animal models. Nanofibrous mat and microporous scaffold of *Antheraea assama* SF (AaSF) were functionalized with recombinant spider silk fusion proteins through silk-silk interactions to fabricate bioactive matrices for wound healing applications. The AaSF matrices with a top-coating of functionalized spider silk variants demonstrated accelerated wound healing properties in comparison to the uncoated counterpart. *In vivo* diabetic rabbit model used to examine healing efficiency of functionalized silk mats revealed excellent skin regeneration in comparison to the commercially used Duoderm dressing and untreated wounds. Similar results are obtained with functionalized freeze-dried silk scaffolds when applied on the burn wounds *via* one-step grafting in rat animal model. The spider silk coatings demonstrated improved granulation tissue development, enhanced angiogenesis, early re-epithelialization and matrix remodelling in both types of studies. The results thus validated the potential of bioactive silk matrices in faster repair of diabetic and burn wounds.

5.1. Introduction

Skin, the largest organ of our body, acts as a protective physical barrier against the outside environment and harmful chemicals or biological agents [352]. Skin injuries impose a great threat to the health of patients, as the body gets exposed to harsh external environment and deadly pathogens. Diabetic patients often suffer from chronic cutaneous wounds due to pathophysiological conditions like neuropathy, and abnormal cellular activity [12]. Unlike small acute wounds, which are healed by the self-repair mechanism of skin tissue, chronic wounds fail to heal by themselves and wound chronicity progresses with time unless treated in an efficient way [8]. In addition, dermal wounds represent a major healthcare problem owing to an increasing number of trauma and burn cases. Burn injuries and chronic wounds affect more than 11 million and 6.5 million people respectively every year, leaving millions of patients with disability, distress and discomfort [9, 10]. The wound chronicity in case of cutaneous ulcers often ends up with limb amputation surgeries [19]. Despite a variety of currently available treatments, healing of complex wounds is still a great challenge due to the poor clinical outcomes [353]. Towards this goal, we aim to develop bioactive matrices that accelerate the healing process of various types of severe wounds.

Diabetic wounds are difficult to manage owing to the extreme level of wound chronicity, hyperglycemia and bacterial infection [12]. Similarly, large trauma wounds and burn injuries become necrotic and wound healing process obstructs at the very initial phase [1, 17]. In such conditions, fibroblasts and blood capillaries fail to invade the wound site, preventing development of a contractile granulation tissue [17]. Cell migration, angiogenesis and proliferation of connective tissue are the critical determinants of initial stage of wound healing [28]. In this context, extensive research is being carried out in the field of tissue engineering to enhance the cell migration and cell adherence through functional biomaterials [7]. Biomaterials like fibrin, present in the natural provisional matrix contains fibronectin, which supports cell adhesion, spreading and proliferation through its cell binding motifs [26, 354]. Such biomaterials are in high demand that confer physical connection between cells and matrix, and also mediate biochemical signals controlling cell growth, proliferation and migration. The matrix should not only provide mechanical support but should also be conducive to rapidly recruit host cells and thereby guide the tissue regeneration [8]. Development of acellular

tissue-engineered constructs, which mimic the attributes of wound provisional matrix is therefore very challenging.

To mimic the cell binding domains of fibronectin, we utilized recombinant spider silk protein 4RepCT (4RC) by functionalizing it with bioactive domains. 4RC is a partial dragline silk protein derived from *Euprosthenops australis* spiders and produced *via Escherichia coli* bacterial system with the help of recombinant DNA technology (RDT) [327, 328]. The spider silk (4RC) protein and its various variants (also known as silk fusion proteins) have inherent self-assembling property, making them a suitable component for matrix fabrication [213, 237, 326, 328]. One variant of 4RC utilized in the present study is FN-4RC, which is the functionalized spider silk containing RGD loop of fibronectin (FN) and possesses integrin mediated cell binding properties [235, 300]. The FN-4RC is well-explored recombinant spider silk fusion protein and has shown excellent binding with various cells like fibroblasts, keratinocytes and endothelial cells, as shown in our previous study (chapter 4) [355]. Further, to combat the bacterial infections, an antimicrobial motif containing spider silk fusion protein (Lac-4RC) was applied using similar technology to achieve antibacterial activity of lactoferricin.

To efficiently use the functionalized spider silk proteins, we used them in form of a thin coating on top a biocompatible bulk substrate made up of silk fibroin (SF) biomaterial. SF with favorable biocompatibility and biodegradable properties could be easily functionalized with spider silk fusion proteins owing to the inherent silk-silk interactions [332, 355]. In our previous chapter, we validated bioactive properties of such functionalized silk matrices in promoting higher cell adhesion and rapid cellular recruitment under *in vitro* conditions. We developed interactive biomaterials by coating functionalized spider silk proteins on SF bulk platform. Interactions of spider silk variants with two types of SF proteins, namely, *Bombyx mori* SF (BmSF) and *Antheraea assama* SF (AaSF) were examined in our previous work. The study revealed enhanced interaction of 4RC variants with the AaSF platform through various physical and biological assays [332, 355]. The previous observations under *in vitro* study provided us evidences about the efficacy of developed constructs under *in vivo* systems. Therefore, in the present study, we used only *A. assama* silk fibroin (AaSF) based matrices as bulk platform and coated them with spider silk fusion proteins to develop bioactive matrices for wound healing applications. We selected AaSF based nanofibrous mats and microporous scaffolds and applied them in the form of wound dressing and bio-artificial

skin. The nanofibrous mats were developed and characterized for wound dressing applications, particularly for chronic diabetic wounds. On the other hand, microporous scaffolds were designed for application in skin grafting, where they could be implanted through one-step surgery on burn wounds. In this work, we hypothesized that the functionalized SF matrices in their respective format may have a promising wound healing impact on both types of wounds, namely, diabetic wounds and third degree burns. The results of this study validated our hypothesis and provided suitable treatments for burn injuries and diabetic foot ulcers at an affordable cost.

5.2. Materials and methods

5.2.1. Isolation of *Antheraea assama* silk fibroin

To isolate AaSF, 5th instar *A. assama* silkworms procured from local sericulture farms of Assam in India were sacrificed. AaSF was directly isolated from the silk glands of larva according to previously described protocol [227]. Protein was carefully extracted out from the glands using forceps. The isolated silk protein was gently washed multiple times and then dissolved in 1 % (w/v) sodium dodecyl sulphate (SDS) (Himedia, India) aqueous solution. Subsequently, the dissolved silk solution was dialyzed against distilled water using a 12 kDa cellulose dialysis membrane (Sigma-Aldrich, USA) for 4 h at 4 °C with frequent water change after every hour. The aqueous solution of AaSF thus obtained was 3 % (w/v) as measured by the gravimetric method.

5.2.2. Fabrication of AaSF nanofibrous mats and microporous scaffolds

Silk based nanofibrous mats were fabricated as previously established [314]. Solutions of AaSF (3 % w/v) and poly(vinyl alcohol) (PVA) (13 % w/v; procured from LobaChemiePvt. Ltd., India) were blended in equal volume to achieve a ratio of 4:1 (PVA: SF) (w/w) with an optimum viscosity for electrospinning to obtain smooth nanofibrous mat. Following parameters were applied to the electrospinning instrument (E-spin nanotech, India) to ensure electrospinning of a AaSF-PVA blend solution: voltage = 25 ± 3 kV, flow rate = 0.800 ± 0.100 mL/h, tip to collector distance (d) = 15 cm and rotating speed of drum collector = 500 rpm. Subsequently, β-sheet in the AaSF electrospun mat was induced by incubating it in 70 % ethanol for 2 h. The nanofibrous mat thus fabricated was washed four to five times with sterile water to remove residual

ethanol. To further sterilize, the nanofibrous mat was placed under ultraviolet (UV) lamp for 20−30 min prior to coating process.

Silk based microporous scaffolds were fabricated as previously established [355]. Microporous scaffolds of AaSF 2.5 % (w/v) were fabricated using freeze drying technique. Briefly, 300 µL of AaSF solution was poured into each well of a 24-well plate, kept frozen at - 20 °C for 12 h and then subjected to lyophilization for 24 h. The freeze-dried AaSF scaffolds thus obtained were immediately treated with ethanol for β-sheet induction. The scaffolds were incubated in 100 % ethanol for 1 h, followed by 70 % ethanol for 6 h. Subsequently, the scaffolds were washed with sterile water multiple times and autoclaved in wet condition for sterilization prior to coating process.

5.2.3. Functionalization of AaSF mats and scaffolds using recombinant spider silk proteins

Two types of recombinant spider silk fusion proteins were used to coat the SF nanofibrous mats, namely, FN-4RC (cell-binding motif with the sequence CTGRGDSPAC from fibronectin fused to 4RepCT) and Lac-4RC (antimicrobial motif of lactoferrin with the sequence FKCRRWQWRMKKLG fused to 4RepCT). Both the recombinant spider silk fusion proteins were provided from Spiber Technologies AB, Sweden. The recombinant proteins were diluted in 20 mM Tris, pH 8.0 to obtain 0.1 mg/mL solutions prior to their coating. Dip coating method was performed wherein the pre-wet AaSF nanofibrous mats were dipped into spider silk solution and incubated at 37 °C for 1 h. Subsequently, the spider silk solution was removed and matrices were washed with Tris buffer twice. Similarly, scaffolds were also coated with spider silk protein using the above-mentioned dip coating method. The scaffolds were coated with only one type of recombinant spider silk fusion protein i.e. FN-4RC; whereas nanofibrous mats were coated with both FN-4RC and Lac-4RC. Both the coated mats and scaffolds were stored in wet conditions at 4 °C prior to applying on the wounds.

5.2.4. *In vivo* study design in diabetic animal model and treatment with nanofibrous mat dressing

The animal experiments in diabetic animal model were performed in accordance with ‘‘Principles of laboratory animal care” from the Institutional Animal Ethical Committee, West Bengal University of Animal and Fishery Sciences, West Bengal, India (Permit No. Pharma/IAEC/136 dated 30.6.2014). Thirty-six New Zealand white healthy rabbits

(1.5 – 1.8 kg) were acclimatized one week prior to study. Diabetic conditions were induced in all the animals using Alloxan based treatment following the standard protocol. Briefly, Acepromazine (1 mL/kg) was administered subcutaneously in order to sedate the rabbits and hair at the back of their ears were shaved off. Required dose of Alloxan in 30 mL saline (Sigma-Aldrich, USA) (150 mg/kg) was subsequently administered at a rate of 1.5 mL/min *via* ear vein. Following the Alloxan treatment, rabbits were given water containing glucose (12 g/L) for a period of 48 h to ensure induction of diabetes condition. Diabetes disease in the animals was confirmed by checking the blood glucose using test strips and meter (Accuchek_test advantage meter, Accu-chek_advantage II strips, Roche Diagnostics, U.K.). Alloxan treated rabbits with blood glucose level more than 300 mg/dL were considered as diabetic or hyperglycaemic animals in comparison to the normal healthy rabbits (glucose level 120-150 mg/dL). The diabetic condition of rabbits was monitored for a period of 4 weeks prior to commencing the wound healing experiment. The animals were then randomized into three groups for time points (day 7, day 14 and day 21). For anaesthesia, animals were given a cocktail dose of saline containing xylazine hydrochloride (6 mg/kg) (Xylaxin®, Indian Immunologicals, India) and ketamine hydrochloride (33 mg/kg) (Ketalar®, Parke-Davis, India) while performing the experiment.

During the wound creation process, proper aseptic conditions were taken and hair of mid thoraco-lumbar region of dorsal surface were shaved off. Skin was wiped with 70 % ethanol and full thickness wounds were created using a biopsy punch of 12 mm diameter. A total number of six wounds were created in each rabbit corresponding to each treatment: 1) Uncoated AaSF mat, 2) AaSF-FN (mat coated with FN-4RC), 3) AaSF-Lac (mat coated with Lac-4RC), 4) AaSF-FN-Lac (mat coated with both FN-4RC and Lac-4RC), 5) Positive control group taken as commercially available Duoderm wound dressing (DD) and 6) Untreated group (UNT). The Duoderm dressing (ConvaTec Duoderm extra thin CGF dressing) used in the study was procured from Ortho Care Pvt. Ltd. through amazon online store (https://www.amazon.com). All the dressing patches were replaced with fresh ones after every three days till 12 days post-operation. Glucose level of all the animals was monitored regularly and found to be in the range of 300 to 350 mg/dL throughout the study. No abnormality was found during the surgery or post-operation and animals were separately placed in individual cages.

5.2.5. *In vivo* study design in burn injury model and treatment with microporous scaffolds

The animal experiments on third degree burn injury model were performed according to the ethical approval received from 'Institutional Animal Ethics Committee (IAEC)', Guwahati medical college and hospital, Guwahati, Assam, India (CPCSEA under the "Principles of laboratory animal care approval no. MC/916/2017/4", Registration No. 351, 3/1/2001). Female wistar rats were procured from National Institute of Nutrition, Hyderabad, India weighing 200-250 grams each and were 6-7 weeks old. To create third degree burn model, standard protocol was followed on the rats and animals were acclimatized for 7-10 days in the animal house prior to experiment [356]. Anaesthesia condition was given to the animals by administering a cocktail dose of Ketamine (80 mg/kg) and Xyalazine (12 mg/kg) (K-X cocktail) *via* intraperitoneal route. Third degree burn injury was inflicted without effecting surrounding and underneath organs using an instrument set-up following an optimized protocol [356].

An instrument consisting of soldering iron fitted with a cylindrical aluminium head of 1 cm diameter was used. A variable autotransformer was connected to the soldering iron to achieve precise control on the temperature of aluminium head. On setting the output of autotransformer to 120 V, necessary temperature of 80 °C was set, which was measured by a Type K temperature probe attached to a digital thermometer. Third degree burn wound was inflicted on each rat by placing head of the device at 90° angle to the skin for 15 sec. The skin was folded parallel to the supporting platform to avoid any thermal insult to the deep tissues. Infliction of third-degree burn was validated by histological examination of burn skin in comparison to normal skin (**Figure A5.1.**). The animals were divided into three groups of 3 time-points (day 7, 14 and 21). Each rat was given only one wound and treatment groups were as follows: 1). Uncoated AaSF scaffold, 2) AaSF-FN (scaffold coated with FN-4RC), 3) Positive control group taken as commercially available Duoderm (DD) wound dressing and 4) Untreated group (UNT). Each group contained four animals (n = 4). The Duoderm dressing (ConvaTec Duoderm extra thin CGF dressing) used in the study was procured from Amazon online store. Grafting of scaffolds was performed following clinical practices and established protocol [48]. The injured burn tissue was excised out using a biopsy punch (1 cm diameter) after 48 h of burn infliction. Wounds were washed with sterile saline following debridement and scaffolds of wound-specific size were applied. To ensure attachment of scaffolds to

the wound site, three skin staples were applied, which were subsequently removed after 3 days of application. The wounds with various treatment were also covered with an occlusive and transparent Tegaderm dressing for protection from infection and prevention from drying. Total three doses of antibiotic Ceftriaxone (20 mg/Kg) and analgesic Meloxicam (5 mg/Kg) were given to all the animals *via* intramuscular route on every alternate day till day 7. In addition, the top dressings of Tegaderm was changed and grafted wounds were cleaned after every 2-3 days till 10-11 days. All the animals were placed in separate cages and monitored daily.

5.2.6. Wound healing estimation

Wound healing efficacy of various treatments was evaluated by measuring the wound size of diabetic wounds. Photographs of the wounds taken periodically were analysed using Image J software, which measured the wound diameter and wound area. Following formula was used to calculate the wound closure:

Wound area (%) = $A_t/A \times 100$ ……...…… (5.1.)

Where A_t was the area of wound at time (t) and A was the wound area at the time of wound creation.

5.2.7. Histological study

Histological examination was performed by collecting the skin biopsies at pre-defined time points, *viz*., day 7, 14 and 21 post-wounding. The biopsies of healing tissues were washed with sterile saline and preserved using 10 % neutral buffer formalin (NBF; Sigma-Aldrich USA). Subsequently, the tissue samples were washed with sterile water 4-5 times and dehydrated using a series of graded ethanol. The dehydrated samples were then embedded in hot paraffin wax and blocks were made. Sections of 5-10 µm thickness were prepared using tissue microtome (Leica) and put on glass slides. The sections were stained with haematoxylin and eosin (H & E) according to the manufacturer's protocol. General morphological observations of wound healing were carried out by microscopic analysis using bright field microscope (EVOS FL, Life technologies, USA).

5.2.8. Immunofluorescence staining

Similar type of paraffin embedded tissue sections (5-7 µm) prepared from skin biopsies were used for immunofluorescence study. Briefly, the sections were rehydrated using

series of graded ethanol and permeabilized with 0.1 % Triton X-100 in PBS for 10 min. Subsequently, blocking was done using 1 % bovine serum albumin (BSA) by incubating for 1 h. The sections were then incubated with specific primary antibody for 1 h at 37 °C. Angiogenesis in the healed tissues (collected on day 7) was determined by staining the sections using anti-CD31 (for rabbit samples) and anti-vWF (for rat samples) procured from Abcam, UK. As secondary antibody, goat anti-rat IgG conjugated with Phycoerythrin (Sigma-Aldrich, USA) was used. Counter staining of nuclei was done by Hoechst 33342 (Invitrogen, USA). Images were taken using a fluorescent microscope (EVOS FL, Life technologies, USA).

5.2.9. Immunohistochemistry assay

The tissue sections made from the skin biopsies were further analysed by IHC. Evaluation of cytokeratin 10 (CK 10) and cytokeratin 14 (CK 14) was performed using IHC kit (Vectastain Elite Universal ABC kit, Vectors lab, U.K.). The sections were rehydrated prior to incubating in blocking serum for 30 min at RT. Subsequently, primary antibodies (anti-CK10 and anti-CK14) were applied on the sections for 1 h at 37 °C. The sections were then incubated with biotinylated universal secondary antibody. After washing, the ABC reagent containing avidin-horseradish peroxidase was applied to the section and incubated for 30 min at RT. Finally, Peroxidase substrate 3,3′-diaminobenzidine (DAB) reagent was applied, which developed a brown reaction product. The sections were then counterstained with haematoxylin to stain nuclei and incubated for 15 min prior to dehydration and mounting. To examine matrix remodelling, the sections of healed tissues collected on day 21 were analysed following the similar process using monoclonal primary antibody against collagen type I (Col I) and collagen type I (Col III) procured from Abcam, U.K. The images were taken using the bright field microscope.

5.2.10. Gene expression study

To determine the gene expression of ECM related proteins, skin biopsies were collected on specific time points, *viz*., day 7, 14 and 21 and preserved in −20 °C using RNA later® (Sigma-Aldrich, USA). The tissue was homogenized in TRIzol reagent (Sigma-Aldrich, USA) and mRNA was isolated following the standard protocol. Briefly, the homogenized tissues were incubated with TRIzol reagent for 30 min at RT and centrifuged at 13,000 rpm for 10 min in 4 °C. mRNA was collected from the supernatant obtained.

Subsequently, chloroform was added to the mRNA containing solution and centrifuged at 13,000 rpm for 15 min at 4 °C. The upper aqueous phase was collected in fresh tube, which contained mRNA and then treated with isopropanol. The mixture was then centrifuged again and mRNA pellet was obtained. The mRNA was further dissolved in RNAase free water and concentration of mRNA was measured. Complementary DNA (cDNA) was synthesized using reverse transcription kit (Applied Biosystems, USA) and PCR equipment (Takara, Japan) according to the manufacturer's instructions. Real-time PCR reactions were performed on the obtained cDNA using SYBR Green PCR Mastermix (Applied Biosystems, USA). Primers listed in **Table 5.1.** were used for examining the gene expressions. Rabbit primers were used for diabetic wound samples and rat primers for burn wound samples. The expression of collagen type I, collagen type III and glyceraldehyde-3-phosphate-dehydrogenase (GAPDH) mRNA transcripts was analysed. The average threshold cycle (Ct) value of a gene of interest (GOI) obtained after the real time reaction was normalized against that of GAPDH gene. Further, fold change of GOI transcript levels between the sample groups were compared with control (untreated group) following the formula: fold change = $2^{-\Delta\Delta Ct}$, where $\Delta\Delta Ct = \Delta Ct_{(sample)} - \Delta Ct_{(control)}$ and $\Delta Ct = Ct_{(GOI)} - Ct_{(GAPDH)}$.

Table 5.1. *Primer sequences used for the gene expression study.*

Target gene	Primer Sequence
Rat GAPDH	**F** 5'-TGACTCTACCCACGGCAAGTTCAA-3'
	R 5'-ACGACATACTCAGCACCAGCATCA-3'
Rat Col-I	**F** 5'-GCGAAGGCAACAGTCGATTC-3'
	R 5'-ACTGTCTTGCCCCAAGTTCC-3'
Rat Col-III	**F** 5'-TGATGGGATCCAATGAGGGAGA-3'
	R 5'-GAGTCTCATGGCCTTGCGTGTTT-3'
Rabbit GAPDH	**F** 5'- TCGGCATTGTGGAGGGGCTC -3'
	R 5'- TCCCGTTCAGCTCGGGGATG -3'
Rabbit Col-I	**F** 5'- CCTGGCACCCCAGGTCCTCA -3'
	R 5'- TCGCTCCCAGGGTTGCCATC -3'
Rabbit Col-III	**F** 5'- AAGCCCCAGCAGAAAATTG -3'
	R 5'- TGGTGGAACAGCAAAAATCA -3'

5.2.11. Statistical analysis

All the *in vivo* experiments were performed for n = 4 animals on each time point. Quantitative data were expressed as mean ± standard deviation as calculated by Microsoft Excel. Further data analysis was carried out using statistical software Origin 9.0 (Origin lab Corporation, USA) at both significant (* $p \leq 0.05$) and highly significant (** $p \leq 0.01$) levels. The data between groups and within groups was compared at significance level by performing one-way analysis of variance (ANOVA) followed by Tukey's test. Histological examination of the *in vivo* explanted samples was performed by analysing the microscopic images using Image J software and images were captured at least 5 fields per section.

5.3. Results

5.3.1. Rationale of the study

Development of functionalized matrices using interactions between silkworm SF and recombinant spider silk fusion proteins has previously been shown in chapter 4. AaSF matrices decorated with top-coating of spider silk proteins demonstrated increased attachment, viability and proliferation of various cell types in different formats like coatings, nanofibrous mats and porous scaffolds under *in vitro* conditions in our previous work [355]. Herein, to further investigate the effect of such functionalized matrices in various wound healing applications under *in vivo* conditions, we used them as wound dressings or skin grafts and examined their healing efficacies. This was accomplished by creating the specific wound models in animal systems and applying the suitable silk dressing for further treatment.

Two separate wound models, namely, diabetic and burn animal models were used for different formats of silk matrices. We developed diabetic wound model in rabbit animals and examined healing efficacy of various coated and non-coated nanofibrous silk mats when applied as wound dressings (**Figure 5.1.**). Burn wound model was created in rat system and healing efficiency of porous scaffolds was investigated when applied as bioengineered skin grafts through one-step grafting surgery. We performed two separate studies using different animal models according to the approved ethical clearances for both. As controls, commercially available dressing Duoderm (DD) was

used as positive control and untreated wounds (UNT) were taken as negative control in both the models. Through a comparative study with the uncoated counterpart, the effect of spider silk coating on AaSF matrices was investigated on the healing outcomes, making the study first of its kind showing impact of spider silk in skin regeneration.

5.3.2. Wound healing efficacy of AaSF nanofibrous dressings coated with recombinant spider silk in treating diabetic wounds

Full-thickness back-skin wounds of diabetic rabbits treated with various dressings were investigated by measuring the wound area through gross wound images (**Figure 5.2.**). AaSF nanofibrous mats, uncoated and coated with different types of spider silk fusion proteins, were applied in the form of primary dressing patch on the wounds and changed every 3 days. The macroscopic appearances of the wounds demonstrated different healing profile among various treatments (**Figure 5.2.A**). Among the treated wounds, spider silk coated AaSF mats (AaSF-FN, AaSF-Lac and AaSF-FN-Lac) promoted wound healing at a much faster rate in comparison with the uncoated counterpart and control group. Quantitative measurement of the wound area showed significant difference in the size of wounds treated with coated mats in comparison to other groups at the initial time-points (day 6 and 9) (**Figure 5.2.B**). Wound area calculation on day 3 also revealed interesting results; AaSF-Lac and AaSF-FN-Lac demonstrated equivalent healing efficacy with 78 ± 4.11 and 77 ± 3.52 % remaining wound area respectively. AaSF-FN showed 93 ± 3.82 % remaining wound area, higher than other coated groups but lower than uncoated AaSF and control groups.

This clearly depicted significance of different spider silk coatings and their healing profile on diabetic wounds. Among all treatments, AaSF-FN-Lac demonstrated the fastest healing owing to dual coating of FN-4RC and Lac-4RC fusion proteins, as wounds were healed within 12-14 days. Treatment with the dressing patch of AaSF-FN and AaSF-Lac resulted in 15-18 % remaining wound area on day 12. In contrast, the corresponding values for AaSF, DD and UNT were 24 ± 2.09, 69 ± 6.45 and 88 ± 6.39 % respectively. This also indicated higher wound healing efficacy of uncoated AaSF mat in comparison to the control groups, validating the regenerative properties of silkworm SF. Spider silk coating on SF further enhanced the healing profile by providing additional bioactivity from fibronectin (FN) and lactoferrin (Lac). The results thus indicated

beneficial effects of bioactivate spider silk fusion proteins in combination with AaSF silk mat in diabetic wound healing.

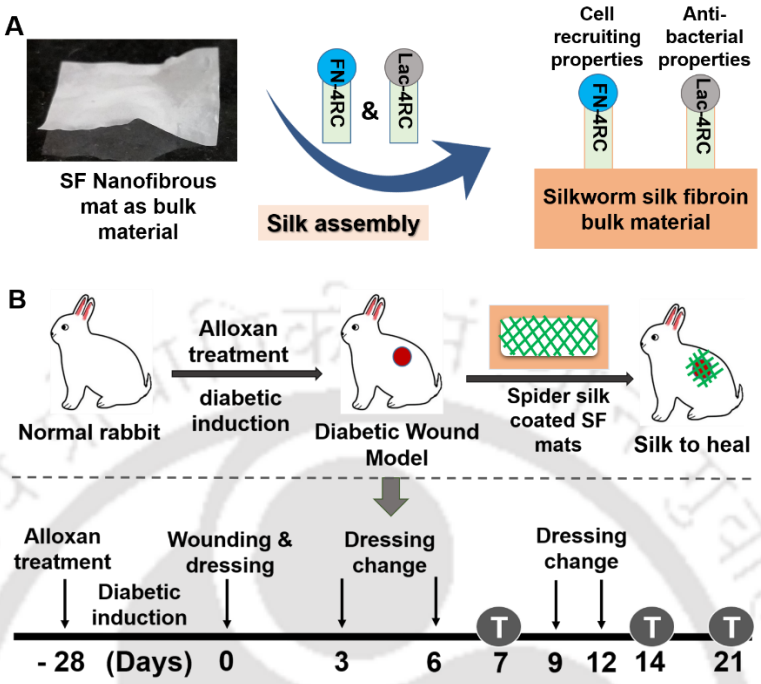

Figure 5.1. *Schematic representation of the experimental design depicting: (A) The methodology to fabricate bioactive silk dressings and (B) The strategy of treating cutaneous wounds in a diabetic rabbit model using silk dressings; diabetes condition was established for 28 days prior to wounding, dressing was changed every 3rd day till day 12, and groups were terminated on day 7, 14 and 21 as represented by (T) in the image.*

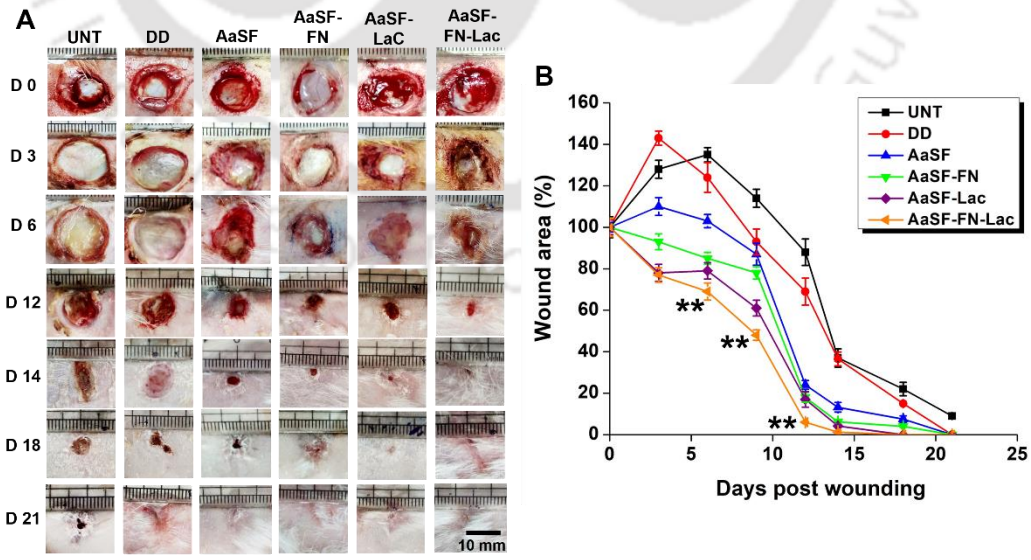

Figure 5.2. *(A) Representative gross images of wounds showing wound morphology by different treatments at various time-points during the course of diabetic wound healing; scale bar represents 10 mm. (B) Graphical representation of wound area at various time-*

*points calculated using Image J software demonstrating wound closure rate by different treatments, ** represents $p \leq 0.01$.*

5.3.3. Histological examination of diabetic wounds

We further evaluated the extent of wound healing through histological analysis of tissue sections collected at various time-points (day 7, 14 and 21). The changes in the wounded tissue were clearly observed in different treatment groups by H & E staining (**Figure 5.3.**). On day 7 post-operation, a growing granulation tissue filling the wound cavity were found in the wounds treated with silk dressings, in comparison to the control groups, where a dried scab mass covered the wounds. Development of thick and mature granulation tissue was evident in wounds treated with AaSF-FN-Lac mats, showing vascularized tissue with regular distribution. Wounds treated with AaSF, AaSF-FN and AaSF-Lac mats developed immature granulation tissue, as depicted by the loose collagen matrix and small blood capillaries in the tissue (**Figure 5.3.A**). In contrast, a delayed onset of healing was observed in the untreated wounds (UNT), as the granulation tissue was not developed and wounds were covered with dried scab of dead tissue. Wounds treated with DD dressing demonstrated a thin layer of tissue matrix, thus showing signs of healing with growing granulation tissue.

On day 14, wounds treated with spider silk coated dressings exhibited moderate to complete epidermal regeneration; whereas the other groups did not show epidermal covering, indicating a slow healing rate (**Figure 5.3.B**). AaSF-FN-Lac promoted complete re-epithelialization, as the wounds were covered with a thick epidermal layer when treated with mats coated with both FN and Lac. The other spider silk coated mats (single coating of FN/Lac) did not show complete re-epithelialization, but a growing epithelial tongue was clearly observed, as depicted by the green arrows in the images. This further validated an accelerated wound healing rate by the treatment of spider silk coated mats.

On day 21, a clear difference in the regenerated skin tissue could be seen among various treatments by the extent of re-epithelialization and dermal organization. Wounds treated with AaSF-FN and AaSF-FN-Lac mats demonstrated a well-formed collagen matrix with structural integrity in the dermal layer (**Figure 5.3.C**). In comparison, wounds treated with uncoated AaSF mats and AaSF-Lac showed loose collagen matrix in the dermal region, indicating remnants of granulation tissue, depicting the wounds in

remodelling stage. All the treated wounds were completely re-epithelialized, but not the untreated (UNT) wounds, where a delayed healing process could be validated. Overall, the spider silk coating on SF mats resulted in more favourable and accelerated wound healing, characterized by mature skin regeneration and well-formed epidermal and dermal layers.

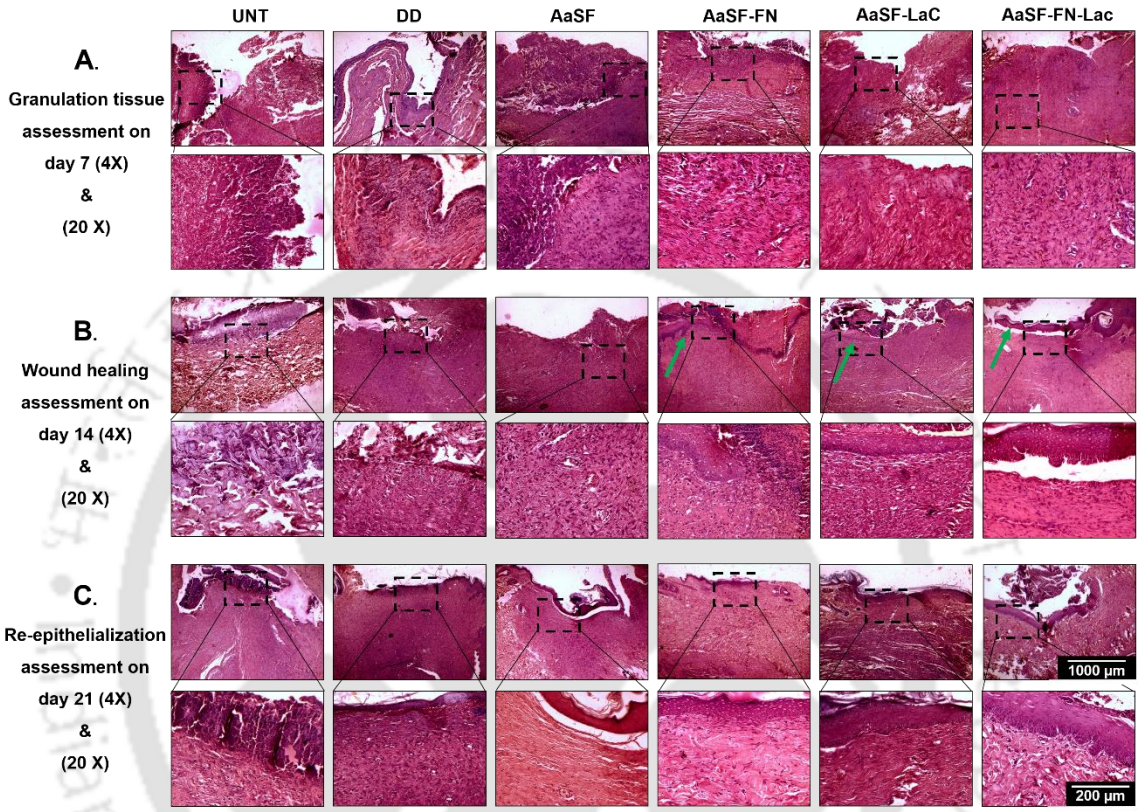

Figure 5.3. *Histological analysis of H and E stained sections of wounded tissues, depicting extent of healing by various treatments in diabetic wounds. (A) Granulation tissue development in the wounds treated by silk mats at early stage (day 7). (B) Commencement of re-epithelialization in the wounds treated with spider silk coated silk mats, shown by growing epithelial tongue (highlighted by green arrows). (C) Regeneration of mature dermal and epidermal layers in all wounds, except the untreated wounds. Images at 4X (scale bar represents 1000 µm) magnification represent histology of cross section of wound tissue; 20X images (scale bar represents 200 µm) of the selected portion represent magnified view of the section.*

5.3.4. Assessment of angiogenesis and re-epithelialization of diabetic wounds

Angiogenic response is the most important step in the healing process, especially in an initial phase. The newly formed blood capillaries during angiogenesis are the only means of nutrients and oxygen supply to the growing granulation tissue during the wound healing process. Early vascular network in the granulation tissue is also considered a

good sign of healing progression. Therefore, we analysed neo-vascularization in the regenerated skin tissue on day 7 post-operation by immunohistological staining of wound sections using CD31 marker of endothelial cells (**Figure 5.4.A**). Among all treatments, wounds with AaSF-FN-Lac and AaSF-FN mats showed higher number of blood capillaries, as also observed in the histological examination presented in figure 5.3., thereby validating more recruitment of endothelial cells due to presence of the fibronectin motif in FN-4RC.

Wounds treated with AaSF-Lac mats showed mixed population of blood capillaries and endothelial cells in the granulation tissue. In wounds treated with uncoated AaSF mats and DD dressings, a comparatively lower number of blood capillaries were observed, although their presence demonstrated growing granulation tissue. In contrast, UNT wounds did not show mature blood capillaries, which might be due to the absence of granulation tissue, as also observed in H & E images. Quantification of blood vessels in the granulation tissue further validated the angiogenic potential of silk mats, especially the ones coated with FN-4RC (**Figure 5.4.B**). The wounds treated with spider silk coated mats showed significantly higher vessel density in comparison to the wounds treated with uncoated AaSF mat and DD dressing, $p \leq 0.01$. The study thus demonstrated that the spider silk coatings enhance neo-vascularization and recruitment of endothelial cells during the early phase of wound healing.

The H & E images provided clues of early onset of epidermal regeneration in the wounds treated with spider silk coated dressings; therefore, next we evaluated the keratin markers (epithelial protein) to further investigate re-epithelialization on day 14 and day 21 using two cytokeratin (CK) markers, namely CK 10 and CK 14 (**Figure 5.5.**). Suprabasal expression of CK 10 was clearly observed in the mature epidermis even on day 14 in the case of wounds treated with AaSF-FN-Lac. Mature epidermis was not observed by the other types of treatments on day 14. However, higher population of keratinocytes expressing CK 10 could be observed on the uppermost layer of regenerated tissue, signifying epidermal layer in its growing stage. On day 21, a mature epidermal layer with keratinocytes expressing CK 10 in the suprabasal layer could be observed in wounds treated with AaSF, AaSF-FN, AaSF-Lac and AaSF-FN-Lac mats, suggesting re-epithelialization with well-structured organization. Similarly, mature epithelial structures expressing CK 14 were observed on day 21, but not on day 14 in the wounds treated with silk mats. However, day 14 sections demonstrated epidermal tongue

containing keratinocytes expressing CK 14 marker in the basal layer of the wounds treated with silk mats. Such epidermal tongue was not observed in the control groups on day 14, suggesting a delayed healing profile in both UNT and DD groups.

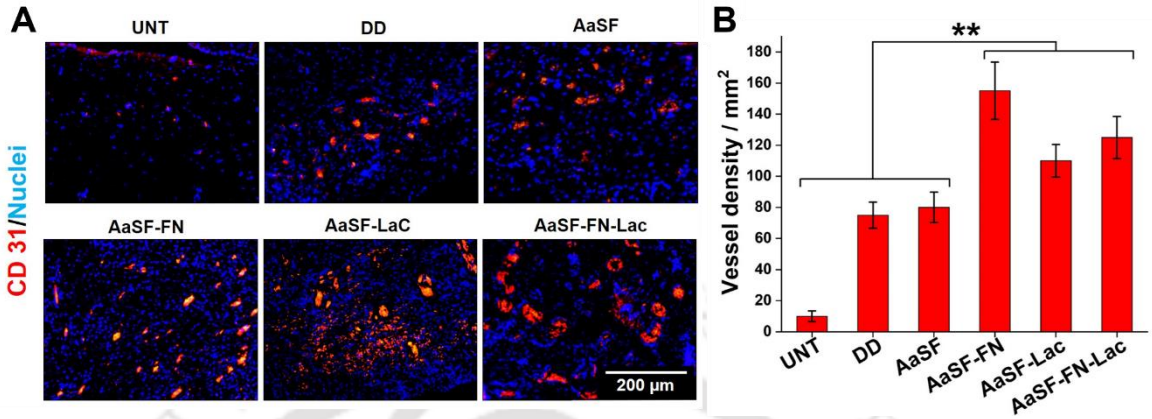

Figure 5.4. *Examination of angiogenesis in variously treated diabetic wounds. (A) Immunostaining using CD31 marker on day 7. Red colour depicts CD31 and blue colour depicts nuclei stained with Hoechst 33342 (scale bar represents 200 µm). (B) Quantification of number of blood vessels in the stained sections demonstrate significantly higher vessel density in the wounds treated with spider silk coated mats in comparison to that of uncoated mat and control groups, ** represents* $p \leq 0.01$.

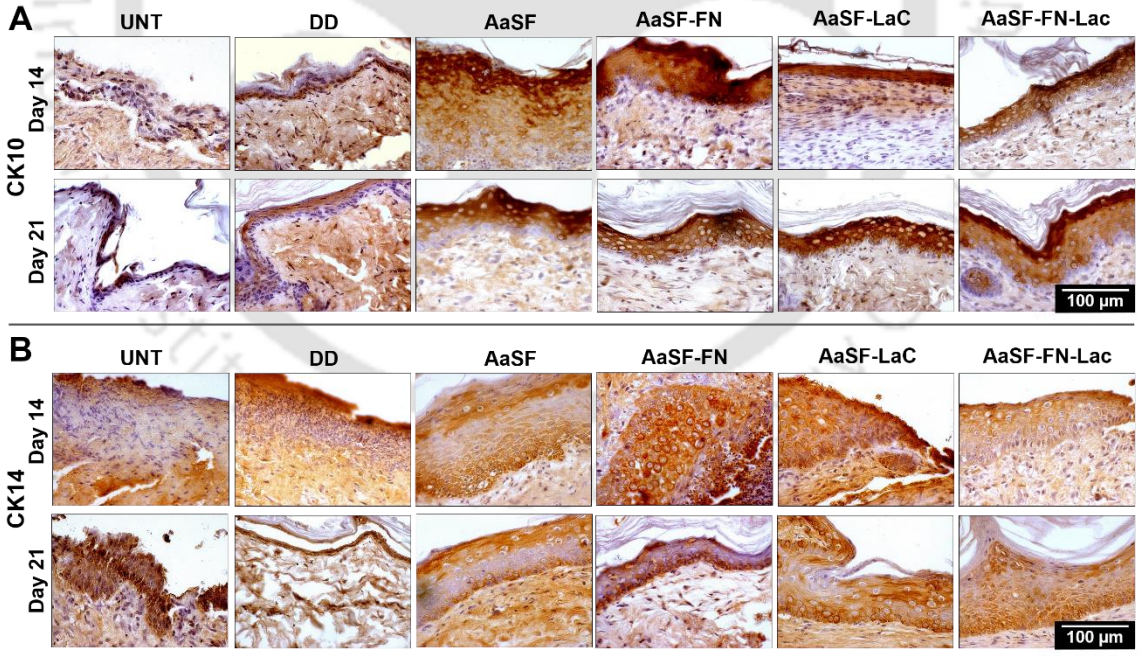

Figure 5.5. *Immunohistochemistry assay of tissue sections using (A) CK 10 and (B) CK 14 markers demonstrates morphology of epithelial cells on day 14 and 21 under hyperglycaemic conditions of diabetic wounds (scale bar represents 100 µm).*

5.3.5. ECM remodelling of diabetic wounds during the wound repair process

A balanced deposition of ECM components in the dermal layer is very crucial during the wound repair process. The dermal matrix continues to remodel from the very beginning till the final completion of healing. Therefore, there is a need to examine the ECM in wounds and regenerated skin tissue. A growing dermal matrix typically shows varied expression of collagen fibres, especially collagen type I (Col I) and collagen type III (Col III). We examined the expression of both types using real time qPCR on day 7, 14 and 21 to evaluate the matrix remodelling stage. In all wounds treated with silk nanofibrous mats, a higher expression of Col I was observed on day 14, revealing a proliferative stage of cells in the wounds at this time point (**Figure 5.6.A**). The mid-stage of a healing process is highly proliferative, where the fibroblasts secrete high amount of ECM components including collagen fibres. In contrast, the wounds treated with commercial Duoderm dressing (DD) demonstrated gradually increasing levels of Col I expression from day 7 to day 21, indicating that the proliferative stage continued till day 21. A typical healing process include proliferation in the early stage and collagen turnover in the later stages of the wound repair process. Such behaviour of matrix remodelling was observed in wounds treated with silk mats, as the expression of Col I regressed on day 21. A significantly lower expression of Col I on day 21 in comparison to day 14 clearly indicated that the proliferative stage was overlapped with remodelling phase in the later phase. This also signified an accelerated rate of wound repair by the AaSF mats and especially those coated with spider silk.

On further investigating the expression of Col III, dermal remodelling was validated in the wounds treated with silk mats (**Figure 5.6.B**). In wounds treated with DD and uncoated AaSF, the expression of Col III was found to be significantly higher on day 14 in comparison to day 7 and 21, $p \leq 0.01$. This signified that the wounds began to contract during the mid-stage (day 14) of the healing process. Collagen III fibres are majorly responsible for contraction of the wound matrix. The fibres are secreted by myofibroblasts and contract the whole matrix, thereby pushing the edges of wound to come close to each other and seal the wound cavity. Early secretion of Col III is also a determinant of accelerated healing process, which was observed in the wounds treated with spider silk coated AaSF mats (AaSF-FN, AaSF-Lac and AaSF-FN-Lac). Higher secretion of Col III in the very initial days (day 7) clearly indicated early onset of wound repair and highly proliferative stage of cells in the wounds. The expression of Col-III

regressed at the later phases (day 14 and 21) suggesting possible collagen turn over or beginning of a tissue remodelling phase. The wounds began to contract on day 7, validating the accelerated rate of healing, as also observed in the gross wound images.

To further validate the collagen matrix deposition in the regenerated skin, we examined the tissue sections by IHC using antibody against collagen type I and collagen type III on day 21 biopsies (**Figure 5.7.A,B**). The dermal regions demonstrated well-distributed bundles of collagen type I in the wounds treated with AaSF mats (coated/uncoated), suggesting an influence on organizing the collagen fibres. Moreover, in the case of AaSF mats coated with spider silk, the organization of collagen bundles was more or less similar, showing regular deposition of ECM guided by the silk mats. In contrast, the control groups did not show well-organized deposition of collagen type I. UNT wounds showed aligned collagen fibres, typical for contraction behaviour of unaided healing. In wounds treated with DD, the collagen fibres were not aligned; however, mature collagen bundles were also absent.

On examining the deposition of collagen type III fibres in the regenerated skin, random small fibres were observed in the dermal regions of all groups, suggesting a lower secretion in comparison to collagen type I. This also demonstrated that the regenerated dermal matrix was majorly composed of collagen type I, thus showing typical characteristics of a normal skin tissue. The morphology of collagen type III was more in the reticular fibre form, in contrast to the bundle like structures seen in case of collagen type I. Deposition of collagen fibres was observed to be homogeneously distributed all over the dermal regions in all wounds, except for the UNT group. The UNT group demonstrated higher secretion at the upper dermal surface in comparison to the lower dermis, suggesting remnants of mature granulation tissue even on day 21, thus validating a delayed healing profile. Such irregular distribution was not observed in the wounds treated with AaSF (coated/uncoated variants) mats, suggesting formation of a mature dermal layer in all the groups due to assistance provided by the silk biomaterial. The results also indicated modulation of the granulation tissue towards a mature dermal matrix within 21 days. Overall, the dermal remodelling was found to be similar in all the wounds treated with silk mats, irrespective of the spider silk coating, which might be attributed to the role of AaSF in ECM deposition.

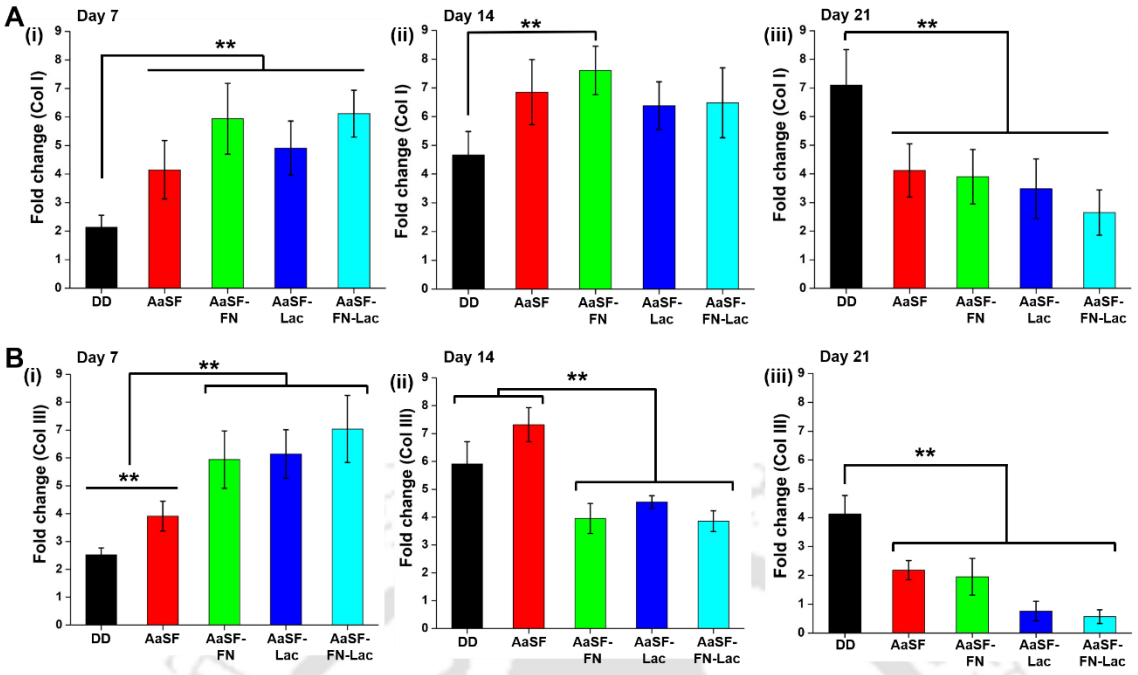

Figure 5.6. *Gene expression study of (a) collagen type I and (b) collagen type I III in the wound tissue shows extracellular matrix remodelling during the healing process on (i) day 7, (ii) day 14 and (iii) day 21 in the diabetic wounds. The graphs represent fold change with respect to the commercially used DD dressing group, ** represents p ≤ 0.01.*

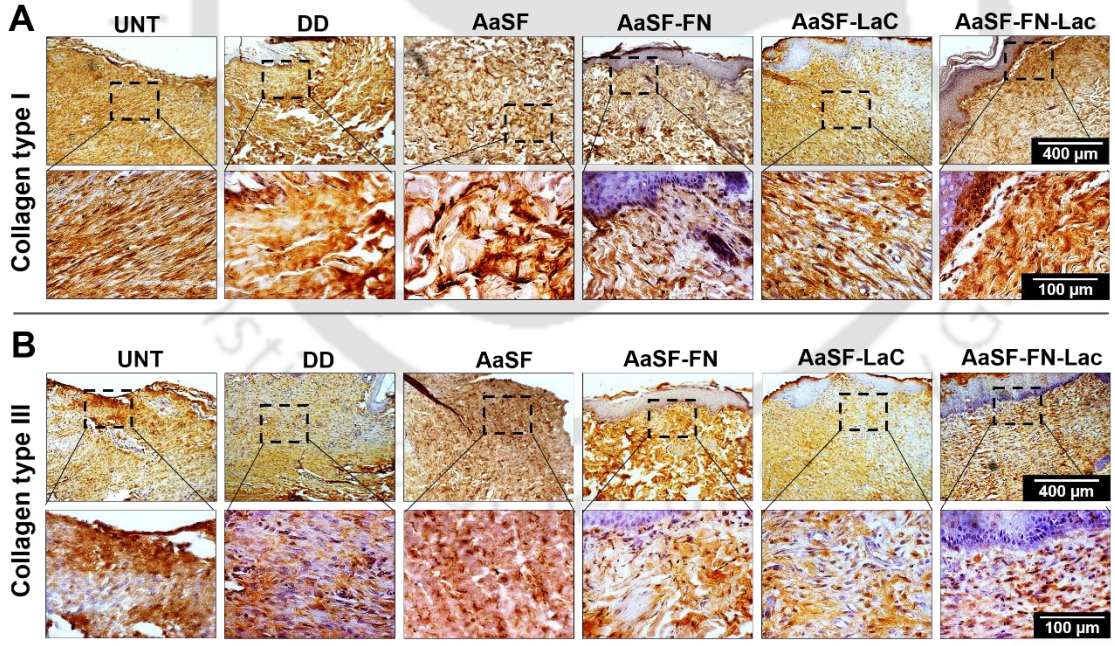

Figure 5.7. *Immunohistochemistry assay showing distribution of (A) Collagen type I and (B) Collagen type III in the regenerated skin tissues in the diabetic model on day 21; Images at 10 x (scale bar represents 400 µm) magnification represent histomorphology of cross section of wound tissue; 40 x images (scale bar represents 100 µm) of the selected portion represent magnified view of collagen fibres.*

5.3.6. One-step grafting of acellular silk scaffolds

Implantation of silk scaffolds was performed through a one-step grafting procedure after 48 h of tissue debridement as demonstrated in the schematic image (**Figure 5.8.**). Both the types of scaffolds (pristine AaSF and with top-coating of FN-4RC) were grafted at the injury site using surgical skin staples. The staples helped in holding the scaffolds in correct position of wound cavity at the time of grafting. Once the scaffolds were integrated with the adjacent skin tissue, staples were no longer required and were carefully removed after 3 days post-implantation. The implantation procedure used in the present study was simple, and did not disturb the wound-bed, to minimize the pain. This procedure indeed helped in one-step grafting of the scaffolds, which were found to be firmly attached at the wound-site.

In order to further validate the integration of scaffolds with wound-bed, the implanted graft site was excised out after 7 days post-implantation using a biopsy punch. Histological analysis of the implanted site clearly indicated integration of the implanted scaffolds with the host tissue as visualized by an upper porous layer over the wound-bed (**Figure 5.9.**). As a reference, histological analysis of wound cavity post-debridement was also performed to reveal creation of full-thickness wounds. The remnants of adipose layer and muscle layer of panniculus carnosus (as observed in the magnified image of the wound cavity) validated the loss of full-thickness cutaneous layer in the wounded region. In comparison to the wound cavity, the wounds grafted with acellular silk scaffolds demonstrated presence of newly developed tissue that filled the wound cavity within 7 days. In addition, invasion of host cells in the porous scaffolds was evident as depicted in the magnified images. The neo-tissue was also found infiltrating in the micropores of silk scaffolds, depicting signs of tissue ingrowth in the scaffolds, thereby attesting successful implantation of the scaffolds.

5.3.7. Wound healing efficacy of AaSF microporous scaffolds coated with recombinant spider silk for treating third degree burn wounds

The support of the AaSF bulk material in the form of microporous scaffold was helpful in covering the wounds and aiding tissue ingrowth at the wound site. Significant difference in the wound healing rate could be detected at the different time-points as the scaffold-treated wounds demonstrated faster wound healing in comparison to the control groups (**Figure 5.10.A**). Among all treatments, the AaSF-FN scaffolds gave significantly

faster wound closure rate, showing only 10.5 ± 2.48 % remaining wound area on day 14 compared to 19.8 ± 2.18 % by the uncoated AaSF counterpart. In contrast, UNT and DD showed 42 ± 3.29 % and 30.3 ± 2.35 % remaining wound area respectively, depicting delayed wound healing as observed on day 14. This indicated ≥ 2 fold accelerated healing rate by AaSF-FN scaffold treatment in comparison to control groups. Notably, early difference in the wound healing profile could not be observed due to presence of intact scaffold over wounds; however, improved healing was clearly evident in the later phase of healing. On day 14, significant differences in the healing profile could be observed for various treatments, depicting faster healing effects of both pristine uncoated AaSF and functionalized AaSF-FN scaffolds.

The gross wound images also showed accelerated wound healing efficacy owing to the bioactivity of spider silk fusion protein present in the AaSF-FN scaffolds (**Figure 5.10.B**). On day 21, AaSF-FN completely healed the wounds, showing no remnants of tissue eschar or scab. Nevertheless, significant difference was not observed between pristine AaSF scaffold and DD dressing on day 21, as remaining wound eschar could be observed on the wounds. On the other hand, UNT wounds showed relatively slower healing rate and demonstrated significantly higher remaining wound area on day 21 in comparison to all treatments. The gross morphology of implanted scaffolds also revealed firm attachment of scaffolds even after removal of staples till day 10. The results can also be validated by the histological examination of implanted scaffolds as shown in figure 5.9. This signified that once implanted at the wound site, the scaffolds promoted rapid tissue ingrowth that helped in adherence of the scaffold to the newly developed tissue matrix of wounds. We observed that the AaSF scaffolds gradually converted into a thin dry layer over the wounds and were then automatically removed after 10 days post-implantation. Representative images of the same have been highlighted in the inset, depicting morphology of dried scaffolds on day 10 and appearance of newly formed skin underneath the scaffold (**Figure 5.10.C**).

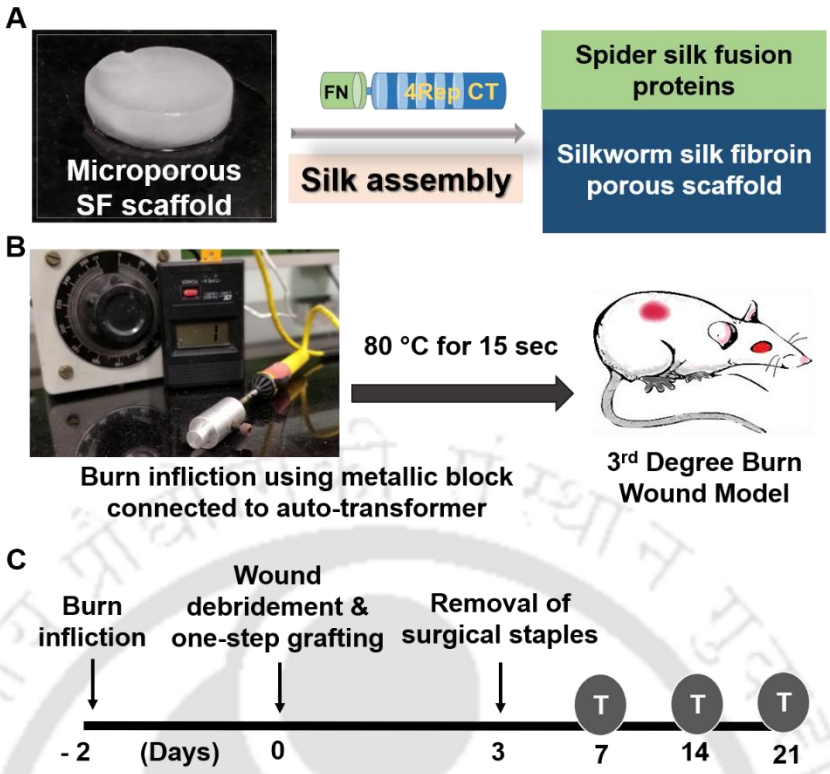

Figure 5.8. *Schematic representation shows: (A) Image of the functionalized silk scaffold, (B) Illustration of the third degree burn wound model obtained using a customized metallic heating block and (C) Experimental set-up depicting treatment of full thickness wounds via one-step grafting procedure. The silk scaffolds were grafted using skin staples post 48 h of burn infliction. Groups were terminated on day 7, 14 and 21 as represented by (T) for wound healing examination.*

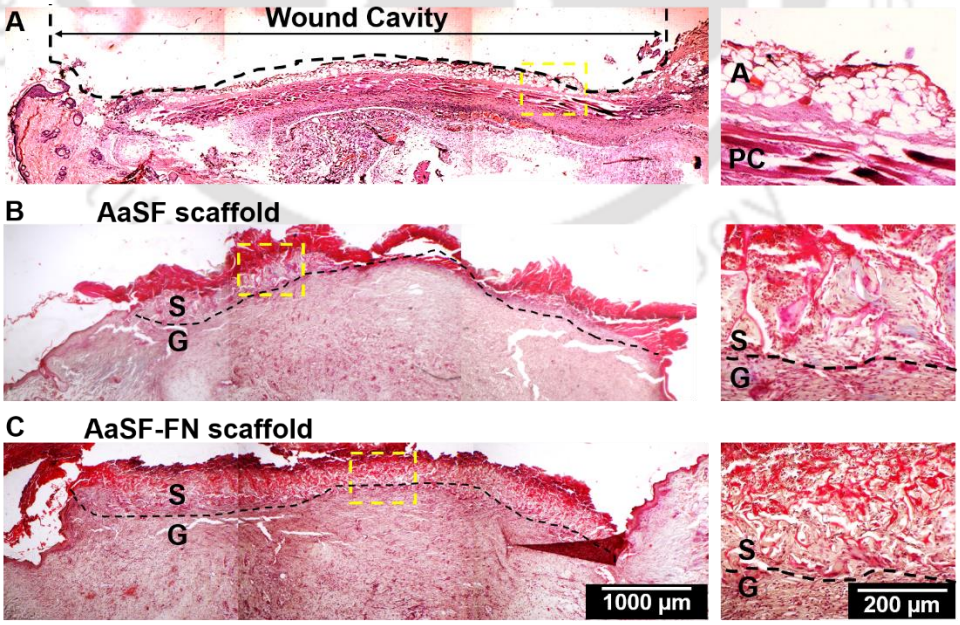

Figure 5.9. *Histological study of the full-length wound biopsies demonstrates wound creation and successful grafting of scaffolds by H and E staining. (A) Wound cavity formed after the debridement of necrotic burn skin; the cavity shows removal of full-*

thickness burn skin after the biopsy. The magnified image shows visible adipose layer (marked as A) and muscle layer of panniculus carnosus (PC). *(B, C) The images depict histology of wound tissue treated silk scaffold on day 7 post-grafting; an upper layer of scaffold (marked as S) well-integrated with the neo-tissue is clearly visible. Granulation tissue (marked as G) developed in the place of wound cavity is also clearly visible underneath the scaffold layer. The magnified images reveal high infiltration of host cells and tissue ingrowth in the implanted scaffolds. Images at 4X magnification represent histomorphology of cross section of full-length wounded tissue (scale bar represents 1000 µm); images at 20X images represent magnified view of the selected portion as highlighted in yellow box (scale bar represents 200 µm).*

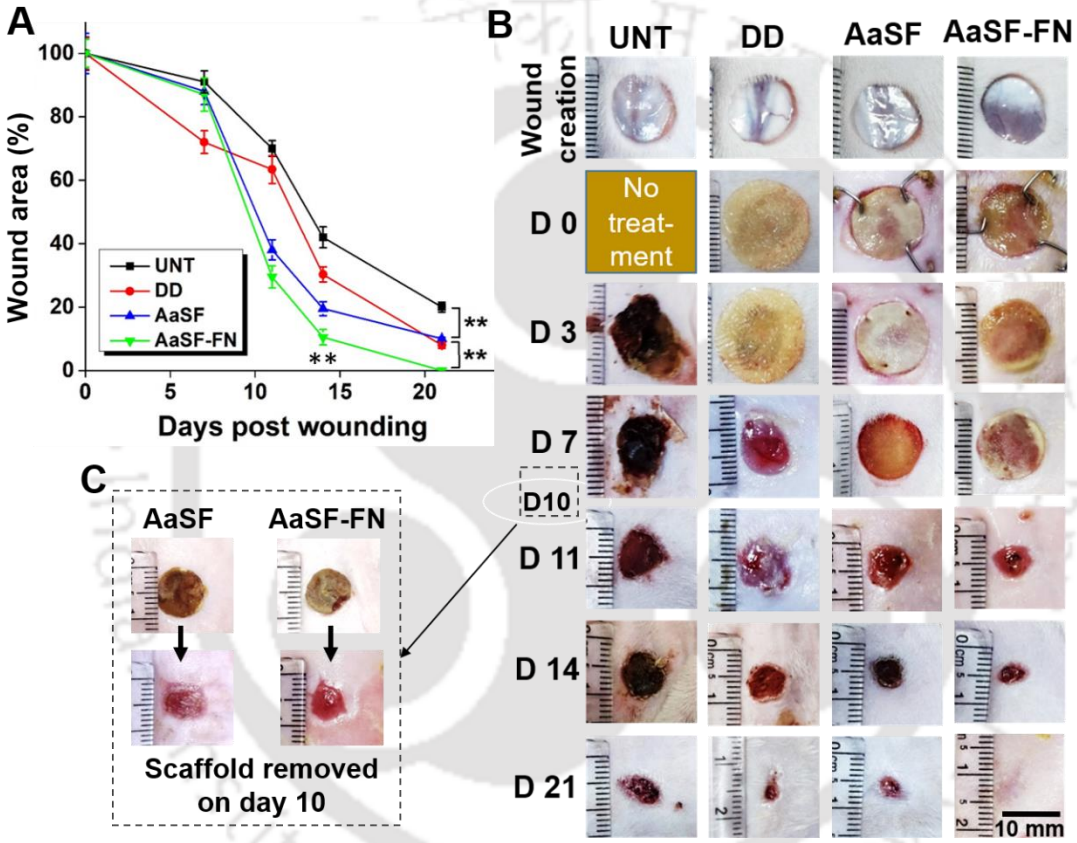

Figure 5.10. *(A) Graphical representation of the wound area at various time-points calculated using Image J software, demonstrating significantly faster wound healing by AaSF-FN treatment, ** represents $p \leq 0.01$. (B) Gross morphology of wounds grafted with silk scaffolds and commercial dressing Duoderm (DD) at various time-points during the course of healing; scale bar represents 10 mm. (C) The inset shows morphology of scaffolds over the wounds and development of regenerated skin visible after removal of scaffolds on day 10.*

5.3.8. Histological examination of burn wounds during the treatment

Histological analysis of the tissue specimens collected on day 7, 14 and 21 revealed timely healing response by the grafted scaffolds (**Figure 5.11.**). Granulation tissue assessment on day 7 indicated early healing response in case of treatment with AaSF scaffolds, as seen by the presence of neotissue ingrowth underneath scaffold layer (**Figure 5.11.A**). When closely observing the tissue section of wound matrix treated by pristine AaSF scaffold, we found gaps in the middle portion of the neomatrix formed (highlighted by dotted yellow line). Such evident gaps were not found in the wounds treated with AaSF-FN, suggesting more recruitment of cells leading to uniform distribution of mature granulation tissue at an early stage of the healing process. The coating of FN-4RC on top of AaSF scaffold clearly demonstrated better wound healing efficiency in comparison to uncoated scaffolds. Among the control groups, treatment with DD dressing demonstrated development of granulation tissue equivalent to treatment with the pristine AaSF scaffold. However, the UNT group showed delayed wound healing response, characterized by a very thin tissue layer over the adipose layer at the wound site. This suggested that in contrast to the treated wounds, granulation tissue was not developed in the untreated wounds till day 7 post-operation.

On day 14, the arrangement of neotissue appeared well-organized, suggesting progression in the wound healing in the treated wounds. Untreated wounds showed granulation tissue development on day 14, which was not formed on day 7, confirming delayed healing process in the untreated wounds. Among the treated groups, AaSF-FN scaffolds demonstrated a growing thick epidermal layer on the uppermost surface of neomatrix, signifying early onset of re-epithelialization (**Figure 5.11.B**). In contrast, neither wounds treated with pristine AaSF nor DD dressing did show any thick epidermal layer. However, complete re-epithelialization was observed on day 21 in all the treated groups (**Figure 5.11.C**). Except for the UNT group, all the treated wounds demonstrated presence of a thick mature epidermal layer. Absence of epidermal layer in the UNT group further corroborated delayed healing profile of untreated wounds, as also observed in the gross wound images. AaSF-FN showed well-formed dermal and epidermal structures as confirmed by the higher magnified images of tissue sections, suggesting improved healing efficacy owing to presence of the FN-4RC spider silk protein.

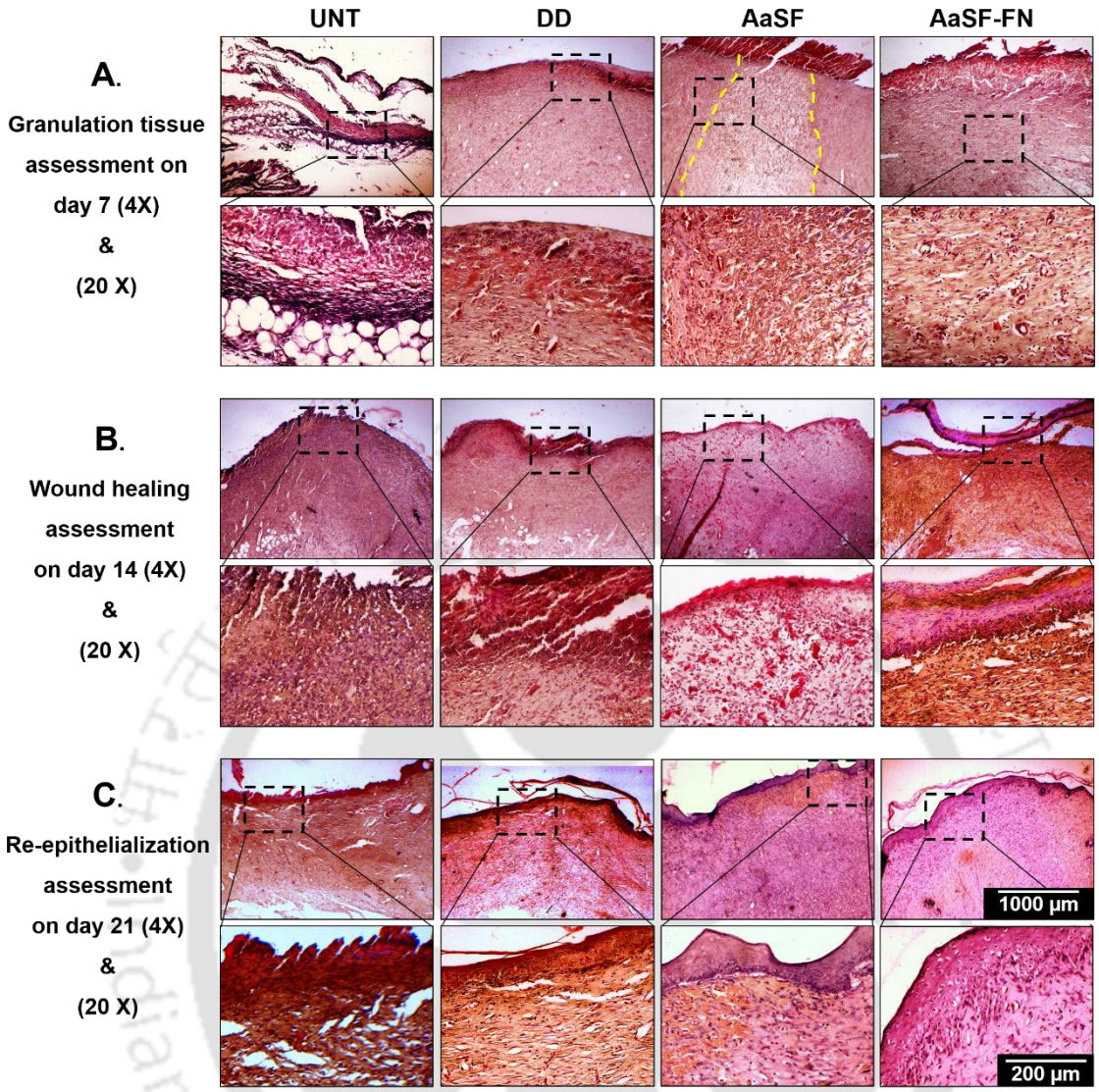

Figure 5.11. *Histological analysis of wounded tissues depicting the extent of healing by various treatments using H and E stain. (A) Granulation tissue development in the treated wounds at an early stage (day 7). (B) Commencement of re-epithelialization in the wounds treated with AaSF-FN scaffold, demonstrating efficacy of FN-4RC coating in the development of epithelial layer (day 14). (C) Regeneration of mature dermal and epidermal layers in all the treatments except the untreated wounds (day 21). Images at 4X magnification represent histomorphology of cross section of wound tissue (scale bar represents 1000 µm); 20X images of the selected portion represent magnified view of the section highlighted in black box (scale bar represents 200 µm).*

5.3.9. Assessment of angiogenesis and re-epithelialization of burn wounds

Next, we evaluated the angiogenic potential of various treatments by immunofluorescence staining of wound sections using vWF marker of endothelial cells (**Figure 5.12.A**). Among all treatments, AaSF-FN treated wounds showed higher number of mature blood capillaries in the wound matrix, indicating signs of angiogenesis and higher recruitment of endothelial cells. The results were consistent with the superior regenerative response, also observed in the H & E stained sections. Formation of a few blood vessels were formed in wounds treated with both pristine AaSF scaffold and DD dressing, depicting presence of growing granulation tissue. However, mature blood capillaries were not observed in the UNT group, as only few endothelial cells could be visible in scattered fashion. Quantification of blood vessels further validated the angiogenic potential of FN-4RC coated scaffolds (**Figure 5.12.B**). The wounds treated with AaSF-FN scaffolds showed significantly higher vessel density in comparison to other groups, $p \leq 0.01$. Neo-vascularization, as observed by the blood capillaries in the granulation tissue, also confirmed angiogenic and healing potential of silk proteins.

We further examined the re-epithelialization of wounds, as it is the most important event in the wound healing process. We investigated the chief markers of epidermal layer, namely, CK 10 and CK 14, in the tissue sections collected on day 14 and day 21 through IHC assay (**Figure 5.13.**). On day 14, CK 10 expression was not observed in the uppermost layer of wound matrix in any of the groups due to absence of mature epithelial layer within this period. However, wounds treated with AaSF-FN demonstrated expression of CK 14 in the growing epithelial tongue on day 14, as highlighted by a black arrow in the respective image. The same section did not reveal expression of CK 10. This support our hypothesis that the epidermal layer observed on the uppermost layer in wounds treated with AaSF-FN was immature and expressed only CK 14 marker. On day 21, CK 10 expression was manifested in the suprabasal layers of the epidermal region of wounds treated with AaSF and AaSF-FN scaffolds, indicating the positive role of silk protein in re-epithelialization.

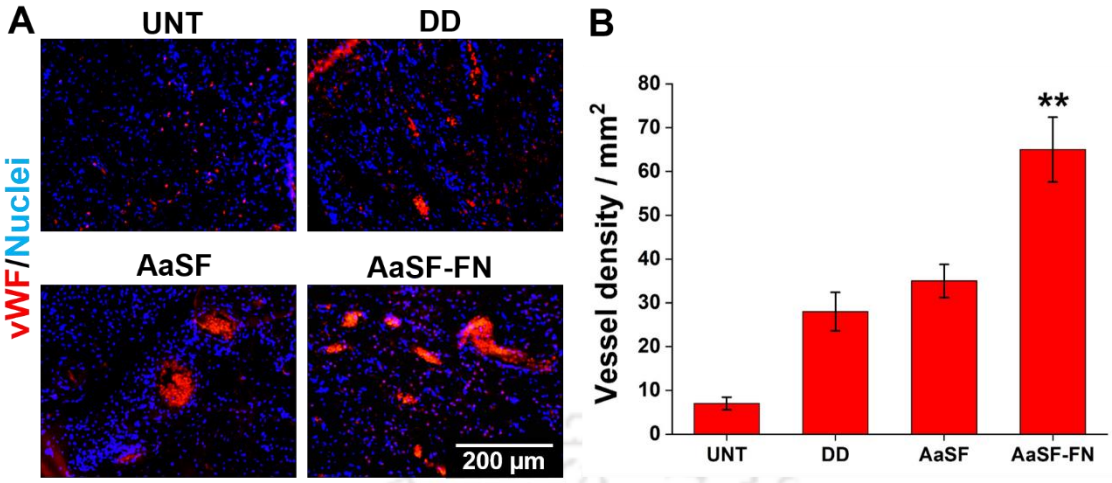

Figure 5.12. *Examination of angiogenesis in the wounds. (A) Immunostaining using vWF marker on day 7. Red colour depicts vWF and blue colour depicts nuclei stained with Hoechst 33342 (scale bar represents 200 µm). (B) Quantification of number of blood vessels in the stained sections demonstrates significantly higher vessel density in the wounds treated with spider silk coated silk scaffolds (AaSF-FN) in comparison to that of other groups, ** represents $p \leq 0.01$.*

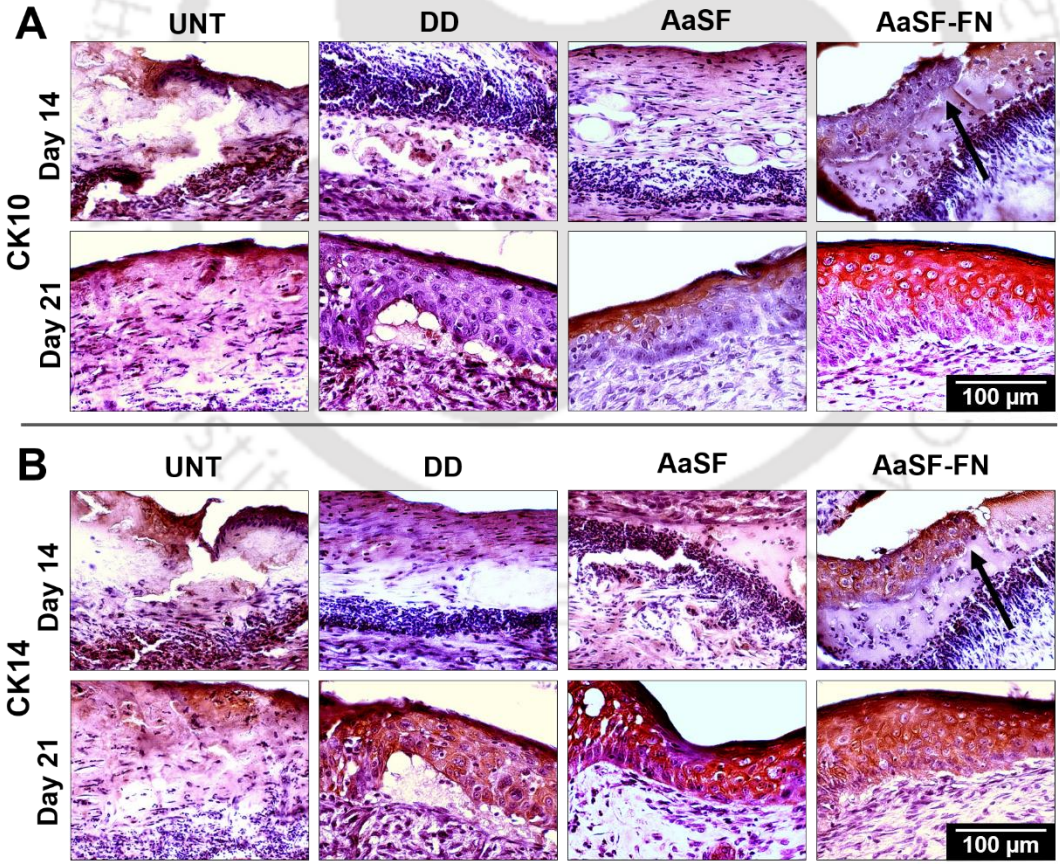

Figure 5.13. *Immunohistochemistry assay of tissue sections using (A) CK 10 and (B) CK 14 markers demonstrates morphology of epithelial cells in the epidermal layer of regenerated skin on day 14 and 21 (scale bar represents 100 µm).*

Untreated wounds and those treated with DD did not demonstrate expression of CK 10 even on day 21, revealing immature epidermal layer still in the growing stage due to delayed healing. CK 14 expression was observed throughout the epidermal layer in all the treated wounds, signifying re-epithelialization of the wounds within 21 days of treatment. Moreover, the IHC images also revealed well-formed epidermal structures (expressing both CK 10 and CK 14) in wounds treated with AaSF and AaSF-FN, indicating improved healing efficacy of silk biomaterials in comparison to the control groups.

5.3.10. Wound remodelling assessment: gene expression study and immunohistology

Finally, we examined the effect of various treatments on the dermal remodelling by analysing the expression and deposition of collagen type I and collagen type III fibres in the regenerated skin biopsies. The real time qPCR revealed significant remodelling between collagen fibres in the wound matrix from day 7 to day 21. The expression of Col I on day 7 indicated early healing profile in case of wounds treated with AaSF and AaSF-FN scaffolds, as the expression was 3-4 fold higher (**Figure 5.14.A**). In contrast, the commercial dressing showed only 1.5-fold increment in Col I expression, suggesting slower healing in comparison to wounds treated with scaffolds. Col I was found to be upregulated on day 14 and day 21, validating tissue formation in the later stages of healing process. In wounds treated with AaSF, the expression on Col I was highest on day 14, confirming ongoing healing stage of the wounds. On the other hand, significantly lower expression on day 21 demonstrated remodelling stage in the later phase of wound healing. Similar expression behaviour was observed in the wounds treated with AaSF-FN. Higher expression of Col I on day 7 and day 14 indicated early granulation tissue development and tissue ingrowth in the wound cavity, suggesting accelerated wound healing profile. A significant regression in the Col I expression on day 21 compared to day 7 and 14 indicated a remodelling stage as the healing process reached the final stage.

The expression study of Col III indicated similar healing pattern (**Figure 5.14.B**). The expression continued to upregulate from day 7 to day 21 in case of DD treatment. This confirmed the ongoing healing phase of wounds throughout the time-period of 3 weeks. In contrast, wounds treated with silk scaffolds demonstrated initial upregulation and regression thereafter, indicating a remodelling stage. Expression of Col III was found

to be significantly higher on day 14 in comparison to day 7 and day 21 in wounds treated with AaSF scaffold. This clearly showed that the highest secretion of collagen type III fibres was during the mid-stage of the healing process, in order to promote wound contraction. Once the wound contraction was completed, the expression was regressed on day 21 in the remodelling stage. IHC assay on the tissue section using antibodies against collagen type I and collagen type III proteins depicted morphology of collagen fibres deposited in the regenerated skin on day 21 (**Figure 5.14.C,D**).

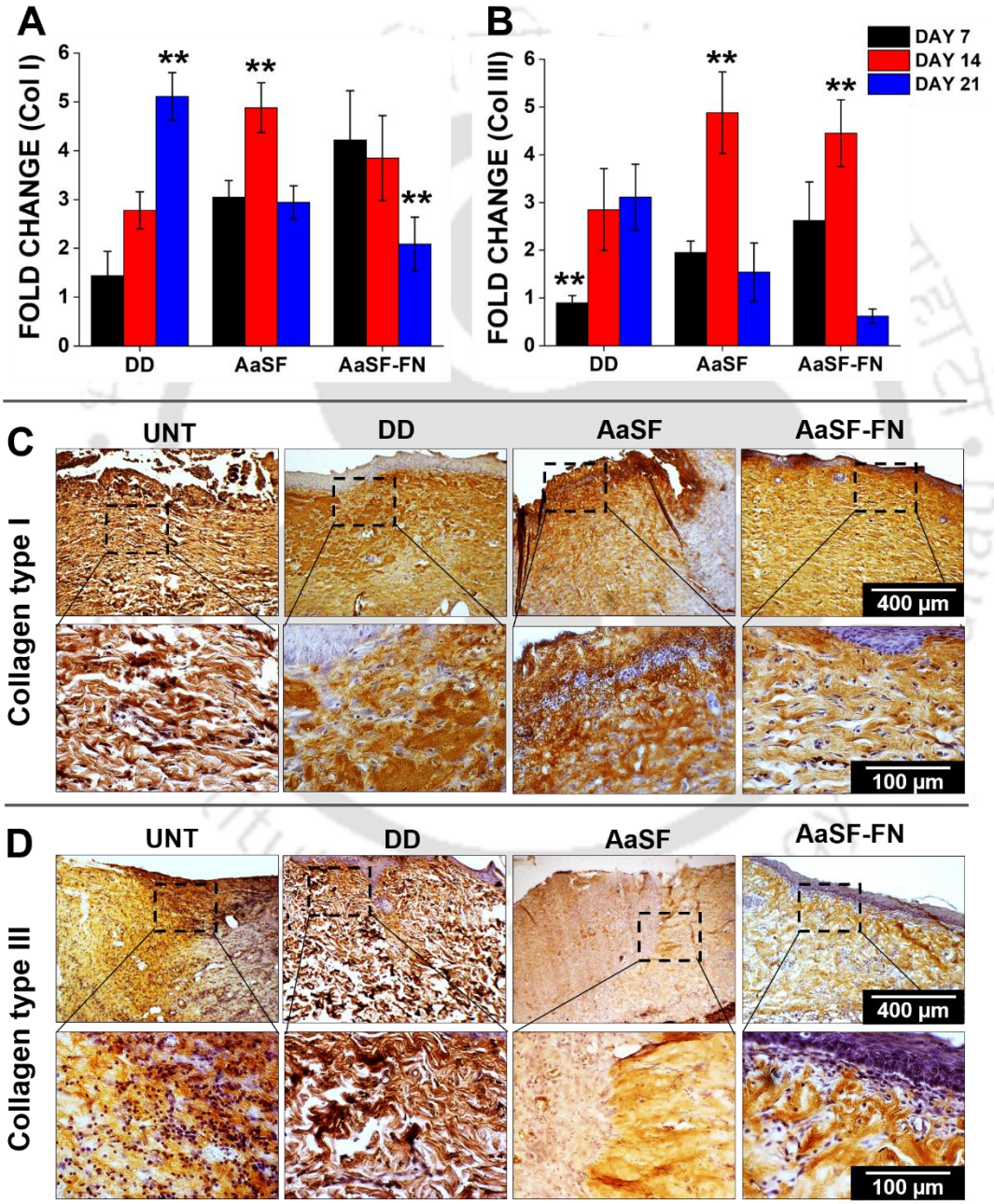

Figure 5.14. *Gene expression study of (A) Collagen type I and (B) Collagen type III in the wounds shows extracellular matrix remodelling during the healing process in burn*

*wounds. Fold change represents expression of particular gene in all the treated wounds with respect to untreated wounds (taken as control), **$p \leq 0.01$. Immunohistochemistry assay showing distribution of (C) Collagen type I and (D) Collagen type III in the regenerated skin tissue on day 21; Images at 10X (scale bar represents 400 µm) magnification represent histomorphology of cross section of wound tissue; 40X images (scale bar represents 100 µm) of the selected portion represent magnified view of collagen fibres and bundles.*

The dermal regions demonstrated well-organized bundles of collagen type I in the treated wounds. In contrast, untreated wounds did not show well-organized deposition of collagen type I bundles, which might be due to the incomplete healing of wounds. Examination of the deposition of collagen type III fibres in the dermal regions of regenerated skin suggested interesting results. Notably, wounds treated with AaSF scaffolds demonstrated collagen type III fibres on the edges and not in the centre of wound matrix. This specified the typical behaviour of collagen type III fibres in wound contraction from the edges towards the central wound matrix. Such morphological observations also revealed that the collagen remodelling was still in the incomplete phase by day 21 in wounds treated with AaSF. On the other hand, wounds treated with AaSF-FN demonstrated homogeneously distributed fibres of collagen type III all over the dermal regions, suggesting characteristics of mature skin regeneration. The results also verified modulation of provisional granulation tissue towards a more resistant and mature dermal matrix within 21 days, revealing final stage of the wound healing process. The regular deposition of collagen fibres in the wounds treated with silk scaffolds suggested a role of silk in guiding the ECM deposition during the tissue regeneration process. The detailed study proved our hypothesis that the functionalized silk scaffolds helped in accelerating the natural healing pathways characterized by the formation of granulation tissue by day 7, commencement of re-epithelialization by day 14 and complete skin regeneration of epidermal and dermal structures by day 21.

.

5.4. Discussion

Silkworm silk biomaterial possesses huge potential in wound healing applications owing to the inherent healing property of SF protein [90]. Despite having the intrinsic regenerative properties, silkworm silk has been further functionalized with growth factors or other bioactive factors in order to enhance the healing efficacy in various previous studies [91, 331]. Another variety of silk is spider silk, which can be successfully produced using recombinant DNA technology [213]. A significant feature of 4RC is that it can be easily functionalized with other motifs at genetic level to produce 4RC conjugated with functional peptides like the tripeptide RGD, cationic antimicrobial peptides, affinity domains, growth factors, and enzymes under near physiological conditions with maintained bioactivity [236, 237, 300, 329, 332]. Herein, we have utilized the recombinant spider silk variants FN-4RC and Lac-4RC to develop multifunctional wound dressings and bioactive scaffolds for the treatment of complex wounds.

The facile methodology of combining both the silk types allows easy construction of stable bioactive matrices without additional crosslinking agent as shown in chapter 4. Results from our previous *in vitro* cell culture study provided evidences that spider silk coated matrices performed better in comparison to the uncoated counterparts [355]. The present study is aimed to evaluate safety and effectiveness of the developed silk constructs for treating critically severe wounds (**Figure 5.1.**). The function of bioactive spider silk coating on wound healing parameters was apparent from the gross wound images (**Figure 5.2.**). Dual coating of FN-4RC and Lac-4RC on top of AaSF mat clearly demonstrated better wound healing efficiency (**Figure 5.3.**), followed by the single coating of Lac-4RC and FN-4RC in case of diabetic wounds. Histological study of the wounded tissues validated the results, as the functionalized matrices helped in the early angiogenesis and granulation tissue formation by day 7 (**Figure 5.4.**). Commencement of re-epithelialization was observed by day 14 in the wounds treated with spider silk coated mats (**Figure 5.5.**). Finally, complete skin regeneration of dermal structures as seen by the morphology of mature collagen fibres was confirmed by day 21 even under the hyperglycaemic condition of diabetic wounds (**Figure 5.7.**).

Reinforcing silk scaffolds with enhanced cell binding activity using recombinant spider silk fusion protein through our facile fabrication process led to the development

of acellular grafts, which could be successfully implanted *via* one-step surgery (**Figure 5.8. and 5.9.**). The coating procedure not only offered functional advantage, but also led to a cost-effective approach. The silkworm silk used as a bulk material is an inexpensive material and its functionalization requires a very low concentration (0.01 %) of recombinant spider silk fusion protein. Our approach thus circumvented the large-scale production problem associated with low yield of recombinant spider silk. Functionalization of silk has previously been done in other studies. For instance, silk fibroin protein containing additional RGD motifs was produced by transgenic silkworms for wound healing applications [357]. In another study, spider silk biomaterial functionalized with fibronectin type II domains was produced [358]. However, production of high amount of such recombinant materials to be used as bulk matrix increase the production cost by many folds.

We also investigated the effect of spider silk coating on AaSF scaffold on the healing outcomes through a comparative study with the uncoated counterpart to unfold the beneficial properties of FN-4RC on burn wound healing for the first time (**Figure 5.10.**). Auto-removal of scaffolds post 10 days of treatment might be attributed to the development of neo-dermal matrix formed beneath the scaffold, which pushed the outer scaffold layer after tissue maturation. Another reason might be the higher mechanical strength and slow biodegradation rate of SF scaffold, which did not contract and remodel along with the wound contraction process. Instead, the scaffolds acted as a provisional matrix and supported development of neo-tissue beneath. Higher wound contraction soon after scaffold removal demonstrated that the scaffolds stimulated cells for faster healing and promoted tissue ingrowth at a faster rate as also observed in the histological analysis (**Figure 5.11.**). In addition, removal of scaffolds in the later phase of healing process did not lead to any major disturbance in the wound matrix since wound healing cascade was already stimulated by the scaffolds in the earlier phase.

Fibronectin present in the natural fibrin clot is the most studied protein in wound healing applications because it plays major role is recruiting cells owing to the presence of a cell adhesion motif (RGD tripeptide) [8, 26, 354]. The RGD sequence is well explored in cell binding applications, as it binds to a wide variety of integrins present on various cells. It plays a major role in wound healing by attracting cells, aiding their growth, migration and proliferation [8, 26, 354]. Thus, AaSF-FN matrices acted as a bioactive platform over the wounds and could stimulate the healing at a faster rate.

Angiogenesis, one of the vital determinants of wound healing progression, indicates proliferation of connective tissue at the initial stage of the healing process [28, 359]. Coating of FN-4RC on the silk matrices provided a local microenvironment suitable for cell adhesion and thereby resulted in higher angiogenesis in the AaSF-FN treated wounds (**Figure 5.4. and 5.12.**).

Diabetic wounds treated with dual coating AaSF-FN-Lac, demonstrated early development of an epidermal layer expressing CK 10 and CK 14 markers even on day 14 (**Figure 5.5.**). This indicated synergistic roles of both FN-4RC and Lac-4RC in promoting wound re-epithelialization. Accelerated healing of wounds treated with AaSF-Lac might be attributed to the antimicrobial and healing properties of lactoferrin. In case of burn wounds, the coating of FN-4RC spider silk stimulated early re-epithelialization of wounds by recruiting keratinocytes (**Figure 5.13.**). Notably, expression of CK 14 observed in the epithelial tongue in case of AaSF-FN treated wounds on day 14 revealed a budding epidermal layer at an early stage. This indicated that FN-4RC played a major role in re-epithelialization of wounds. The coated silk scaffolds demonstrated enhanced cell-material interactions and formation of bilayer keratinized skin layer in the *in vitro* studies conducted in our previous work [355]. The present study thus highlighted keratinization potential of FN-4RC coating present in the implanted scaffolds. By providing artificial cell conducive microenvironments through silk materials, we could achieve improved healing outcomes in both types of wounds.

Further, regular deposition of collagen fibres in the silk treated wounds suggested role of silk matrix in guiding the ECM deposition (**Figure 5.6. and 5.14.**). This might be attributed to ECM deposition assisted by cell-material interactions. Similar results were previously obtained in our previous study as shown in chapter 2 and 3, which demonstrated a role of AaSF in the regulation and deposition of ECM. The dermal layer of cutaneous system majorly consists of 80 – 85 % collagen type I fibres and 10 – 20 % collagen type III fibres, which collectively provide integral stability and tensile strength to the skin [360-362]. The secretion of collagen type III remains more or less constant in the intact skin; however, the secretion increases in the wounded skin in order to facilitate wound contraction with the help of collagen type III fibres [362, 363]. Therefore, early secretion of collagen type III fibres is also considered as a sign of wound contraction and accelerated wound healing process [362]. Further, in case of normal healing process, the deposition of collagen fibres diminishes with time because persistent secretion of

collagen fibres is associated with scar or keloid formation [362, 364]. Higher expression of collagen fibres in the mid-stage (day 14) and lower expression in the later phase of wound healing (day 21) by silk treatments indicated regulated expression of collagen fibres. Overall, the results suggest that wounds treated with silk matrices were at a more advanced stage of healing compared to control groups.

The current gold standard for chronic wounds and large-scale skin replacement in trauma injuries is autologous split-thickness skin grafting (STSG) [1, 18]. However, limitations like donor site availability, long term treatments, prolonged hospital stays and most importantly highly expensive treatments are still limiting the application of STSG [1, 18]. Artificially developed bioactive wound dressings using inexpensive strategies thus offer a promising alternative to overcome the limitations associated with current costly treatments. The bulk material of SF, being a cost-effective material may provide an additional advantage over the currently used highly-priced products. The encouraging results by spider silk coated matrices revealed remarkable contribution of both types of silks in treating hard-to-heal wounds. Overall, the present work demonstrated that the functionalized silk matrices can be used in the form of a ready-to-use, off-the-shelf acellular matrices. Thus, our simplistic approach of developing bioactive matrices using silk biomaterials resulted in possible treatments for chronic diabetic wounds and burn injuries. The facile approach of using combined spider silk and silkworm silk biomaterials in treating difficult wounds encourages a conceivable translation from bench to bedside in future.

5.5. Significant findings

The salient findings of this chapter are as follows:

1. The *in vivo* study in two different types of wound models validated the healing efficiencies of spider silk coated silkworm silk matrices. The engineered matrices in the form nanofibrous mats and acellular porous grafts demonstrated great potential in wound healing applications.
2. The silk matrices not only accelerated the wound healing rate but also showed improved angiogenesis, early re-epithelialization and regulated collagen synthesis, thereby depicting complete wound repair.
3. Dual coating of FN-4RC and Lac-4RC showed better wound healing efficiency in comparison to single individual coatings; thus, depicting improved healing potential of multifunctional dressings.
4. The bioactive silk scaffolds used herein provided a functional niche in the form of an artificial provisional matrix over the wounds, and stimulated cell migration and tissue ingrowth towards quick wound repair.
5. The acellular porous silk grafts implanted on full-thickness burn wounds by one-step grafting procedure revealed temporary graft integration with the host tissue, which helped in accelerating the healing process and overall skin regeneration.

Despite having an intrinsic regenerative property in the silkworm silk, additional functionalization with bioactive recombinant spider silk fusion proteins provided multifunctional assets to the bulk matrices. The encouraging results obtained by the spider silk coated silkworm AaSF matrices under *in vivo* conditions provide a research route of its possible translation from bench to bedside. Our study also paves the way for further pre-clinical and clinical studies using the fabricated matrices in tissue engineering and regenerative medicine.

Chapter 6

Development of *in situ* forming silk hydrogel for treating full thickness burn wounds

This chapter describes the methodology of developing an in situ forming hydrogel for application in full-thickness skin wounds associated with deep burns. The facile fabrication approach demonstrates cross-linker free gelation mechanism towards a stable silk hydrogel that provides an instructive and supportive matrix to aid wound healing.

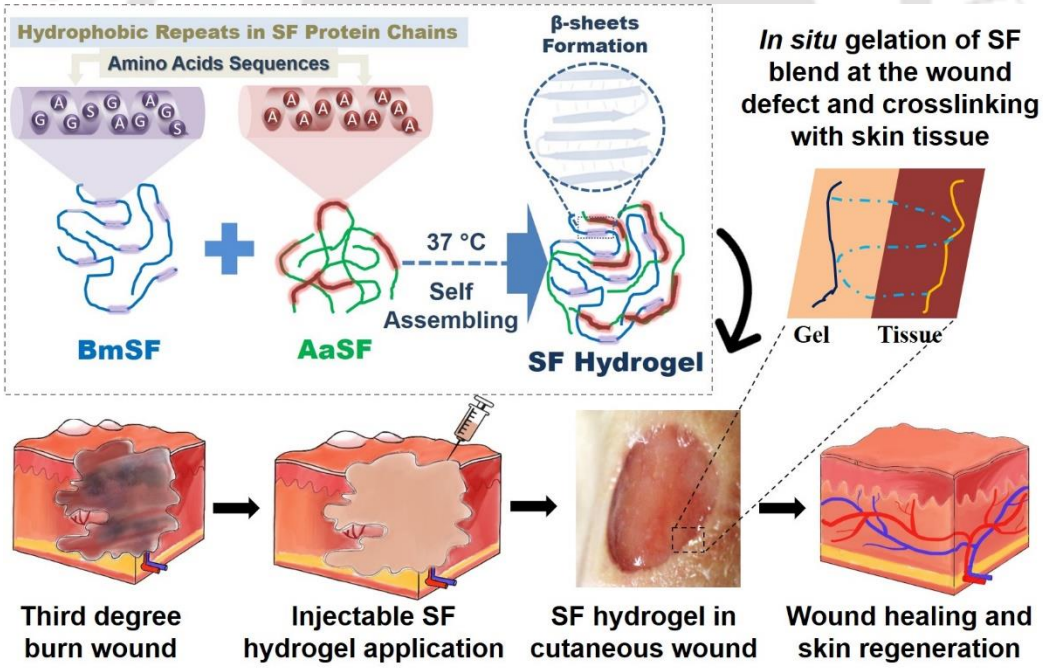

The work embodied in this chapter is published:
Chouhan D, Lohe TU, Samudrala PK, Mandal BB. In situ forming silk fibroin hydrogel promotes skin regeneration in full thickness burn wounds. *Advanced Healthcare Materials* 2018; e1801092.

ABSTRACT

Full-thickness skin wounds, associated with deep burns or chronic wounds pose a major clinical problem. Significant progress has been made in treating such wounds using autografts, allografts and bioengineered constructs. However, efficient, safe and affordable skin regeneration therapeutics still remain a major challenge. Herein, we report the development of *in situ* forming hydrogel using natural silk fibroin (SF) biomaterial for treating third degree burn wounds. Blends of SF solutions isolated from *Bombyx mori* (BmSF) and *Antheraea assama* (AaSF) showed inherent self-assembly between the two types of silk proteins and led to fabrication of stable hydrogel matrix. Investigation of gelation mechanism revealed inherent crosslinking due to formation of β-sheet structures as examined by X-ray diffraction and Fourier transform infrared spectroscopy. Rheological studies demonstrated temperature and concentration dependent gelation of SF hydrogel, thereby depicting tunable gelation mechanism. *In vitro*, SF hydrogel supported proliferation of primary human dermal fibroblasts and aided active migration of keratinocytes. *In vivo*, the efficacy and healing mechanism of SF hydrogel was examined by taking collagen gel as control in third-degree burn rat model. A 3-week comparative study indicated that SF hydrogel not only promoted wound healing, but also showed transitions from inflammation to proliferation stage as observed through the expression of TNF-α and CD163 genes. The *in situ* forming SF hydrogel provided an instructive and supportive matrix to the full-thickness wounds, thereby promoting granulation tissue formation, angiogenesis, re-epithelialization and tissue remodelling. Thus, SF hydrogel proved to be an effective and inexpensive formulation towards a potential therapeutic approach for burn wound treatment.

6.1. Introduction

Burn injuries give rise to complex wounds and may be life threatening to third degree burn patients [17, 365]. More than 100 million people are affected by burn injuries every year worldwide according to the World Health Organization (WHO) [365]. If not treated timely, wound necrosis progresses towards nearby tissue and lead to fatal consequences [366]. In addition, obstructed blood in the necrotic wounds further hampers the inherent healing pathway [367]. Treatment of burn wounds is difficult and clinical outcomes are often poor due to additional complications like scarring and disability in movement [5]. The treatment of burn wounds has largely been centred on the use of autografts or artificial skin constructs [1, 5]. The standard-of-care for third degree burn wounds is the application of autologous split-thickness skin grafts (STSGs). However, STSGs suffer from drawbacks like skin contracture, prolonged hospital stays, secondary donor site wounds and high expenditure [1, 5]. Therefore, dermal reconstruction or regeneration with the help of artificial template is pivotal to improve wound healing mechanism.

The existing treatment mostly prefer natural biomaterials over synthetic materials owing to the former's better biocompatibility and ability to interact with host tissue [25]. Matrices commonly used for skin engineering are made up of protein polymers such as collagen or fibrin gels as they form a regenerative template, mimicking the skin physiology [1, 25]. However, biological effects of collagen-based matrices are compromised by its poor mechanical properties, leading to faster contraction of the grafts [67, 68]. In addition, the collagen and fibrin based matrices are costly, creating a huge gap between need and availability [368, 369]. In 2013, the estimated hospital care cost incurred in high-income countries was approximately $ 88,000 per burn patient [370]. The cost to heal is indeed an important factor that needs to be considered to bridge the gap. Therefore, management of burn wounds poses a challenging clinical and economical problem. This has encouraged the exploration and development of affordable novel matrices with ideal physical and biological properties [1]. Developing a matrix with capacity to innately guide cell migration and proliferation while also holding suitable mechanical properties, remains a big challenge in tissue engineering.

As such, affordable natural biomaterial like silk fibroin (SF) possessing inherent tissue regeneration property holds great potential in wound healing [90]. According to a recent study, the underlying mechanism of wound healing by SF protein is regulated by

the NF-κB signalling pathway [255]. In addition, SF also possesses tunable mechanical properties to match the desired resilience and elasticity of native tissues [22]. SF supports cell proliferation and extracellular matrix (ECM) deposition, thus making direct contribution towards wound repair and tissue regeneration process [238]. SF based constructs like porous scaffolds, nanofibrous mats and thin films have been highly explored for treating acute and chronic wounds [23, 90, 238]. The present study deals with the development of silk based soft hydrogels for treating burn wounds. Hydrogels have advantages over other formats, as they provide an ideal hydration environment required for burn wounds [56]. Maintaining tissue hydration in burn wounds is an essential criterion to facilitate autolytic debridement of necrotic eschar tissue and prevent wound necrosis [55, 56]. Most important, hydrogels are an ideal physicochemical mimetic of the skin ECM due to similarities in their hygroscopic nature [55, 56].

Herein, we have developed a silk gel formulation that allows *in situ* gelation at 37 °C due to self-assembly between two different silk proteins. Two types of silk fibroin proteins isolated from mulberry silkworm *Bombyx mori* and non-mulberry silkworm *Antheraea assama* were blended in equal ratio to develop SF hydrogel. The inherent self-assembly property between the two silk types was exploited to generate *in situ* hydrogel formulation for treating third degree burn wounds. Our formulation of developing SF hydrogel does not require any additional cross-linking agent and thereby can be used as injectable or *in situ* forming hydrogel in aqueous form. This provided an additional advantage to the hydrogels to crosslink with ECM of wound edges, thereby preventing further suture application. In this study, we evaluated efficacy of the unique class of blended SF hydrogel as a template for skin regeneration through extensive study under *in vivo* conditions. We first investigated the gelation kinetics and examined physical properties of SF hydrogel in order to assess their utility in the context of soft tissue engineering applications. Next, we studied biocompatibility of the hydrogel under *in vitro* conditions followed by its application on third degree burn wounds *in vivo*. Healing events during the wound repair by SF hydrogel were thoroughly evaluated by comparing to those with collagen (Col) gel. The comparable results with Col gel thus demonstrate efficacy of the *in situ* forming SF hydrogel for treating burn wounds.

6.2. Materials and Methods

6.2.1. Isolation and preparation of silk aqueous solutions

SF from *A. assama* (AaSF) and *B. mori* (BmSF) were isolated from *A. assama* silk glands and *B. mori* cocoons respectively following the standard protocols [215, 227]. Briefly, 5th instar larva of *A. assama* were dissected to obtain silk glands, from which silk protein was extruded out by squeezing using forceps. The silk protein was washed with distilled water, subsequently dissolved in 1 % (w/v) sodium dodecyl sulphate (SDS) (Himedia, India) aqueous solution and dialyzed against water for 4 h at 4 °C. To obtain BmSF, *B. mori* cocoons were cut into small pieces, washed and degummed using 0.02 M sodium carbonate (Merck, India). The dried degummed fibres were subsequently dissolved in 9.3 M LiBr at 60 °C for 4 h. An aqueous solution of BmSF was obtained after dialyzing the dissolved solution against water using a 12 kDa cellulose dialysis membrane (Sigma Aldrich, USA) for 3 days at room temperature (RT). BmSF was sterilized by autoclaving method; whereas sterilization of AaSF was performed under UV irradiation for 40 min. Isolation procedure of SF from both the silk varieties was completely aqueous and further fabrication steps also involved all-aqueous procedures bringing green synthesis of the hydrogel.

6.2.2. Fabrication of silk and collagen hydrogels

Both AaSF (3 % w/v) and BmSF (3 % w/v) aqueous solutions were mixed in equal volume to fabricate SF hydrogel. The blend solution was incubated at 37 °C for 30 min for self-gelation. Collagen type I isolated from rat tail (ThermoFisher Scientific, USA) was used for the fabrication of collagen gel according to manufacturer's protocol. Briefly, desired concentration of collagen precursor solution was taken and neutralized to pH 7 using 1 N sodium hydroxide (NaOH). The solution was added with 1/10th part of 10 X phosphate buffer saline (PBS) and the total volume was adjusted by adding sterile water to form hydrogel lattice of 2 mg/mL concentration. The whole process was performed on ice and the final solution was incubated at 37 °C for gelation.

6.2.3. Characterization of silk hydrogel

SF hydrogel thus prepared by blending BmSF and AaSF solutions were photographed in different shapes to examine their ability to take shapes of specific moulds. Injectable property of the hydrogel was confirmed by pushing the blend solution in its pre-gelation

phase through a 5 mL syringe. Internal morphology of the hydrogel was observed using field-emission scanning electron microscope (FESEM; Sigma 300, Zeiss). For preparing samples for FESEM analysis, the hydrogel was freeze dried and placed on a stub covered with carbon tape. The samples were sputter coated with gold for 130 s, and characterized at an accelerating voltage of 2−4 kV.

Crystallinity induced by self-assembly in the SF hydrogel was analysed by wide angle X ray diffraction (WAXD) and FTIR. Pristine AaSF (3 % w/v), pristine BmSF (3 % w/v) and blend of AaSF and BmSF (3: 3 w/w) solutions were air dried at 37 °C for analysis. X ray diffraction (XRD; GE Inspection Technologies, 3003 TT) under Cu Ka radiation was used with a scanning rate of 1° min^{-1} in thin film mode. All scans were extended from 5° to 50° in 2θ and were smoothened by taking average of 5 points using the Origin 8.5 software. The secondary structures of silk proteins were examined using FTIR spectrophotometer (PerkinElmer BX) in attenuated total reflection (ATR) mode. For each measurement, 32 scans were taken with the resolution of 4 cm^{-1}, and the wavenumbers ranged from 400 to 4000 cm^{-1}.

6.2.4. Water content analysis and hydration properties of silk hydrogels

Water content analysis or swelling properties were studied by measuring the amount of absorbed water. The hydrogel made by blending SF solutions (AaSF:BmSF; 3:3 w/w) were freeze dried using a lyophilizer (Alpha 1-4 LD plus, Martin Christ Gefriertrocknungsanlagen) prior to the experiment. Swelling behaviour of dried hydrogels was monitored by immersing the dried hydrogels in PBS at 37 °C for 30 min. Col gel were taken under similar conditions for comparative study. Water content of hydrogels was calculated from the following equation:

$$\text{Water gain (\%)} = (M_t - M_0)/M_0 \times 100 \quad \text{(6.1.)}$$

Where M_t is the mass of swollen gel at time t, and M_0 is the mass of freeze-dried gel.

Following water absorption, the hydrogels were further studied for estimating its dehydration rate. Weight of the hydrogels immediately after gelation was measured and subsequently placed in an incubator at 37 °C. Their weights were measured at pre-defined time-points until found to be completely dry to determine water loss (%) using the same formula mentioned in equation 1.

6.2.5. Gelation time estimation

The gelation time (t_{gel}) of SF hydrogel was measured by turbidity measurement method. SF blend solution (AaSF:BmSF; 3:3 w/w) was taken into wells of 96 well plate and optical density (O.D.) was measured at 550 nm using multi-plate reader (Tecan ProM200) at a frequency of 5 min. The experiment was performed independently at 25 °C and 37 °C. The measurements were stopped once a constant reading was obtained and the initial saturation time point was considered as t_{gel}.

6.2.6. Rheological and mechanical properties

Rheological measurements were conducted on various solutions at different blending ratio to determine gelation time (t_{gel}) and moduli after gelation using (Modular Compact Rheometer, MCR 302, Anton-Paar). SF solutions analysed were: pristine AaSF (3 % w/v), pristine BmSF (3 % w/v), blend of 3 % AaSF + 3 % BmSF (AB33), blend of 3 % AaSF + 6 % BmSF (AB36), blend of 6 % AaSF + 3 % BmSF (AB63) and blend of 6 % AaSF and 6 % BmSF (AB66). The hydrogels were named as AB63, AB33, AB36 and AB66, corresponding to the ratio of AaSF to BmSF protein mixtures. The respective SF solution (750 µL) was loaded under the specific geometry of rheometer and rheological measurements were performed using two different methods. (1) A time sweep test to evaluate gelation time and storage modulus post-gelation. This experiment was conducted independently at both 25 °C and 37 °C to examine temperature dependent gelation kinetics. The storage modulus (G′) and loss modulus (G″) were calculated with respect to time during the gelation process.

Hydrogels of concentration higher than 3 % SF were found to be stiff and hence not suitable for application in wound healing. Therefore, 3 % SF blend from equal volume of AaSF and BmSF (AB33) was selected as optimum and termed as SF hydrogel in the subsequent studies. (2) Strain amplitude sweep and frequency sweep tests were carried on the pre-formed gel of AB33 at 37 °C to obtain the critical strain and visco-elastic behaviour. The SF hydrogel (3 % blend) was placed between parallel plates and strain amplitude sweep test was performed with constant frequency of 10 rad/s. Amplitude oscillatory strains were switched from small strain (γ = 1.0 %) to subsequent large strain (γ = 100 %) with 100 s for every strain interval. Frequency sweep test was performed with 1 % constant strain and a constant frequency of 10 rad/s.

Compression tests were performed by a uniaxial compression test method using a universal testing machine (Instron 5944, USA), fitted with 100 N load cell and Bluehill version 3.66 software. SF hydrogels were made into cylinder shape with diameter of 10 mm and height of 10 mm. Compressive modulus (CM) and ultimate compressive strength (UCS) were calculated from the stress versus strain plots. Further, based on the strain measured under compression test, the hydrogels were subjected to cyclic compression testing to assess their recovery following multiple compression cycles. The hydrogels were given 15 preloading cycles at 10 % strain (half of the UTS obtained previously) in order to eliminate artefacts. All testing was conducted at a constant crosshead speed of 1 mm min^{-1}.

6.2.7. *In vivo* degradation study under subcutaneous pocket of mice

The experiment was conducted on Swiss (I.B.) mice each weighing 30-35 g after an acclimatization period of 7 days in animal house. The mice were anaesthetized by inhalant isoflurane along with 1-3 % oxygen with a precision vapourizer. The operative regions were wiped with 70 % ethanol prior to the operation. 1 mm incisions were made in the lateral side of the thoraco-lumbar region of each mice under treatment. Sterile SF hydrogel (200 µL) was injected subcutaneously and the incisions were closed using non-absorbable nylon suture stitches. Total 4 mice were taken, kept in separate cages and sacrificed after 4 weeks post cervical dislocation. The tissues containing the implanted SF hydrogel and surrounding native tissue were carefully peeled off and stored using 10 % NBF for histological examination. The implants fixed with 10 % NBF were washed using PBS, dehydrated through a series of graded ethanol, embedded in paraffin and sliced with a microtome (Leica, RM2235, Germany) to obtain sections of 5-7 µm thickness. Slides containing sections were then stained with haematoxylin and eosin (H & E) for general morphological observations.

6.2.8. *In vitro* degradation studies and integral stability of silk hydrogel

Integral stability and *in vitro* degradation of SF hydrogel fabricated by SF blend solution (AaSF: BmSF; 3:3 w/w) were analysed using 2 U/mL Protease XIV solution (from *S. griseus*, Sigma-Aldrich, USA). Briefly, SF and Col hydrogels (10 mm diameter, 20 mm height) were fabricated and their weights were measured prior to freeze drying. The hydrogels were then placed in 2 mL protease solution at 37 °C for a period of 2 weeks.

Every 3 days, protease solution was removed; hydrogels were washed twice with PBS and freeze dried to measure their weight prior to addition of fresh protease solution. Protease free PBS solution was taken as control to examine integral stability of the hydrogels. Degradation was calculated as the remaining mass compared to original mass following the formula:

Percent mass remaining = (mass at time t / initial mass) x 100 ……..… (6.2.)

6.2.9. Cell encapsulation study within hydrogels and cell morphology

Primary human dermal fibroblast (HDF, passage 4 – 5) (Himedia, India) and HaCaT (keratinocytes cell line procured from NCCS, India) were used in the cellular assays. The cells were expanded in T-75 flask using high glucose DMEM with 10 % FBS at 37 °C and 5 % CO_2. HDF at a cell density of 5×10^7 cells/mL were used for encapsulation study. Cells were mixed with solution of AaSF-BmSF blend (3 % w/w) in its pre-gelation state and in Col gel. Each well of 24 well plate contained 500 µL of the hydrogel forming solution containing cells and incubated at 37 °C and 5 % CO_2 for 30 min. Subsequently, 500 µL media was added to the hydrogels. Fresh media was replenished every alternate day. Proliferation of encapsulated cells was assessed by DNA quantification assay. Briefly, at each time point, cell laden hydrogels from each group were washed with PBS and homogenized in cell lysis buffer. DNA content was measured using PicoGreen assay (Molecular Probes) according to the manufacturer's instructions. Fluorometric measurement was performed by taking readings at an excitation wavelength of 480 nm and an emission wavelength of 528 nm using Tecan Infinite M200. DNA content was calculated by comparing the standard curve.

For morphological observation of cells on top of hydrogels, HDF were seeded at 10,000 cells/cm^2 density on top of the pre-formed hydrogels and cultured for day 3 and day 7 separately. The cells were fixed using 10 % neutral buffer formalin (NBF) (Sigma-Aldrich, USA) and stained with Rhodamine Phalloidin and Hoechst 33342 (Invitrogen, USA). Samples were permeabilized using 0.1 % Triton X-100 solution for 10 min and blocked with 1 % bovine serum albumin (BSA) for 30 min prior to staining. Images were taken using fluorescent microscope (EVOS FL).

6.2.10. Cell migration study on hydrogels using agarose drop migration assay

Thin coatings of SF and Col gels were fabricated in individual wells of 24 well plate by adding 150 µL of respective solutions in their pre-gelation state and incubated at 37 °C for 3 h. To perform agarose drop assay, a pre-warmed 0.5 % agarose drop (20 µL) containing 5,000 HaCaT cells was gently placed on the centre of SF and Col gels and the plate was placed at 4 °C for 15 min for agarose solidification. 300 µL of media was gently added afterwards and incubated at 37 °C cell incubator. The migration of cells from agarose gel towards SF or Col gels was observed after 24 h and 72 h of culture using phase contrast microscopy.

6.2.11. *In vivo* burn injury model and treatment

All animal experiments were performed in accordance with ‘‘Principles of laboratory animal care approval no. MC/916/2017/4” from the ‘Institutional Animal Ethics Committee (IAEC)’, Guwahati medical college and hospital, Guwahati, Assam, India (CPCSEA Registration No. 351, 3/1/2001). Female wistar albino rats of age 6-7 week old weighing 200-250 grams each were procured from animal house of National Institute of Nutrition, Hyderabad, India. Animals were acclimatized for 1 week at the animal house prior to experiment. A cocktail dose of Ketamine (80 mg/kg) and Xyalazine (12 mg/kg) (K-X cocktail) was used for anaesthesia *via* intraperitoneal (IP) route. To inflict size specific third degree burn injury without effecting surrounding and underneath organs, an instrument set-up was designed following an optimized protocol [356].

The instrument was built using a commercially available soldering iron. The head of the soldering iron was removed and replaced with one cylindrical aluminium head of 1 cm diameter (**Figure A6.1.**). A Type K temperature probe attached to a digital thermometer was used to detect the temperature. The set-up was further attached to a variable autotransformer, leading to a precise control of its temperature. The necessary temperature of 80 °C was set by the output on the autotransformer to 120 V as also described in chapter 5. To create burn wounds, head of the device was held at 90° angle to the skin for 15 sec. Significant thermal insult to the deep tissues was avoided by folding the skin of rats parallel to the platform. Three different batches for 3 time-points (day 7, 14 and 21) were taken and each batch contained three treatment groups (collagen, SF and untreated). Each group contained four animals (n = 4), hence 36 rats were used for the main study. Each animal was given 1 wound. Following clinical practices, the

injured tissue was debrided using a biopsy punch (1 cm diameter) after 48 h [48]. Following debridement, wounds were washed with sterile saline and different treatments were applied. SF gel in its pre-gelation phase (200 µL) was injected in the wounds, which formed hydrogel *in situ* after 10 min as shown in the schematic design.

For comparative study, pre-formed Col gel (diameter 1 cm and height 2 mm) was applied to the wounds. The wounds filled with SF or Col gels were subsequently covered with an occlusive and transparent Tegaderm dressing to enable hydrogel placement, protection from infection and prevention from drying. In the untreated group, also referred as control group, wounds were sealed with only Tegaderm soon after the excision of necrotic skin. Soft cotton gauze was applied to the whole trunk portion of rats of all groups using one top-layer of adhesive tape. Antibiotic Ceftriaxone 20 mg/Kg and analgesic Meloxicam 5 mg/Kg was administered *via* intra-muscular route on day 1, 3 and 5 to all the animals. Additional dressings (Tegaderm and sterile gauze) applied on top of the hydrogels were changed three times a week till 14 days. Further, due to low survival rate and high severity of wounds, the groups containing wounds without any dressing or intramuscular antibiotic dose were discontinued in the study. As a result, three groups were finally considered for the study: 1. wounds treated with SF gel covered with Tegaderm, 2. Wounds treated with Col gel covered with Tegaderm and 3. Untreated (Unt) wounds covered with Tegaderm (also denoted as control group). The animals of all the three groups were caged separately and monitored daily.

6.2.12. Wound healing estimation

Wound size was measured by analysing the images of wounds taken on pre-defined time points. Central diameter of the wounds was calculated using Image J software and accordingly wound area was measured following the formula:

$$\text{Wound area (\%)} = A_t/A \times 100 \quad \text{(6.3.)}$$

Where A_t was the area of wound at time (t) and A was the initial wound area.

Further, microscopic analysis was performed by staining paraffin embedded tissue sections (5-7 µm) prepared from skin biopsies. Haematoxylin and eosin staining (H & E) and Masson's Trichrome (MT) staining kit (Sigma-Aldrich, USA) was used according to the manufacturer's protocol for general histological observations.

6.2.13. Immunohistochemical assay

For immunohistochemical (IHC) assay, the sections (5-7 µm) were stained for antibodies against collagen type I (5 µg/mL), collagen type III (5 µg/mL), cytokeratin 10 (CK10; 1 µg/mL) and cytokeratin 14 (CK14; 1 µg/mL) purchased from Abcam, U.K. IHC kit (Vector Laboratories Inc., CA) was used according to manufacturer's protocol and 3,3'-diaminobenzidine (DAB) peroxidase substrate solution was used. Counterstaining was performed with haematoxylin for nuclei and images were taken using bright field microscope (Evos FL). For immunofluorescence assay, the tissue sections were blocked using horse serum and permeabilized using 1 % Triton X prior to applying primary antibody. Primary antibodies (rabbit anti-rat) were used at the following concentrations: van Willbrand factor (vWF, 10 µg/mL), CD68 (1 µg/mL) and Involucrin (INV, 4 µg/mL) procured from Abcam, UK. Secondary antibody used was goat anti-rat IgG (Sigma-Aldrich, USA) conjugated with Phycoerythrin/FITC. Counter staining was performed using Hoechst 33342 (Invitrogen, USA) and images were taken using the fluorescent microscope. For vessel density analysis, 3 different sections stained with anti-vWF were imaged and at least 5 different locations per slide were considered for quantification in the whole wound area. Histological images (H & E and IHC of collagen type I and collagen type III) were taken and three separate images were merged to visualize full length sections.

6.2.14. Gene expression study

Skin biopsies taken on day 7, 14 and 21 were preserved in −20 °C using RNA later (Sigma-Aldrich, USA) and mRNA was isolated after homogenizing the tissue in TRIzol reagent (Sigma-Aldrich, USA). Complementary DNA (cDNA) was subsequently synthesized using reverse transcription kit (Applied Biosystems, USA) and PCR equipment (Takara, Japan according to the manufacturer's instructions. The expression of collagen type I, collagen type III, Tumour Necrosis Factor-α (TNF–α), CD68, CD163 and glyceraldehyde-3-phosphate-dehydrogenase (GAPDH) mRNA transcripts was analysed by Real-time PCR reactions using SYBR Green PCR Mastermix on a 7500 Fast Real-Time System (Applied Biosystems, USA). **Table 6.1.** lists the sequences of rat primer used in the reaction. The average threshold cycle (Ct) values for a gene of interest (GOI) were normalized against the average Ct values for GAPDH gene. Fold change of GOI transcript levels between SF or Col group was compared with untreated wounds

(control) following the formula: fold change = $2^{-\Delta\Delta Ct}$, where $\Delta\Delta Ct = \Delta Ct_{(sample)} - \Delta Ct_{(control)}$ and $\Delta Ct = Ct_{(GOI)} - Ct_{(GAPDH)}$.

Table 6.1. *Primer sequences used for the gene expression study.*

Target gene	Forward primer	Reverse primer
Rat GAPDH	5'-TGACTCTACCCACGGCAAGTTCAA-3’	5'-ACGACATACTCAGCACCAGCATCA-3'
Rat Col-I	5'-GCGAAGGCAACAGTCGATTC-3’	5'-ACTGTCTTGCCCCAAGTTCC-3'
Rat Col-III	5'-TGATGGGATCCAATGAGGGAGA-3’	5'-GAGTCTCATGGCCTTGCGTGTTT-3'
Rat TNF-α	5'-AACACACGAGACGCT-3’	5'-TCCAGTGAGTTCCGAAAGCC-3'
Rat CD68	5’-CGCATCTTGTACCTGACCCA-3’	5’-TGAGAGAGCCAAGTGGGGAT-3’
Rat CD163	5'-ACCCACTGAGGTTGGCATTT-3’	5'-TGTAGCTGTGGTCATCCGTG-3'

6.2.15. Statistical analysis

All the experiments were carried out for n = 4 samples unless otherwise specified. Data analysis was done using statistical software OriginPro 8 (Origin lab Corporation, USA). The significance level was measured by comparing the data between groups and within groups by performing one-way analysis of variance (ANOVA) followed by Tukey’s test. Significance levels were set at * $p \leq 0.05$ and ** $p \leq 0.01$. Histological examination was performed by capturing at least 5 fields per section and images were analysed using Image J software. Unless otherwise indicated, all graphical data are reported as mean ± standard deviation.

6.3. Results

6.3.1. Silk hydrogel fabrication and characterization

In situ forming SF hydrogel was readily fabricated by blending two different silk proteins owing to their inherent self-assembly property (**Figure 6.1.A**). The intrinsic cross-linking between *A. assama* SF (AaSF, 3 % w/v) and *B. mori* SF (BmSF, 3 % w/v) proteins led to irreversible gelation. Rapid gelation was observed with steady decrease in transparency and increase in matrix stiffness. The SF blend solution was visually transparent with flowing properties at room temperature, which was transformed into an opaque gel after 15 - 20 min when incubated at 37 °C (**Figure 6.1.B and Table 6.2.**). The blend solution could be used as an injectable gel as shown in the representative image (**Figure 6.1.C**). The pre-formed hydrogel lattice also appeared as stable matrix, which could be easily handled using a forcep (**Figure 6.1.D**). The ultrastructure of freeze-dried hydrogel matrix revealed porous architecture of the construct as observed under FESEM image (**Figure 6.2.A**). The average pore size of the hydrogel matrix was 155 ± 60 µm, which was suitable for tissue engineering applications. Microporous hydrogel matrices with similar range of this pore size have been found to be beneficial for cellular growth, vascularization and wound healing applications as also observed in similar studies.

Post-gelation crosslinking between AaSF and BmSF in the blend solution was confirmed by WAXD (**Figure 6.2.B**). The peaks shown of BmSF, AaSF and blend matrices were found to be distinct. Sharp peaks at $2\theta = 12°$ and 21° were observed for AaSF; whereas a single broad peak around 20° was observed for BmSF, depicting amorphous nature of silk fibroin proteins. In contrast, the SF hydrogel matrix made by blending AaSF and BmSF demonstrated sharp peak at 20° with higher intensity. This suggested more crystallization as a result of physical crosslinking in the blend between two silk varieties compared to individual silk proteins.

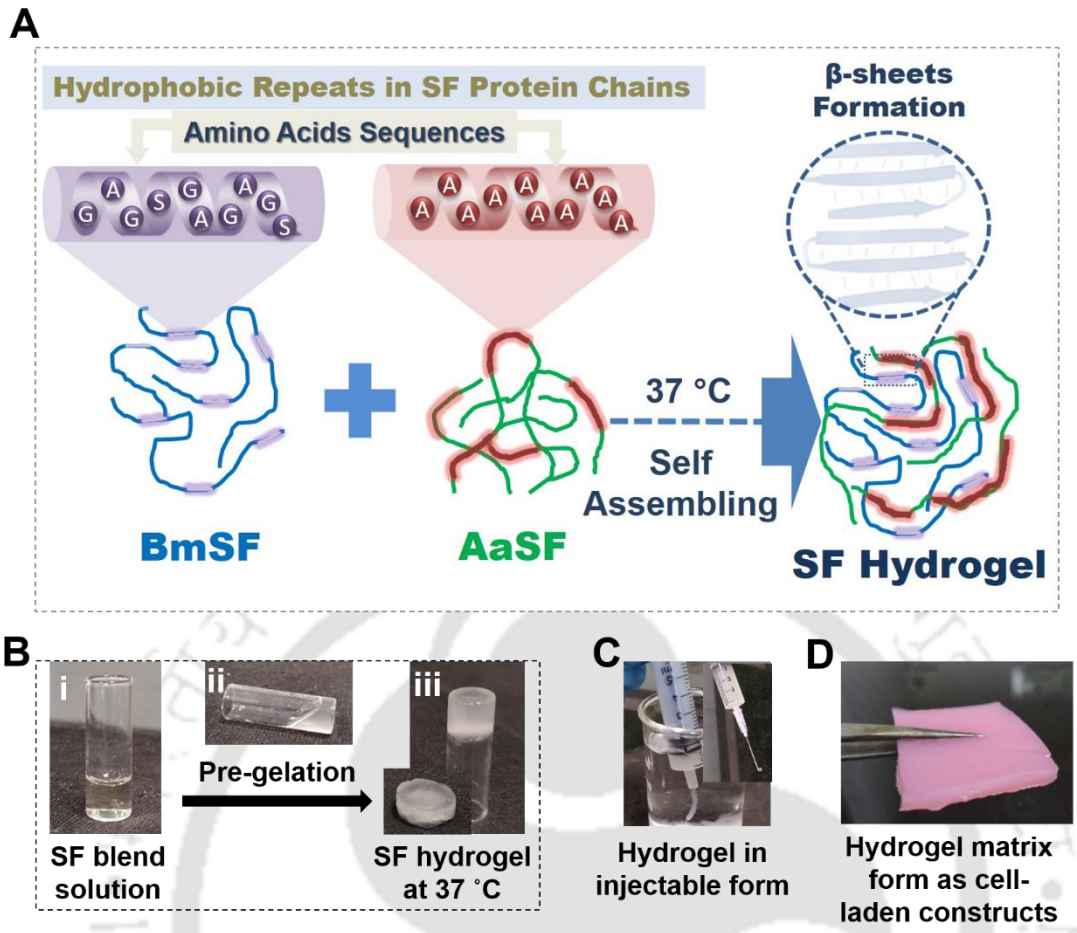

Figure 6.1. *(A) Schematic representation shows development of in situ forming SF blend hydrogel at 37 °C for wound healing applications. (B) Representative images of SF blend solution (i) soon after blending AaSF and BmSF proteins, (ii) during pre-gelation state and (iii) post gelation. (C, D) Images of SF hydrogel depicting its application in the form of an injectable gel and pre-formed matrix respectively.*

The observation was further validated using FTIR (**Figure 6.2.C**). BmSF and AaSF in pristine conditions demonstrated sharp characteristic peaks of amide I, amide II and amide III at 1645, 1516 and 1230 cm^{-1} respectively. All three characteristic peaks of the silk fibroin protein were also shown at high intensity in the blend matrix. It is to be observed that the peak at 1627 cm^{-1} associated with the C=O stretching vibrations was sharp in case of blend matrix. This region corresponded to the β-sheet conformational backbone (amide I) and thus attested presence of β-sheet structures formed due to self-assembling between silk molecules in the blend [371, 372]. Further, the spectral area from 3000 to 3600 cm^{-1} depicted a broad peak in case of blend hydrogel matrix, demonstrating higher O–H stretching in the blend [276]. The broader peak of O-H stretch shown in the blend matrix compared to pristine BmSF and AaSF confirmed highly crosslinked molecules in SF hydrogel due to hydrogen bonding.

Table 6.2. *Gelation time of various SF solutions in pristine and blended forms at various concentrations and temperatures.*

Sample	Concentration	Gelation time (t_{gel})
BmSF (pristine silk)	BmSF concentration: 6 %	~ 14 days at 37˚C [219]
		~ 40 days at RT [219]
BmSF (pristine silk)	BmSF concentration: 3 %	15-20 days at 37˚C (This study)
		25-30 days at RT (This study)
AaSF (pristine silk)	AaSF concentration: 3 %	2-3 h at 37˚C (This study)
		5-6 h at RT (This study)
SF blend	BmSF:AaSF = 3: 3	480 s at 37˚C (This study)
	Total SF concentration: 3 % (w/w)	2350 s at RT (This study)

Water content analysis further validated the hydrogel characteristics of SF blend matrix (**Figure 6.2.D**). Hydrogels are defined as the crosslinked hydrophilic polymers with a high intrinsic content of water [221]. Presence of hydrophobic β-sheet structures (in this case SF) further provides long term stable hydrogel networks [221]. Stable hydrogel matrix of SF blend might be attributed to the synergistic effects of hydrophobic interaction and hydrogen bonding between AaSF and BmSF proteins. The freeze-dried hydrogels absorbed high water content and showed 200 % swelling capacity when placed in PBS solution. To elucidate the stability of hydrogel networks due to formation of β-sheet structures in SF gel, water loss was measured with respect to time. For comparative study, Col gel was taken, which showed significantly faster dehydration rate. On incubating under non-humidified chamber at 37 °C, SF hydrogel showed 75 % water retention in comparison to only 20 % in Col gel after 12 h. After 36 h of study, SF hydrogel contained 40 % water, significantly higher than that of Col gel, $p \leq 0.01$. This also attested the presence of hydrogel networks in SF gel, leading to higher water holding capacity.

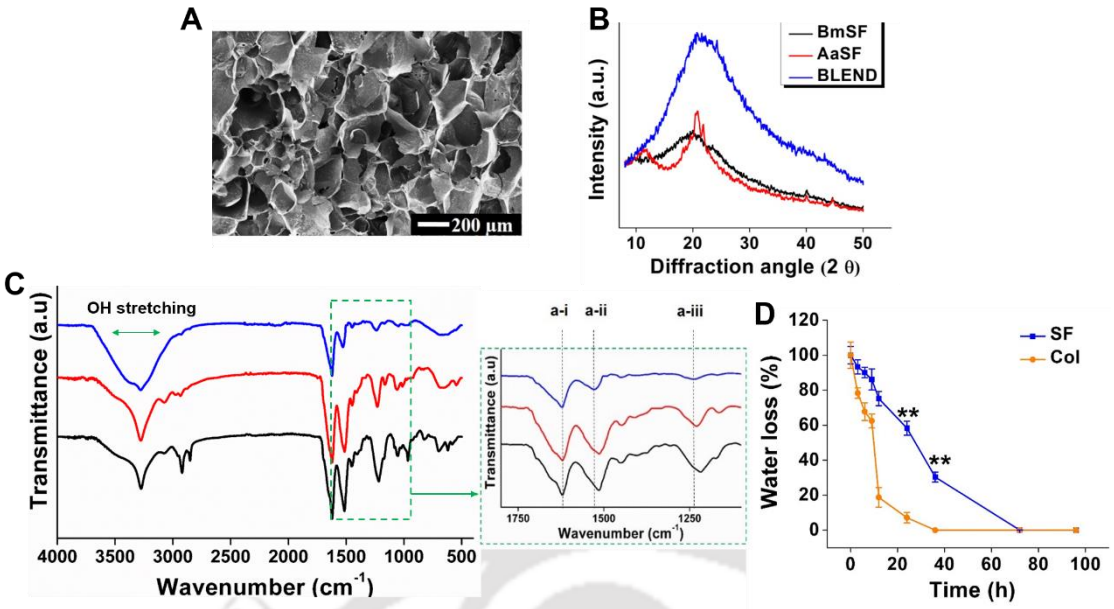

Figure 6.2. *(A) FESEM image representing porous architecture of SF hydrogel matrix. (B, C) XRD and FTIR-ATR spectra of pristine AaSF, pristine BmSF and the blend SF matrices respectively, suggesting conformational changes in the blend SF matrix. (D) Dehydration study of SF hydrogel in comparison to Col gel demonstrating water loss with respect to time.*

6.3.2. Gelation properties

The dynamics of gelation mechanism in the SF blend was determined by calculating the change in absorbance value at 550 nm with time on comparing with pristine individual silk solutions (**Figure 6.3.A**). In contrast to the constant O.D. value of individual silk proteins (BmSF or AaSF), the blend solution showed varied optical density in an increasing order. Saturation at a constant high value demonstrated completion of crosslinking and hence depicted hydrogel fabrication. The study also showed temperature dependent gelation process. At 37 °C, the gelation time was 20 min; whereas, it was as found to be 45 min at 25 °C, demonstrating faster crosslinking at 37 °C. Moreover, the pre-gelation time period of SF blend (8-20 min at 37 °C and 25-40 min at 25 °C; highlighted in the box) was sufficient, indicating its application in the injectable systems.

In order to further investigate the gelation behaviour of SF blend, rheological study was performed on the blends of BmSF and AaSF (**Figure 6.3.B**). Blend of BmSF and AaSF at 1:1 ratio with 3 % (w/v) concentration readily formed hydrogel at 37 °C after 8 minutes (480 s) suggesting t_{gel} = 8 min. In contrast, there was no change in the modulus and viscosity of the same blend solution at 25 °C even after 20 min; the gel was

formed after 40 min (**Figure 6.4.A**). This validated the temperature dependent gelation kinetics of silk molecules as also observed by measuring O.D. with time. Further, pristine AaSF and pristine BmSF did not show change in the moduli with respect to time, suggesting no gelation in the pristine silk solutions (**Figure 6.4.B**). The storage modulus (G′) increased dramatically in the SF blend solution and eventually exceeded the loss modulus (G″) value after 8 min when run at 37 °C, displaying characteristic transition from a liquid-like state to an elastic gel-like state. Storage modulus (336.42 Pa) was found to be significantly higher than loss modulus (11.269 Pa) post gelation. Further, strain sweeps acquired in the pre-formed 3 % SF gel maintained their stability till 10 % shear strain application. The stability started failing at 50 % shear strain (**Figure 6.3.C,D**). Constant modulus at frequency from 0.1 to 10 rad/s validated linear visco-elastic nature in the range of 0 to 10 % shear strain. This demonstrated visco-elastic behaviour of the gel with potential of withstanding significant shear strain.

Furthermore, time sweep study between various concentrations of silk proteins showed that gelation time was dependent on the concentration of individual silks (**Figure 6.5.A**). Blends with higher silk concentration demonstrated shorter gelation time compared to 3 % SF blend. Blended hydrogel containing higher concentration of either protein (AB63 and AB36) showed a gelation time of 280 s and 350 s respectively. This showed quicker hydrogel formation due increased concentration of overall SF blend. The hydrogels made up 6 % BmSF and 6 % AaSF (AB66) further revealed interesting results (**Figure 6.4.C and 6.5.B**). This combination instantly formed a gel and thus the storage modulus was found to be higher than the loss modulus throughout the complete time sweep. Similar behaviour was observed in the case of Col gel, which immediately formed gel and demonstrated higher storage modulus than loss modulus from the initial point. However, storage modulus of Col was low, which was constant throughout the time. In addition, silk hydrogel (AB66) made up of 6 % concentration showed time dependent increment in both storage and loss modulus suggesting shear stress induced hydrogel stiffness. On comparing the storage modulus at the end time point, SF hydrogel (3 %; used throughout the study) showed significantly higher storage modulus (336.42 Pa) than Col gel (~ 28 Pa), $p \leq 0.01$ (**Figure 6.5.B**). The SF hydrogel made by blending 3 % BmSF and 3 % AaSF in equal volume was therefore selected in the present study owing to their suitable physical properties in soft tissue engineering applications.

Compression tests on SF hydrogel (3 % gel selected from the rheological study) showed a compressive strength of 2960 ± 75 Pa and strain of 20 % before eventuating break down (**Figure 6.5.C**). Compressive modulus of SF hydrogel was found to be 7367 Pa, suggesting compression properties of soft hydrogels. The cyclic compression of SF hydrogel observed at 10 % strain also showed complete recovery of the gel after multiple cycles of compression (**Figure 6.5.D**). The study showed no change in the compressive stress from cycle 1 to 15 of loading and unloading. The hydrogel also showed reversible deformation within 15 cycles, indicating high stability sustainable for a prolonged period along with flexibility. Such robust physical properties of the hydrogel could also be comprehended from the ease of manually handling the same with forceps with minimal breakage.

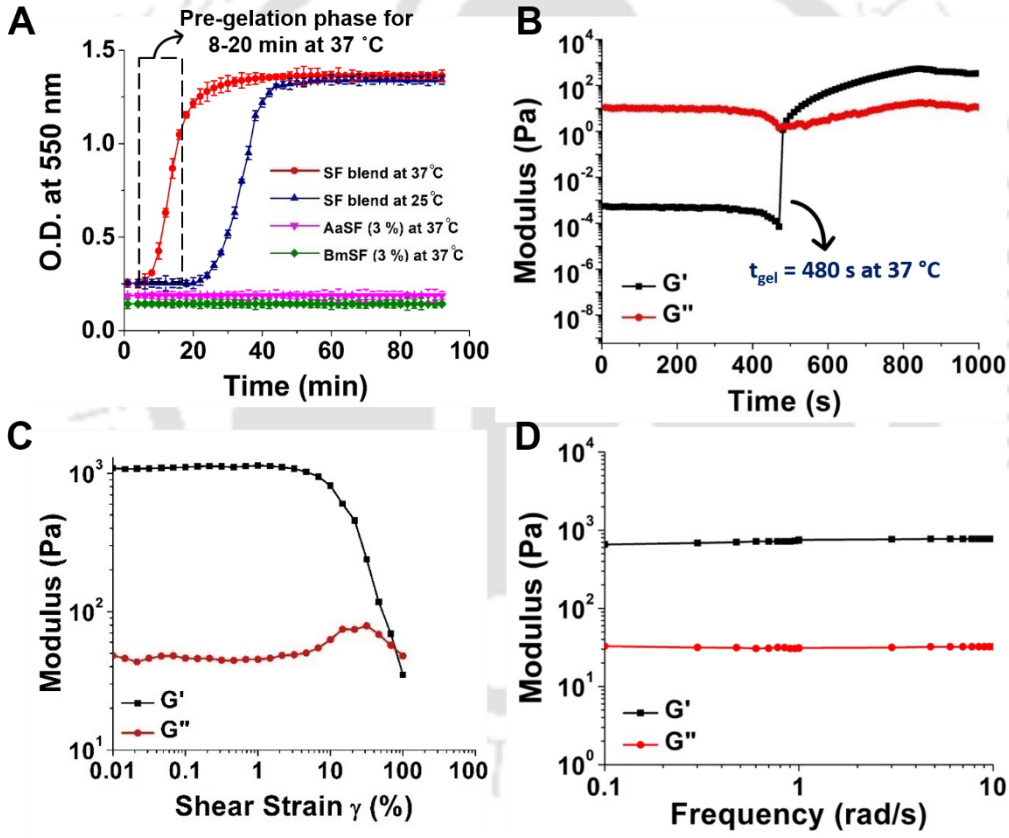

Figure 6.3. *(A) Gelation characterization of the SF blend hydrogel as determined by optical density measurement at 25 °C and 37 °C; pristine AaSF and BmSF solutions showed constant O.D. in contrast to varied O.D. exhibited by the blend SF solution. (B) Rheology property of the SF blend solution (AaSF + BmSF = 3 % w/v blend) displaying storage modulus (G') and loss modulus (G") in time sweep test: Gel behaviour of SF blend was demonstrated by the change in moduli at gelation time* t_{gel} *= 480 s at 37 °C. (C) Frequency sweep measurement and (D) Strain sweep of the pre-formed 3 % SF hydrogel showing linear viscoelasticity of the matrix up to 10 % strain.*

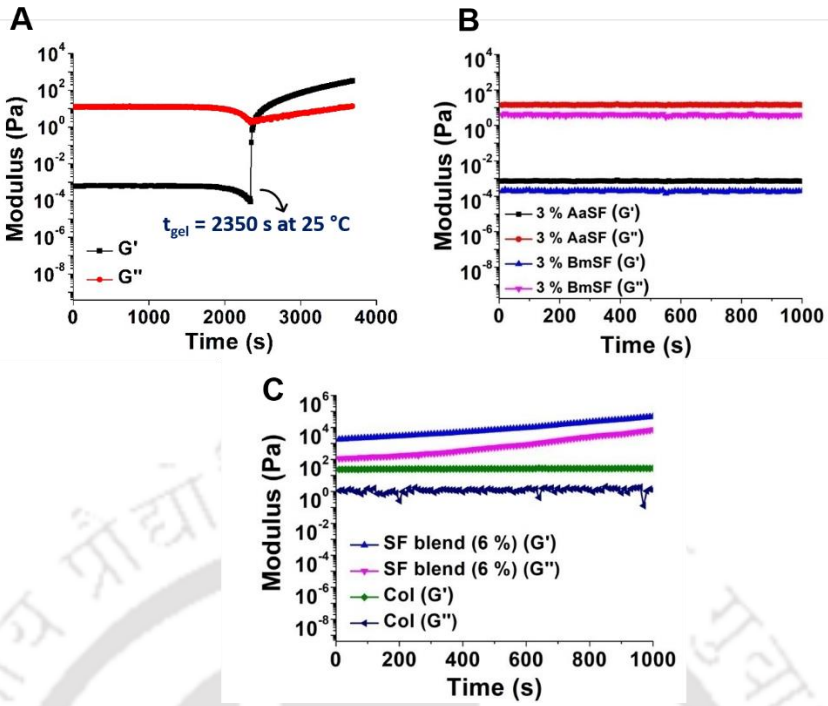

Figure 6.4. *(A) Rheology behaviour of the SF blend solution (AaSF + BmSF; 3 % w/v blend) displaying storage modulus (G') and loss modulus (G'') in time sweep test demonstrating change in moduli at the gelation time. (B) Pristine AaSF and BmSF solutions demonstrated constant moduli at 37 °C, suggesting no gelation in their pure form. (C) Time sweep test of 6 % SF blend displaying higher storage modulus than loss modulus indicated instant gelation similar to collagen (Col) gel.*

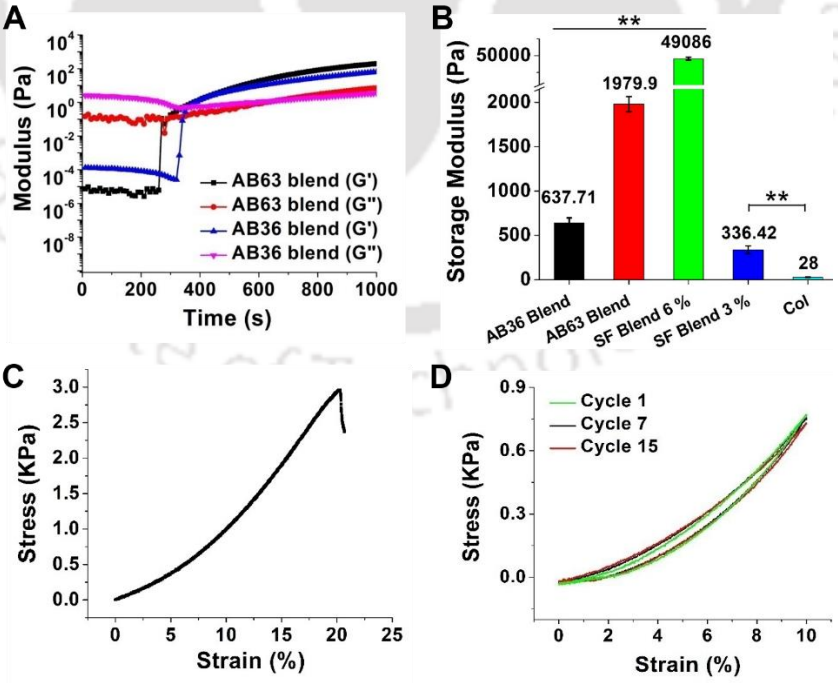

Figure 6.5. *(A) Time sweep test on varying the concentration of AaSF and BmSF in SF blend depicts concentration dependent gelation time. (B) Storage modulus of SF hydrogels at various SF concentrations in comparison to Col gel. (C) Compression test*

depicting stress - strain curve of pre-formed SF hydrogel depicting compressive modulus of SF hydrogel (D) Cyclic compression test on the SF hydrogel showing matrix stability examined for 15 cycles.

6.3.3. Biodegradability and biocompatibility of the silk hydrogel

Biodegradability of SF hydrogel was examined under both *in vivo* and *in vitro* conditions. Histological analysis by H & E staining of subcutaneously implanted SF hydrogel revealed degradation of the injected hydrogel as examined after 4 weeks of implantation (**Figure 6.6.**). Moreover, the experiment not only demonstrated *in vivo* biodegradability, but also showed *in vivo* biocompatibility as depicted by intersection area of SF and host tissue. The H & E analysis suggested infiltration of host cells in the SF hydrogel along with void area, suggesting possible biodegradation occurred within 4 weeks of time period, which also allowed cell recruitment. Biodegradation profile of SF hydrogel was further determined under *in vitro* conditions based on the measurable differences in their weights over a period of 2 weeks (**Figure 6.7.A**). In the protease free solution, SF hydrogel showed 97 % and 85 % mass remaining after 7 and 14 days respectively. In contrast, Col gel retained 75 to 65 % mass after 7 to 14 days, indicating significantly lower integral stability compared to SF hydrogel, $p \leq 0.01$. In the presence of protease, Col gel showed only 25 % mass retention on day 7 and degraded completely after 10 days; whereas SF showed 70 - 50 % mass retention from day 7 to day 10. Thus, the biodegradation studies indicated slow degradation rate of SF hydrogel in comparison to Col gel.

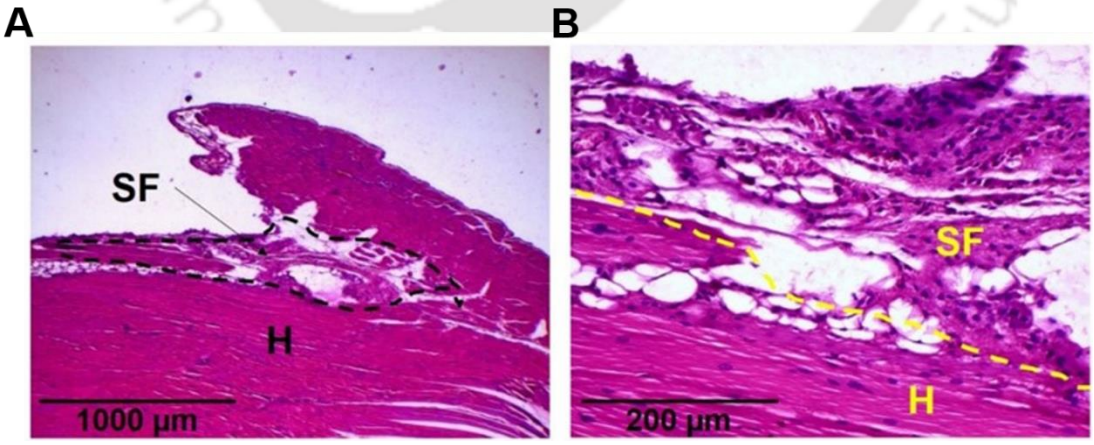

Figure 6.6. *(A) Histological analysis by H & E staining of subcutaneously implanted SF hydrogel examined after 4 weeks of implantation, showing in vivo biodegradability under the subcutaneous pocket of mice. (B) Magnified image depicts intersection area of SF and host tissue, suggesting infiltration of host cells in the SF hydrogel and void area.*

'SF' represents silk fibroin hydrogel present in the subcutaneous pocket of mice and 'H' represents host tissue.

Next, we examined biocompatibility of SF hydrogel using human dermal fibroblasts (HDF) under *in vitro* conditions (**Figure 6.7.B**). In order to prove its possible application as an *in situ* injectable gel system, cells were encapsulated in pre-gel solution of SF blend and subsequently incubated at 37 °C for gelation. The hydrogels encapsulated with HDF were examined for total DNA content after 1, 3, 7 and 14 days and revealed an increase in cellular population with time. Col gel used as a positive control showed significantly higher DNA content on day 3 and day 7 in comparison to SF, $p \leq 0.01$. However, on day 14, SF hydrogel demonstrated higher DNA content in comparison to Col gel. Interestingly, the Col gel encapsulating HDF showed significant size reduction, depicting gel contraction behaviour within 7 days (**Figure 6.7.C**). On the other hand, SF gel did not show gel contraction and remained intact throughout the culture conditions.

Higher cell proliferation in SF on day 14 in comparison with Col might be attributed to the reduced cell proliferation in contracted Col gels. Cell proliferation inside SF hydrogel was further validated by microscopy, which demonstrated cells encapsulated in the hydrogel (**Figure 6.8.**). HDF tagged with cytotracker molecules were encapsulated in SF gel; higher cell density on day 3 compared to day 1 attested cell proliferation. Higher cell proliferation inside SF matrix as evidenced here further demonstrated its application in cell delivery system. In addition, HDF seeded on top surface of the hydrogels were stained for morphological observations (**Figure 6.7.D**). The cells showed extended and spread out morphology as observed on day 3 and 7 suggesting comparable biocompatibility of SF gel with Col gel. To examine migration of keratinocytes on SF hydrogel, we performed gel drop migration assay using HaCaT cells encapsulated in agarose gel (**Figure 6.7.E**). On day 1, the cells resided within the agarose gel placed on top of SF or Col gels. However, on day 3 of culture, the cells migrated from agarose gel towards SF and Col coatings, depicting comparable cell recruitment and cell migration capability of both the materials.

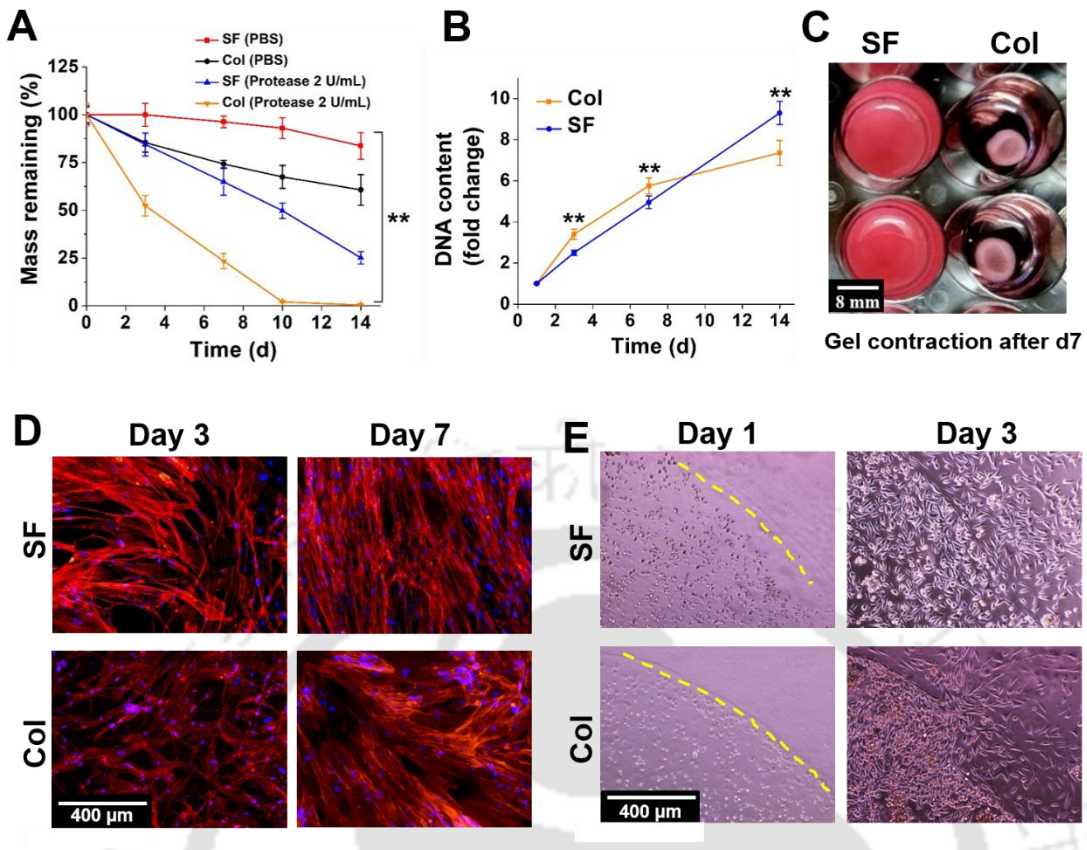

Figure 6.7. *(A) In vitro degradation behaviour of SF and Col hydrogels in both proteolytic and non-proteolytic solutions for 14 days. (B) Proliferation rate of HDF cells encapsulated in SF and Col hydrogels as determined by dsDNA content quantification assay. (C) Image of HDF encapsulated hydrogels showing contraction of Col gels after 14 days of culture. (D) Morphology of HDF cultured on top of the hydrogels stained with Rhodamine Phalloidin and Hoechst 33342. (E) Migration of HaCaT cells from agarose gels towards SF or Col gels as determined by the gel drop migration assay for 3 days. Scale bar represents 400 µm.*

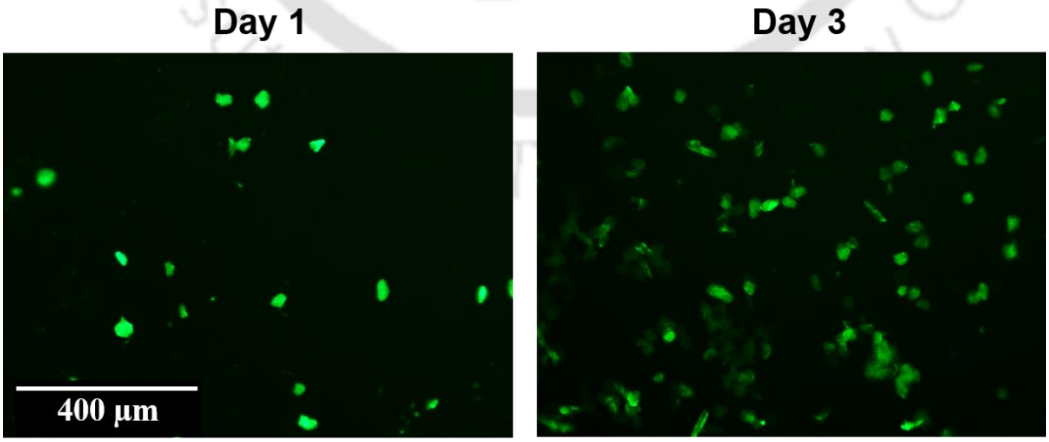

Figure 6.8. *HDF cells tagged with cytotracker-FITC encapsulated in the SF hydrogel on day 1 and 3, suggesting proliferation of cells when encapsulated in the hydrogel.*

6.3.4. *In vivo* wound healing assessment using third degree burn model

Efficacy of *in situ* forming SF hydrogel was analysed on debrided third-degree wounds by injecting the SF blend solution at its pre-gel stage. It also facilitated *in situ* crosslinking with the wound edges of native tissue. SF blend solution once injected at the wound defect formed gel after 10 min and firmly attached to the native tissue as observed by the histological analysis of injected hydrogel at the wound site after 3 days of application (**Figure A6.2.**). A clear demarcation between wound edge and SF hydrogel was visible, suggesting possible crosslinking between the native tissue and the hydrogel at the time of *in situ* gelation stage. In contrast, when a pre-formed SF hydrogel was applied at the wound defect, it failed to attach to the native tissue and remained separated to the wound edges.

Application of SF blend solution in its injectable form also prevented an additional requirement of glues or sutures. Among the three groups: SF, Col and control (Unt; untreated wounds sealed with Tegaderm dressing), healing of untreated wounds was significantly delayed. The gross examination of wound images revealed comparable wound closure by SF and Col treatments (**Figure 6.9.A**). By day 7, Col hydrogels appeared to be well integrated within the wound bed and SF hydrogels were observed to be superficial to the native tissue, acting as a provisional matrix. SF hydrogels remained firmly attached to the underneath native tissue till day 14. After day 14, dry thin layer of wound eschar along with portion of remaining hydrogel detached from the wound site by itself. Underneath the dried mass, neo-epidermis was regenerated and complete wound closure was observed.

The results were further validated by histological observations through MT staining (**Figure 6.9.B**). By day 7, thick granulation tissue was developed in SF and Col treated wounds, but untreated group did not show granulation tissue development. By day 14, the difference was found to be more prominent because SF and Col treated wounds showed substantial re-epithelialized wounds. In contrast, untreated group showed areas of necrotic tissues and delayed granulation tissue formation on day 14. Mature collagen bundles were not developed on day 7 and day 14 in SF and Col treated wounds as demonstrated by the lack of blue stain in the central region. However, on day 21, SF treated wounds represented mature collagen bundles evenly distributed in the dermis area throughout the section as compared to control wounds. Thus, SF hydrogel

demonstrated similar rate of wound healing progression with Col gel. Correspondingly, only 40 % wound area remained open in SF hydrogel treated wounds compared to 80 % area of untreated wounds on day 14, $p \leq 0.01$ (**Figure 6.9.C**). This revealed 2-fold accelerated healing rate of SF hydrogel in comparison to untreated wounds. No significant difference was observed between SF and Col on comparing the wound area. On examining gross wound closure on day 21, we observed that SF and Col hydrogel-treated wounds were completely closed, whereas almost 30 % of the wound area remained open in the untreated wounds. Sequential healing process from day 7 to day 21 was also validated by H & E stained sections (**Figure 6.10.**).

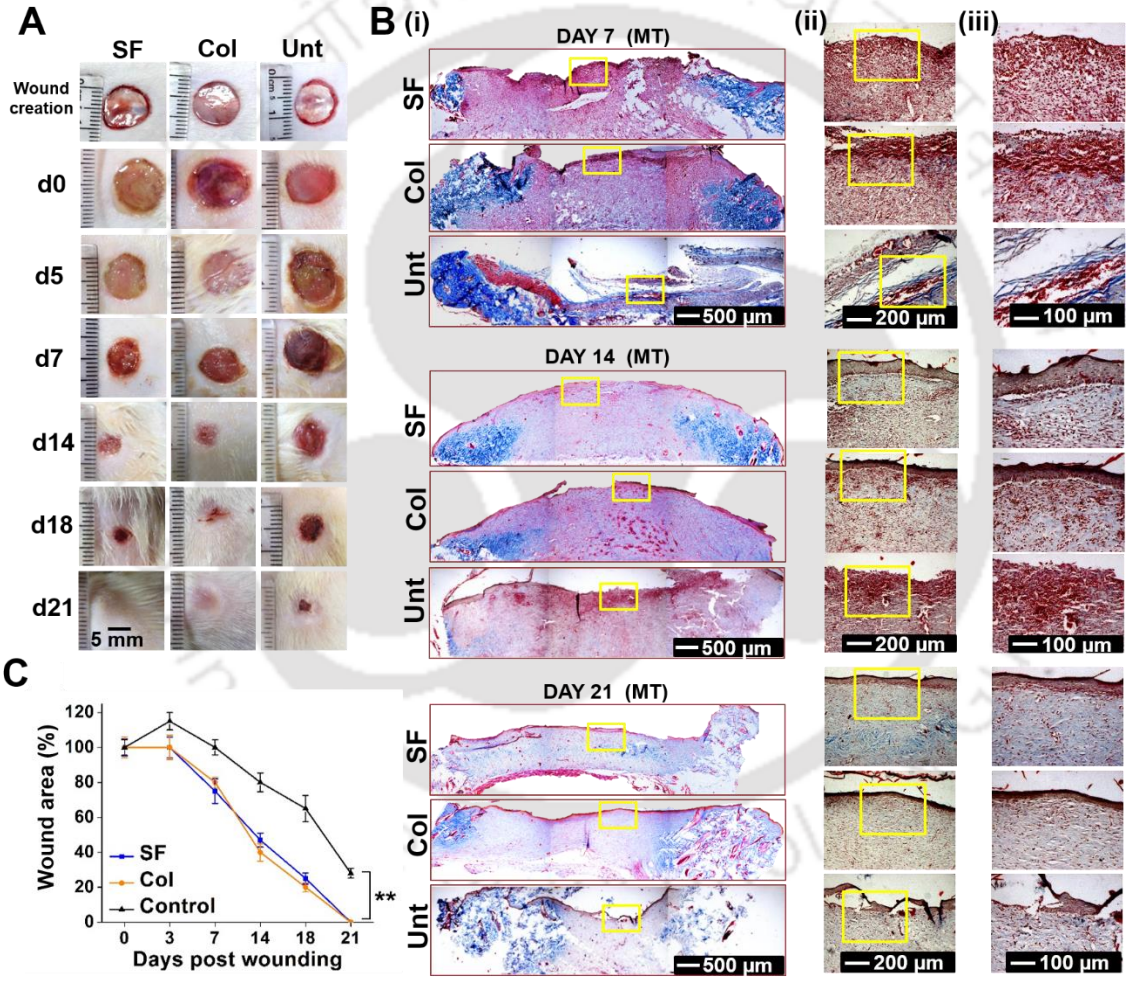

Figure 6.9. *Wound healing profile of SF and Col hydrogels representing: (A) Gross images of wounds implanted with respective hydrogel on excised 3rd degree burn wounds, showing extent of wound healing with respect to time. (B) Histology analysis of healed skin biopsies on day 7, 14 and 21 by MT stain: (i) Section of full wound biopsy observed at 4X magnification, (ii and iii) images at 10X and 20X magnification respectively (highlighted in yellow box). (C) Percentage of wound area as determined by Image J software.*

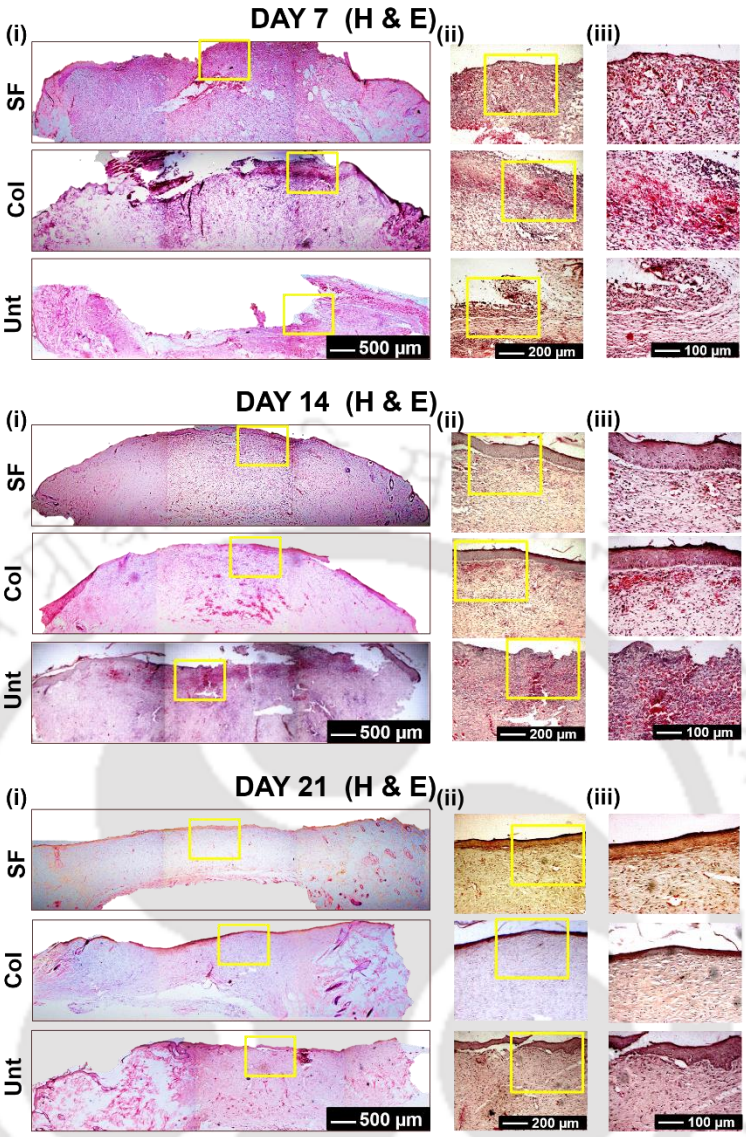

Figure 6.10. *Histological analysis of healed skin biopsies on day 7, 14 and 21 by H & E stain depicting wound morphology at various stages of wound healing. (i) Section of full wound biopsy observed at 4X magnification, (ii and iii) Images at 10X and 20X magnification respectively represents the magnified portion of central wound area (highlighted in yellow box).*

6.3.5. Angiogenic potential

Consistent with the superior regenerative response, hydrogel treated wounds exhibited significantly higher angiogenic potential compared to untreated wounds (**Figure 6.11.A,B**). Immunofluorescence staining for vWF performed on the tissue sections showed formation of small blood vessels in both SF and Col treated wounds on day 7. In contrast, untreated group demonstrated lack of blood vessels due to delay in granulation tissue development. Hydrogel vascularization, quantified as vessel density in the granulation tissue confirmed angiogenic potential of SF hydrogel. Col gel showed

significantly higher vessel density in comparison to SF showing superior angiogenic potential of Col in comparison with SF, $p \leq 0.01$. On comparing with untreated group, SF hydrogel showed 10-fold increment in vessel density, thereby demonstrating superior healing potential of SF hydrogel when compared with untreated. This also suggested that although vessel density in SF treated wounds was lower in comparison to Col treated wounds, vascularized granulation tissue was developed in SF treated wounds when compared to untreated. This depicts early recruitment of endothelial cells and angiogenic potential of SF gel.

6.3.6. Immune response to the hydrogels

We next examined immune response of the host tissue towards SF and Col hydrogels grafted onto the wounds by immunostaining and gene expression study of macrophage markers. Staining of tissue sections using antibody against CD68, a macrophage marker revealed an abundance of macrophages throughout the tissue on day 7 (**Figure 6.11.C**). This suggested high inflammation during the early phase of healing in SF and Col treated wounds. However, relatively lower density of CD68 positive cells on day 14 and 21 demonstrated regression of immune response and suppression of the inflammatory phase. Similar results were obtained from the expression study of CD68 gene (**Figure 6.11.D**). The expression of CD68 was significantly higher on day 7 compared to day 14 and day 21 in all the treatments. On comparing between SF and Col treatments, wounds treated with SF gel showed significantly lower expression of CD68 in comparison to Col on day 7, $p \leq 0.01$. This suggested higher immune response towards Col, which might be attributed to the allogenic collagen type I source. SF gel did not provoke prolonged immune response during the healing process, demonstrating biocompatibility of the material. CD68 expression regressed 2.5-fold and 3-fold on day 14 in case of Col and SF groups respectively. This suggested that the inflammatory phase did not persist, indicating prominent proliferative phase of the wounds.

This was further validated by gene expression study using pro-inflammatory (TNF-α) and anti-inflammatory (CD163) markers of macrophages [373]. Gene expression study of TNF-α and CD163 revealed interesting results (**Figure 6.11.E,F**). Higher expression of TNF-α on day 7 suggested higher inflammatory phase at the beginning of healing process. This might be attributed to the host response against foreign materials (here SF and Col gel) in addition to the initial inflammatory phase of

wound healing. Moreover, the regressed expression of TNF-α in SF treated wounds on day 14 and 21 further proved biocompatibility of SF material. To study more into the details of immune response towards SF gel, gene expression of CD163 was determined. CD163 is a marker of M2 type of macrophage, which helps in tissue regeneration and is also known as anti-inflammatory marker [374, 375]. Significantly higher expression of CD163 in SF treated wounds was observed on day 21 in comparison to day 7 and day 14, depicting tissue regeneration and promotion in healing. Significant higher expression of CD163 on day 14 in comparison to day 7 suggested early beginning of regenerative phase, $p \leq 0.01$. Col treatment also showed similar trend of regenerative phase as observed from the significantly higher CD163 expression on day 21 compared to day 7 and day 14, $p \leq 0.01$.

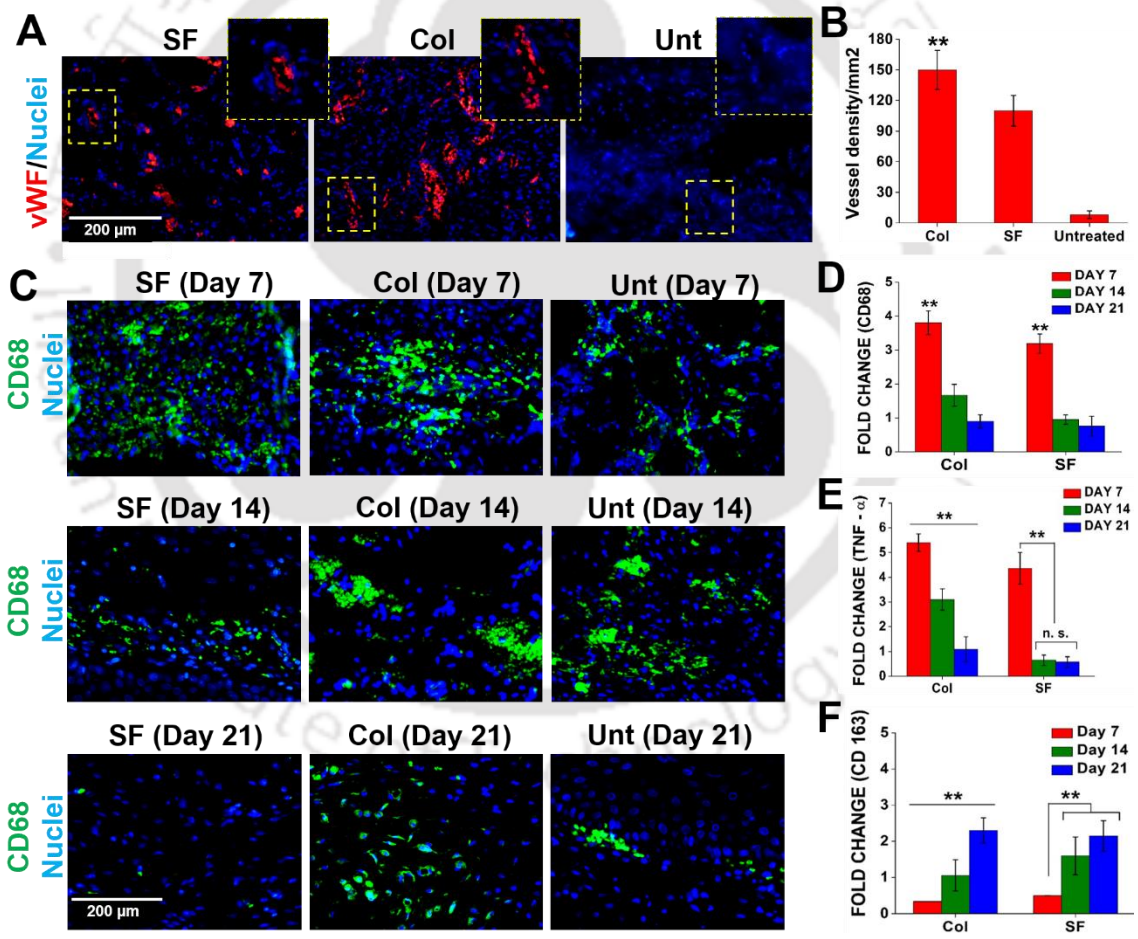

Figure 6.11. *(A) Immunostaining for vWF marker in the wound area demonstrating vascular ingrowth in the SF and Col gel treated wounds on day 7. Inset image depicts magnified blood vessel from the same image; red depicts vWF positive endothelial cells and blue depicts nuclei stained with Hoechst 33342. (B) Quantification of vWF stained blood vessels in the wounds showing vessel density on day 7. (C) Immunostaining for CD68 marker in the wound area depicting macrophage population in the tissue in*

response to SF and Col hydrogel grafts on day 7, 14 and 21. Green depicts CD68 positive macrophage cells and blue depicts nuclei stained with Hoechst 33342. (D-F) Relative gene expression of CD68, TNF-α and CD163 demonstrating fold change expression of the respective genes by taking the untreated group as control.

6.3.7. Wound remodelling assessment: immunohistology and gene expression studies

Next, we examined the effect of SF hydrogel treatment on dermal remodelling by analysing regeneration of extracellular matrix composition (collagen type I and collagen type III fibres) in the healed tissues. Increasing collagen type I secretion from day 7 to day 21 was clearly observed in both SF and Col treated wounds from the IHC images (**Figure 6.12.**). On day 14, prominent mature collagen fibres (both type I and type III) were clearly visible in the hydrogel treated wounds in comparison to untreated wounds. This suggested relatively delayed healing process in the untreated group. Overall, an increasing secretion of collagen type I was observed from day 7 to day 14 in all the wounds, indicating wound healing progression. However, the pattern was different for collagen type III. In case of SF treated wounds, highest secretion of collagen type III was observed on day 14 in comparison to day 7 and day 21. This indicated higher secretion of collagen type III by the fibroblast cells in the proliferative phase due to the support of SF hydrogel. Further, collagen type III fibres were observed homogeneously distributed throughout the lower portion of dermis layer on day 21 in SF treated wounds.

Gene analysis of collagen type I and collagen type III also revealed their significant upregulation and downregulation during different stages of wound healing (**Figure 6.13.**). In the Col gel treated wounds, collagen type I expression was 6-fold higher than untreated (taken as control) on day 7, but the expression regressed to 3.7-fold on day 14. It further upregulated to almost 9-fold on day 21, suggesting an overall increment of collagen type I expression from day 7 to 21. In contrast, expression of collagen type III showed reverse pattern in the Col gel treated wounds. The expression continued to downregulate from day 7 to day 21, suggesting initial upregulation and regression thereafter. Similarly, SF treated wounds exhibited similar expression of collagen type I as observed in Col treated wounds. Expression of collagen type I continued to upregulate from day 7 to day 21 and the expression was 8-fold higher than control. On day 14, collagen type III expression was found to be 5-fold higher than

control, which regressed on day 21. This suggested that SF-treated wounds were at a more advanced stage of remodelling.

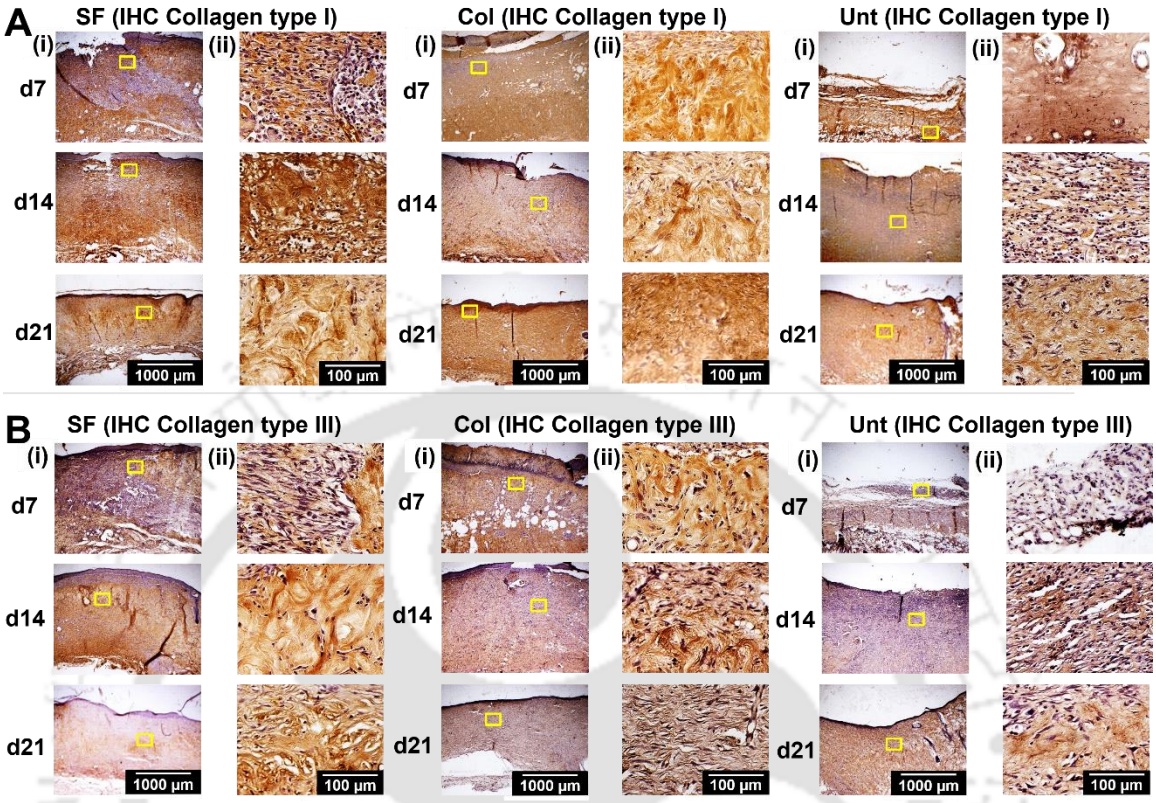

Figure 6.12. *Immunohistochemistry of (A) Collagen type I and (B) Collagen type III in the wounds depicting distribution of respective collagen fibres in the regenerated skin tissues supported by SF and Col hydrogels: (i) section of central wound portion at 4X magnification and (ii) 40X magnified area (highlighted in yellow box of image i) representing respective collagen fibres and bundles at different time points.*

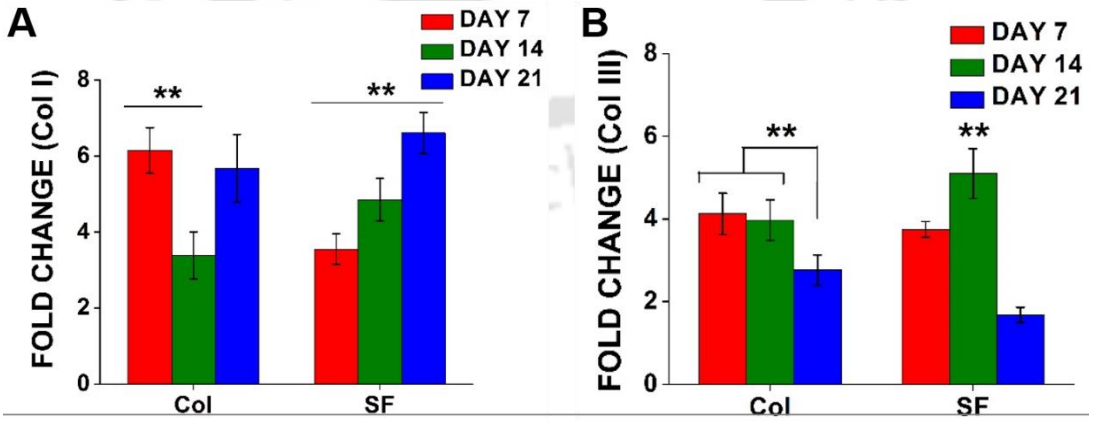

Figure 6.13. *Relative gene expression of (A) Collagen type I and (B) Collagen type III respectively in the wounds treated with SF and Col hydrogels with respect to untreated group taken as control.*

6.3.8. Re-epithelialization assessment

Re-epithelialization of wounds is the most important event in wound healing process. Examination of chief markers of epidermal layer performed after 21 days of wound healing revealed regenerated epidermis (**Figure 6.14.**). The expression of suprabasal keratin marker cytokeratin 10 (CK10), basal keratin marker cytokeratin 14 (CK14) and marker of terminally differentiated keratinocytes Involucrin (INV) were examined by immunostaining. Both SF and Col treated wounds demonstrated comparable regeneration of epidermis. Differentiated keratinocytes of regenerated epidermal layers express CK10 [91]. Expression of CK10 and CK14 at the suprabasal and basal epithelial layers respectively was clearly visible in both SF and Col treated wounds. In contrast, untreated wounds did not exhibit cytokeratin expression by day 21, validating delayed healing conditions. Involucrin appeared mostly in the uppermost stratified layer in SF and Col treated wounds. In contrast, untreated wounds did not show Involucrin expression by day 21. The observation suggests that hydrogels could fasten wound healing by inducing differentiation of keratinocytes.

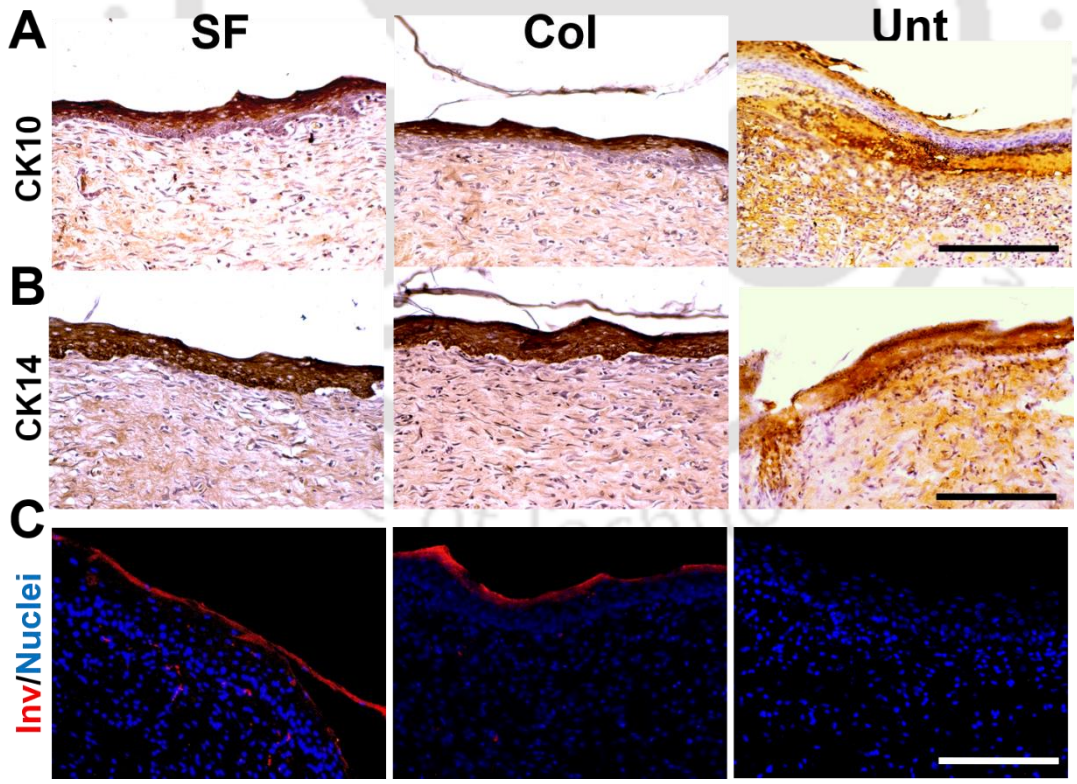

Figure 6.14. *Immunohistochemistry (IHC) of (A) CK 10 marker in the wounds depicting suprabasal expression of CK10 in the epidermis on the wounds on day 21. (B) IHC of CK 14 marker in the wounds depicting its expression in the whole epidermis on the wounds on day 21. Scale bar represents 200 µm. (C) Immunostaining of Involucrin*

marker (a marker of terminally differentiated keratinocytes) in the wounds on day 21 demonstrating mature epidermis in the SF and Col gel treated wounds. Red colour depicts Involucrin and blue colour depicts nuclei stained with Hoechst 33342. Scale bar represents 200 µm.

6.4. Discussion

Injectable hydrogel systems based on natural biomaterials provide great advantage in addressing challenges in surgical interventions [57]. In addition, *in situ* forming gels that rapidly cross-link with surrounding tissue have drawn significant attention as potent healing materials [57]. Shape of wounds can be easily taken up by injectable gels as they fill irregular shaped wounds and large cavities. By using flexible biomaterials like silk fibroin, which possesses tunable mechanical strength, hydrogels with varying stiffness were readily engineered. In the present study, self-assembly property of silk fibroin was utilized to achieve *in situ* gelation for application on third degree burn wounds for improved skin regeneration. Blend of two different silk varieties (AaSF and BmSF) crosslinked at body temperature (37 °C) led to the fabrication of stable hydrogel matrix (**Figure 6.1.**). This natural cross-linking between SF blend is majorly attributed to β-sheet formation in its structure due to permanent physical entanglements between them as verified by XRD and FTIR spectra (**Figure 6.2.B,C**). Stable hydrogel matrix of SF blend might be attributed to the synergistic effects of hydrophobic interaction and hydrogen bonding between AaSF and BmSF proteins.

BmSF and AaSF have different amino acid sequence, with variations in the number of hydrophobic and hydrophilic amino acids. BmSF contains majority of (GAGAGS)n repeats in the protein sequence, which tend to form β-sheet structure on applying physical forces like vortexing, sonication or by electrogelation [222-224]. AaSF protein sequence contains conserved polyalanine blocks alternated with glycine-rich sequence, depicting stretches of hydrophopic blocks [214]. Temperature dependent self-gelation of BmSF is a well-known phenomenon as the interactions among protein chains increases, thereby leading to physical crosslinking [219]. Blending of BmSF with polymers like poly(ethylene oxide) (PEO) or PEG also drives sol-gel transitions leading to faster gelation due to movement of water molecules, thus facilitating inter- and intramolecular interactions [219, 376]. Similarly, blending of BmSF with AaSF induced such inter- and intramolecular interactions, thus leading to self-gelation of the blend

solution. We speculated that the difference between hydrophilicity and hydrophobicity between BmSF and AaSF might attribute to inherent self-assembly between them. Further, the gelation time was dependent on temperature and concentration (**Table 6.2.**) as also observed in previous studies.

Our approach of hydrogel formation by inherent crosslinking between the two silk types also resulted in crosslinker-free gelation. Temperature and concentration dependency on the gelation kinetics further demonstrated flexibility of system (**Figure 6.3. and 6.4.**). On comparing the storage modulus at the end time point, SF hydrogels of concentration higher than 3 % (AB36, AB63 and AB66) were found to be stiff with very high storage modulus (**Figure 6.5.A,B**). Such stiff hydrogels might not be suitable for soft tissues like skin or in wound healing applications. In contrast, hydrogels with less than 3 % concentration formed loose matrix, which were not self-supporting and breaking down easily. Therefore, 3 % SF blend from equal volume of AaSF and BmSF (AB33) was selected as optimum and termed as SF hydrogel in the subsequent studies. Silk being a bulk protein, is well-known for its remarkable mechanical properties within the physiological range for soft tissues [73]. The compressive modulus of SF hydrogel was found to be suitable for wound healing applications, as this much strength is required to maintain its shape and structure under prolonged cell culture conditions (**Figure 6.5.C,D**). Other soft hydrogels such as collagen and fibrin, suffer from contraction and matrix failure due to low mechanical strength [73]. Thus, the soft mechanical properties of SF hydrogel might offer favourable physical and biological properties for skin regeneration applications.

Biodegradability and biocompatibility of SF hydrogel was confirmed by the subcutaneous implantation for 4 weeks (**Figure 6.6.**). In addition, SF gel demonstrated high integral stability in comparison to Col gel as determined by enzymatic degradation studies (**Figure 6.7.A**). Higher stability of SF gel might be attributed to higher molecular weight of SF protein and stable β-sheet networks in comparison to Col. In addition, SF gel did not show gel contraction and remained intact throughout the culture conditions (**Figure 6.7.B,C**). Hence, cell culture studies on SF hydrogel not only revealed its cytocompatibility but also demonstrated matrix stability. Contraction mechanism of Col gel is a well-known phenomenon and therefore strategies to prevent gel contraction have been applied by increasing the mechanical strength *via* chemical or physical crosslinking in previous reports [69-71]. Higher mechanical strength and stability of silk protein thus

offered beneficial properties to the SF gel. In addition, AaSF protein possesses inherent RGD motifs, well known for its cell binding activity, thereby aiding in enhanced cellular proliferation and migration (**Figure 6.7.D and 6.8.**) [214]. Cell migration is an important parameter to assess for biomaterials developed for wound healing applications. The cells residing in wound edges, especially keratinocytes, migrate towards wound site to heal the wound by taking the support of provisional matrix [28]. Migration of keratinocytes from agarose gel to SF matrix within 3 days validated the role of SF in cellular recruitment and migration as observed under *in vitro* conditions (**Figure 6.7.E**).

Thermal wounds, especially third-degree burns are complex acute wounds due to tissue necrosis and loss of full thickness skin. We applied the *in situ* forming injectable SF hydrogel to investigate its wound healing attributes. This offered one step grafting procedure requiring no additional sutures or glue for graft attachment. Wound healing potential of SF hydrogel was found to be comparable with Col gel, as observed from gross wound images (**Figure 6.9.**). Wound healing assessment of SF hydrogel in comparison with Col gel also provided a proof of concept on its application for tissue regeneration. Histological analysis by H & E and MT stain demonstrated that SF gel healed the wounds in a regenerative manner, characterized by rapid development of granulation tissue by 7 days, early re-epithelialization by 14 days and mature epidermo-dermal regeneration by 21 days (**Figure 6.9.B and 6.10.**). Rapid wound closure in SF-treated burns might also be attributable to a combination of both biological and physical properties optimum for wound healing. Moist environment provided by the hydrogel matrix for prolonged time prevents dehydration and thus leads to faster cell migration. Higher water retention capacity of SF aided in maintaining moisture conditions during skin regeneration. Higher cellular proliferation in the SF hydrogel matrix assayed under *in vitro* conditions validated its effective cell migration property.

In the context of biomaterial-induced healing, vascularization potential and macrophage response towards the construct are primary concerns. Events like high blood vessel density in the granulation tissue and high density of CD68 positive macrophages on day 7 confirmed overlapping inflammatory and proliferation phases during the initial healing process by SF hydrogel (**Figure 6.11.A,B**). Angiogenesis at the early phase of healing process is a determinant of granulation tissue development and beginning of proliferative stage of wound healing. Both BmSF and AaSF holds great potential in vascularization as also reported in previous studies. Immunostaining of macrophage

marker (CD68) revealed reduction in their density from day 7 to day 21, suggesting wound healing advancement (**Figure 6.11.C**). This also demonstrated biocompatibility property of the SF matrix because there was no aggressive or prolonged immune reaction by the host. Gene expression analysis from day 7 to 21 further revealed interesting aspects of macrophages during the wound repair process (**Figure 6.11.D**). Inflammation was significantly reduced in the later phases of wound healing, as also observed by low TNF-α and CD68 expression. Higher expression of TNF- α in SF treated wounds on day 7 and lower expression on day 14 and 21 suggested initial inflammatory phase and regenerative phase thereafter (**Figure 6.11.E**). This was further validated by the expression of CD163, a marker of regenerative macrophages which was lower on day 7 and higher on day 14 and 21 (**Figure 6.11.F**). This further explained persistent mild inflammation in Col treated wounds on day 14 because the expression of TNF- α was higher and CD163 was lower. This might be attributed to the host inflammatory response towards allogenic collagen source of Col gel. However, the inflammation was reduced on day 21 owing to the regenerative capacity of Col gel as validated by higher CD163 expression.

Furthermore, wound remodelling by different treatments was assessed by examining gene expression of collagen type I and collagen type III in the regenerated tissue by IHC and gene expression studies (**Figure 6.12.**). In case of SF treated wounds, collagen remodelling was clearly observed by higher deposition of collagen type III on day 7 and 14, but lower on day 21. ECM in the regenerate skin was dominated by collagen type I on day 21, suggesting tissue remodelling at the later stages of wound repair by SF hydrogel. Such distinct collagen remodelling was not observed in Col gel treated wounds. However, this might be attributed to the integration of Col gel matrix with the native tissue and thus collagen type III fibres were not clearly visible. However, gene expression study of collagen type I and type III revealed collagen remodelling and dynamic wound repair process in both SF and Col treated wound (**Figure 6.13.**). The major components of dermis include collagen type I (80-85 %) and collagen type III (8-11 %), which together provide tensile strength and integral stability to the skin [360]. This is an important aspect of wound healing as early secretion of collagen type III helps in accelerated repair process. Persistent or higher deposition of collagen type III is also associated with scar formation during wound healing [377]. Therefore, suppressed collagen type III observed in later wound healing stage (day 21) demonstrated that its

expression was regulated and did not persist in the later phases. Expression of CK10, CK14 and Involucrin at the respective layers further validated regeneration of mature epidermis in SF and Col treated wounds (**Figure 6.14.**). Early re-epithelialization might be attributed to the biocompatible property of SF gel, aiding in recruitment and migration of keratinocytes as also observed under *in vitro* condition. We could speculate that the moist hydrogel treatment of SF might further promote rapid re-epithelialization with mature keratin proteins.

The combination of BmSF and AaSF in SF hydrogel resulted in accelerated healing with normal wound repair process. Combining our findings obtained from the *in vivo* study, SF hydrogel demonstrated enhanced neovascularization and did not provoke persistent inflammation at the onset of wound healing process, suggesting biocompatibility of the material. Next, early development of granulation tissue and guided deposition of collagen type I and type III by SF matrix showed dynamic tissue remodelling during the wound repair process. Thus, our study established a unique SF gel system for treating hard to heal third-degree burns. Our findings report SF hydrogel as an alternative to current therapeutics for treating dermal injuries at a very low-cost. The injectable hydrogel system might also be used to deliver cells by encapsulating it with desired autologous cells. The hydrogel can also be easily functionalized by incorporating bioactive molecules such as specific drugs, antibiotics or growth factors for targeted drug delivery applications. Further investigation of the hydrogel matrix incorporating bioactive molecules or cells may be performed in future to study other applications.

6.5. Significant findings

The salient findings of this chapter are as follows:

1. *In situ* forming hydrogel developed using the facile strategy by blending two types of SF proteins offered advantages over the use of preformed constructs in terms of taking shape of wounds, convenience of application, and host tissue integration.
2. The inherent self-assembly between the two silk proteins resulted in rapid gel formation without any cross-linker or external physical stimulus as compared to individual proteins, which failed to form gel. The faster gelation under physiological like conditions allowed easy encapsulation of viable cells.
3. The long-term moist environment provided by SF hydrogel proved to be beneficial in accelerating the healing process and enhancing re-epithelialization.
4. The silk hydrogel was biocompatible and acted as a supportive matrix for regenerating skin tissue with neo-dermis and neo-epithelium.
5. The detailed *in vivo* study indicates that the silk hydrogel not only promoted wound healing, but also showed transitions from inflammation to proliferation stage, an important event during burn wound healing.

In conclusion, this chapter provides details of a biocompatible *in situ* forming gel system, which may substantially improve healing quality at an affordable cost. Comparable results with collagen biomaterial demonstrate the silk hydrogel as an effective and inexpensive formulation toward a potential therapeutic approach for wound healing applications. This can pave way for further clinical studies on the same to improve the treatment of severe burn injuries.

SUMMARY AND FUTURE PERSPECTIVES

SUMMARY AND FUTURE PERSPECTIVES

Full-thickness skin wounds like third degree burns and chronic cutaneous ulcers are complex wounds that affect a large population due to increasing cases of trauma and pathophysiological conditions. The limited clinical outcomes and costly treatments are major drawbacks at present, which has led to an increasing demand of bioactive matrices that are affordable and available off-the-shelf. To tackle this pressing health problem, we have developed silk based matrices by exploring and investigating the properties of various types of silk for wound healing applications. Also, the current fabrication strategies include application of harsh chemicals or organic solvents for matrix development, which might lead to undetected toxicity in future. In order to combat such fabrication related problems, our focus has primarily been on green approach, which do not include chemical crosslinking and usage of harsh organic solvents. The facile approaches taken herein as demonstrated in various chapters demonstrate huge potential in skin regeneration therapeutics. The relevant advancement of the study and the future prospects associated with it, are briefly enumerated in the following section:

(1) Exploring various varieties of silk fibroin helped in investigating the role of non-mulberry silk and its potential in wound healing applications for the first time. Further, functionalization of silk matrices was facilitated through various strategies including recombinant growth factors and spider silk fusion proteins. The revelation of the *in vitro* studies was fascinating, since the non-mulberry silk demonstrated improved cellular activities in comparison to well-explored mulberry silk. The detailed wound healing assessment *in vivo* further revealed extraordinary properties of various silk varieties for scarless healing and diabetic wound healing. It is foreseen that the silk-based wound dressings developed herein, might find applications in treating chronic cutaneous ulcers like diabetic foot ulcers.

(2) Growth factors and antibacterial compounds are important additives for graft implantation and play crucial roles in tissue regeneration. Functionalized silk-based matrices developed herein demonstrate efficacy of sustained delivery of such bioactive molecules and thus, can also be utilized for drug delivery applications or other tissue regeneration therapeutics.

(3) The prospect of a crosslinker-free approach for hydrogel fabrication opens immense avenues in tissue regeneration applications. The silk hydrogel developed herein holds *in situ* gelation and injectable properties apart from the regenerative properties, which make this hydrogel suitable for healing internal injuries through minimally invasive surgeries.

(4) The research work revealed the potential of various silk biomaterials like mulberry silk, non-mulberry silk and recombinant spider silk fusion proteins in wound healing applications. Besides this, various types of constructs have been developed to harness the regenerative properties of silk material. This technology is not only limited with skin wound healing applications, but it can also be utilized for various tissue engineering applications and regenerative therapeutics.

(4) In the near future, these silk-based matrices may be assessed for developing cellular constructs using autologous cells to fabricate laboratory grown living skin equivalents for patient specific treatments.

(5) The silk-based matrices can also be utilized to develop *in vitro* viable models for drug testing, drug screening and other applications. Another prospective application of such matrices is development of *in vitro* disease models such as melanoma model to study the disease pathways and possible treatment pathways. The matrices if cultured with disease specific human cells might be matured into artificial tissues, mimicking the disease conditions. Such models are great tools for understanding the disease and its diagnosis.

In summary, silk-based matrices have been successfully developed for wound healing applications. Various strategies made it possible to harness the regenerative properties of natural silk biomaterial for treating hard-to-heal wounds. The promising outcome of the *in vitro* and *in vivo* experiments highlights the potential of developed silk matrices for the treatment of complex wounds like burn injuries and diabetic wounds. Moreover, this work brings forward the potential of non-mulberry silk and recombinant spider silk fusion proteins for wound healing applications for the first time. Further exploration of such biomaterials and the developed matrices have immense prospects in tissue engineering and regenerative medicine.

Bibliography

[1] Shevchenko RV, James SL, James SE. A review of tissue-engineered skin bioconstructs available for skin reconstruction. Journal of the royal society, Interface 2010; 7:229-58.
[2] Lee SH, Jeong SK, Ahn SK. An update of the defensive barrier function of skin. Yonsei medical journal 2006; 47:293-306.
[3] Pourmoussa A, Gardner DJ, Johnson MB, Wong AK. An update and review of cell-based wound dressings and their integration into clinical practice. Annals of translational medicine 2016; 4:457.
[4] Groeber F, Holeiter M, Hampel M, Hinderer S, Schenke-Layland K. Skin tissue engineering-in vivo and in vitro applications. Advanced drug delivery reviews 2011; 63:352-66.
[5] MacNeil S. Progress and opportunities for tissue-engineered skin. Nature 2007; 445:874-80.
[6] Martin P. Wound healing-aiming for perfect skin regeneration. Science 1997; 276:75-81.
[7] Yildirimer L, Thanh NT, Seifalian AM. Skin regeneration scaffolds: a multimodal bottom-up approach. Trends in biotechnology 2012; 30:638-48.
[8] Clark RA, Ghosh K, Tonnesen MG. Tissue engineering for cutaneous wounds. Journal of investigative dermatology 2007; 127:1018-29.
[9] Niu Y, Li Q, Ding Y, Dong L, Wang C. Engineered delivery strategies for enhanced control of growth factor activities in wound healing. Advanced drug delivery reviews 2018.
[10] Sen CK, Gordillo GM, Roy S, Kirsner R, Lambert L, Hunt TK, et al. Human skin wounds: a major and snowballing threat to public health and the economy. Wound repair and regeneration 2009; 17:763-71.
[11] Snyder BJ, Waldman BJ. Venous thromboembolism prophylaxis and wound healing in patients undergoing major orthopedic surgery. Advances in skin & wound care 2009; 22:311-5.
[12] Falanga V. Wound healing and its impairment in the diabetic foot. Lancet 2005; 366:1736-43.
[13] Papini R. Management of burn injuries of various depths. Bmj 2004; 329:158-60.
[14] Ojeh N, Pastar I, Tomic-Canic M, Stojadinovic O. Stem cells in skin regeneration, wound healing, and their clinical applications. International journal of molecular sciences 2015; 16:25476-501.
[15] Chua AW, Khoo YC, Tan BK, Tan KC, Foo CL, Chong SJ. Skin tissue engineering advances in severe burns: review and therapeutic applications. Burns & trauma 2016; 4:3.
[16] Herndon DN, Barrow RE, Rutan RL, Rutan TC, Desai MH, Abston S. A comparison of conservative versus early excision. Therapies in severely burned patients. Annals of surgery 1989; 209:547-52.
[17] Bottcher-Haberzeth S, Biedermann T, Reichmann E. Tissue engineering of skin. Burns 2010; 36:450-60.
[18] Holzer PW, Leonard DA, Shanmugarajah K, Moulton KN, Ng ZY, Cetrulo CL, Jr., et al. A comparative examination of the clinical outcome and histological appearance of

cryopreserved and fresh split-thickness skin grafts. Journal of burn care & research 2017; 38:e55-e61.
[19] Moura LI, Dias AM, Carvalho E, de Sousa HC. Recent advances on the development of wound dressings for diabetic foot ulcer treatment-a review. Acta biomaterialia 2013; 9:7093-114.
[20] Suarato G, Bertorelli R, Athanassiou A. Borrowing from nature: biopolymers and biocomposites as smart wound care materials. Frontiers in bioengineering and biotechnology 2018; 6:137.
[21] Mir M, Ali MN, Barakullah A, Gulzar A, Arshad M, Fatima S, et al. Synthetic polymeric biomaterials for wound healing: a review. Progress in biomaterials 2018; 7:1-21.
[22] Altman GH, Diaz F, Jakuba C, Calabro T, Horan RL, Chen J, et al. Silk-based biomaterials. Biomaterials 2003; 24:401-16.
[23] Holland C, Numata K, Rnjak-Kovacina J, Seib FP. The biomedical use of silk: past, present, future. Advanced healthcare materials 2019; 8:e1800465.
[24] Kundu SC, Kundu B, Talukdar S, Bano S, Nayak S, Kundu J, et al. Invited review nonmulberry silk biopolymers. Biopolymers 2012; 97:455-67.
[25] Mogosanu GD, Grumezescu AM. Natural and synthetic polymers for wounds and burns dressing. International journal of pharmaceutics 2014; 463:127-36.
[26] Clark RA. Fibrin and wound healing. Annals of the New York academy of sciences 2001; 936:355-67.
[27] Yucel T, Lovett ML, Kaplan DL. Silk-based biomaterials for sustained drug delivery. Journal of controlled release 2014; 190:381-97.
[28] Eming SA, Martin P, Tomic-Canic M. Wound repair and regeneration: mechanisms, signaling, and translation. Science translational medicine 2014; 6:265sr6.
[29] Sun G, Shen YI, Harmon JW. Engineering pro-regenerative hydrogels for scarless wound healing. Advanced healthcare materials 2018; 7:e1800016.
[30] Johnson NR, Wang Y. Drug delivery systems for wound healing. Current pharmaceutical biotechnology 2015; 16:621-9.
[31] Chaudhari AA, Vig K, Baganizi DR, Sahu R, Dixit S, Dennis V, et al. Future prospects for scaffolding methods and biomaterials in skin tissue engineering: a review. International journal of molecular sciences 2016; 17.
[32] Pereira RF, Barrias CC, Granja PL, Bartolo PJ. Advanced biofabrication strategies for skin regeneration and repair. Nanomedicine 2013; 8:603-21.
[33] Boyce ST, Lalley AL. Tissue engineering of skin and regenerative medicine for wound care. Burns & trauma 2018; 6:4.
[34] Nyame TT, Chiang HA, Orgill DP. Clinical applications of skin substitutes. The surgical clinics of North America 2014 ;94:839-50.
[35] Tenenhaus M, Rennekampff HO. Current concepts in tissue engineering: skin and wound. Plastic and reconstructive surgery 2016 ;138:42-50.
[36] Shafiee A, Atala A. Tissue engineering: toward a new era of medicine. Annual review of medicine 2017; 68:29-40.

[37] Burke JF, Yannas IV, Quinby WC, Jr., Bondoc CC, Jung WK. Successful use of a physiologically acceptable artificial skin in the treatment of extensive burn injury. Annals of surgery 1981; 194:413-28.
[38] Gould DJ. Tissue engineering for plastic surgeons: a primer commentary. Aesthetic plastic surgery 2014; 38:222-3.
[39] Ng WL, Wang S, Yeong WY, Naing MW. Skin bioprinting: impending reality or fantasy? Trends in biotechnology 2016; 34:689-99.
[40] Chen S, Liu B, Carlson MA, Gombart AF, Reilly DA, Xie J. Recent advances in electrospun nanofibers for wound healing. Nanomedicine 2017; 12:1335-52.
[41] Hakimi N, Cheng R, Leng L, Sotoudehfar M, Ba PQ, Bakhtyar N, et al. Handheld skin printer: in situ formation of planar biomaterials and tissues. Lab on a chip 2018; 18:1440-51.
[42] Vrana NE, Lavalle P, Dokmeci MR, Dehghani F, Ghaemmaghami AM, Khademhosseini A. Engineering functional epithelium for regenerative medicine and in vitro organ models: a review. Tissue engineering Part B, Reviews 2013; 19:529-43.
[43] Bhardwaj N, Kundu SC. Electrospinning: a fascinating fiber fabrication technique. Biotechnology advances 2010; 28:325-47.
[44] Liu M, Zhang Y, Sun S, Khan AR, Ji J, Yang M, et al. Recent advances in electrospun for drug delivery purpose. Journal of drug targeting 2019; 27:270-82.
[45] Lee OJ, Ju HW, Kim JH, Lee JM, Ki CS, Kim JH, et al. Development of artificial dermis using 3D electrospun silk fibroin nanofiber matrix. Journal of biomedical nanotechnology 2014; 10:1294-303.
[46] Dong RH, Jia YX, Qin CC, Zhan L, Yan X, Cui L, et al. In situ deposition of a personalized nanofibrous dressing via a handy electrospinning device for skin wound care. Nanoscale 2016; 8:3482-8.
[47] Bhardwaj N, Sow WT, Devi D, Ng KW, Mandal BB, Cho NJ. Silk fibroin-keratin based 3D scaffolds as a dermal substitute for skin tissue engineering. Integrative biology 2015; 7:53-63.
[48] Shen YI, Song HG, Papa A, Burke J, Volk SW, Gerecht S. Acellular hydrogels for regenerative burn wound healing: translation from a porcine model. Journal of investigative dermatology 2015; 135:2519-29.
[49] Akita S, Hayashida K, Yoshimoto H, Fujioka M, Senju C, Morooka S, et al. Novel application of cultured epithelial autografts (CEA) with expanded mesh skin grafting over an artificial dermis or dermal wound bed preparation. International journal of molecular sciences 2017; 19.
[50] Yu J, Wang MY, Tai HC, Cheng NC. Cell sheet composed of adipose-derived stem cells demonstrates enhanced skin wound healing with reduced scar formation. Acta biomaterialia 2018; 77:191-200.
[51] Jiang S, Li SC, Huang C, Chan BP, Du Y. Physical properties of implanted porous bioscaffolds regulate skin repair: focusing on mechanical and structural features. Advanced healthcare materials 2018; 7:e1700894.
[52] Eke G, Mangir N, Hasirci N, MacNeil S, Hasirci V. Development of a UV crosslinked biodegradable hydrogel containing adipose derived stem cells to promote vascularization for skin wounds and tissue engineering. Biomaterials 2017; 129:188-98.

[53] Loh QL, Choong C. Three-dimensional scaffolds for tissue engineering applications: role of porosity and pore size. Tissue engineering Part B, Reviews 2013; 19:485-502.
[54] Marino D, Luginbuhl J, Scola S, Meuli M, Reichmann E. Bioengineering dermo-epidermal skin grafts with blood and lymphatic capillaries. Science translational medicine 2014; 6:221ra14.
[55] Rustad KC, Wong VW, Sorkin M, Glotzbach JP, Major MR, Rajadas J, et al. Enhancement of mesenchymal stem cell angiogenic capacity and stemness by a biomimetic hydrogel scaffold. Biomaterials 2012; 33:80-90.
[56] Madaghiele M, Demitri C, Sannino A, Ambrosio L. Polymeric hydrogels for burn wound care: advanced skin wound dressings and regenerative templates. Burns & trauma 2014; 2:153-61.
[57] Nguyen MK, Lee DS. Injectable biodegradable hydrogels. Macromolecular bioscience 2010; 10:563-79.
[58] Zhao L, Niu L, Liang H, Tan H, Liu C, Zhu F. pH and glucose dual-responsive injectable hydrogels with insulin and fibroblasts as bioactive dressings for diabetic wound healing. ACS applied materials & interfaces 2017; 9:37563-74.
[59] Williams DF. Biomaterials and biocompatibility. Medical progress through technology 1976; 4:31-42.
[60] Hussein KH, Park KM, Kang KS, Woo HM. Biocompatibility evaluation of tissue-engineered decellularized scaffolds for biomedical application. Materials science & engineering C 2016; 67:766-78.
[61] Rameshbabu AP, Bankoti K, Datta S, Subramani E, Apoorva A, Ghosh P, et al. Silk sponges ornamented with a placenta-derived extracellular matrix augment full-thickness cutaneous wound healing by stimulating neovascularization and cellular migration. ACS applied materials & interfaces 2018; 10:16977-91.
[62] Thurber AE, Omenetto FG, Kaplan DL. In vivo bioresponses to silk proteins. Biomaterials 2015; 71:145-57.
[63] Tenekecioglu E, Farooq V, Bourantas CV, Silva RC, Onuma Y, Yilmaz M, et al. Bioresorbable scaffolds: a new paradigm in percutaneous coronary intervention. BMC cardiovascular disorders 2016; 16:38.
[64] Wang Y, Rudym DD, Walsh A, Abrahamsen L, Kim HJ, Kim HS, et al. In vivo degradation of three-dimensional silk fibroin scaffolds. Biomaterials 2008; 29:3415-28.
[65] Ushiki T. Collagen fibers, reticular fibers and elastic fibers. A comprehensive understanding from a morphological viewpoint. Archives of histology and cytology 2002; 65:109-26.
[66] Levy-Mishali M, Zoldan J, Levenberg S. Effect of scaffold stiffness on myoblast differentiation. Tissue engineering Part A 2009; 15:935-44.
[67] Bell E, Ivarsson B, Merrill C. Production of a tissue-like structure by contraction of collagen lattices by human fibroblasts of different proliferative potential in vitro. Proceedings of the national academy of sciences of the United States of America 1979; 76:1274-8.

[68] Ng KW, Khor HL, Hutmacher DW. In vitro characterization of natural and synthetic dermal matrices cultured with human dermal fibroblasts. Biomaterials 2004; 25:2807-18.
[69] Brinkman WT, Nagapudi K, Thomas BS, Chaikof EL. Photo-cross-linking of type I collagen gels in the presence of smooth muscle cells: mechanical properties, cell viability, and function. Biomacromolecules 2003; 4:890-5.
[70] Davidenko N, Schuster CF, Bax DV, Raynal N, Farndale RW, Best SM, et al. Control of crosslinking for tailoring collagen-based scaffolds stability and mechanics. Acta biomaterialia 2015; 25:131-42.
[71] Orban JM, Wilson LB, Kofroth JA, El-Kurdi MS, Maul TM, Vorp DA. Crosslinking of collagen gels by transglutaminase. Journal of biomedical materials research Part A 2004; 68:756-62.
[72] Park SN, Lee HJ, Lee KH, Suh H. Biological characterization of EDC-crosslinked collagen-hyaluronic acid matrix in dermal tissue restoration. Biomaterials 2003; 24:1631-41.
[73] Hopkins AM, De Laporte L, Tortelli F, Spedden E, Staii C, Atherton TJ, et al. Silk hydrogels as soft substrates for neural tissue engineering. Advanced functional materials 2013; 23:5140-9.
[74] Kamoun EA, Kenawy ES, Chen X. A review on polymeric hydrogel membranes for wound dressing applications: PVA-based hydrogel dressings. Journal of advanced research 2017; 8:217-33.
[75] Celebi N, Erden N, Gonul B, Koz M. Effects of epidermal growth factor dosage forms on dermal wound strength in mice. The Journal of pharmacy and pharmacology 1994; 46:386-7.
[76] Vidal SEL, Tamamoto KA, Nguyen H, Abbott RD, Cairns DM, Kaplan DL. 3D biomaterial matrix to support long term, full thickness, immuno-competent human skin equivalents with nervous system components. Biomaterials 2019; 198:194-203.
[77] Gilmartin DJ, Soon A, Thrasivoulou C, Phillips AR, Jayasinghe SN, Becker DL. Sustained release of Cx43 antisense oligodeoxynucleotides from coated collagen scaffolds promotes wound healing. Advanced healthcare materials 2016; 5:1786-99.
[78] Koppenol DC, Vermolen FJ, Niessen FB, van Zuijlen PPM, Vuik K. A biomechanical mathematical model for the collagen bundle distribution-dependent contraction and subsequent retraction of healing dermal wounds. Biomechanics and modeling in mechanobiology 2017; 16:345-61.
[79] Price BL, Lovering AM, Bowling FL, Dobson CB. Development of a novel collagen wound model to simulate the activity and distribution of antimicrobials in soft tissue during diabetic foot infection. Antimicrobial agents and chemotherapy 2016; 60:6880-9.
[80] Chen J, Liu Z, Chen M, Zhang H, Li X. Electrospun gelatin fibers with a multiple release of antibiotics accelerate dermal regeneration in infected deep burns. Macromolecular bioscience 2016; 16:1368-80.
[81] Huang S, Zhang Y, Tang L, Deng Z, Lu W, Feng F, et al. Functional bilayered skin substitute constructed by tissue-engineered extracellular matrix and microsphere-incorporated gelatin hydrogel for wound repair. Tissue engineering Part A 2009; 15:2617-24.

[82] Nunes PS, Rabelo AS, Souza JC, Santana BV, da Silva TM, Serafini MR, et al. Gelatin-based membrane containing usnic acid-loaded liposome improves dermal burn healing in a porcine model. International journal of pharmaceutics 2016; 513:473-82.
[83] Tchemtchoua VT, Atanasova G, Aqil A, Filee P, Garbacki N, Vanhooteghem O, et al. Development of a chitosan nanofibrillar scaffold for skin repair and regeneration. Biomacromolecules 2011; 12:3194-204.
[84] Kong Y, Xu R, Darabi MA, Zhong W, Luo G, Xing MM, et al. Fast and safe fabrication of a free-standing chitosan/alginate nanomembrane to promote stem cell delivery and wound healing. International journal of nanomedicine 2016; 11:2543-55.
[85] Boucard N, Viton C, Agay D, Mari E, Roger T, Chancerelle Y, et al. The use of physical hydrogels of chitosan for skin regeneration following third-degree burns. Biomaterials 2007; 28:3478-88.
[86] Skardal A, Murphy SV, Crowell K, Mack D, Atala A, Soker S. A tunable hydrogel system for long-term release of cell-secreted cytokines and bioprinted in situ wound cell delivery. Journal of biomedical materials research Part B 2017; 105:1986-2000.
[87] Tokatlian T, Cam C, Segura T. Porous hyaluronic acid hydrogels for localized nonviral DNA delivery in a diabetic wound healing model. Advanced healthcare materials 2015; 4:1084-91.
[88] Yang Y, Zhang W, Li Y, Fang G, Zhang K. Scalded skin of rat treated by using fibrin glue combined with allogeneic bone marrow mesenchymal stem cells. Annals of dermatology 2014; 26:289-95.
[89] Sun T, Haycock J, Macneil S. In situ image analysis of interactions between normal human keratinocytes and fibroblasts cultured in three-dimensional fibrin gels. Biomaterials 2006; 27:3459-65.
[90] Farokhi M, Mottaghitalab F, Fatahi Y, Khademhosseini A, Kaplan DL. Overview of silk fibroin use in wound dressings. Trends in biotechnology 2018; 36:907-22.
[91] Gil ES, Panilaitis B, Bellas E, Kaplan DL. Functionalized silk biomaterials for wound healing. Advanced healthcare materials 2013; 2:206-17.
[92] Vasconcelos A, Cavaco-Paulo A. Wound dressings for a proteolytic-rich environment. Applied microbiology and biotechnology 2011; 90:445-60.
[93] Fu S-Z, Meng X-H, Fan J, Yang L-L, Wen Q-L, Ye S-J, et al. Acceleration of dermal wound healing by using electrospun curcumin-loaded poly(ε-caprolactone)-poly(ethylene glycol)-poly(ε-caprolactone) fibrous mats. Journal of biomedical materials research 2014; 102:533-42.
[94] Hinrichs WL, Lommen EJ, Wildevuur CR, Feijen J. Fabrication and characterization of an asymmetric polyurethane membrane for use as a wound dressing. Journal of applied biomaterials 1992; 3:287-303.
[95] Khil MS, Cha DI, Kim HY, Kim IS, Bhattarai N. Electrospun nanofibrous polyurethane membrane as wound dressing. Journal of biomedical materials research Part B, 2003; 67:675-9.
[96] Chen G, Sato T, Ohgushi H, Ushida T, Tateishi T, Tanaka J. Culturing of skin fibroblasts in a thin PLGA-collagen hybrid mesh. Biomaterials 2005; 26:2559-66.

[97] Marston WA. Dermagraft, a bioengineered human dermal equivalent for the treatment of chronic nonhealing diabetic foot ulcer. Expert review of medical devices 2004; 1:21-31.
[98] Kumbar SG, Nukavarapu SP, James R, Nair LS, Laurencin CT. Electrospun poly(lactic acid-co-glycolic acid) scaffolds for skin tissue engineering. Biomaterials 2008; 29:4100-7.
[99] Said SS, El-Halfawy OM, El-Gowelli HM, Aloufy AK, Boraei NA, El-Khordagui LK. Bioburden-responsive antimicrobial PLGA ultrafine fibers for wound healing. European journal of pharmaceutics and biopharmaceutics 2012; 80:85-94.
[100] Li M, Minoura N, Dai L, Zhang L. Preparation of porous poly(vinyl alcohol)-silk fibroin (PVA/SF) blend membranes. Macromolecular materials and engineering 2001; 286:529-33.
[101] Metcalfe AD, Ferguson MW. Tissue engineering of replacement skin: the crossroads of biomaterials, wound healing, embryonic development, stem cells and regeneration. Journal of the royal society, interface 2007; 4:413-37.
[102] Catalano E, Cochis A, Varoni E, Rimondini L, Azzimonti B. Tissue-engineered skin substitutes: an overview. Journal of artificial organs 2013; 16:397-403.
[103] Zhong SP, Zhang YZ, Lim CT. Tissue scaffolds for skin wound healing and dermal reconstruction. Wiley interdisciplinary reviews Nanomedicine and nanobiotechnology 2010; 2:510-25.
[104] Brett D. A review of collagen and collagen-based wound dressings. Wounds : a compendium of clinical research and practice 2008; 20:347-56.
[105] Auger FA, Rouabhia M, Goulet F, Berthod F, Moulin V, Germain L. Tissue-engineered human skin substitutes developed from collagen-populated hydrated gels: clinical and fundamental applications. Medical & biological engineering & computing 1998; 36:801-12.
[106] Rastogi S, Modi M, Sathian B. The efficacy of collagen membrane as a biodegradable wound dressing material for surgical defects of oral mucosa: a prospective study. Journal of oral and maxillofacial surgery 2009; 67:1600-6.
[107] Takagi R, Ishimaru J, Sugawara A, Toyoshima KE, Ishida K, Ogawa M, et al. Bioengineering a 3D integumentary organ system from iPS cells using an in vivo transplantation model. Science advances 2016; 2:e1500887.
[108] Powell HM, Boyce ST. Wound closure with EDC cross-linked cultured skin substitutes grafted to athymic mice. Biomaterials 2007; 28:1084-92.
[109] Ono I, Tateshita T, Inoue M. Effects of a collagen matrix containing basic fibroblast growth factor on wound contraction. Journal of biomedical materials research 1999; 48:621-30.
[110] Yeh M-k, Liang Y-m, Cheng K-m, Dai N-T, Liu C-c, Young J-j. A novel cell support membrane for skin tissue engineering: gelatin film cross-linked with 2-chloro-1-methylpyridinium iodide. Polymer 2011; 52:996-1003.
[111] Deng C-M, He L-Z, Zhao M, Yang D, Liu Y. Biological properties of the chitosan-gelatin sponge wound dressing. Carbohydrate polymers 2007; 69:583-9.

[112] Wang TW, Sun JS, Wu HC, Tsuang YH, Wang WH, Lin FH. The effect of gelatin-chondroitin sulfate-hyaluronic acid skin substitute on wound healing in SCID mice. Biomaterials 2006; 27:5689-97.
[113] Li Y, Yao M, Wang X, Zhao Y. Effects of gelatin sponge combined with moist wound-healing nursing intervention in the treatment of phase III bedsore. Experimental and therapeutic medicine 2016; 11:2213-6.
[114] Liu H, Mao J, Yao K, Yang G, Cui L, Cao Y. A study on a chitosan-gelatin-hyaluronic acid scaffold as artificial skin in vitro and its tissue engineering applications. Journal of biomaterials science Polymer edition 2004; 15:25-40.
[115] Shi C, Zhu Y, Ran X, Wang M, Su Y, Cheng T. Therapeutic potential of chitosan and its derivatives in regenerative medicine. The Journal of surgical research 2006; 133:185-92.
[116] Huang S, Fu X. Naturally derived materials-based cell and drug delivery systems in skin regeneration. Journal of controlled release 2010; 142:149-59.
[117] Peramo A, Marcelo CL. Bioengineering the skin-implant interface: the use of regenerative therapies in implanted devices. Annals of biomedical engineering 2010; 38:2013-31.
[118] Mizuno K, Yamamura K, Yano K, Osada T, Saeki S, Takimoto N, et al. Effect of chitosan film containing basic fibroblast growth factor on wound healing in genetically diabetic mice. Journal of biomedical materials research Part A 2003; 64:177-81.
[119] Ma L, Gao C, Mao Z, Zhou J, Shen J, Hu X, et al. Collagen/chitosan porous scaffolds with improved biostability for skin tissue engineering. Biomaterials 2003; 24:4833-41.
[120] Kiyozumi T, Kanatani Y, Ishihara M, Saitoh D, Shimizu J, Yura H, et al. The effect of chitosan hydrogel containing DMEM/F12 medium on full-thickness skin defects after deep dermal burn. Burns 2007; 33:642-8.
[121] Veleirinho B, Coelho DS, Dias PF, Maraschin M, Ribeiro-do-Valle RM, Lopes-da-Silva JA. Nanofibrous poly(3-hydroxybutyrate-co-3-hydroxyvalerate)/chitosan scaffolds for skin regeneration. International journal of biological macromolecules 2012; 51:343-50.
[122] Madihally SV, Matthew HW. Porous chitosan scaffolds for tissue engineering. Biomaterials 1999; 20:1133-42.
[123] Adekogbe I, Ghanem A. Fabrication and characterization of DTBP-crosslinked chitosan scaffolds for skin tissue engineering. Biomaterials 2005; 26:7241-50.
[124] Harris PA, di Francesco F, Barisoni D, Leigh IM, Navsaria HA. Use of hyaluronic acid and cultured autologous keratinocytes and fibroblasts in extensive burns. Lancet 1999; 353:35-6.
[125] Price RD, Berry MG, Navsaria HA. Hyaluronic acid: the scientific and clinical evidence. Journal of plastic, reconstructive & aesthetic surgery 2007; 60:1110-9.
[126] Murashita T, Nakayama Y, Hirano T, Ohashi S. Acceleration of granulation tissue ingrowth by hyaluronic acid in artificial skin. British journal of plastic surgery 1996; 49:58-63.
[127] Yang JA, Kim ES, Kwon JH, Kim H, Shin JH, Yun SH, et al. Transdermal delivery of hyaluronic acid - human growth hormone conjugate. Biomaterials 2012; 33:5947-54.

[128] Wang F, Garza LA, Kang S, Varani J, Orringer JS, Fisher GJ, et al. In vivo stimulation of de novo collagen production caused by cross-linked hyaluronic acid dermal filler injections in photodamaged human skin. Archives of dermatology 2007; 143:155-63.
[129] Currie LJ, Sharpe JR, Martin R. The use of fibrin glue in skin grafts and tissue-engineered skin replacements: a review. Plastic and reconstructive surgery 2001; 108:1713-26.
[130] Qi C, Xu L, Deng Y, Wang G, Wang Z, Wang L. Sericin hydrogels promote skin wound healing with effective regeneration of hair follicles and sebaceous glands after complete loss of epidermis and dermis. Biomaterials science 2018; 6:2859-70.
[131] Lamboni L, Gauthier M, Yang G, Wang Q. Silk sericin: A versatile material for tissue engineering and drug delivery. Biotechnology advances 2015; 33:1855-67.
[132] Sugihara A, Sugiura K, Morita H, Ninagawa T, Tubouchi K, Tobe R, et al. Promotive effects of a silk film on epidermal recovery from full-thickness skin wounds. Proceedings of the society for experimental biology and medicine society for experimental biology and medicine 2000; 225:58-64.
[133] Wang HY, Zhang YQ. Processing silk hydrogel and its applications in biomedical materials. Biotechnology progress 2015; 31:630-40.
[134] Li X, You R, Luo Z, Chen G, Li M. Silk fibroin scaffolds with a micro-/nano-fibrous architecture for dermal regeneration. Journal of materials chemistry B 2016; 4:2903-12.
[135] Xie SY, Peng LH, Shan YH, Niu J, Xiong J, Gao JQ. Adult stem cells seeded on electrospinning silk fibroin nanofiberous scaffold enhance wound repair and regeneration. Journal of nanoscience and nanotechnology 2016; 16:5498-505.
[136] Yoon H, Kim G. A three-dimensional polycaprolactone scaffold combined with a drug delivery system consisting of electrospun nanofibers. Journal of pharmaceutical sciences 2011; 100:424-30.
[137] Kamel RA, Ong JF, Eriksson E, Junker JP, Caterson EJ. Tissue engineering of skin. Journal of the American college of surgeons 2013; 217:533-55.
[138] Bleasdale B, Finnegan S, Murray K, Kelly S, Percival SL. The use of silicone adhesives for scar reduction. Advances in wound care 2015; 4:422-30.
[139] Golas AR, Hernandez KA, Spector JA. Tissue engineering for plastic surgeons: a primer. Aesthetic plastic surgery 2014; 38:207-21.
[140] Pyun do G, Choi HJ, Yoon HS, Thambi T, Lee DS. Polyurethane foam containing rhEGF as a dressing material for healing diabetic wounds: synthesis, characterization, in vitro and in vivo studies. Colloids and surfaces B, biointerfaces 2015; 135:699-706.
[141] Chua AW, Ma DR, Song IC, Phan TT, Lee ST, Song C. In vitro evaluation of fibrin mat and tegaderm wound dressing for the delivery of keratinocytes-implications of their use to treat burns. Burns 2008; 34:175-80.
[142] Vacik J, Dvorankova B, Michalek J, Pradny M, Krumbholcova E, Fenclova T, et al. Cultivation of human keratinocytes without feeder cells on polymer carriers containing ethoxyethyl methacrylate: in vitro study. Journal of materials science Materials in medicine 2008; 19:883-8.
[143] Boyce ST. Cultured skin substitutes: a review. Tissue engineering 1996; 2:255-66.

[144] Gwak SJ, Kim SS, Sung K, Han J, Choi CY, Kim BS. Synergistic effect of keratinocyte transplantation and epidermal growth factor delivery on epidermal regeneration. Cell transplantation 2005; 14:809-17.
[145] Horch RE, Kopp J, Kneser U, Beier J, Bach AD. Tissue engineering of cultured skin substitutes. Journal of cellular and molecular medicine 2005; 9:592-608.
[146] Boyce ST, Goretsky MJ, Greenhalgh DG, Kagan RJ, Rieman MT, Warden GD. Comparative assessment of cultured skin substitutes and native skin autograft for treatment of full-thickness burns. Annals of surgery 1995; 222:743-52.
[147] Blanpain C, Fuchs E. Epidermal stem cells of the skin. Annual review of cell and developmental biology 2006; 22:339-73.
[148] Topol BM, Haimes HB, Dubertret L, Bell E. Transfer of melanosomes in a skin equivalent model in vitro. Journal of investigative dermatology 1986; 87:642-7.
[149] Biernaskie J, Paris M, Morozova O, Fagan BM, Marra M, Pevny L, et al. SKPs derive from hair follicle precursors and exhibit properties of adult dermal stem cells. Cell stem cell 2009; 5:610-23.
[150] Maxson S, Lopez EA, Yoo D, Danilkovitch-Miagkova A, Leroux MA. Concise review: role of mesenchymal stem cells in wound repair. Stem cells translational medicine 2012; 1:142-9.
[151] Cerqueira MT, Pirraco RP, Martins AR, Santos TC, Reis RL, Marques AP. Cell sheet technology-driven re-epithelialization and neovascularization of skin wounds. Acta biomaterialia 2014; 10:3145-55.
[152] Hunyadi J, Farkas B, Bertenyi C, Olah J, Dobozy A. Keratinocyte grafting: a new means of transplantation for full-thickness wounds. Journal of dermatologic surgery and oncology 1988; 14:75-8.
[153] Navarro FA, Stoner ML, Park CS, Huertas JC, Lee HB, Wood FM, et al. Sprayed keratinocyte suspensions accelerate epidermal coverage in a porcine microwound model. The Journal of burn care & rehabilitation 2000; 21:513-8.
[154] Sriram G, Bigliardi PL, Bigliardi-Qi M. Fibroblast heterogeneity and its implications for engineering organotypic skin models in vitro. European journal of cell biology 2015; 94:483-512.
[155] Wong T, McGrath JA, Navsaria H. The role of fibroblasts in tissue engineering and regeneration. The British journal of dermatology 2007; 156:1149-55.
[156] Driskell RR, Watt FM. Understanding fibroblast heterogeneity in the skin. Trends in cell biology 2015; 25:92-9.
[157] Greaves NS, Iqbal SA, Baguneid M, Bayat A. The role of skin substitutes in the management of chronic cutaneous wounds. Wound repair and regeneration 2013; 21:194-210.
[158] Tumbar T, Guasch G, Greco V, Blanpain C, Lowry WE, Rendl M, et al. Defining the epithelial stem cell niche in skin. Science 2004; 303:359-63.
[159] Zheng Y, Du X, Wang W, Boucher M, Parimoo S, Stenn K. Organogenesis from dissociated cells: generation of mature cycling hair follicles from skin-derived cells. Journal of investigative dermatology 2005; 124:867-76.
[160] Falanga V, Iwamoto S, Chartier M, Yufit T, Butmarc J, Kouttab N, et al. Autologous bone marrow-derived cultured mesenchymal stem cells delivered in a fibrin

spray accelerate healing in murine and human cutaneous wounds. Tissue engineering 2007; 13:1299-312.
[161] Guo Z, Higgins CA, Gillette BM, Itoh M, Umegaki N, Gledhill K, et al. Building a microphysiological skin model from induced pluripotent stem cells. Stem cell research & therapy 2013; 4 Suppl 1:S2.
[162] Monfort A, Soriano-Navarro M, Garcia-Verdugo JM, Izeta A. Production of human tissue-engineered skin trilayer on a plasma-based hypodermis. Journal of tissue engineering and regenerative medicine 2013; 7:479-90.
[163] Yoshikawa T, Mitsuno H, Nonaka I, Sen Y, Kawanishi K, Inada Y, et al. Wound therapy by marrow mesenchymal cell transplantation. Plastic and reconstructive surgery 2008; 121:860-77.
[164] Zhang CL, Huang T, Wu BL, He WX, Liu D. Stem cells in cancer therapy: opportunities and challenges. Oncotarget 2017; 8:75756-66.
[165] Martino MM, Tortelli F, Mochizuki M, Traub S, Ben-David D, Kuhn GA, et al. Engineering the growth factor microenvironment with fibronectin domains to promote wound and bone tissue healing. Science translational medicine 2011; 3:100ra89.
[166] Gainza G, Villullas S, Pedraz JL, Hernandez RM, Igartua M. Advances in drug delivery systems (DDSs) to release growth factors for wound healing and skin regeneration. Nanomedicine 2015; 11:1551-73.
[167] Brown GL, Curtsinger LJ, White M, Mitchell RO, Pietsch J, Nordquist R, et al. Acceleration of tensile strength of incisions treated with EGF and TGF-beta. Annals of surgery 1988; 208:788-94.
[168] Berlanga J, Fernandez JI, Lopez E, Lopez PA, del Rio A, Valenzuela C, et al. Heberprot-P: a novel product for treating advanced diabetic foot ulcer. MEDICC review 2013; 15:11-5.
[169] Schneider MR, Antsiferova M, Feldmeyer L, Dahlhoff M, Bugnon P, Hasse S, et al. Betacellulin regulates hair follicle development and hair cycle induction and enhances angiogenesis in wounded skin. Journal of investigative dermatology 2008; 128:1256-65.
[170] Yu A, Niiyama H, Kondo S, Yamamoto A, Suzuki R, Kuroyanagi Y. Wound dressing composed of hyaluronic acid and collagen containing EGF or bFGF: comparative culture study. Journal of biomaterials science Polymer edition 2013; 24:1015-26.
[171] Xie Z, Paras CB, Weng H, Punnakitikashem P, Su LC, Vu K, et al. Dual growth factor releasing multi-functional nanofibers for wound healing. Acta biomaterialia 2013; 9:9351-9.
[172] Elcin YM, Dixit V, Gitnick G. Extensive in vivo angiogenesis following controlled release of human vascular endothelial cell growth factor: implications for tissue engineering and wound healing. Artificial organs 2001; 25:558-65.
[173] Goldman R. Growth factors and chronic wound healing: past, present, and future. Advances in skin & wound care 2004; 17:24-35.
[174] Penn JW, Grobbelaar AO, Rolfe KJ. The role of the TGF-beta family in wound healing, burns and scarring: a review. International journal of burns and trauma 2012; 2:18-28.

[175] auf demKeller U, Krampert M, Kumin A, Braun S, Werner S. Keratinocyte growth factor: effects on keratinocytes and mechanisms of action. European journal of cell biology 2004; 83:607-12.
[176] Valente S, Ciavarella C, Pasanisi E, Ricci F, Stella A, Pasquinelli G. Hepatocyte growth factor effects on mesenchymal stem cells derived from human arteries: a novel strategy to accelerate vascular ulcer wound healing. Stem cells international 2016; 2016:3232859.
[177] Kim DS, Cho HJ, Yang SK, Shin JW, Huh CH, Park KC. Insulin-like growth factor-binding protein contributes to the proliferation of less proliferative cells in forming skin equivalents. Tissue engineering Part A 2009; 15:1075-80.
[178] Cianfarani F, Zambruno G, Brogelli L, Sera F, Lacal PM, Pesce M, et al. Placenta growth factor in diabetic wound healing: altered expression and therapeutic potential. The American journal of pathology 2006; 169:1167-82.
[179] Zhang Y, Hu X, Tian R, Wei W, Hu W, Chen X, et al. Angiopoietin-related growth factor (AGF) supports adhesion, spreading, and migration of keratinocytes, fibroblasts, and endothelial cells through interaction with RGD-binding integrins. Biochemical and biophysical research communications 2006; 347:100-8.
[180] Shi X, Wang L, Clark JD, Kingery WS. Keratinocytes express cytokines and nerve growth factor in response to neuropeptide activation of the ERK1/2 and JNK MAPK transcription pathways. Regulatory peptides 2013; 186:92-103.
[181] Hu X, Sun H, Han C, Wang X, Yu W. Topically applied rhGM-CSF for the wound healing: a systematic review. Burns 2011; 37:729-41.
[182] Schneider A, Wang XY, Kaplan DL, Garlick JA, Egles C. Biofunctionalized electrospun silk mats as a topical bioactive dressing for accelerated wound healing. Acta biomaterialia 2009; 5:2570-8.
[183] Choi JK, Jang J-H, Jang W-H, Kim J, Bae I-H, Bae J, et al. The effect of epidermal growth factor (EGF) conjugated with low-molecular-weight protamine (LMWP) on wound healing of the skin. Biomaterials 2012; 33:8579-90.
[184] Greenhalgh DG, Sprugel KH, Murray MJ, Ross R. PDGF and FGF stimulate wound healing in the genetically diabetic mouse. American journal of pathology 1990; 136:1235-46.
[185] LeGrand EK. Preclinical promise of becaplermin (rhPDGF-BB) in wound healing. American journal of surgery 1998; 176:48S-54S.
[186] Pierre EJ, Perez-Polo JR, Mitchell AT, Matin S, Foyt HL, Herndon DN. Insulin-like growth factor-I liposomal gene transfer and systemic growth hormone stimulate wound healing. The Journal of burn care & rehabilitation 1997; 18:287-91.
[187] Tateshita T, Ono I, Kaneko F. Effects of collagen matrix containing transforming growth factor (TGF)-beta(1) on wound contraction. Journal of dermatological science 2001; 27:104-13.
[188] Haik J, Kornhaber R, Blal B, Harats M. The feasibility of a handheld electrospinning device for the application of nanofibrous wound dressings. Advances in wound care 2017; 6:166-74.

[189] Sofokleous P, Stride E, Bonfield W, Edirisinghe M. Design, construction and performance of a portable handheld electrohydrodynamic multi-needle spray gun for biomedical applications. Materials science and engineering: C 2013; 33:213-23.
[190] Xu, SC, Qin CC, Yu M, Dong RH, Yan X, Zhao H, et al. A battery-operated portable handheld electrospinning apparatus. Nanoscale 2015; 7:12351-55.
[191] Veazey WS, Anusavice KJ, Moore K. Mammalian cell delivery via aerosol deposition. Journal of biomedical materials research B applied biomaterials 2005; 72:334-38.
[192] Esteban-Vives R, Young MT, Zhu T, Beiriger J, Pekor C, Ziembicki J, et al. Calculations for reproducible autologous skin cell-spray grafting. Burns 2016; 42:1756-1765.
[193] Duncan CO, Shelton RM, Navsaria H, Balderson DS, Papini RPG, Barralet JE. In vitro transfer of keratinocytes: comparison of transfer from fibrin membrane and delivery by aerosol spray. Journal of biomedical materials research B applied biomaterials 2005; 73:221-28.
[194] Martin YH, Jubin K, Smalley S, Wong JPF, Brown RA, Metcalfe AD. A novel system for expansion and delivery of human keratinocytes for the treatment of severe cutaneous injuries using microcarriers and compressed collagen. Journal of tissue engineering and regenerative medicine 2017; 11:3124-33.
[195] Devalliere J, Chang WG, Andrejecsk JW, Abrahimi P, Cheng CJ, Jane-wit D, et al. Sustained delivery of proangiogenic microRNA-132 by nanoparticle transfection improves endothelial cell transplantation. The journal of the federation of American societies for experimental biology 2014; 28:908-22.
[196] Castellano D, Sanchis A, Blanes M, Pérez Del Caz MD, Ruiz-Saurí A, Piquer-Gil M, et al. Electrospun poly(hydroxybutyrate) scaffolds promote engraftment of human skin equivalents via macrophage M2 polarization and angiogenesis. Journal of tissue engineering and regenerative medicine 2018; 12:e983-e994.
[197] Eaton KV, Yang HL, Giachelli CM, Scatena M. Engineering macrophages to control the inflammatory response and angiogenesis. Experimental cell research 2015; 339:300-09.
[198] Ellis S, Lin EJ, Tartar D. Immunology of wound healing. Current dermatology reports 2018; 7:350-58.
[199] Xuguang L, Dai Y, Shen T, Gao C. Induced migration of endothelial cells into 3D scaffolds by chemoattractants secreted by pro-inflammatory macrophages in situ. Regenerative biomaterials 2017; 4:139-48.
[200] Lisovsky A, Chamberlain MD, Wells LA, Sefton MV. Cell interactions with vascular regenerative MAA-based materials in the context of wound healing. Advanced healthcare materials 2015; 4:2375-87.
[201] Shen YI, Cho H, Papa AE, Burke JA, Chan XY, Duh EJ, et al. Engineered human vascularized constructs accelerate diabetic wound healing. Biomaterials 2016; 102:107-19.
[202] Klar AS, Güven S, Biedermann T, Luginbühl J, Böttcher-Haberzeth S, Meuli-Simmen C, et al. Tissue-engineered dermo-epidermal skin grafts prevascularized with adipose-derived cells. Biomaterials 2014; 35:5065-78.

[203] van Dongen JA, Stevens HP, Parvizi M, van der Lei B, Harmsen MC. The fractionation of adipose tissue procedure to obtain stromal vascular fractions for regenerative purposes. Wound repair and regeneration 2016; 24:994-1003.
[204] Klar AS, Güven S, Zimoch J, Zapiórkowska NA, Biedermann T, Böttcher-Haberzeth S, et al. Characterization of vasculogenic potential of human adipose-derived endothelial cells in a three-dimensional vascularized skin substitute. Pediatric surgery international 2016; 32:17-27.
[205] Seavey JG, Masters ZA, Balazs GC, Tintle SM, Sabino J, Fleming ME, et al. Use of a bioartificial dermal regeneration template for skin restoration in combat casualty injuries. Regenerative medicine 2016; 11:81-90.
[206] Lagus H, Sarlomo-Rikala M, Böhling T, Vuola J. Prospective study on burns treated with Integra®, a cellulose sponge and split thickness skin graft: comparative clinical and histological study-randomized controlled trial. Burns 2013; 39:1577-87.
[207] Nicoletti G, Brenta F, Bleve M, Pellegatta T, Malovini A, Faga A, et al. Long-term in vivo assessment of bioengineered skin substitutes: a clinical study. Journal of tissue engineering and regenerative medicine 2015; 9:460-68.
[208] Harding K, Sumner M, Cardinal M. A prospective, multicentre, randomised controlled study of human fibroblast-derived dermal substitute (Dermagraft) in patients with venous leg ulcers. International wound journal 2013; 10:132-37.
[209] Caputo WJ, Vaquero C, Monterosa A, Monterosa P, Johnson E, Beggs D, et al. A retrospective study of cryopreserved umbilical cord as an adjunctive therapy to promote the healing of chronic, complex foot ulcers with underlying osteomyelitis. Wound repair and regeneration 2016; 24:885-93.
[210] Lavery LA, Fulmer J, Shebetka KA, Regulski M, Vayser D, Fried D, et al. Grafix diabetic foot ulcer study group, the efficacy and safety of Grafix(®) for the treatment of chronic diabetic foot ulcers: results of a multi-centre, controlled, randomised, blinded, clinical trial. International wound journal 2014; 11:554-60.
[211] Löndahl M, Tarnow L, Karlsmark T, Lundquist R, Nielsen AM, Michelsen M, et al. Use of an autologous leucocyte and platelet-rich fibrin patch on hard-to-heal DFUs: a pilot study. Journal of wound care 2015; 24:172-74.
[212] Towler MA, Rush EW, Richardson MK, Williams CL. Randomized, prospective, blinded-enrollment, head-to-head venous leg ulcer healing trial comparing living, bioengineered skin graft substitute (Apligraf) with living, cryopreserved, human skin allograft (TheraSkin). Clinics in podiatric medicine and surgery 2018; 35:357–65.
[213] Widhe M, Johansson J, Hedhammar M, Rising A. Current progress and limitations of spider silk for biomedical applications. Biopolymers 2012; 97:468-78.
[214] Gupta AK, Mita K, Arunkumar KP, Nagaraju J. Molecular architecture of silk fibroin of Indian golden silkmoth, Antheraea assama. Scientific reports 2015; 5:12706.
[215] Rockwood DN, Preda RC, Yucel T, Wang X, Lovett ML, Kaplan DL. Materials fabrication from Bombyx mori silk fibroin. Nature protocols 2011; 6:1612-31.
[216] Inoue S, Tanaka K, Arisaka F, Kimura S, Ohtomo K, Mizuno S. Silk fibroin of Bombyx mori is secreted, assembling a high molecular mass elementary unit consisting of H-chain, L-chain, and P25, with a 6:6:1 molar ratio. The Journal of biological chemistry 2000; 275:40517-28.

[217] Konwarh R, Gupta P, Mandal BB. Silk-microfluidics for advanced biotechnological applications: a progressive review. Biotechnology advances 2016; 34:845-58.
[218] Zhou Z, Zhang S, Cao Y, Marelli B, Xia X, Tao TH. Engineering the future of silk materials through advanced manufacturing. Advanced materials 2018; 30:1706983.
[219] Kim UJ, Park J, Li C, Jin HJ, Valluzzi R, Kaplan DL. Structure and properties of silk hydrogels. Biomacromolecules 2004; 5:786-92.
[220] McGill M, Coburn JM, Partlow BP, Mu X, Kaplan DL. Molecular and macro-scale analysis of enzyme-crosslinked silk hydrogels for rational biomaterial design. Acta biomaterialia 2017; 63:76-84.
[221] Matsumoto A, Chen J, Collette AL, Kim UJ, Altman GH, Cebe P, et al. Mechanisms of silk fibroin sol-gel transitions. The journal of physical chemistry B 2006; 110:21630-8.
[222] Wang X, Kluge JA, Leisk GG, Kaplan DL. Sonication-induced gelation of silk fibroin for cell encapsulation. Biomaterials 2008; 29:1054-64.
[223] Yucel T, Cebe P, Kaplan DL. Vortex-induced injectable silk fibroin hydrogels. Biophysical journal 2009; 97:2044-50.
[224] Leisk GG, Lo TJ, Yucel T, Lu Q, Kaplan DL. Electrogelation for protein adhesives. Advanced materials 2010; 22:711-5.
[225] Pei Y, Liu X, Liu S, Lu Q, Liu J, Kaplan DL, et al. A mild process to design silk scaffolds with reduced beta-sheet structure and various topographies at the nanometer scale. Acta biomaterialia 2015; 13:168-76.
[226] Gupta P, Kumar M, Bhardwaj N, Kumar JP, Krishnamurthy CS, Nandi SK, et al. Mimicking form and function of native small diameter vascular conduits using mulberry and non-mulberry patterned silk films. ACS applied materials & interfaces 2016; 8:15874-88.
[227] Mandal BB, Kundu SC. A novel method for dissolution and stabilization of non-mulberry silk gland protein fibroin using anionic surfactant sodium dodecyl sulfate. Biotechnology and bioengineering 2008; 99:1482-9.
[228] Bratzel G, Buehler MJ. Sequence-structure correlations in silk: poly-ala repeat of N. clavipes MaSp1 is naturally optimized at a critical length scale. Journal of the mechanical behavior of biomedical materials 2012; 7:30-40.
[229] Kluge JA, Rabotyagova O, Leisk GG, Kaplan DL. Spider silks and their applications. Trends in biotechnology 2008; 26:244-51.
[230] Tokareva O, Jacobsen M, Buehler M, Wong J, Kaplan DL. Structure–function–property–design interplay in biopolymers: spider silk. Acta biomaterialia 2014; 10:1612-26.
[231] Schacht K, Scheibel T. Processing of recombinant spider silk proteins into tailor-made materials for biomaterials applications. Current opinion in biotechnology 2014; 29:62-9.
[232] Lewis R. Unraveling the weave of spider silk: one of nature's wondrous chemical structures is being dissected so that it can be used in human inventions. BioScience 1996; 46:636-8.

[233] Zheng K, Ling S. De novo design of recombinant spider silk proteins for material applications. Biotechnology journal 2019; 14:1700753.
[234] Lazaris A, Arcidiacono S, Huang Y, Zhou JF, Duguay F, Chretien N, et al. Spider silk fibers spun from soluble recombinant silk produced in mammalian cells. Science 2002; 295:472-76.
[235] Widhe M, Johansson U, Hillerdahl CO, Hedhammar M. Recombinant spider silk with cell binding motifs for specific adherence of cells. Biomaterials 2013; 34:8223-34.
[236] Thatikonda N, Nilebäck L, Kempe A, Widhe M, Hedhammar M. Bioactivation of spider silk with basic fibroblast growth factor for in vitro cell culture: a step toward creation of artificial ECM. ACS biomaterials science & engineering 2018; 4:3384-96.
[237] Nilebäck L, Hedin J, Widhe M, Floderus LS, Krona A, Bysell H, et al. Self-assembly of recombinant silk as a strategy for chemical-free formation of bioactive coatings: a real-time study. Biomacromolecules 2017; 18:846-54.
[238] Zhang W, Chen L, Chen J, Wang L, Gui X, Ran J, et al. Silk fibroin biomaterial shows safe and effective wound healing in animal models and a randomized controlled clinical trial. Advanced healthcare materials 2017; 6.
[239] Guan G, Bai L, Zuo B, Li M, Wu Z, Li Y, et al. Promoted dermis healing from full-thickness skin defect by porous silk fibroin scaffolds (PSFSs). Bio-medical materials and engineering 2010; 20:295-308.
[240] Lu G, Ding Z, Wei Y, Lu X, Lu Q, Kaplan DL. Anisotropic biomimetic silk scaffolds for improved cell migration and healing of skin wounds. ACS applied materials & interfaces 2018; 10:44314-23.
[241] Yu K, Lu F, Li Q, Zou Y, Xiao Y, Lu B, et al. Accelerated wound-healing capabilities of a dressing fabricated from silkworm cocoon. International journal of biological macromolecules 2017; 102:901-13.
[242] Kawabata S, Kanda N, Hirasawa Y, Noda K, Matsuura Y, Suzuki S, et al. The utility of silk-elastin hydrogel as a new material for wound healing. Plastic and reconstructive surgery 2018; 6:e1778.
[243] Ju HW, Lee OJ, Lee JM, Moon BM, Park HJ, Park YR, et al. Wound healing effect of electrospun silk fibroin nanomatrix in burn-model. International journal of biological macromolecules 2016; 85:29-39.
[244] Seo SR, Lee MS, So BP, Kim JC. In vivo pressure sore-healing efficacy of beta-cyclodextrin/polyethyleneimine/silk fibroin xerogel. International journal of dermatology 2012; 51:987-95.
[245] Kim MK, Yoo KY, Kwon KJ, Kim SG, Park YW, Lee KG, et al. Powdered wound dressing materials made from wild silkworm Antheraea pernyi silk fibroin on full-skin thickness burn wounds on rats. Maxillofacial plastic and reconstructive surgery 2014; 36:111-5.
[246] Setooni Z, Mohammadi M, Hashemi A, Hashemi M, Mozafari F, Simi F, et al. Evaluation of wound dressing made from spider silk protein using in a rabbit model. The international journal of lower extremity wounds 2018; 17:71-7.
[247] Liebsch C, Bucan V, Menger B, Kohne F, Waldmann KH, Vaslaitis D, et al. Preliminary investigations of spider silk in wounds in vivo - implications for an innovative wound dressing. Burns 2018; 44:1829-38.

[248] Kundu B, Rajkhowa R, Kundu SC, Wang X. Silk fibroin biomaterials for tissue regenerations. Advanced drug delivery reviews 2013; 65:457-70.
[249] Wenk E, Merkle HP, Meinel L. Silk fibroin as a vehicle for drug delivery applications. Journal of controlled release 2011; 150:128-41.
[250] Bhunia BK, Kaplan DL, Mandal BB. Silk-based multilayered angle-ply annulus fibrosus construct to recapitulate form and function of the intervertebral disc. Proceedings of the national academy of sciences of the United States of America 2018; 115:477-82.
[251] Chiarini A, Freddi G, Liu D, Armato U, Dal Pra I. Biocompatible silk noil-based three-dimensional carded-needled nonwoven scaffolds guide the engineering of novel skin connective tissue. Tissue engineering Part A 2016; 22:1047-60.
[252] Kundu B, Schlimp CJ, Nürnberger S, Redl H, Kundu SC. Thromboelastometric and platelet responses to silk biomaterials. Scientific reports 2014; 4:4945.
[253] Pignatelli C, Perotto G, Nardini M, Cancedda R, Mastrogiacomo M, Athanassiou A. Electrospun silk fibroin fibers for storage and controlled release of human platelet lysate. Acta biomaterialia 2018; 73:365-76.
[254] Martinez-Mora C, Mrowiec A, Garcia-Vizcaino EM, Alcaraz A, Cenis JL, Nicolas FJ. Fibroin and sericin from Bombyx mori silk stimulate cell migration through upregulation and phosphorylation of c-Jun. PloS one 2012; 7:e42271.
[255] Park YR, Sultan MT, Park HJ, Lee JM, Ju HW, Lee OJ, et al. NF-kappaB signaling is key in the wound healing processes of silk fibroin. Acta biomaterialia 2018; 67:183-95.
[256] Li AB, Kluge JA, Guziewicz NA, Omenetto FG, Kaplan DL. Silk-based stabilization of biomacromolecules. Journal of controlled release 2015; 219:416-30.
[257] Zhang J, Pritchard E, Hu X, Valentin T, Panilaitis B, Omenetto FG, et al. Stabilization of vaccines and antibiotics in silk and eliminating the cold chain. Proceedings of the national academy of sciences of the United States of America 2012; 109:11981-6.
[258] Tsioris K, Raja WK, Pritchard EM, Panilaitis B, Kaplan DL, Omenetto FG. Fabrication of silk microneedles for controlled-release drug delivery. Advanced functional materials 2012; 22:330-5.
[259] Hu X, Kaplan D, Cebe P. Determining beta-sheet crystallinity in fibrous proteins by thermal analysis and infrared spectroscopy. Macromolecules 2006; 39:6161-70.
[260] Hines DJ, Kaplan DL. Mechanisms of controlled release from silk fibroin films. Biomacromolecules 2011; 12:804-12.
[261] Singer AJ, Clark RAF. Cutaneous wound healing. New England journal of medicine 1999; 341:738-46.
[262] Stevens MM, George JH. Exploring and engineering the cell surface interface. Science 2005; 310:1135.
[263] Abrigo M, McArthur SL, Kingshott P. Electrospun nanofibers as dressings for chronic wound care: advances, challenges, and future prospects. Macromolecular bioscience 2014; 14:772-92.
[264] Sood A, Granick MS, Tomaselli NL. Wound dressings and comparative effectiveness data. Advances in wound care 2013; 3:511-29.

[265] Bygd HC, Akilbekova D, Muñoz A, Forsmark KD, Bratlie KM. Poly-l-arginine based materials as instructive substrates for fibroblast synthesis of collagen. Biomaterials 2015; 63:47-57.
[266] Schultz GS, Sibbald RG, Falanga V, Ayello EA, Dowsett C, Harding K, et al. Wound bed preparation: a systematic approach to wound management. Wound repair and regeneration 2003; 11:S1-S28.
[267] Eliopoulos GM, Gardella A, Moellering RC. In vitro activity of ciprofloxacin, a new carboxyquinoline antimicrobial agent. Antimicrobial agents and chemotherapy 1984; 25:331.
[268] Jeong L, Lee KY, Liu JW, Park WH. Time-resolved structural investigation of regenerated silk fibroin nanofibers treated with solvent vapor. International journal of biological macromolecules 2006; 38:140-4.
[269] Boyle VJ, Fancher ME, Ross RW. Rapid, modified Kirby-Bauer susceptibility test with single, high-concentration antimicrobial disks. Antimicrobial agents and chemotherapy 1973; 3:418.
[270] Goldner J. A modification of the masson trichrome technique for routine laboratory purposes. The American journal of pathology 1938; 14:237-43.
[271] Proctor GB, Horobin RW. Chemical structures and staining mechanisms of Weigert'S Resorcin-Fuchsin and related elastic fiber stains. Stain Technology 1988; 63:101-11.
[272] Gridley MF. A modification of the silver impregnation method of staining reticular fibers. American journal of clinical pathology 1951; 21:897-9.
[273] Wang Q, Jin Y, Deng X, Liu H, Pang H, Shi P, et al. Second-harmonic generation microscopy for assessment of mesenchymal stem cell-seeded acellular dermal matrix in wound-healing. Biomaterials 2015; 53:659-68.
[274] van Zuijlen PPM, Ruurda JJB, van Veen HA, van Marle J, van Trier AJM, Groenevelt F, et al. Collagen morphology in human skin and scar tissue: no adaptations in response to mechanical loading at joints. Burns 2003; 29:423-31.
[275] Shankhwar N, Kumar M, Mandal BB, Robi PS, Srinivasan A. Electrospun polyvinyl alcohol-polyvinyl pyrrolidone nanofibrous membranes for interactive wound dressing application. Journal of Biomaterials Science, Polymer Edition 2016; 27:247-62.
[276] Coates J. Interpretation of infrared spectra, a practical approach: in encyclopedia of analytical chemistry, John Wiley & Sons, Ltd, 2006.
[277] Asakura T, Tanaka C, Yang M, Yao J, Kurokawa M. Production and characterization of a silk-like hybrid protein, based on the polyalanine region of Samia cynthia ricini silk fibroin and a cell adhesive region derived from fibronectin. Biomaterials 2004; 25:617-24.
[278] Queen D, Gaylor JDS, Evans JH, Courtney JM, Reid WH. The preclinical evaluation of the water vapour transmission rate through burn wound dressings. Biomaterials 1987; 8:367-71.
[279] Meinel L, Hofmann S, Karageorgiou V, Kirker-Head C, McCool J, Gronowicz G, et al. The inflammatory responses to silk films in vitro and in vivo. Biomaterials 2005; 26:147-55.

[280] Kobayashi M, Chang Y-S, Oka M. A two year in vivo study of polyvinyl alcohol-hydrogel (PVA-H) artificial meniscus. Biomaterials 2005; 26:3243-8.
[281] Luo Q, Chen Z, Hao X, Zhu Q, Zhou Y. Preparation and properties of nanometer silk fibroin peptide/polyvinyl alcohol blend films for cell growth. International journal of biological macromolecules 2013; 61:135-41.
[282] Rho KS, Jeong L, Lee G, Seo B-M, Park YJ, Hong S-D, et al. Electrospinning of collagen nanofibers: Effects on the behavior of normal human keratinocytes and early-stage wound healing. Biomaterials 2006; 27:1452-61.
[283] Xu R, Luo G, Xia H, He W, Zhao J, Liu B, et al. Novel bilayer wound dressing composed of silicone rubber with particular micropores enhanced wound re-epithelialization and contraction. Biomaterials 2015; 40:1-11.
[284] Dado D, Sagi M, Levenberg S, Zemel A. Mechanical control of stem cell differentiation. Regenerative medicine 2011; 7:101-16.
[285] Geerligs M, van Breemen L, Peters G, Ackermans P, Baaijens F, Oomens C. In vitro indentation to determine the mechanical properties of epidermis. Journal of biomechanics 2011; 44:1176-81.
[286] Chiellini E, Corti A, Del Sarto G, D'Antone S. Oxo-biodegradable polymers – effect of hydrolysis degree on biodegradation behaviour of poly(vinyl alcohol). Polymer degradation and stability 2006; 91:3397-406.
[287] Horan RL, Antle K, Collette AL, Wang Y, Huang J, Moreau JE, et al. In vitro degradation of silk fibroin. Biomaterials 2005; 26:3385-93.
[288] Fonder MA, Lazarus GS, Cowan DA, Aronson-Cook B, Kohli AR, Mamelak AJ. Treating the chronic wound: a practical approach to the care of nonhealing wounds and wound care dressings. Journal of the American academy of dermatology 2008; 58:185-206.
[289] Schunck M, Neumann C, Proksch E. Artificial barrier repair in wounds by semi-occlusive foils reduced wound contraction and enhanced cell migration and reepithelization in mouse skin. Journal of investigative dermatology 2005; 125:1063-71.
[290] Mi F-L, Shyu S-S, Wu Y-B, Lee S-T, Shyong J-Y, Huang R-N. Fabrication and characterization of a sponge-like asymmetric chitosan membrane as a wound dressing. Biomaterials 2001; 22:165-73.
[291] Kong HH, Segre JA. Skin microbiome: looking back to move forward. Journal of investigative dermatology 2012; 132:933-9.
[292] Smith SM, Eng RH. Activity of ciprofloxacin against methicillin-resistant Staphylococcus aureus. Antimicrobial agents and chemotherapy 1985; 27:688.
[293] Marchesan S, Qu Y, Waddington LJ, Easton CD, Glattauer V, Lithgow TJ, et al. Self-assembly of ciprofloxacin and a tripeptide into an antimicrobial nanostructured hydrogel. Biomaterials 2013; 34:3678-87.
[294] Huang R, Li W, Lv X, Lei Z, Bian Y, Deng H, et al. Biomimetic LBL structured nanofibrous matrices assembled by chitosan/collagen for promoting wound healing. Biomaterials 2015; 53:58-75.
[295] Tanaka T, Magoshi J, Magoshi Y, ichi Inoue S, Kobayashi M, Tsuda H, et al. Thermal properties of bombyx mori and several wild silkworm silks phase transition of liquid silk. Journal of thermal analysis and calorimetry 2002; 70:825-32.

[296] Trengove NJ, Stacey MC, Macauley S, Bennett N, Gibson J, Burslem F, et al. Analysis of the acute and chronic wound environments: the role of proteases and their inhibitors. Wound repair and regeneration 1999; 7:442-52.
[297] Gorouhi F, Shah NM, Krishna Raghunathan V, Mohabbati Y, Abbott NL, Isseroff RR, et al. Epidermal growth factor–functionalized polymeric multilayer films: interplay between spatial location and bioavailability of EGF. Journal of investigative dermatology 2014; 134:1757-60.
[298] Seeger MA, Paller AS. The roles of growth factors in keratinocyte migration. Advances in wound care 2014; 4:213-24.
[299] Bellis SL. Advantages of RGD peptides for directing cell association with biomaterials. Biomaterials 2011; 32:4205-10.
[300] Widhe M, Shalaly ND, Hedhammar M. A fibronectin mimetic motif improves integrin mediated cell biding to recombinant spider silk matrices. Biomaterials 2016; 74:256-66.
[301] Gailit J, Clark RAF. Wound repair in the context of extracellular matrix. Current opinion in cell biology 1994; 6:717-25.
[302] Gogoi D, Choudhury AJ, Chutia J, Pal AR, Khan M, Choudhury M, et al. Development of advanced antimicrobial and sterilized plasma polypropylene grafted muga (antheraea assama) silk as suture biomaterial. Biopolymers 2014; 101:355-65.
[303] Lutolf MP, Hubbell JA. Synthetic biomaterials as instructive extracellular microenvironments for morphogenesis in tissue engineering. Nature biotechnology 2005; 23:47.
[304] Godwin J, Kuraitis D, Rosenthal N. Extracellular matrix considerations for scar-free repair and regeneration: insights from regenerative diversity among vertebrates. The international journal of biochemistry & cell biology 2014; 56:47-55.
[305] Kim YS, Lew DH, Tark KC, Rah DK, Hong JP. Effect of recombinant human epidermal growth factor against cutaneous scar formation in murine full-thickness wound healing. Journal of Korean medical science 2010; 25:589-96.
[306] Heo YS, Song HJ. Characterizing cutaneous elastic fibers by eosin fluorescence detected by fluorescence microscopy. Annals of dermatology 2011; 23:44-52.
[307] Mimura Y, Ihn H, Jinnin M, Asano Y, Yamane K, Tamaki K. Epidermal growth factor affects the synthesis and degradation of type I collagen in cultured human dermal fibroblasts. Matrix biology 2006; 25:202-12.
[308] Ushiki T. Collagen fibers, reticular fibers and elastic fibers: a comprehensive understanding from a morphological viewpoint. Archives of histology and cytology 2002; 65:109-26.
[309] Urtreger A, Porro F, Puricelli L, Werbajh S, Baralle FE, Bal de Kier Joffé E, et al. Expression of RGD minus fibronectin that does not form extracellular matrix fibrils is sufficient to decrease tumor metastasis. International journal of cancer 1998; 78:233-41.
[310] Kulkarni M, O'Loughlin A, Vazquez R, Mashayekhi K, Rooney P, Greiser U, et al. Use of a fibrin-based system for enhancing angiogenesis and modulating inflammation in the treatment of hyperglycemic wounds. Biomaterials 2014; 35:2001-10.

[311] Carretero M, Escámez MJ, García M, Duarte B, Holguín A, Retamosa L, et al. In vitro and in vivo wound healing-promoting activities of human cathelicidin LL-37. Journal of investigative dermatology 2008; 128:223-36.
[312] Rayman G, Rayman A, Baker NR, Jurgeviciene N, Dargis V, Sulcaite R, et al. Sustained silver-releasing dressing in the treatment of diabetic foot ulcers. British journal of nursing 2005; 14:109-14.
[313] Lopez Barreiro D, Yeo J, Tarakanova A, Martin-Martinez FJ, Buehler MJ. Multiscale modeling of silk and silk-based biomaterials - a review. Macromolecular bioscience 2018:e1800253.
[314] Chouhan D, Chakraborty B, Nandi SK, Mandal BB. Role of non-mulberry silk fibroin in deposition and regulation of extracellular matrix towards accelerated wound healing. Acta biomaterialia 2017; 48:157-74.
[315] Liang C-C, Park AY, Guan J-L. In vitro scratch assay: a convenient and inexpensive method for analysis of cell migration in vitro. Nature protocols 2007; 2:329.
[316] Gomes AP, Mano JF, Queiroz JA, Gouveia IC. Incorporation of antimicrobial peptides on functionalized cotton gauzes for medical applications. Carbohydrate polymers 2015; 127:451-61.
[317] Merritt JH, Kadouri DE, O'Toole GA. Growing and analyzing static biofilms. Current protocols in microbiology 2011; 22:1B..-B..18.
[318] Dinis TM, Elia R, Vidal G, Auffret A, Kaplan DL, Egles C. Method to form a fiber/growth factor dual-gradient along electrospun silk for nerve regeneration. ACS applied materials & interfaces 2014; 6:16817-26.
[319] Mottola C, Mendes JJ, Cristino JM, Cavaco-Silva P, Tavares L, Oliveira M. Polymicrobial biofilms by diabetic foot clinical isolates. Folia microbiologica 2016; 61:35-43.
[320] Martin JM, Zenilman JM, Lazarus GS. Molecular microbiology: new dimensions for cutaneous biology and wound healing. Journal of investigative dermatology 2010; 130:38-48.
[321] Hu SC, Lan CE. High-glucose environment disturbs the physiologic functions of keratinocytes: focusing on diabetic wound healing. Journal of dermatological science 2016; 84:121-7.
[322] Stamenkovic I. Extracellular matrix remodelling: the role of matrix metalloproteinases. The journal of pathology 2003; 200:448-64.
[323] Simeon A, Monier F, Emonard H, Gillery P, Birembaut P, Hornebeck W, et al. Expression and activation of matrix metalloproteinases in wounds: modulation by the tripeptide-copper complex glycyl-L-histidyl-L-lysine-Cu2+. Journal of investigative dermatology 1999; 112:957-64.
[324] Muthukumar T, Anbarasu K, Prakash D, Sastry TP. Effect of growth factors and pro-inflammatory cytokines by the collagen biocomposite dressing material containing Macrotyloma uniflorum plant extract-in vivo wound healing. Colloids and surfaces B, biointerfaces 2014; 121:178-88.
[325] Stadelmann WK, Digenis AG, Tobin GR. Physiology and healing dynamics of chronic cutaneous wounds. American journal of surgery 1998; 176:26S-38S.

[326] Widhe M, Bysell H, Nystedt S, Schenning I, Malmsten M, Johansson J, et al. Recombinant spider silk as matrices for cell culture. Biomaterials 2010; 31:9575-85.
[327] Hedhammar M, Rising A, Grip S, Martinez AS, Nordling K, Casals C, et al. Structural properties of recombinant nonrepetitive and repetitive parts of major ampullate spidroin 1 from Euprosthenops australis: implications for fiber formation. Biochemistry 2008; 47:3407-17.
[328] Stark M, Grip S, Rising A, Hedhammar M, Engstrom W, Hjalm G, et al. Macroscopic fibers self-assembled from recombinant miniature spider silk proteins. Biomacromolecules 2007; 8:1695-701.
[329] Jansson R, Thatikonda N, Lindberg D, Rising A, Johansson J, Nygren P-Å, et al. Recombinant spider silk genetically functionalized with affinity domains. Biomacromolecules 2014; 15:1696-706.
[330] Gholipourmalekabadi M, Seifalian AM, Urbanska AM, Omrani MD, Hardy JG, Madjd Z, et al. 3D protein-based bilayer artificial skin for the guided scarless healing of third-degree burn wounds in vivo. Biomacromolecules 2018; 19:2409-22.
[331] Chouhan D, Janani G, Chakraborty B, Nandi SK, Mandal BB. Functionalized PVA-silk blended nanofibrous mats promote diabetic wound healing via regulation of extracellular matrix and tissue remodelling. Journal of tissue engineering and regenerative medicine 2018; 12:e1559-e70.
[332] Nileback L, Chouhan D, Jansson R, Widhe M, Mandal BB, Hedhammar M. Silk-silk interactions between silkworm fibroin and recombinant spider silk fusion proteins enable the construction of bioactive materials. ACS applied materials & interfaces 2017; 9:31634-44.
[333] Mehrotra S, Chouhan D, Konwarh R, Kumar M, Jadi PK, Mandal BB. A comprehensive review on silk at nanoscale for regenerative medicine and allied applications. ACS Biomaterials Science & Engineering 2019.
[334] Bhardwaj N, Singh YP, Devi D, Kandimalla R, Kotoky J, Mandal BB. Potential of silk fibroin/chondrocyte constructs of muga silkworm Antheraea assamensis for cartilage tissue engineering. Journal of materials chemistry B 2016; 4:3670-84.
[335] Janani G, Nandi SK, Mandal BB. Functional hepatocyte clusters on bioactive blend silk matrices towards generating bioartificial liver constructs. Acta biomaterialia 2018; 67:167-82.
[336] Harvey D, Bardelang P, Goodacre SL, Cockayne A, Thomas NR. Antibiotic spider silk: site-specific functionalization of recombinant spider silk using “click” chemistry. Advanced materials 2017; 29:1604245.
[337] Kumar M, Coburn J, Kaplan DL, Mandal BB. Immuno-informed 3D silk biomaterials for tailoring biological responses. ACS applied materials & interfaces 2016; 8:29310-22.
[338] Sobers CJ, Wood SE, Mrksich M. A gene expression-based comparison of cell adhesion to extracellular matrix and RGD-terminated monolayers. Biomaterials 2015; 52:385-94.
[339] James GA, Swogger E, Wolcott R, Pulcini Ed, Secor P, Sestrich J, et al. Biofilms in chronic wounds. Wound repair and regeneration 2008; 16:37-44.

[340] Costa F, Carvalho IF, Montelaro RC, Gomes P, Martins MCL. Covalent immobilization of antimicrobial peptides (AMPs) onto biomaterial surfaces. Acta biomaterialia 2011; 7:1431-40.
[341] Zasloff M. Antimicrobial peptides of multicellular organisms. Nature 2002; 415:389-95.
[342] Yeung ATY, Gellatly SL, Hancock REW. Multifunctional cationic host defence peptides and their clinical applications. Cellular and molecular life sciences 2011; 68:2161.
[343] Bellamy W, Takase M, Wakabayashi H, Kawase K, Tomita M. Antibacterial spectrum of lactoferricin B, a potent bactericidal peptide derived from the N-terminal region of bovine lactoferrin. The journal of applied bacteriology 1992; 73:472-9.
[344] Takayama Y, Aoki R. Roles of lactoferrin on skin wound healing. Biochemistry and cell biology 2012; 90:497-503.
[345] Gifford JL, Hunter HN, Vogel HJ. Lactoferricin. Cellular and molecular life sciences 2005; 62:2588.
[346] Clark RA, Tonnesen MG, Gailit J, Cheresh DA. Transient functional expression of alphaVbeta 3 on vascular cells during wound repair. The American journal of pathology 1996; 148:1407-21.
[347] Brooks PC, Clark RA, Cheresh DA. Requirement of vascular integrin alpha v beta 3 for angiogenesis. Science 1994; 264:569-71.
[348] Janani G, Nandi SK, Mandal BB. Functional hepatocyte clusters on bioactive blend silk matrices towards generating bioartificial liver constructs. Acta biomaterialia 2018; 67:167-82.
[349] Larouche D, Cuffley K, Paquet C, Germain L. Tissue-engineered skin preserving the potential of epithelial cells to differentiate into hair after grafting. Tissue engineering Part A 2011; 17:819-30.
[350] Yaffe MB, Murthy S, Eckert RL. Evidence that involucrin is a covalently linked constituent of highly purified cultured keratinocyte cornified envelopes. Journal of investigative dermatology 1993; 100:3-9.
[351] Wendt H, Hillmer A, Reimers K, Kuhbier JW, Schafer-Nolte F, Allmeling C, et al. Artificial skin-culturing of different skin cell lines for generating an artificial skin substitute on cross-weaved spider silk fibres. PloS one 2011; 6:e21833.
[352] Bhardwaj N, Chouhan D, Mandal BB. Tissue engineered skin and wound healing: current strategies and future directions. Current pharmaceutical design 2017; 23:3455-82.
[353] Zelen CM, Serena TE, Gould L, Le L, Carter MJ, Keller J, et al. Treatment of chronic diabetic lower extremity ulcers with advanced therapies: a prospective, randomised, controlled, multi-centre comparative study examining clinical efficacy and cost. International wound journal 2016; 13:272-82.
[354] Lenselink EA. Role of fibronectin in normal wound healing. International wound journal 2015; 12:313-6.
[355] Chouhan D, Thatikonda N, Nileback L, Widhe M, Hedhammar M, Mandal BB. Recombinant spider silk functionalized silkworm silk matrices as potential bioactive

wound dressings and skin grafts. ACS applied materials & interfaces 2018; 10:23560-72.
[356] Venter NG, Monte-Alto-Costa A, Marques RG. A new model for the standardization of experimental burn wounds. Burns 2015; 41:542-7.
[357] Baba A, Matsushita S, Kitayama K, Asakura T, Sezutsu H, Tanimoto A, et al. Silk fibroin produced by transgenic silkworms overexpressing the Arg-Gly-Asp motif accelerates cutaneous wound healing in mice. Journal of biomedical materials research Part B, applied biomaterials 2019; 107:97-103.
[358] Pereira AM, Machado R, da Costa A, Ribeiro A, Collins T, Gomes AC, et al. Silk-based biomaterials functionalized with fibronectin type II promotes cell adhesion. Acta biomaterialia 2017; 47:50-9.
[359] Kim S, Bell K, Mousa SA, Varner JA. Regulation of angiogenesis in vivo by ligation of integrin alpha5beta1 with the central cell-binding domain of fibronectin. The American journal of pathology 2000; 156:1345-62.
[360] Kular JK, Basu S, Sharma RI. The extracellular matrix: Structure, composition, age-related differences, tools for analysis and applications for tissue engineering. Journal of tissue engineering 2014; 5:2041731414557112.
[361] Lovell CR, Smolenski KA, Duance VC, Light ND, Young S, Dyson M. Type I and III collagen content and fibre distribution in normal human skin during ageing. The British journal of dermatology 1987; 117:419-28.
[362] Xue M, Jackson CJ. Extracellular matrix reorganization during wound healing and its impact on abnormal scarring. Advances in wound care 2015; 4:119-36.
[363] Hayakawa T, Hashimoto Y, Myokei Y, Aoyama H, Izawa Y. Changes in type of collagen during the development of human post-burn hypertrophic scars. Clinica chimica acta; international journal of clinical chemistry 1979; 93:119-25.
[364] Gauglitz GG, Korting HC, Pavicic T, Ruzicka T, Jeschke MG. Hypertrophic scarring and keloids: pathomechanisms and current and emerging treatment strategies. Molecular medicine 2011; 17:113-25.
[365] Silva JP, Dhall S, Garcia M, Chan A, Costa C, Gama M, et al. Improved burn wound healing by the antimicrobial peptide LLKKK18 released from conjugates with dextrin embedded in a carbopol gel. Acta biomaterialia 2015; 26:249-62.
[366] Wang Y, Beekman J, Hew J, Jackson S, Issler-Fisher AC, Parungao R, et al. Burn injury: challenges and advances in burn wound healing, infection, pain and scarring. Advanced drug delivery reviews 2018; 123:3-17.
[367] Shakespeare P. Burn wound healing and skin substitutes. Burns 2001; 27:517-22.
[368] Spotnitz WD. Fibrin sealant: the only approved hemostat, sealant, and adhesive-a laboratory and clinical perspective. ISRN surgery 2014; 2014:203943.
[369] Vig K, Chaudhari A, Tripathi S, Dixit S, Sahu R, Pillai S, et al. Advances in skin regeneration using tissue engineering. International journal of molecular sciences 2017; 18.
[370] Hop MJ, Polinder S, van der Vlies CH, Middelkoop E, van Baar ME. Costs of burn care: a systematic review. Wound repair and regeneration 2014; 22:436-50.
[371] Numata K, Katashima T, Sakai T. State of water, molecular structure, and cytotoxicity of silk hydrogels. Biomacromolecules 2011; 12:2137-44.

[372] Zhong J, Ma M, Li W, Zhou J, Yan Z, He D. Self-assembly of regenerated silk fibroin from random coil nanostructures to antiparallel beta-sheet nanostructures. Biopolymers 2014; 101:1181-92.
[373] Martinez FO, Gordon S. The M1 and M2 paradigm of macrophage activation: time for reassessment. F1000prime reports 2014; 6:13.
[374] Jiang D, Qi Y, Walker NG, Sindrilaru A, Hainzl A, Wlaschek M, et al. The effect of adipose tissue derived MSCs delivered by a chemically defined carrier on full-thickness cutaneous wound healing. Biomaterials 2013; 34:2501-15.
[375] Barros MH, Hauck F, Dreyer JH, Kempkes B, Niedobitek G. Macrophage polarisation: an immunohistochemical approach for identifying M1 and M2 macrophages. PloS one 2013; 8:e80908.
[376] Wang X, Partlow B, Liu J, Zheng Z, Su B, Wang Y, et al. Injectable silk-polyethylene glycol hydrogels. Acta biomaterialia 2015; 12:51-61.
[377] Volk SW, Wang Y, Mauldin EA, Liechty KW, Adams SL. Diminished type III collagen promotes myofibroblast differentiation and increases scar deposition in cutaneous wound healing. Cells, tissues, organs 2011; 194:25-37.

APPENDIX

APPENDIX

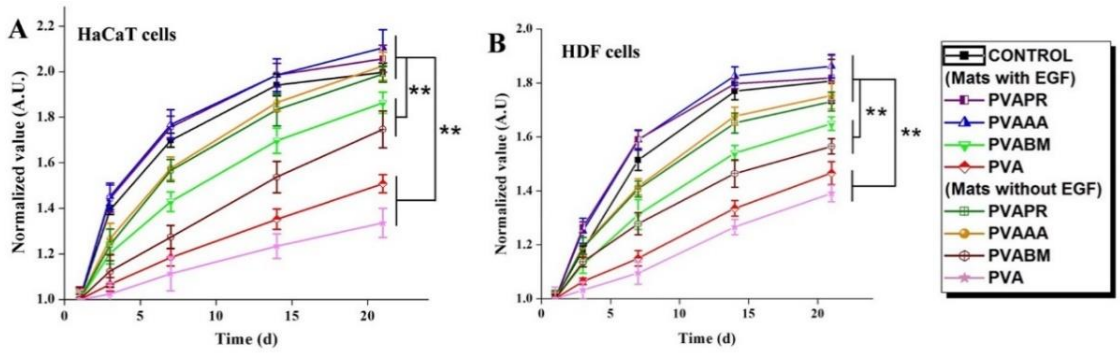

Figure A2.1. *(A, B) Proliferation profile of HaCaT and HDF cells on various mats (blank as well as functionalized) on day 21 respectively. Mats containing NMSF had significant difference with mulberry SF blend and PVA at* $p \leq 0.01$. *Functionalized hybrid mats showed higher cell proliferation compared to respective blank mats. (*p ≤ 0.05, **p ≤ 0.01).*

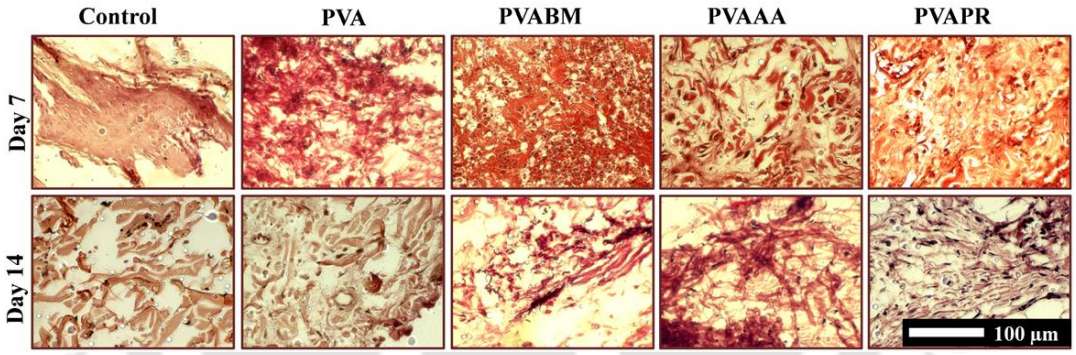

Figure A2.2. *Elastin fibres stained by Weigert Resorcin–Fuschin method in the dermal region of regenerated skin by various treatments on day 7 and day 14. Scale bar represents 100 µm.*

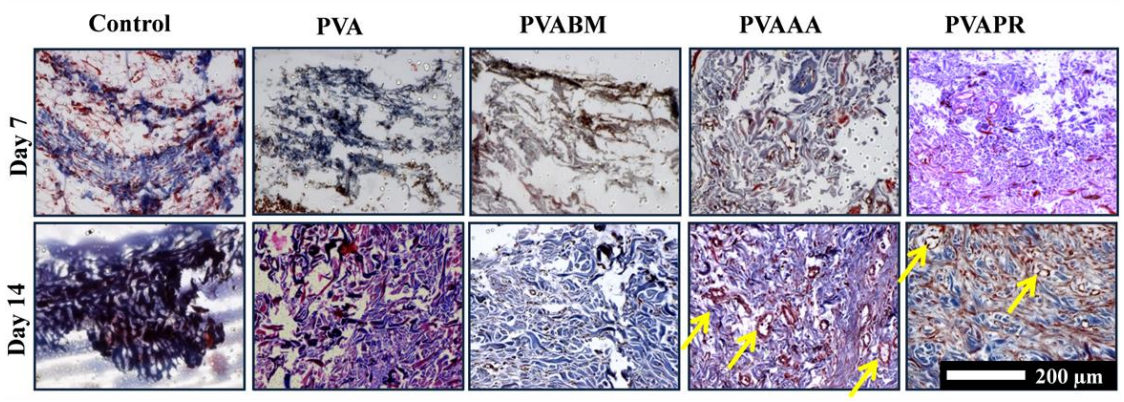

Figure A2.3. *Collagen fibres stained by Masson trichrome method in the dermal region of regenerated skin by various treatments on day 7 and day 14. Scale bar represents 200 µm. Yellow arrows represent blood vessels.*

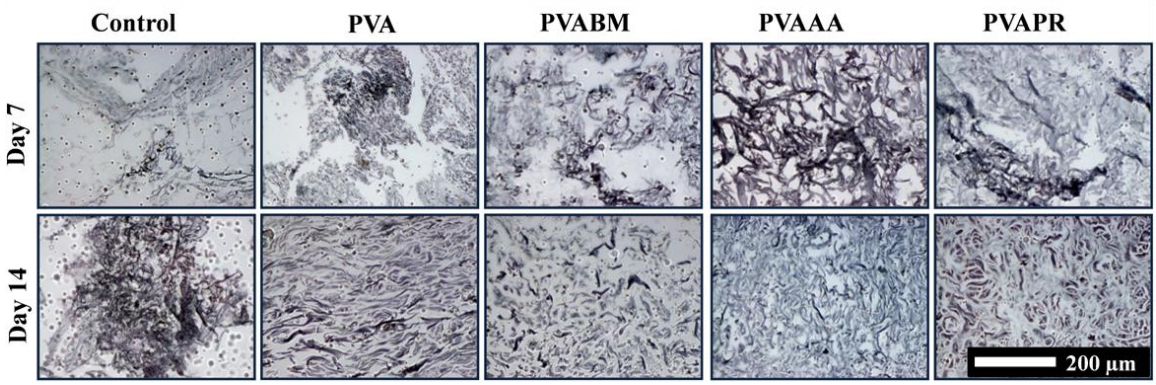

Figure A2.4. *Reticulin fibres stained by Gridley silver impregnation method in the dermal region of regenerated skin by various treatments on day 7 and day 14. Scale bar represents 200 µm.*

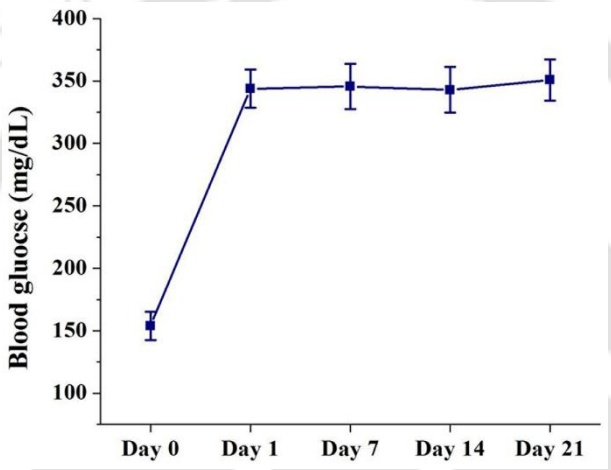

Figure A3.1. *Glucose levels of rabbits before (day 0) and after Alloxan induction (day 1, 7, 14 and 21) for making diabetic model.*

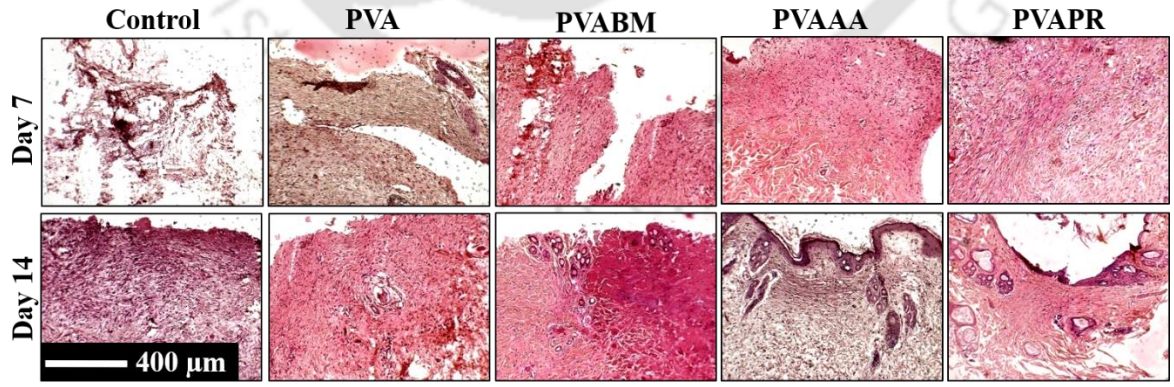

Figure A3.2. *Histological study of wound healing process by H & E stained sections on day 7 and 14 post wound creation in healthy rabbits.*

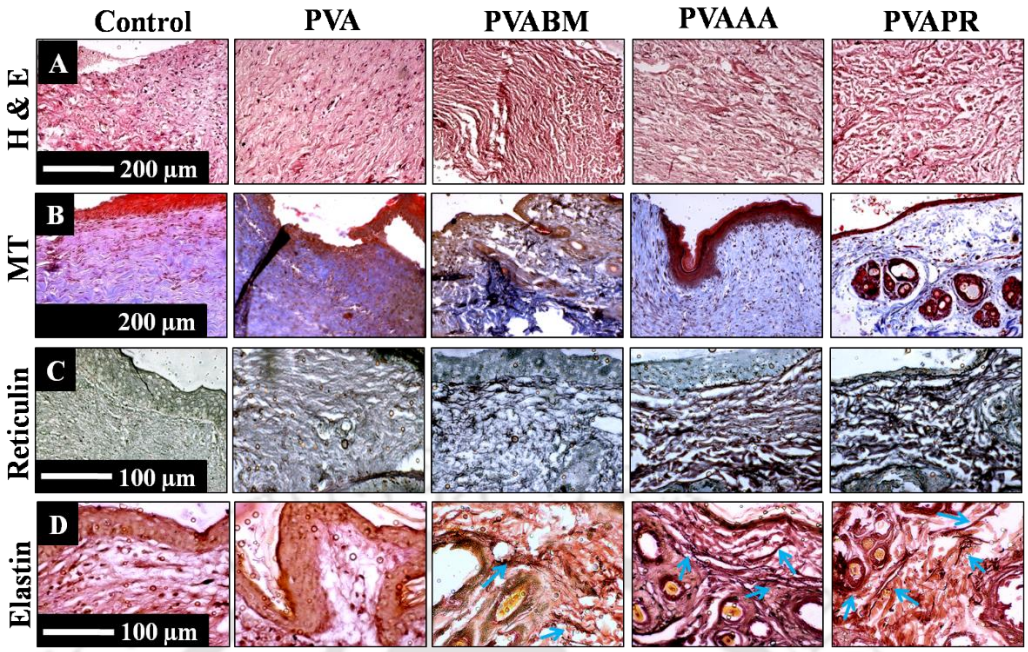

Figure A3.3. *(A) H & E stained sections of healed skin tissue showing matrix morphology in the dermal region of diabetic rabbits on day 28 post wounding. (B) Deposition of collagen bundles in wounds by Masson trichrome stain (C, D) Deposition of reticulin and elastin fibres in the regenerated skin of diabetic rabbits.*

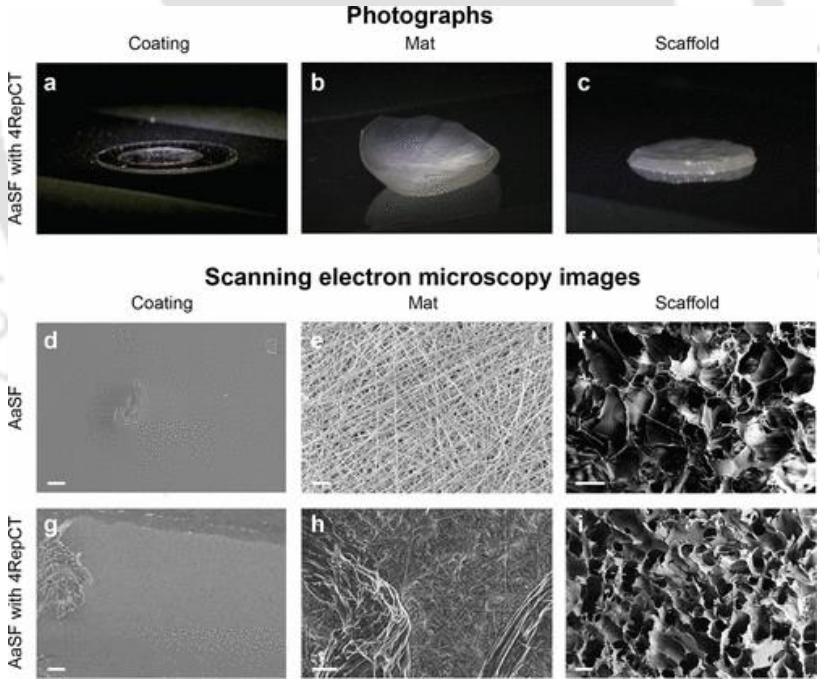

Figure A4.1. *Various formats of AaSF coated with 4RepCT. Photographs of AaSF as (a) coating (7 mm wide) on a circular coverslip, (b) electrospun mat (12 mm wide), and (c) microporous scaffold (6 mm wide) with 4RepCT top coating. SEM images of AaSF coating, electrospun mat, and microporous scaffold alone (d–f) and with 4RepCT top coating (g–i). Scale bars are 2 µm for coatings and mats and 100 µm for microporous scaffolds. (Reproduced with permission from [332] ©2018 American Chemical Society).*

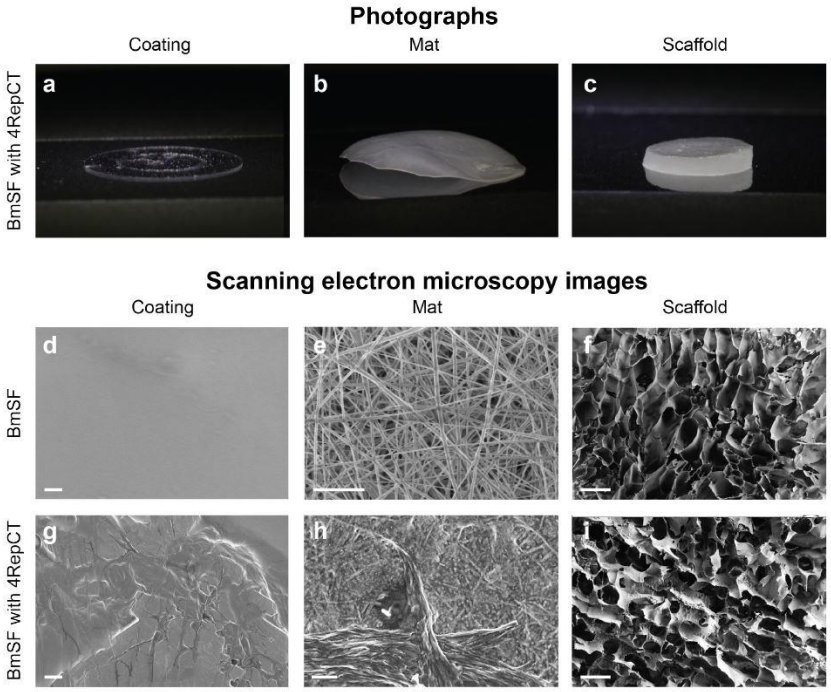

Figure A4.2. *Various formats of BmSF coated with 4RepCT. Photographs of BmSF coating on a circular cover slip (a), electrospun mat (b), and microporous scaffold (c) coated with 4RepCT. SEM images of BmSF coatings (d, g), electrospun mats (e, h), and microporous scaffolds (f, i) alone (d, e, f) and with 4RepCT top-coating (g, h, i). Scale bars are 2 μm for coatings and mats, and 100 μm for microporous scaffolds. Areas with occasional irregularities are shown for top-coated materials (g-i), which were otherwise similar to materials without top-coatings (d-f). (Reproduced with permission from [332] ©2018 American Chemical Society).*

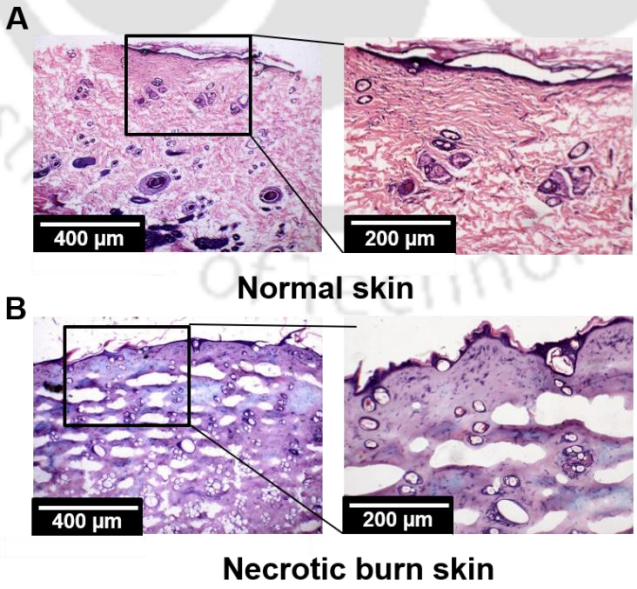

Figure A5.1. *Histological analysis by H & E staining: (A) Normal rat skin showing intact dermal and epidermal structures and (B) Necrotic burn skin after infliction of third degree burn on skin.*

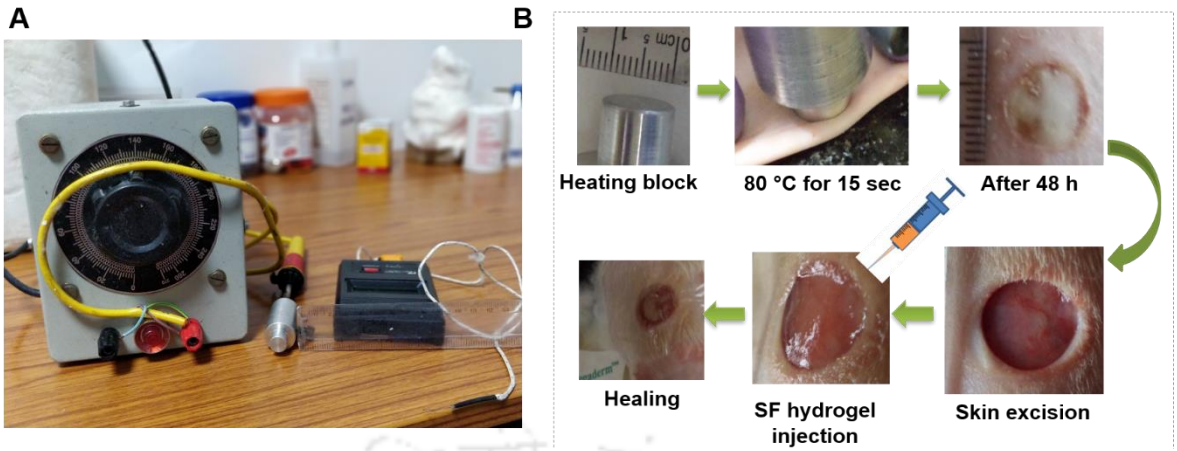

Figure A6.1. *(A) Image of the instrument designed for inflicting third degree burn on the rats. (B) Schematic representation depicting methodology of burn wound infliction and injecting SF hydrogel for wound healing application.*

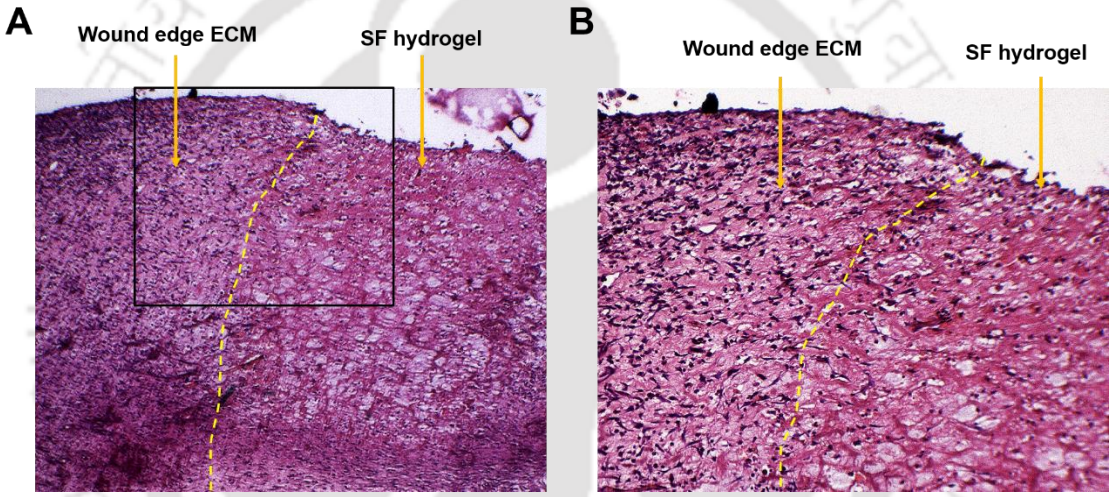

Figure A6.2. *H & E staining of tissue section depicting the interface between wound edge ECM and SF hydrogel after 3 days of application: (A) A clear demarcation between wound edge and SF hydrogel is visible in the tissue section. (B) Magnified image of the intersection between wound edge ECM and SF hydrogel.*

LIST OF PUBLICATIONS

List of Publications

Publications from Ph.D. Thesis:

(A) Journal Publications:

1. **Dimple Chouhan**, Tshewuzo-u Lohe, Pavan K. Samudrala, Biman B. Mandal. "In situ forming silk fibroin hydrogel promotes skin regeneration in full thickness burn wounds". *Advanced Healthcare Materials*, 2018; e1801092.
2. **Dimple Chouhan**, Janani Guru, Bijayashree Chakraborty, Samit K. Nandi, Biman B Mandal. "Functionalized PVA-Silk blended nanofibrous mats promote diabetic wound healing via regulation of extracellular matrix and tissue remodeling". *Journal of Tissue Engineering and Regenerative Medicine*, 2018; 12: e1559-1570.
3. **Dimple Chouhan**, Naresh Thatikonda, Linnea Nileback, Mona Widhe, My Hedhammar, Biman B. Mandal. "Recombinant spider silk functionalized silkworm silk matrices as potential bioactive wound dressings and skin grafts". *ACS Applied Materials and Interfaces*, 2018; 10: 23560-23572.
4. **Dimple Chouhan**, Bijayashree Chakraborty, Samit K. Nandi, Biman B Mandal. "Role of non-mulberry silk fibroin in deposition and regulation of extracellular matrix towards accelerated wound healing". *Acta Biomaterialia*, 2017; 48: 157-174.
5. Nandana Bhardwaj, **Dimple Chouhan**, Biman B. Mandal. "Tissue engineered skin and wound healing: current strategies and future directions". *Current Pharmaceutical Design*, 2017; 23: 3455-82.
6. **Dimple Chouhan**, Nandana Bhardwaj, Biman B. Mandal. "Emerging and innovative approaches for wound healing and skin regeneration: current status and advances" *(Revision submitted in Biomaterials).*
7. **Dimple Chouhan**, Piyali Das, Naresh Thatikonda, Samit K. Nandi, My Hedhammar, Biman B. Mandal. "Silkworm silk matrices coated with functionalized spider silk accelerate healing of diabetic wounds" *(Revision submitted in ACS Biomaterials Science & Engineering).*
8. **Dimple Chouhan**, Tshewuzo-u Lohe, Naresh Thatikonda, VGM Naidu, My Hedhammar, Biman B. Mandal. "Recombinant spider silk coated silkworm silk fibroin matrices accelerate healing of third degree burn wounds" *(under review).*

Publications from Other Collaborative Research Projects:

1. **Dimple Chouhan**, Shreya Mehrotra, Omkar Majumder, Biman B. Mandal. "Magnetic actuator device assisted modulation of cellular behavior and tuning of drug release on silk platform". *ACS Biomaterials Science & Engineering*, 2019; 5, 92–105.
2. Sween Gilotra, **Dimple Chouhan**, Nandana Bhardwaj, Samit K. Nandi, Biman B. Mandal. "Potential of silk sericin based nanofibrous mats for wound dressing applications". *Materials Science and Engineering C*, 2018; 90: 420-432.
3. Linnea Nileback, **Dimple Chouhan**, Ronnie Jansson, Mona Widhe, Biman B. Mandal and My Hedhammar. "Silk-silk interactions between silkworm fibroin and recombinant spider silk fusion proteins enable the construction of bioactive materials". *ACS Applied Materials and Interfaces*, 2017; 9: 31634-44.
4. Shreya Mehrotra, **Dimple Chouhan**, Rocktotpal Konwarh, Manishekhar Kumar, Praveen Kumar Jadi, Biman B. Mandal. "A comprehensive review on silk at nanoscale for regenerative medicine and allied applications". *ACS Biomaterials Science & Engineering*, 2019.

(B) Patents:

1. Biman B. Mandal and **Dimple Chouhan**, "Silk Hydrogel for Treatment of Burn Wounds", Indian patent, Application No. 201831022013.
2. Biman B. Mandal, Yogendra Pratap Singh, Ashutosh Bandyopadhyay, Shreya Mehrotra, Joseph Christakiran Moses, Bibhas Kumar Bhunia, G. Janani and **Dimple Chouhan**, "Development of silk based bioinks for 3D bioprinting and uses thereof", Indian patent, Application No. 201831038727.
3. Biman B. Mandal, **Dimple Chouhan**, Bibrita Bhar, Rajiv Borah, "Silk fibroin – Aloe vera composite matrices for wound healing, Indian Patent, Application no. 201931004617.

(C) Book Chapter:

1. Nandana Bhardwaj, **Dimple Chouhan**, Biman B. Mandal, "Functional 3D Tissue Engineering Scaffolds". 345–365, 2018. (Book Chapter, *Woodhead Publishing*).

(D) Conference Proceedings:

1. **Second position** in TE SIG Poster Award in the 'Annual Meeting of Society for Biomaterials' held at Seattle, U.S.A. on the topic "Silk-ECM composite 3D printed constructs for burn wound healing", 2019.
2. **First position** in Springer Oral Contest in the 'Advances in Polymer Science and Technology' held at Kathmandu, Nepal on the topic "Silk fibroin hydrogel as an affordable alternative solution for treatment of third degree burn wounds", 2018.
3. **Best poster award** in the Research Conclave 2018, on the topic "Exploring silk fibroin based nanofibrous matrix as skin substitute material", IITG, 2018.
4. **Fourth position** in 'Talent Search Contest' organized by Guwahati Biotech Park, Topic: "Smart and affordable wound dressings for treatment of chronic diabetic foot ulcers" in 2018.
5. **Conference paper**: Biman B. Mandal, Dimple Chouhan, Naresh Thatikonda, Linnea Nileback, Mona Widhe, My Hedhammar. "Functionalization of silk fibroin matrices using recombinant spider silk fusion proteins for developing bioactive wound dressing". 5th TERMIS World Congress – 2018 Kyoto, Japan.
6. **Second position** in 'TechExpo Competition' organized by Techniche, IITG, Topic: "Silk based affordable grafts and healthcare products" in 2017.
7. **Best poster award** in the international conference 'Biomaterials, Biodiagnostics, Tissue Engineering, Drug delivery and Regenerative medicine' (BiTERM) on the topic "Silk fibroin based functionalized nanofibrous mats as potential wound dressing material" conducted by IIT Delhi, India, 2016.
8. **Conference paper**: Dimple Chouhan, Samit K. Nandi, Biman B. Mandal. "Non-mulberry silk fibroin based smart nanofibrous wound dressing for chronic cutaneous ulcers". *European cells & materials*, 2016; 31:239, TERMIS-EU Meeting, Uppsala, Sweden.
9. **Second position** in 'Innovation Competition' organized by Technology Incubation Centre, IITG, Topic: "Smart silk based nanofibrous wound dressing: To treat non-healing diabetic foot ulcers" in 2016.
10. **Conference paper**: Mimi Adhikary, Prerak Gupta, Manishekhar Kumar, Salma Jasmine, Nandana Bhardwaj, Dimple Chouhan, Biman B. Mandal. "Hydroxyapatite-silk fiber-silk fibroin tri-composite scaffolds for bone tissue engineering". *European cells & materials*, 2016; 31:18, TERMIS-EU Meeting, Uppsala, Sweden.